SMALL-*x* BEHAVIOUR OF DIS STRUCTURE FUNCTIONS IN THE FRAMEWORK OF LINEAR AND NONLINEAR QCD EVOLUTION EQUATIONS AND SIGNATURES OF GLUON SHADOWING

A thesis submitted in partial fulfillment
of the requirements for award
of the degree of
Doctor of Philosophy

by,

MAYURI DEVEE
Registration No: 005 of 2012

Department of Physics
School of Sciences
Tezpur University
Napaam, Tezpur-784028
Assam, India

December, 2014

I dedicate this humble effort of mine to my beloved parents

Mrs. Tarulata Devee (Maa)

and

Mr. Narayan Chandra Nath (Baba)

whose love, endless support, encouragement, sacrifices and prayers throughout my life enable me to get success

Abstract

Structure functions in lepton-nucleon deep inelastic scattering (DIS) are the well-established observables exploring Quantum Chromodynamics (QCD), the theory of the strong interaction, and they provide exclusive information about the deep structure of hadrons. Predominantly, the structure functions form the foundation of our knowledge of the parton densities, which are indispensable for analysis of hard scattering processes at proton-(anti-)proton colliders like the TEVATRON and the Large Hadron Collider (LHC). Parton distributions are the vital ingredients for most of the theoretical calculations at hadron colliders and they provide the number densities of the colliding partons (quarks and gluons) inside their parent hadrons at a given momentum fraction x, where x is the Bjorken scaling variable, and scale Q^2.

The small-x behavior of parton densities is one of the challenging issues of QCD. The chief and most salient phenomena in the region of small-x which determine the physical picture of the parton evolution are the increase of the parton density at $x \to 0$, the growth of the mean transverse momentum of a parton inside the parton cascade at small-x, and the saturation of the parton density. Therefore the determination of parton densities or to a great degree the gluon densities in the small-x region is particularly important because the gluon distribution function controls the physics at high energy or small-x in DIS. Moreover, precise knowledge of gluon distribution functions at small-x is useful to estimate backgrounds and explore new physics at the LHC. That being so, the dynamics of the the high density QCD, the regime of large gluon densities, is one of the present-day highly demanding undecided issues in the area of high energy or small-x physics.

The standard and the key tools for theoretical investigation of DIS structure functions are the Dokshitzer-Gribov-Lipatov-Altarelli-Parisi (DGLAP) evolution equations. These equations can delineate the available experimental data in a decent manner considering a large domain of x and Q^2 with appropriate parameterizations. Consequently, the solutions of the DGLAP evolution equations have been reported in recent years with significant phenomenological success. The DGLAP evolution equation at the twist-2 level prognosticates a sharp growth of the gluon densities as x grows smaller which is clearly observed in the DIS experiments at HERA as well. In consequence, this generates cross sections which in the high-energy or small-x

limit fail to comply with the Froissart bound. Subsequently, the growing number of gluon densities, so as to approach small-x, demands a formulation of the QCD at high partonic density incorporating the unitarity corrections in a suitable manner.

Gluon recombination is usually assumed to be accountable for the unitarization of the cross section at high energies or a possible saturation of the gluon density at small-x. At small-x the likelihood of interaction between two gluons can no longer be neglected and sooner or later, the individual gluons necessarily start to overlap or shadow each other. Consequently, nonlinear phenomena are expected to arise which eventually bring about a taming of the maximum gluon density per unit of phase-space. Moreover, the pioneering finding of the geometrical scaling in HERA data as well as the existence of geometrical scaling in the production of inclusive jets in the LHC data provides strong experimental evidences of the saturation effects. The multiple gluon interactions towards small-x induce nonlinear corrections in the conventional linear DGLAP equation and accordingly the corrections of the higher order QCD effects have become the focus of in-depth studies in the last few years.

Gribov, Levin and Ryskin, at the onset, investigated the shadowing corrections of gluon recombination to the parton distributions. Following that Mueller and Qiu completed the equation numerically using a perturbative calculation of the recombination probabilities in the DLLA, and also formulated the equation for the change of gluons to sea-quarks. This is a great achievement as it authorises the GLR-MQ equation to be applied phenomenologically and thus provides the connection to experiments. This equation predicts a critical line separating the perturbative regime from the saturation regime, and it is legitimate just in the edge of this critical line. The study of the GLR-MQ equation is extremely important for the interpretation of the non-linear effects of gluon-gluon recombination due to high gluon density at sufficiently small-x as well as for the determination of the saturation momentum. Moreover, the Balitsky-Kovchegov (BK), Modified-DGLAP (MD-DGLAP), Modified-Balitsky-Fadin-Kuraev-Lipatov (MD-DGLAP) and Jalilian-Marian-Iancu-McLerran-Weigert-Leonidov-Kovner (JIMWLK) are some of other widely studied nonlinear evolution equations relevant at high gluon densities.

The work presented in this thesis is focused on the study of the small-x and Q^2 behaviours of the singlet and nonsinglet structure functions and gluon distribution

functions in the context of linear DGLAP and nonlinear GLR-MQ evolution. The first part of this thesis is concerned with the study of the linear DGLAP equation upto next-to-next-to-leading order (NNLO); the second part is more specifically dedicated to the higher order QCD corrections in small-x physics where we address the issue of gluon-gluon recombination or shadowing corrections at very small values of x. In this work, we intend to check whether at very small-x the DGLAP equations can be ruled out in favour of the GLR-MQ equations which would mean evidence for gluon recombination. The structure of the thesis is organized as follows:

Chapter 1 is a general introduction of the elementary particles with a brief account of QCD, DIS, structure functions and parton distribution functions (PDFs). The importance of small-x physics and gluon shadowing are also concisely described here. Various high energy experiments as well as parametrization groups extracting PDFs from global data analyses are also briefly summarized.

Chapter 2 is an overview of the different QCD linear and nonlinear evolution equations with a more or less detailed description of the DGLAP and the GLR-MQ equations. The numerical as well as analytical solutions of the evolution equations, widely available in the literature are also outlined very briefly in this chapter.

It is always very alluring to explore the prospect of obtaining analytical solutions of DGLAP equations somewhat in the restricted domain of small-x. In **chapter 3**, we solve the DGLAP equations for the singlet and non-singlet structure functions analytically at LO, NLO and NNLO by using a Taylor series expansion valid at small-x and obtain the Q^2 and x-evolutions of deuteron structure function, $F_2^d(x, Q^2)$, along with the Q^2-evolution of proton structure function, $F_2^p(x, Q^2)$, upto NNLO. We compare our predictions with NMC, E665 and H1 experimental data as well as with the NNPDF parametrizations. The results obtained are in agreement with perturbative QCD fits at small-x and can explain the general trend of data in a decent manner. Moreover the inclusion of NNLO contributions provide excellent consistency with the experimental data and parametrizations.

In **chapter 4**, we find analytical expressions for gluon distribution function, $G(x, Q^2)$, at LO, NLO and NNLO by solving the corresponding DGLAP evolution equations using a Taylor series expansion as in chapter 3 and evaluate the Q^2 and x-evolutions of $G(x, Q^2)$ upto NNLO. We note that the NNLO approximation has

appreciable contribution in the particular range of x and Q^2 under study. The obtained results can be described within the framework of perturbative QCD. We check the compatibility of our predicted gluon distributions and find satisfactory agreement with the GRV1998, MRST2004, MSTW2008 and JR09 global analysis as well as with the BDM model.

Although, the linear DGLAP equations can delineate the available experimental data, as far as HERA data are concerned, in a decent manner covering a large domain of x and Q^2 with appropriate parameterizations, however, in the very small-x region, due to the nonlinear corrections of gluon-gluon interactions, the conventional linear DGLAP evolution equation is expected to breakdown. We, therefore, turn our attention to the gluon recombination processes in **chapter 5** and estimate the importance of the corrections of these higher order QCD effects, which eventually saturate the growth of the gluon densities in the framework of nonlinear GLR-MQ equation. We investigate the effect of shadowing corrections on the small-x and moderate Q^2 behavior of gluon distribution by solving the nonlinear GLR-MQ equation in leading twist approximation incorporating the well known Regge ansatz in the kinematic region $10^{-5} \leq x \leq 10^{-2}$ and $1 \leq Q^2 \leq 30$ GeV^2. We also derive the condition of compatibility of the LO solution of linear DGLAP equation for gluon with the DLA solution in a finite range of x and Q^2. The predicted gluon distributions from GLR-MQ equation are compared with the GRV1998, GJR2008, MRST2001, MSTW2008, NNPDF, HERAPDF0.1 and CT10 parametrizations as well as with the H1 data. Our predictions are also compared with the EHKQS and BZ models respectively. We further analyse the ratio of the prediction of nonlinear GLR-MQ equation to that of linear DGLAP equation for $G(x, Q^2)$ and observe that the ratio decreases as x grows smaller signifying that the effect of nonlinearity increases towards small-x. It is enticing to note that, the rapid growth of gluon densities towards small-x is tamed by the gluon recombination processes. Results also indicate significant effect of shadowing corrections at $R = 2$ GeV^{-1} when the gluons are concentrated at the hot spots.

In **chapter 6**, we solve the nonlinear GLR-MQ equation for sea quark distribution in leading twist approximation incorporating the well known Regge like ansatz and investigate the effect of shadowing corrections to the small-x and Q^2 behaviour

of singlet structure function $F_2^S(x, Q^2)$ in the kinematic region $10^{-4} \leq x \leq 10^{-1}$ and $0.6 \leq Q^2 \leq 30$ GeV^2. Our predictions are compared with NMC and E665 data as well as with the results of NNPDF collaboration. Results show that $F_2^S(x, Q^2)$ increases with increasing Q^2 and decreasing x, but this behaviour is slowed down towards small-x with the inclusion of the nonlinear terms. The logarithmic derivative, of singlet structure function with shadowing corrections is also calculated and compared with the H1 data. The behaviour of $\partial F_2^S(x, Q^2)/\partial \ln Q^2$ is seen to be tamed due to gluon recombination at small-x.

Chapter 7 concerns with the comparative analysis of the GLR-MQ equation with the more precise and more complicated BK equation as well as with the MD-DGLAP equation. It is interesting to note that the predictions of nonlinear gluon density obtained from the GLR-MQ equation are in very good agreement with the results of the BK equation. Our predictions are also observed to be almost comparable with those of the MD-DGLAP equation, however a flatter gluon distribution is observed in our predictions due to significant shadowing corrections at small-x.

Finally, the conclusions and the future outlooks of this work are drawn in **chapter 8**.

DECLARATION

I hereby declare that the thesis entitled "**Small-*x* Behaviour of DIS Structure Functions in the Framework of Linear and Nonlinear QCD Evolution Equations and Signatures of Gluon Shadowing**" being submitted to Tezpur University, Tezpur, Assam in partial fulfillment of the requirements for the award of the degree of Doctor of Philosophy, has previously not formed the basis for the award of any degree, diploma, associateship, fellowship or any other similar title or recognition.

Date:
Place: Napaam, Tezpur

(Mayuri Devee)
Department of Physics
Tezpur University
Tezpur- 784 028 (Assam)

Tezpur University

CERTIFICATE

This is to certify that the thesis entitled "**Small-*x* Behaviour of DIS Structure Functions in the Framework of Linear and Nonlinear QCD Evolution Equations and Signatures of Gluon Shadowing**" submitted to the School of Sciences, Tezpur University in partial fulfillment for the award of the degree of Doctor of Philosophy in Physics is a record of research work carried out by Ms. Mayuri Devee under my supervision and guidance.

All help received by her from various sources have been duly acknowledged.

No part of this thesis has been submitted elsewhere for award of any other degree.

Signature of the Supervisor:

Name of the Supervisor: Dr. Jayanta Kumar Sarma

Designation: Professor

School: Sciences

Department: Physics

Place: Napaam, Tezpur. **Date:**

Acknowledgement

I would like to take this opportunity to express my deepest appreciation to all those who supported me throughout the period of my research work in some or the other way.

Firstly I would like to thank Prof. Jayanta Kumar Sarma for his guidance and helpfulness during my research work, and for providing me with a nice atmosphere for doing research. I am grateful to him for his encouragement and for giving me freedom to learn on my own.

I am thankful to Tezpur University for providing me with the research facility and the institutional scholarship for the first two years of my research. I also extend my sincere thanks to all the administrative staffs. My thanks also goes to all the staffs of the central library for their wonderful services.

I offer my heartfelt gratitude to all the faculty members of Physics Department, Tezpur University for their inspiration and valuable suggestions. I wish to express my special thanks to Prof. N. Das and Prof. N. Bhattacharyya for their encouragement and invaluably constructive criticism. Moreover, I am thankful to all the technical and non technical staffs of Physics Department for their help during my research work.

I must acknowledge the University Grants Commission for financial support in the form of a research project, I got in some part of my research period.

I would like to offer my heartiest thanks to all my friends and colleagues at Tezpur University, specially Sovan, Nayanmoni, Nomita, Sourav, Rathinda, Momiba, Sanchita ba, Ranjitda, Anjanda, Ananya, Mahmuda and Bobby baideu for their wonderful company, help and well wishes. I really enjoyed the wonderful moments spent with my friends and colleagues at TU.

I would also like to thank the anonymous reviewers of my publications for their constructive comments and helpful suggestions that greatly contributed to improve the quality of my work.

Finally, from the depth of my heart with love and faith, I would like to thank my family- my beloved parents, my dearest younger brother and my darling husband for their constant support and encouragement, without which this work would not have

been possible. Their appreciation, even for small achievements, has always been a source of motivation for me. It is their unconditional love and care that enables me to deal with the tough situations. I find no words to convey how much I love them. I am very much indebted to Maa and Baba (my parents), who have always been there for me and believed in all my efforts. Their invaluable advices, suggestions, blessings and prayers helped me at every stage of my personal as well as academic life. Especially, I would like to thank my mother for being a continual source of my strength and support. She has faith in me and my ability even when I felt like giving up. My mother, taught me that even the largest task can be accomplished if it is done one step at a time. Her love, sacrifice, patience, optimism, sense of humour, and guidance was more valuable than one could ever imagine. Without her presence, this thesis would probably never have existed. She is always the role model and the biggest inspiration of my life. I further owe my love and deepest gratitude to my younger brother Amit who always encourages me to work hard and achieve my goals. Being a software engineer by profession, he has helped me a lot in all computer related matters throughout my research work, enabling me to its successful completion. His love, endless support, care and inspiration have always been invaluable to my life. I am also very grateful to my husband who supported me in every possible way to see the completion of this work. The love, support and constant patience of my husband have taught me much about sacrifice and compromise. I thank him for always being there, cheering me up and standing by me through ups and downs of my life. I also owe to him as he spent endless hours proofreading my thesis.

Above all, I thank the Almighty GOD for his blessings and mercy, and granting me the knowledge, fitness and strength to complete this work.

Date: (Mayuri Devee)

Contents

List of Figures

List of Tables

Abstract

Abstract

Structure functions in lepton-nucleon deep inelastic scattering (DIS) are the well-established observables exploring Quantum Chromodynamics (QCD), the theory of the strong interaction, and they provide exclusive information about the deep structure of hadrons. Predominantly, the structure functions form the foundation of our knowledge of the parton densities, which are indispensable for analysis of hard scattering processes at proton-(anti-)proton colliders like the TEVATRON and the Large Hadron Collider (LHC). Parton distributions are the vital ingredients for most of the theoretical calculations at hadron colliders and they provide the number densities of the colliding partons (quarks and gluons) inside their parent hadrons at a given momentum fraction x, where x is the Bjorken scaling variable, and scale Q^2.

The small-x behavior of parton densities is one of the challenging issues of QCD. The chief and most salient phenomena in the region of small-x which determine the physical picture of the parton evolution are the increase of the parton density at $x \to 0$, the growth of the mean transverse momentum of a parton inside the parton cascade at small-x, and the saturation of the parton density. Therefore the determination of parton densities or to a great degree the gluon densities in the small-x region is particularly important because the gluon distribution function controls the physics at high energy or small-x in DIS. Moreover, precise knowledge of gluon distribution functions at small-x is useful to estimate backgrounds and explore new physics at the LHC. That being so, the dynamics of the the high density QCD, the regime of large gluon densities, is one of the present-day highly demanding undecided issues in the area of high energy or small-x physics.

The standard and the key tools for theoretical investigation of DIS structure functions are the Dokshitzer-Gribov-Lipatov-Altarelli-Parisi (DGLAP) evolution equations. These equations can delineate the available experimental data in a decent manner considering a large domain of x and Q^2 with appropriate parameterizations. Consequently, the solutions of the DGLAP evolution equations have been reported in recent years with significant phenomenological success. The DGLAP evolution equation at the twist-2 level prognosticates a sharp growth of the gluon densities as x grows smaller which is clearly observed in the DIS experiments at HERA as well. In consequence, this generates cross sections which in the high-energy or small-x

limit fail to comply with the Froissart bound. Subsequently, the growing number of gluon densities, so as to approach small-x, demands a formulation of the QCD at high partonic density incorporating the unitarity corrections in a suitable manner.

Gluon recombination is usually assumed to be accountable for the unitarization of the cross section at high energies or a possible saturation of the gluon density at small-x. At small-x the likelihood of interaction between two gluons can no longer be neglected and sooner or later, the individual gluons necessarily start to overlap or shadow each other. Consequently, nonlinear phenomena are expected to arise which eventually bring about a taming of the maximum gluon density per unit of phase-space. Moreover, the pioneering finding of the geometrical scaling in HERA data as well as the existence of geometrical scaling in the production of inclusive jets in the LHC data provides strong experimental evidences of the saturation effects. The multiple gluon interactions towards small-x induce nonlinear corrections in the conventional linear DGLAP equation and accordingly the corrections of the higher order QCD effects have become the focus of in-depth studies in the last few years.

Gribov, Levin and Ryskin, at the onset, investigated the shadowing corrections of gluon recombination to the parton distributions. Following that Mueller and Qiu completed the equation numerically using a perturbative calculation of the recombination probabilities in the DLLA, and also formulated the equation for the change of gluons to sea-quarks. This is a great achievement as it authorises the GLR-MQ equation to be applied phenomenologically and thus provides the connection to experiments. This equation predicts a critical line separating the perturbative regime from the saturation regime, and it is legitimate just in the edge of this critical line. The study of the GLR-MQ equation is extremely important for the interpretation of the non-linear effects of gluon-gluon recombination due to high gluon density at sufficiently small-x as well as for the determination of the saturation momentum. Moreover, the Balitsky-Kovchegov (BK), Modified-DGLAP (MD-DGLAP), Modified-Balitsky-Fadin-Kuraev-Lipatov (MD-BFKL) and Jalilian-Marian-Iancu-McLerran-Weigert-Leonidov-Kovner (JIMWLK) are some of the widely studied nonlinear evolution equations relevant at high gluon densities.

The work presented in this thesis is focused on the study of the small-x and Q^2 behaviours of the singlet and nonsinglet structure functions and gluon distribution

functions in the context of linear DGLAP and nonlinear GLR-MQ evolution. The first part of this thesis is concerned with the study of the linear DGLAP equation upto next-to-next-to-leading order (NNLO); the second part is more specifically dedicated to the higher order QCD corrections in small-x physics where we address the issue of gluon-gluon recombination or shadowing corrections at very small values of x. In this work, we intend to check whether at very small-x the DGLAP equations can be ruled out in favour of the GLR-MQ equations which would mean evidence for gluon recombination. The structure of the thesis is organized as follows:

Chapter 1 is a general introduction of the elementary particles with a brief account of QCD, DIS, structure functions and parton distribution functions (PDFs). The importance of small-x physics and gluon shadowing are also concisely described here. Various high energy experiments as well as parametrization groups extracting PDFs from global data analyses are also briefly summarized.

Chapter 2 is an overview of the different QCD linear and nonlinear evolution equations with a more or less detailed description of the DGLAP and the GLR-MQ equations. The numerical as well as analytical solutions of the evolution equations, widely available in the literature are also outlined very briefly in this chapter.

It is always very alluring to explore the prospect of obtaining analytical solutions of DGLAP equations somewhat in the restricted domain of small-x. In **chapter 3**, we solve the DGLAP equations for the singlet and non-singlet structure functions analytically at LO, NLO and NNLO by using a Taylor series expansion valid at small-x and obtain the Q^2 and x-evolutions of deuteron structure function, $F_2^d(x, Q^2)$, along with the Q^2-evolution of proton structure function, $F_2^p(x, Q^2)$, upto NNLO. We compare our predictions with NMC, E665 and H1 experimental data as well as with the NNPDF parametrizations. The results obtained are in agreement with perturbative QCD fits at small-x and can explain the general trend of data in a decent manner. Moreover the inclusion of NNLO contributions provide excellent consistency with the experimental data and parametrizations.

In **chapter 4**, we find analytical expressions for gluon distribution function, $G(x, Q^2)$, at LO, NLO and NNLO by solving the corresponding DGLAP evolution equations using a Taylor series expansion as in chapter 3 and evaluate the Q^2 and x-evolutions of $G(x, Q^2)$ upto NNLO. We note that the NNLO approximation has

appreciable contribution in the particular range of x and Q^2 under study. The obtained results can be described within the framework of perturbative QCD. We check the compatibility of our predicted gluon distributions and find satisfactory agreement with the GRV1998, MRST2004, MSTW2008 and JR09 global analysis as well as with the BDM model.

Although, the linear DGLAP equations can delineate the available experimental data, as far as HERA data are concerned, in a decent manner covering a large domain of x and Q^2 with appropriate parameterizations, however, in the very small-x region, due to the nonlinear corrections of gluon-gluon interactions, the conventional linear DGLAP evolution equation is expected to breakdown. We, therefore, turn our attention to the gluon recombination processes in **chapter 5** and estimate the importance of the corrections of these higher order QCD effects, which eventually saturate the growth of the gluon densities in the framework of nonlinear GLR-MQ equation. We investigate the effect of shadowing corrections on the small-x and moderate Q^2 behavior of gluon distribution by solving the nonlinear GLR-MQ equation in leading twist approximation incorporating the well known Regge ansatz in the kinematic region $10^{-5} \leq x \leq 10^{-2}$ and $1 \leq Q^2 \leq 30$ GeV^2. We also derive the condition of compatibility of the LO solution of linear DGLAP equation for gluon with the DLA solution in a finite range of x and Q^2. The predicted gluon distributions from GLR-MQ equation are compared with the GRV1998, GJR2008, MRST2001, MSTW2008, NNPDF, HERAPDF0.1 and CT10 parametrizations as well as with the H1 data. Our predictions are also compared with the EHKQS and BZ models respectively. We further analyse the ratio of the prediction of nonlinear GLR-MQ equation to that of linear DGLAP equation for $G(x, Q^2)$ and observe that the ratio decreases as x grows smaller signifying that the effect of nonlinearity increases towards small-x. It is enticing to note that, the rapid growth of gluon densities towards small-x is tamed by the gluon recombination processes. Results also indicate significant effect of shadowing corrections at $R = 2$ GeV^{-1} when the gluons are concentrated at the hot spots.

In **chapter 6**, we solve the nonlinear GLR-MQ equation for sea quark distribution in leading twist approximation incorporating the well known Regge like ansatz and investigate the effect of shadowing corrections to the small-x and Q^2 behaviour

of singlet structure function $F_2^S(x, Q^2)$ in the kinematic region $10^{-4} \leq x \leq 10^{-1}$ and $0.6 \leq Q^2 \leq 30$ GeV^2. Our predictions are compared with NMC and E665 data as well as with the results of NNPDF collaboration. Results show that $F_2^S(x, Q^2)$ increases with increasing Q^2 and decreasing x, but this behaviour is slowed down towards small-x with the inclusion of the nonlinear terms. The logarithmic derivative, of singlet structure function with shadowing corrections is also calculated and compared with the H1 data. The behaviour of $\partial F_2^S(x, Q^2)/\partial \ln Q^2$ is seen to be tamed due to gluon recombination at small-x.

Chapter 7 concerns with the comparative analysis of the GLR-MQ equation with the more precise and more complicated BK equation as well as with the MD-DGLAP equation. It is interesting to note that the predictions of nonlinear gluon density obtained from the GLR-MQ equation are in very good agreement with the results of the BK equation. Our predictions are also observed to be almost comparable with those of the MD-DGLAP equation, however a flatter gluon distribution is observed in our predictions due to significant shadowing corrections at small-x.

Finally, the conclusions and the future outlooks of this work are drawn in **chapter 8**.

Chapter 1

Introduction

1.1 Fundamental structure of matter

The fundamental research in physics evolves the understanding of mankind at a great rate in the last century. The everlasting hunt to determine what are we made of or what is the fundamental structure of matter has led to a broadly adopted classification of fundamental particles. In the course of time, physicists become triumphant in portraying matter to be made up of some smaller entities. The origin of today's world is supposed to be the so called big bang, during which time, space, matter and energy emerged as reality. In ancient time it was believed that there were four set of classical elements: earth, water, air, and fire; sometimes including a fifth element called aether in ancient Greece and akasha in India [1]. The idea of the five elements established a background of analysis in both Hinduism and Buddhism. This theory of classical elements prevailed to the seventeenth century until the beginning of the modern chemistry when the great chemist Robert Boyle gave the new definition for an element. About a hundred years later the British chemist John Dalton proposed the modern atomic theory in 1809 and gave a list of elements that is a clear outrider to today's tabulation of the hundred and more elements. In 1897, the first subatomic particle called the electron was discovered by Joseph John Thomson. The discovery of proton by Ernest Rutherford in 1911 in his famous scattering experiment superseded Thomsons plum pudding model of the atom. Later in 1932 Rutherford's student James Chadwick discovered the neutron following which the detailed picture of atomic nuclei was undocked.

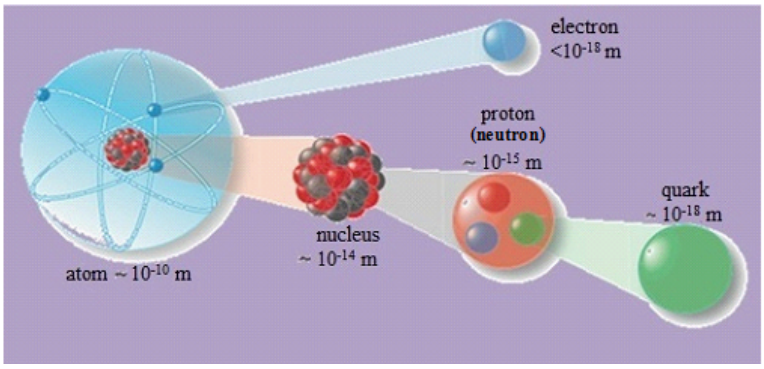

Figure 1.1: The structure within the atom

By the 1960s more and more new particles like proton and neutron, called hadrons, were discovered and it was justifiable to admit that the strongly bound hadrons were not truly fundamental particles, but were composed of some further anonymous elementary entities. In 1964 Murray Gell-mann and George Zweig independently proposed that these entities were a family of spin 1/2 particles which they named quarks [2, 4] and according to their theory each hadron was consisted of either three quarks, known as baryons, or a quark and anti-quark pair, known as mesons. Then, in 1968, the high energy electron-proton scattering experiments at the Stanford Linear Accelerator Center (SLAC) revealed the existence of hard scattering centers inside the proton, thus confirming, undoubtedly, that it surely was a composite particle. Richard Feynman in 1969 proposed the parton model in which the hadrons were supposed to be composite objects of some more fundamental particles, the so-called partons [5]. Later it was identified that these partons represent the same objects nowadays usually referred to as 'quarks' and 'gluons'. The main difference between Rutherford's experiment and the electron-proton scattering experiments comes from the fact that, the dimension of an atom is typically 10^{-10} m whereas that of a proton is about 1 fm = 10^{-15} m (Figure 1.1). From the uncertainty principle $\Delta E.\Delta x \geq hc \approx 0.2$ GeVfm, it is clear that the smaller the distance to be probed the higher must be the beam energy. The probing inside the proton ($x << 1$ fm) requires a beam energy $E >> 1$ GeV. The requirement of this high energy acceleration technique is responsible for more than 50 years gap between the two experiments.

The quark model possessed various puzzling features regardless of its achievement that included the probable absence of isolated quarks as well as two quark (qq) or

four quark combinations (qqqq). Over the past decade, however, particle-accelerator activities all over the world have assembled some indication that a few different kinds of four-quark particles might exist. Very recently using the most powerful particle collider in the world, the Large Hadron Collider (LHC), a research group at CERN has produced a particle made of four quarks go by the name $Z(4430)^-$ [6]. They exist only in exceedingly high-energy ambiance for an extremely short period of time. Moreover the presence of pentaquark states was announced by various experiments in the middle of the year 2000, but subsequent experiments and reanalysis of the data revealed them to be statistical effects instead of true resonances. A further problem was associated with the Δ^{++} baryon as the quantum numbers of this particle turned out to violate the Pauli exclusion principle. These enigmas were sooner or later resolved by the addition of another degree of freedom referred to as color and to that end along with all other quantum numbers quarks also carry a color charge. Nevertheless due to color confinement all particles observed in nature must be color singlet, and so the only permissible quark combinations appear to be simply the three quarks or three antiquarks as well as a quark and an antiquark compositions.

Our current understanding of the basic building blocks of matter and how do they interact with each other can be explained by a theory, known as the Standard Model (SM) [6-9]. Over time and through many experiments, physicists have successfully developed the SM into a well-tested theory of particle physics that marks a milestone in our present knowledge on what the world is and what holds it together. It was flourished during the latter half of the 20th century, as a joint endeavor of scientists throughout the world. The present formulation was established in the middle of 1970s consequent to the experimental evidence for the existence of quarks. Ever since the discoveries of the W and Z bosons in 1981 [10], the top quark in 1995 [11], the tau neutrino in 2000 [12], and more recently the Higgs boson with spin 0, the first elementary scalar particle ever discovered in nature, in 2012 [13] at the worlds largest particle accelerator, the CERN's Large Hadron Collider (LHC) have added further credibility to the already established SM. According to this theory, the most fundamental building blocks of all matter in the universe are quarks and leptons along with their antiparticles. Nonetheless, the experiments colliding beam of protons at the highest LHC energies will be awaiting to see whether quarks themselves contain

more fundamental constituents. Each of these particles comes in six distinct types and their interactions are mediated by the force carrier particles. The particles that make up ordinary matter i.e. leptons and quarks are fermions, whereas the force carriers are bosons. The six quarks form three doublets of the electroweak symmetry group SU(2).

The SM organizes the elementary particles into three generations, including two quarks and two leptons in each generation as shown in Figure 1.2. Particles in generation I are less massive than those in generation II, which are less massive than those in generation III. The up quark, the down quark, the electron and the electron neutrino are placed in the first generation; the second generation includes the charm quark, the strange quarks, the muon and the muon neutrino; while the third generation consists of the top and bottom quarks and the tau and tau neutrino. The ordinary matter, for example the stable atoms made of electrons, protons, and neutrons with effectively infinite life spans, is exclusively made up of first-generation particles. Being heavier higher generations particles quickly disintegrate into first-generation particles, and thus are not usually experienced. The hadron with longest life time containing a second generation quark is the lambda particle, made of an up, down, and strange quark. It has a mean lifetime less than a billionth of a second, which is comparatively long-lasting for an unstable hadron. Particles of third generation are divided according to their behavior. The bottom quark does not differ much from a strange quark. On the other hand the top quark is very short-lived and breaks down before anything realizes its existence. They can only be recognized from their decay products.

There are four fundamental forces in the universe: the strong force, the electromagnetic force, the weak force and the gravitational force. The SM includes the electromagnetic, strong and weak forces and all their carrier particles, and explains well how these forces act on all of the matter particles. However, the most familiar force in our everyday lives, gravity, is not a part of the SM. The weak and strong forces are effective only over a very short range and dominate only at the level of subatomic particles whereas the electromagnetic force acts over an infinite range. Gravity is the weakest of the four fundamental forces and appears to have infinite range unlike the strong or weak force. It is speculated that the gravitational force is mediated

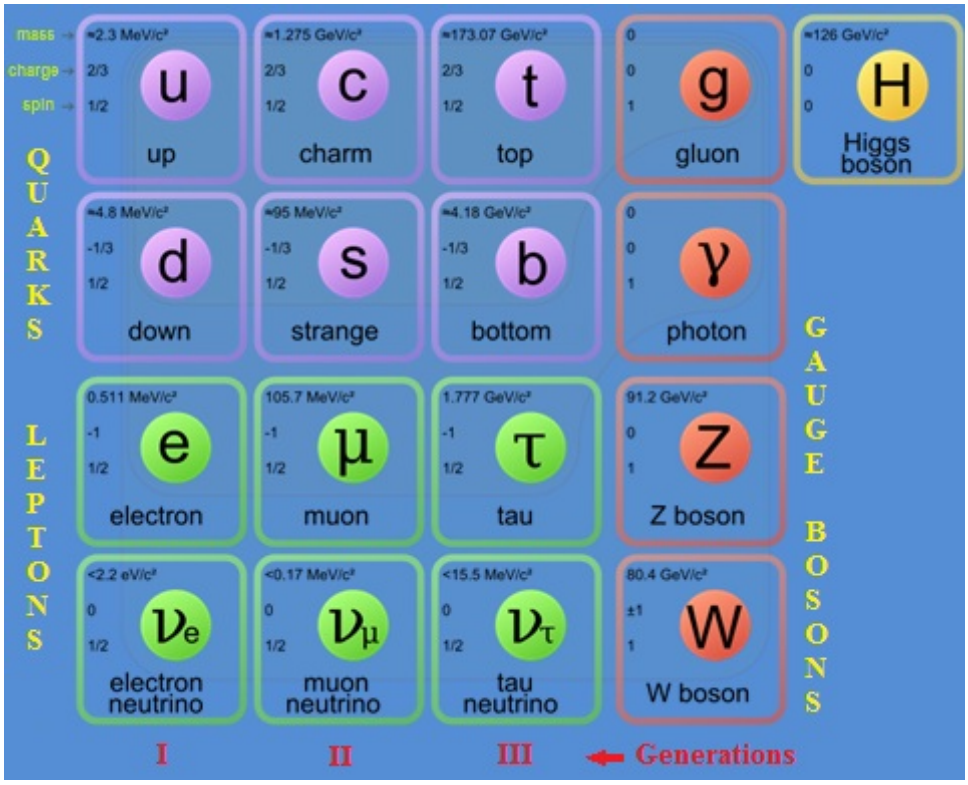

Figure 1.2: Standard model of elementary particles

by a massless spin-2 particle called the graviton, yet to be discovered. The LHC experiments could give indication for extra dimensions apart from the four dimensions we experience and allow the study of higher-dimensional gravitons. Nevertheless, some theories predict that high-energy experiments at LHC could create gravitons escaping into the extra dimensions. Quantum electrodynamics (QED), a quantum field theory, mathematically describes all phenomena involving electrically charged particles, interacting by means of exchange of photon, the massless, uncharged, spin 1 gauge boson. The weak interaction is accountable for both the radioactive decay and nuclear fusion of subatomic particles. The weak interaction affects all the fermions of the SM, as well as the Higgs boson and is mediated by two massive gauge bosons: the charged $W^{\pm}$ or the neutral Z^0, also known as intermediate vector bosons. Neutrinos are the only particles to feel just one of the fundamental forces, the weak interaction, which is what makes them so hard to investigate. The weak interaction is best understood in terms of Glashow, Salam, and Weinbergs electro-weak theory (EWT) which unifies both the weak and electromagnetic forces into one at higher energies [7-9].

The strong force, as the name implies, is the strongest of all four fundamental

interactions. Quarks and gluons are the only fundamental particles that carry color charge, and hence participate in strong interactions. The quantum field theory that describes strong interactions is named as Quantum Chromodynamics (QCD) for this property of color. The strong interactions among the quarks are exchanged by gluons, the massless gauge boson with spin 1, like photons. However, unlike photons, which are not electrically charged and therefore do not feel the electromagnetic force, gluons do take part in strong interaction and can interact among themselves. But the behavior of this crucial, prevalent binding force is exceptionally difficult to understand. A new electron-ion collider (EIC) [14] could successfully unfold the enigmas of the glue. Within short range about 10^{-15} metre, approximately the diameter of a proton or a neutron, the strong force becomes stronger with distance, unlike the other forces. However, the strong force between quarks becomes weaker at short distances. That is Quarks behave independently when they are close, but they can not be pulled apart. Due to this property, known as the asymptotic freedom [15-17], the various interactions between the quarks can possibly be neglected when probing the hadron with a high energy particle. Consequently free quarks are not observed in nature but rather they are permanently confined within colorless hadrons.

So far so good, but there are many shortcomings in the SM as it fails to explain the complete picture, such as the strong CP problem, neutrino oscillations, matter-antimatter asymmetry, and the dark matter and dark energy etc. Another problem with SM is that it incorporates only three out of the four fundamental forces, omitting gravity. The model is also unsuccessful in explaining why gravity is so much weaker than the electromagnetic or strong forces. Moreover it cannot provide justification for the three generations of quarks and leptons with such a diverse mass scale. The hierarchy problem is also associated with the Higgs boson mass. Last but not the least, the SM only describes visible matter, but it cannot explain the nature of the dark matter and dark energy. Many attempts in the theoretical and experimental physics are going on to extend the SM through supersymmetry or to discard it in favor of new theories like Minimal Supersymmetric Standard Model (MSSM), string theory and extra dimensions. Regardless of the deficiencies, the SM is the most successful theory of particle physics to date.

1.2 Quantum chromodynamics

QCD is the theory that describes the dynamics of the strong interactions between quarks and gluons. Its phenomenological utilizations to a large extent, concerning which people go on learning, are still very interesting topics of active research. QCD is a special case of a non-abelian Yang-Mills theory with the gauge group SU(3), the Special Unitary group in 3 dimensions [18]. This gauge group involves the additional degree of freedom known as color, completely unrelated to the everyday familiar phenomenon of color, which plays an essential part in the dynamics of the theory. The concept of color first originated from the discovery of the Δ^{++} baryon composed of three strange quarks with parallel spins when its quantum numbers seemed to violate the Pauli exclusion principle. The idea of color as the origin of a strong field was evolved into the theory of QCD in the 1970s by the physicists Harald Fritzsch and Heinrich Leutwyler, together with Murray Gell-Mann [19]. According to QCD quarks carry a color charge of red (R), green (G) or blue (B) and antiquarks have a color charge of antired (cyan), antigreen (megenta) and antiblue (yellow) i.e. $\bar{R}$, $\bar{G}$, $\bar{B}$ [18]. Especially, it is of great importance that the gauge bosons of QCD, the gluons, carry color as well and therefore can interact among themselves. In this way apart from the well known fermion-boson vertex, the QCD Lagrangian further involves three-gluon and four-gluon vertices. Figure 1.3 shows the schematic representation of the basic QCD Feynman diagrams. Due to the specific characteristic of gluon self coupling in QCD it is feasible to have a convincing theory including only the gauge fields without any fermion, and so in some situations the contributions arising from only the gauge part are likely to be separated from the fermionic contributions. Moreover the existence of jets in QCD is subjected to these gluon-gluon interactions. Gluons have a combination of a color and an anticolor of a different kind in a superposition of states which are equivalent to the Gell-Mann matrices. Unlike the single photon of QED or the three $W^{\pm}$ and Z^0 bosons of the weak interaction, there are evidently eight kinds of gluons in QCD listed as follows [18]: $R\bar{G}$, $R\bar{B}$, $G\bar{R}$, $G\bar{B}$, $B\bar{R}$, $B\bar{G}$, $(R\bar{R}-G\bar{G})/\sqrt{2}$ and $(R\bar{R}+G\bar{G}-2B\bar{B})/\sqrt{6}$. In other words, the gluons belong to a $SU(3)$ color octet. The remaining combination, the $SU(3)$ color singlet, $(R\bar{R}+G\bar{G}+B\bar{B})/\sqrt{3}$ does not take part in the interaction.

Two outstanding features of QCD are confinement and asymptotic freedom [15-

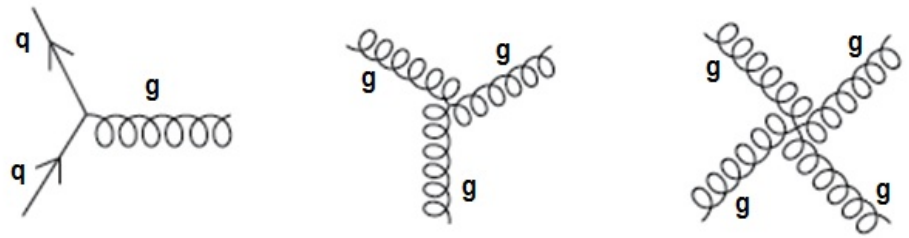

Figure 1.3: Basic QCD Feynmann diagrams

17]. The perturbative analysis of QCD is well grounded based on the fact that the theory is asymptotically free, that is, at short distance the quarks and gluons behave as quasi-free particles whereas at longer distance the force of attraction between quarks and gluons becomes stronger and stronger. Therefore no free color charge has ever been observed in nature, rather they are confined within the experimentally observed color neutral composite states of hadrons. The coupling constant which is a measure of the effectiveness of the strong force that holds quarks and gluons together into composite particles introduces a dependence on the absolute scale, implying more radiation at low scales than at high ones and it is usually referred to as running coupling constant [20]. The running is logarithmic with energy, and is governed by the so-called beta function,

$$\frac{\partial \alpha_s}{\partial \ln (Q^2)} = \beta(\alpha_s), \tag{1.1}$$

where

$$\beta(\alpha_s) \equiv \frac{\partial \alpha_s(Q)^2}{\partial \ln (Q^2)} = -\frac{\beta_0}{4\pi}\alpha_s^2 - \frac{\beta_1}{16\pi^2}\alpha_s^3 - \frac{\beta_2}{64\pi^2}\alpha_S^4 + \mathcal{O}(\alpha_s^5) \tag{1.2}$$

with one-loop, two-loop and three-loop coefficients

$$\beta_0 = \frac{11}{3}N_c - \frac{4}{3}T_f = 11 - \frac{2}{3}N_f,$$

$$\beta_1 = \frac{34}{3}N_c^2 - \frac{10}{3}N_c N_f - 2C_F N_f = 102 - \frac{38}{3}N_f,$$

and

$$\begin{aligned} \beta_2 &= \frac{2857}{54}N_c^3 + 2C_F^2 T_f - \frac{205}{9}C_F N_c T_f - \frac{1415}{27}N_c^2 T_f + \frac{44}{9}C_F T_f^2 + \frac{158}{27}N_c T_f^2 \\ &= \frac{2857}{2} - \frac{6673}{18}N_f + \frac{325}{54}N_f^2. \end{aligned}$$

Here N_f is the number of active fermion flavors and N_c is the number of colors. We use $N_f = 4$, $N_c = 3$, $T_f = \frac{1}{2}N_f$ and $C_F = \frac{N_c^2-1}{2N_c}$, C_F being the color factor associated

with the color group SU(3). Numerically, the value of the strong coupling is usually specified by two parameters, the renormalization scale (μ) and the corresponding value of the coupling at that point, from which we can obtain its value at any other scale from Eq.1.1,

$$\alpha_s(Q^2) = \frac{\alpha_s(\mu^2)}{1 + \alpha_s(\mu^2)\beta_0 \ln(Q^2/\mu^2) + \mathcal{O}(\alpha_s^2)}. \tag{1.3}$$

These two parameters can be replaced for a single parameter Λ so that the running coupling can be expressed as

$$\alpha_s(Q^2) = \frac{1}{\beta_0 \ln(Q^2/\Lambda^2)}. \tag{1.4}$$

The coupling would clearly diverge at the scale Λ, called the Landau pole, which specifies the energy scale at which the perturbative coupling would nominally become infinite. Its value is experimentally found to be $\Lambda \approx 200$ GeV. This implies that the perturbation calculations are allowed only at energy scales of or higher than 1 GeV. Moreover, the structure of hadrons cannot be determined applying perturbation theory as a result of confinement. Alternatively, the quark and gluon content of hadrons are computed by parametrizations of the distribution functions obtained from high energy scattering experiments. Being universal these distribution functions are very useful to make prognostications for other experiments.

1.3 Deep inelastic scattering and structure functions

Deep inelastic scattering (DIS) [21, 22] has long been an excellent tool of exploring the inner structure of a hadron, say proton. DIS provides the first conceivable indication of the reality of quarks which so far had been considered by many to be merely a mathematical fact. In lepton-nucleon DIS for example, electrons and protons are accelerated to very high energies and then allowed them to collide. The four-momentum squared (Q^2) of the exchanged virtual photon in this process determines the resolving power. The spatial resolution with which structure of the proton is probed is roughly the De Broglie wavelength of the virtual photon $\lambda \sim 1/Q$. At large Q^2, the wavelength associated with the electron are much smaller than the size of a proton, thereby resolving smaller distances within the proton, i.e. a single quark

inside the proton scatters off the photon. Thus DIS assist us to extract information on the the parton dynamics and the momentum distributions of quarks and gluons inside the proton to a great extent. Over and above that DIS is solicitous to the discovery and interpretation of new physics which could be observed in extreme conditions of high parton densities at very small Bjorken-x. The first DIS experiments were performed at SLAC in California in 1968 following which a lot of other DIS experiments exploring the proton structure have been carried out until 2007 with the high energy HERA electron-proton collider at DESY in Hamburg. Most recently a new colliding beam facility, the Large Hadron Electron Collider (LHeC) [23], is proposed at CERN for lepton-nucleon scattering which will produce an unprecedented kinematic domain for lepton-nucleon scattering with the centre of mass energy of 1.3 TeV being four times larger than the previous highest attainable energy at HERA. In lepton-nucleon neutral-current (NC) DIS, a neutral boson, i.e. a photon or a Z^0,

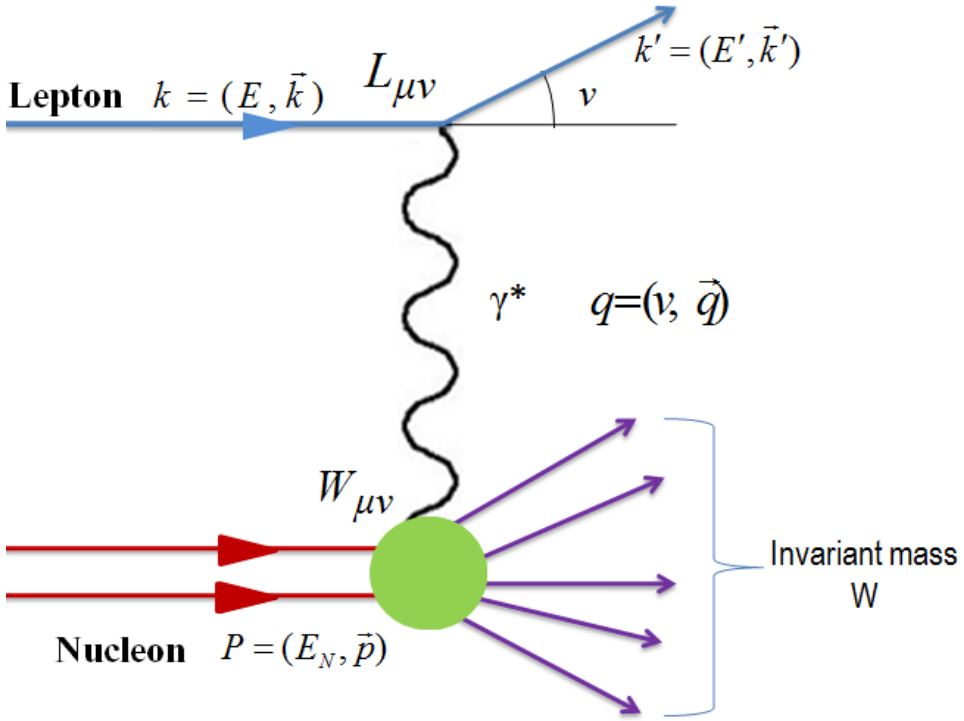

Figure 1.4: Schematic representation of DIS

is exchanged between the electron (or positron) and the quark, in contrast to the charged-current (CC) DIS where a charged $W^{\pm}$ boson is exchanged when a neutrino interacts with a nucleon. The resulting process of DIS is inclusive when this hadronic final state remains undetected, or semi-inclusive when apart from the lepton some

produced hadrons are detected or exclusive when all final products are identified. The basic process of NC DIS where the lepton with four momentum k interacts with the proton with four momentum p through the exchange of a virtual photon whose momentum is q is depicted in Figure1.4. The cross section of the process can be described by the following Lorentz invariant kinematic variables [18]:
Exchanged four momentum squared or virtuality of photon:

$$Q^2 \equiv -q^2 = (k - k');$$

Square of the invariant mass of the final state hadronic jet:

$$W^2 = (p + q)^2 = M^2 + 2p.q + q^2;$$

Center of mass energy squared:

$$s = (p + k)^2;$$

Energy transfer from the lepton to the proton:

$$\nu = p.q;$$

Bjorken scaling variable representing the fracton of proton's four momentum carried by a parton:

$$x = \frac{Q^2}{2\nu} \text{ and}$$

Fraction of energy lost by the electron in the proton rest frame (inelasticity):

$$y = \frac{p.q}{p.k} = 1 - E'/E.$$

Here k denotes the four momentum of the incoming electron and k' the four momentum of the scattered electron, E and E' are the initial and final electron energies in the rest frame of the target proton and M is the mass of the proton. Q^2 and ν are the two independent variables in DIS. The dimensionless x is related to the variables y, Q^2 and s via the approximate relation $Q^2 = xys$. Since the proton is the lightest baryon, therefore $W > M$. It is necessary to measure E, E' and the scattering angle θ in the laboratory reference frame to determine the full kinematics. The aforementioned kinematic variables have a finite range of allowed values: $0 < x < 1$; $0 < y < 1$; $0 < Q^2 < s$ and $M < W < \sqrt{s}$.

The scattering cross section can be splitted into a leptonic part describing the emission of the virtual photon by the lepton and a hadronic part describing the interaction of the virtual photon with the proton,

$$d\sigma \sim L_{\mu\nu} W^{\mu\nu}. \tag{1.5}$$

The most general form of the tensor $W_{\mu\nu}$ can be constructed out of $g^{\mu\nu}$ and independent momenta p and q as

$$W^{\mu\nu} = \Big(g^{\mu\nu} - \frac{q^\mu q^\nu}{q^2}\Big) W_1(x, Q^2) + \Big(p^\mu + \frac{1}{2x} q^\mu\Big)\Big(p^\nu + \frac{1}{2x} q^\nu\Big) W_2(x, Q^2). \tag{1.6}$$

The proton structure function is characterised by two measurable functions W_1 and W_2 or equivalently the so-called structure functions F_1 and F_2:

$$F_1(x, Q^2) = W_1(x, Q^2),$$

$$F_2(x, Q^2) = \nu W_2(x, Q^2). \tag{1.7}$$

Structure functions are the established observables in DIS providing unique information about the deep structure of hadrons as well as their interactions. They allow perturbative QCD to be precisely tested and and to a great degree, they form the backbone of our understanding concerning the parton densities which are indispensable to investigate the hard scattering processes. In terms of F_1 and F_2 the unpolarized DIS cross section can be expressed as

$$\frac{d^2\sigma}{dx dQ^2} = \frac{4\pi\alpha_S^2(Q^2)}{Q^4}\Big[xy^2 F_1(x, Q^2) + (1-y) F_2(x, Q^2)\Big], \tag{1.8}$$

where the first term F_1 corresponds to the absorption of a transversely polarized photon, while the longitudinally polarized component of the cross section is given by $F_L(x, Q^2) = F_2(x, Q^2) - 2xF_1(x, Q^2)$. Further in the limit $Q^2 \to \infty$ and fixed x, any strong interactions among the partons can be neglected and the proton structure functions can be estimated from an incoherent sum of the partons. Then F_1 and F_2 become independent of Q^2 and are functions of the dimensionless kinematical variable x only. This is known as the so-called Bjorken scaling [24]. The well-known SLAC-MIT experiment on DIS observed that the measured DIS cross section exhibit approximate scaling behavior [25]. In the Bjorken limit the quarks in the proton can absorb only the transversely polarized photons, whereas the the longitudinally

polarized photons can not be absorbed due to halicity conservation and therefore the longitudinal part of the cross section turns out to vanish. In that case F_1 and F_2 are related through the famous Callan-Gross relation $2xF_1(x) = F_2(x)$ which is a direct consequence of the existence of point like quarks with spin 1/2 within proton.

QCD extends the naive quark parton model by allowing interactions between the partons via the exchange of gluons. The processes that generate the parton interactions to first order in α_s are gluon radiation ($q \to qg$), gluon splitting ($g \to gg$) and quark pair production ($g \to q\bar{q}$). In DIS, at smaller values of Q^2 the photon can resolve only the valence quarks with relatively large values of x with a finite resolution proportional to $1/Q$. On the other hand, at higher values of Q^2 the photon, having a smaller wavelength, can resolve the quarks at smaller distance scales. Thus in the high Q^2 region gluon radiation leads to the creation of quark-antiquark pairs with relatively small values of x. The parton densities will thus increase with increasing Q^2. Analysis of the cross section shows that this increase mainly occurs at small-x. Therefore, QCD persuades the requirement of an additional scale Q^2 for the representation of the parton densities. Accordingly beyond the bounds of parton model approximation the PDFs and therefore the structure functions come to have a Q^2 dependence through higher order corrections in $\alpha_s(Q^2)$ resulting in sizeable scaling violations [26]. The HERA experiments, H1 and ZEUS [27-30] measured the proton structure function F_2 extensively and perfectly established its scaling violations anticipated by QCD over a wide kinematic region. The predicted scale dependence further enables the factual estimation of $\alpha_s(Q^2)$ as well as provides an explicit verification of QCD.

1.4 Parton distribution functions

Perturbative QCD or any other cross sections involving initial-state hadrons can not provide first-hand appraisal of structure functions owing to the fact that the initial-state particles in the experiments of different high energy collider viz. HERA, Tevatron as well as LHC are not quarks and gluons, but the composite hadrons. Therefore, it is a prerequisite to know the momentum distributions of the partons (quarks and gluons) inside the colliding hadrons in order to correlate theoretical QCD calculations with experimental data. To zeroth order in α_s, the structure functions

are precisely measured in respect of parton distribution functions (PDFs). In the parton model approximation, the proton is composed of a number of free constituents, each of which carry a fraction x of the protons total momentum. In this framework the structure functions are usually identified by the summation over the incoherent sum of the parton's momentum distributions $q_i(x)$ for each quark flavor i,

$$F_2(x) = 2xF_1(x) = \sum_i e_i^2 x q_i(x), \tag{1.9}$$

where the sum implies summation over all flavours of quarks and antiquarks. e_i is the electric charge of a parton of type i. The functions $q_i(x)$ are known as the PDFs describing the probability of finding a parton of flavor i inside the proton with a longitudinal momentum fraction x at resolution scale Q^2. The proton consists of three valence quark flavors uud along with the many quark-antiquark flavors $u\bar{u}$, $d\bar{d}$, $s\bar{s}$ and so on, known as the 'sea' quarks. As a first approximation, we may assume the three lightest quark flavors u, d and s, having roughly the same fequency and momentum distribution, to occur in the sea and neglect the possibility of sizeable presence of heavier quark flavors. To recover the quantum numbers of proton, the net numbers of quarks need to satisfy the following sum rule:

$$\int_0^1 (u(x) - \bar{u}(x))dx = 2; \int_0^1 (d(x) - \bar{d}(x))dx = 1; \int_0^1 (s(x) - \bar{s}(x))dx = 0, \tag{1.10}$$

resulting charge=+1, baryon no.=1, strangeness=0. Another important sum rule is the momentum sum rule which demands that the sum of the momenta of all partons must be equal to the momentum of the proton, i.e.

$$\sum_i \int_0^1 x q_i(x) dx = 1. \tag{1.11}$$

The PDFs, being non-perturbative, cannot be fully obtained by perturbative QCD. These are rather derived by fitting observables to experimental data. Nevertheless, within QCD one can study the rate of change of the PDFs with the resolution scale Q^2 and it is controlled by the QCD evolution equations for parton densities. As mentioned earlier, QCD predicts a dependence of the structure function on the scale Q^2 induced by corrections in $\alpha_s(Q^2)$ arises from diagrams with real gluon emission. So QCD modifies the F_2 structure function as

$$F_2(x, Q^2) = \sum_i e_i^2 x(q_i(x, Q^2)). \tag{1.12}$$

Thus the structure function as well as the parton distributions now have a Q^2 dependence resulting in scaling violation. The general strategy to determine PDFs is comprised of parametrizing the dependence of the parton distributions on the variable x at some small value of $Q^2 = Q_0^2$, either by constructing a rough presumption on their analytical forms or by employing the neural-net technology, and evolving these input distributions to high Q^2 via the evolution equations. Be that as it may, there is still not a particular set of PDFs commonly acknowledged. Presently the parametrizations of PDFs are accomplished by several groups, mainly the GRV/GJR [31, 32], MRST/MSTW [33-35], NNPDF [36, 37], HERAPDF [38, 39] and CTEQ [40, 41]. We will further discuss these PDFs groups in more detail in section 1.6.2 of this chapter. These groups differ mainly in the input data, the methods of parametrizations, the treatment of heavy quarks and the value of the coupling constant α_s as well the methods of analysis. To comprehend the common features and ambiguity as well as the discrepancies between the predictions of the PDF groups an active association has been set up at CERN in recent times.

1.5 Gluon shadowing at small-x

One of the present most fascinating issues of QCD is the growth of hadronic cross sections at high energies or in other words at small-x. At very high energies hadronic interactions have been manifested to be impelled by states with high partonic densities and accordingly many phenomenological and theoretical efforts have been made to explain it. A vital finding of the past years is the prepotent role of gluons with very small fractional momentum x in nucleons when observed by a high energy probe. Thus increase of energy causes a rapid growth of the gluon density in the limit $x \to 0$ eventually leading to the saturation effects [42-44]. That being so, the study of lepton-nucleon DIS or most importantly the determination of the gluon density in the region of small-x is considerably relevant as it could be a measure of perturbative QCD or a probe of novel effects and further because it is the primary factor in numerous other analysis of different high energy hadronic processes. There have been enormous phenomenological and experimental activities for decades regarding the interpretation of small-x QCD from DIS at HERA to heavy ions collisions at RHIC. Moreover the study of this kinematic regime is of uttermost importance to

compute particle production in the proton-proton collisions at LHC.

The small-x demeanor of structure functions for fixed Q^2 exhibits the high-energy nature of the total cross section with growing total center of mass energy squared s since $s \simeq Q^2(\frac{1}{x} - 1)$ [44]. At very high energies, one can therefore access the region of smaller and smaller values of x. At small-x, the likelihood for the photon of detecting a small-x parton increases and for sufficiently small values of x the virtual photon no longer interacts with each parton deliriously, rather there may be multiple scattering off various partons. However the sharp growth of the gluon density towards small-x will eventually have to slow down in order to restore the Froissart bound [45, 46] on physical cross sections. This bound controls the upper limit for the increase of the cross section at asymptotically large values of s and is established on analyticity and unitarity constraints. The Froissart bound indicates that the total cross section does not grow faster than the logarithm squared of the energy as $s \to \infty$ or, equivalently, as $x \to 0$, i.e., $\sigma_{total} = \frac{\pi}{m_\pi^2}(\ln s)^2$, where m_π measures the range of the strong force. It seems that there should be some process which restricts the growth of the gluon distribution at small-x and subsequently prohibits the cross section from growing very rapidly. Gluon recombination is generally regarded as the mechanism liable for this taming or a potential saturation of the gluon distribution function at very small-x.

As x decreases for fixed Q^2, the number of gluons increases, and at some value of $x = x_{crit}$ the entire transverse area inhabited by gluons turns out to be comparable to or larger than the transverse area of a proton. In consequence, at sufficiently high energy the semi-hard processes, which complements the interactions of gluons with a very small fraction of the proton's momentum, may affluently contend the soft processes [42]. In other words, at very small values of x the number densities of gluons will be so high that the probability of interaction between two gluons can no longer be overlooked. That is to say, at very small-x ($x < x_{crit}$) gluons start to overlap spatially and so the processes of recombination of gluons will be as essential as their emission. In this way the increase in the number of small-x gluons becomes limited by gluon recombination ($gg \to g$) processes which eventually leads to gluon saturation [42, 43, 47]. The phenomena of gluon recombination is also known as absorptive corrections, shadowing, nonlinear effects, screening or unitarity corrections. The gluon saturation

is one of the most fascinating problems of the small-x physics, which is presumed on theoretical basis and there is emerging indications of its existence. The pioneering finding of the geometrical scaling in HERA data [48] as well as the existance of geometrical scaling in the production of comprehensive jets in the LHC data [49] provides strong experimental evidences of the saturation effects.

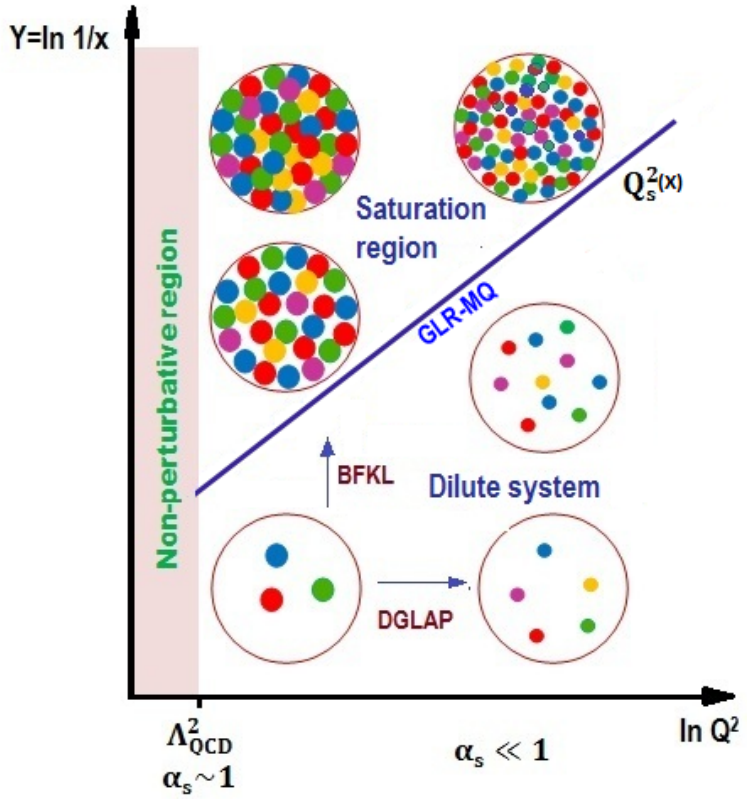

Figure 1.5: Schematic picture of parton saturation

In conjunction with energy the inception of saturation also depends on the size of the gluons, defined as $r \sim 1/Q$ in DIS. With larger sized gluons the available hadron area will be teemed earlier and the gluons start to re-interact whereas, when the size is small the saturation will be deferred to larger energies. The process of gluon saturation is schematically portrayed in Figure 1.5. There is a typical transverse momentum scale Q_s related to saturation which separates the dilute regime from the saturated regime. It is known as the saturation scale and it signifies the scale at which the nonlinear effects become important. Q_s is proportional to the density of gluons per unit area [50]:

$$Q_s^2(x) \simeq \frac{\alpha_s}{N_c} \frac{x g(x, Q^2)}{\pi R^2} \sim x^{-\lambda}, \tag{1.13}$$

where R is the radius of the hadron where gluons populate. The saturation scale is the key parameter in saturation physics [47-54] and grows with $1/x$. Therefore, for sufficiently small-x, $Q_s^2 >> \Lambda^2$ with Λ being the QCD cut off parameter and thus the small coupling approach is legitimate. Below the saturation scale the nonlinear effects begins to decelerate and ultimately saturate the rapid growth of the gluon densities.

The conventional perturbative QCD methods cannot be pertained in the kinematic region of small-x and large-Q^2, where α_s continues to be small but the density of gluons becomes high enough. The interactions among the gluons in this dense system disagree with the fundamental presumption of the QCD improved parton model where the partons are considered to be noninteracting. The physics that controls this high density region is non-perturbative, but of a nature unlike the one analogous to large distances [47, 55]. Nevertheless there is a transition region between perturbative QCD and high density QCD where some aspects of the aforementioned dense system of gluons can be studied and this transition region is likely to analyse through perturbative approach. The linear QCD evolution equations, such as the DGLAP [56-58] and the Balitsky-Fadin-Kuraev-Lipatov (BFKL) [59-61], are therefore expected to breakdown in the kinematic region of very small-x where the gluon recombination processes give rise to nonlinear corrections. A comprehensive study of this region was first performed by Gribov, Levin and Ryskin, and by Mueller and Qiu (GLR-MQ) in their pioneering papers [42, 43] and they suggested that the higher twist phenomena of gluon recombination or shadowing corrections could be expressed in a new evolution equation which is nonlinear in gluon density. This nonlinear evolution equation is nowadays referred to as the GLR-MQ equation. In the recent years various alternative nonlinear evolution equations admissible at high gluon densities have been derived and analysed widely and subsequently the structure functions from DIS or more particularly the PDFs have been investigated in the framework of saturation models. These are the Modified-DGLAP (MD-DGLAP) [62], Balitsky-Kovchegov (BK) [63, 64], Modified-BFKL (MD-BFKL) [65] and Jalilian-Marian-Iancu-McLerran-Weigert-Leonidov-Kovner (JIMWLK) [66, 67]. We present a brief account of these linear and nonlinear QCD evolution equations in Chapter 2 of this thesis.

The picture of high gluon density in QCD can be quantitatively executed by a

crucial parameter [55]

$$\widetilde{W} = \frac{\alpha_s(Q^2)}{Q^2}\rho(x, Q^2), \tag{1.14}$$

which represents the probability of gluon recombination throughout the cascade. Here $\rho = \frac{xg(x,Q^2)}{\pi R^2}$ is the the density of gluons in the transverse plane, $xg(x, Q^2)$ number of gluons per unit of rapidity ($Y = \ln(1/x)$) which interacts with the probe and $\alpha_s/Q^2 \sim \sigma_{gg\to g}$ represents the cross section of gluon-gluon interaction. This parameter controls the precision of calculations involving gluon-gluon interactions. The unitarity constraint on physical cross sections can be expressed as $\widetilde{W} \leq 1$ [55]. In the region of x and Q^2 where $\widetilde{W} << 1$, the interaction of gluons is negligible and we may proceed with the evolution equations linear in gluon density. However, at small-x the gluon density becomes so large that $\widetilde{W}$ can become appreciable in which case higher twist effects of gluon-gluon interactions can no longer be ignored and in that case the evolution is governed by the nonlinear evolution equations. The correlation radius of two interacting gluons is characterized by R and its value depends on how the gluons ladders couple to different partons. If the gluons originate from sources which occupy distinct regions in longitudinal coordinate space then R is of the order of proton radius, i.e. $R = 5$ GeV^{-1} [42]. In that case recombination probability is very negligible. On the other hand, if the gluon ladders couple to the same quark or gluon then the gluons are expected to be concentrated in small areas inside the proton, the so-called hot-spots [43, 68]. Such hot spots of high gluon density can enumerate the rapid onset of gluon-gluon interactions in the environs of the emitting parton and so uplift the recombination effect or shadowing corrections. In such hot spots R is considered to be of the order of the transverse size of a valence quark, i.e. $R = 2$ GeV^{-1}.

Gluon saturation as well as the high parton density regime within hadronic and nuclear wave functions at small-x are properly described in the effective theory of Color Glass Condensate (CGC) [69-71] and related formalisms. It is predicted by the theorists that, when Q_s^2 is large the interactions among the individual gluons are feeble but they jointly form a very strong coherent classical color field analogous to Bose-Einstein condensates and glassy materials, and is therefore marked as the CGC. The CGC is expected to be the universal restrain for the constituents of a comprehensible hadron wave function which is, as a whole, high density of gluons

and for resolving momenta below the saturation scale.

As a general comment, we note that exploring the dynamics of the high density QCD at small-x is one of the current most demanding problems in high energy physics and there has been significant breakthrough formulated to comprehend gluon recombination or shadowing. Numerous theoretical and phenomenological endeavours have been done in the recent years to investigate the saturation phenomena based on perturbative QCD [72-79].

1.6 Experiments and parametrizations

1.6.1 Experiments

The structure functions measurements have been accomplished by several high energy experiments over the past years. The DIS experiments utilizing charged and neutral lepton beams have steadily enhanced the understanding of the structure functions in recent years. The first electron-proton DIS experiments were performed at SLAC in 1968 in California [80]. Following this the progress of the E26 [81], CHIO [82], Bologna-CERN-Dubna-Munich-Saclay (BCDMS) [83], European Muon Collaboration (EMC) [84], New Muon Collaboration (NMC) [85] and E665 [86] muon scattering experiments at Fermilab and CERN, and the HERA [27-30, 87] at DESY have been established in the past years. These muon scattering experiments were improved by a course of high energy neutrino scattering experiments as well at Fermilab and CERN. The most recent high energy experiments of p-p collisions are the Large Hadron Collider (LHC) [88, 89] which is the latest addition to CERN's accelerator complex. The LHC is the biggest and most complicated experimental facilities ever constructed and is likely to confront some of the unanswered queries of physics, promoting knowledge of physical laws. A brief account of some of these experiments are given below.

SLAC

The SLAC experiments were fixed target experiments operated during the time period from 1968 to 1985 using 21 GeV electrons scattered off hydrogen and deuterium targets. The first DIS experiments exploring the proton structure were performed at SLAC in 1968. The SLAC measurements [80] covered a kinematic range

$0.06 \leq x \leq 0.9$ and $0.6 \leq Q^2 \leq 30$ GeV^2. The overall normalization error of the experiments is about 2.1%. The structure function F_2 was obtained using R_{SLAC}, where R is the ratio of the longitudinally polarized virtual photon absorption cross section to that of transversely polarized.

BCDMS

The BCDMS experiment (NA4) at CERN ran parallel to EMC from 1978 up to 1985 and included a DIS of muons on a hydrogen target using beams of 100, 120, 200 and 280 GeV. The the kinematic range covered in these measurements is [83] $0.06 \leq x \leq 0.8$ and $7 \leq Q^2 \leq 260$ GeV^2. The structure function F_2 was extracted using R_{QCD} and an overall normalization error is around 3% was reported.

EMC

The EMC experiment (NA28) at CERN was performed using a beam of 280 GeV muons on a deuterium as well as heavier elements target. The kinematic range $0.0025 \leq x \leq 0.14$ and $0.25 \leq Q^2 \leq 7.2$ GeV^2 provided a good description of the measurements [84] whereas the rest of their measurements is superseded by the more precise measurements of NMC described below. There is an overall normalization error of 7%. The F_2 structure function was obtained using R_{CHIO} of CHIO collaboration.

NMC

The NMC-NA37 experiment was an extension of the EMC experiment with an upgraded apparatus performed by the new muon collaboration at the M2 muon beam line of the CERN SPS. This experiment measured simultaneously the proton and deuteron differential cross sections using two similar pairs of 3 m long targets exposed off and on to the muon beam and these measurements considerably reduced the uncertainty of the relative normalization between the proton and deuteron structure functions. An overall normalization error of 2% is claimed. An iterative method based on a Monte Carlo simulation of the experiment was applied to determine the structure functions. For each period of data taking individual simulations were performed to allow changes in the beam and the detector to be considered. The values of $F_2(x, Q^2)$ were obtained performing a comparison of the normalized outputs of data

and accepted Monte Carlo events. The structure functions were computed from an initial selection of F_2 and a fixed parametrization of the ratio, $R(x, Q^2)$, obtained from a global analysis of SLAC data [80]. The proton and deuteron structure functions F_2^p and F_2^d were measured in the kinematic range $0.006 < x < 0.6$ and $0.5 < Q^2 < 75$ GeV^2, by inclusive DIS with beams of 90, 120, 200 and 280 GeV muons on hydrogen and deuterium targets [85].

E665

The E665 experiment at Fermilab is a fixed-target muon scattering experiment, with the highest energy of about 490 GeV muon beams. The E665 experiment took data using liquid hydrogen and deuterium targets, as well as heavy targets and measured the structure functions and their ratios as well as investigated the hadronic final states produced in the muon interaction. The F_2 measurements are reported in the kinematic range $8.9 \times 10^{-4} \leq x \leq 0.39$ and $0.2 \leq Q^2 \leq 75$ GeV^2 [86]. The overall normalization error is of 1.8%. There is a significant overlap in x and Q^2 of the E665 measurements with those of NMC and the two measurements are accorded well in the region of overlap. The E665 data being at lower Q^2 at fixed x, these measurements overlap in x with the HERA data as well. Like NMC, the E665 analysis of F_2 also use the parametrization of R obtained from a global analysis of SLAC data [80].

H1 and ZEUS

H1 and ZEUS are the two major experiments at the particular lepton-proton collider HERA, hosted by DESY in Hamburg, Germany to investigate the DIS processes. H1 is an international collaboration involving about 250 scientists from 20 institutes and 12 countries whereas ZEUS collaboration is handled by 450 physicists from 12 countries, forming it a genuinely international scientific collaboration. The outset of operation of the HERA collider provides an important landmark for the measurements of the proton structure. Both the H1 and ZEUS experiments at HERA have measured the inclusive $e^{\pm}p$ NC and CC DIS cross sections. HERA collides 920 GeV protons off 27.5 GeV electrons inducing a large center of mass energy of the collisions $\sqrt{s} \approx 320$ GeV. The maximum value of Q^2 at H1 and ZEUS experiments measures to $90,200$ GeV^2 whereas the calibrated x-range have been remarkably extended to a smaller value of $x \sim 10^{-5}$ [27-30, 87]. The operation of HERA have been carried out

in two stages, HERA-I, from 1992-2000, and HERA-II, from 2002-2007. The utmost precise determination of the proton structure is measured by the H1 and ZEUS collaborations using the HERA-I data. During the HERA-I period, HERA was mostly operating with positrons due to restrictions of the electron beam life time. However this problem has been resolved for HERA-II and during the period from 2004 to 2006 HERA operated with electron beams allowing a more precise measurement of the xF_3 structure function. In the year 2007, HERA performed a series of runs with lowered proton beam energies of 460 and 575 GeV producing data sets essential for the first direct measurement of F_L. The H1-ZEUS combined results [87] have reduced the uncertainties to a large extent compared to the individual experiments and act as a basis for a precise fit of the proton PDFs. In both experiments the structure function F_2 was extracted using R_{QCD}. The kinematic range of the NC data is $6 \times 10^{-7} \leq x \leq 0.65$ and $0.045 \leq Q^2 \leq 30000$ GeV^2, for values of inelasticity y between 0.005 and 0.95. On the other hand, the kinematic range of the CC data is $1.3 \times 10^{-2} \leq x \leq 0.40$ and $300 \leq Q^2 \leq 30000$ GeV^2, for values of y between 0.037 and 0.76. The total uncertainty of the combined data set is 1% for NC scattering in the region $20 < Q^2 < 100$ GeV^2. Even though HERA ended its 15 years of operation in 2007, dynamic analyses of full data sets are continuing and outstanding improvements are being generated.

LHC

The LHC is the world's largest and most powerful particle accelerator, built by CERN in collaboration with over 10,000 scientists and engineers from over 100 countries, as well as hundreds of universities and laboratories. The LHC weighs more than 38,000 tonnes and runs for 27 km in a circular tunnel 100 metres beneath the Swiss-French border at Geneva, Switzerland. The LHC started up on 2008 successfully circulating the proton beams in the main ring of the LHC for the first time, but stopped operating due to a faulty electrical connection. However in 2009 LHC successfully circulated the proton beams with the first reported p-p collisions at the injection energy of 450 GeV per beam. In 2010 two 3.5 TeV proton beams were made to collide, which is a world history for the highest-energy artifial particle collisions. In 2013 LHC went into shutdown and planned to reopen in early 2015 upgrading the

beam energy to 13 TeV, which is almost double its current maximum energy and more than seven times any predecessor collider. As of 2012 data from over 3×10^{14} LHC proton-proton collisions had been analyzed LHC and the LHC Computing Grid, which provide global computing resources to store, distribute and analyse the ~ 30 Petabytes of data annually generated by the LHC, had become the world's largest computing grid. There are seven experiments at the LHC analysing the innumerable particles produced in the accelerator. The biggest of these experiments, A Toroidal LHC Apparatus (ATLAS) and the Compact Muon Solenoid (CMS), use two independently designed general-purpose detectors to explore a vast range, from the search for the Higgs boson to extra dimensions and dark matter. ALICE (A Large Ion Collider Experiment) is a heavy-ion detector on the LHC ring designed to investigate the formation of the quark-gluon plasma. The purpose of LHC beauty (LHCb) experiment is to study the differences between matter and antimatter. The Total Elastic and diffractive cross section Measurement (TOTEM) and LHC forward (LHCf) experiments study forward particles, protons or heavy ions, and focus on physics that cannot be accessed in the general-purpose experiments. The Monopole and Exotics Detector at the LHC (MOEDAL) approved in 2010 uses detectors to search directly for the magnetic monopole. In 2012, the ATLAS and CMS experiments at LHC announced the observation of a new particle in the mass region around 126 GeV [88, 89]. Later the new particle is confirmed to be the Higgs boson [13] which physicists have been looking for since its prediction about 50 years ago. It is one of the greatest discoveries of the present-day and the Nobel Prize in Physics 2013 was undoubtedly awarded jointly to F. Englert and P. W. Higgs for the theoretical prediction of the Higgs mechanism.

1.6.2 Parametrizations

The PDFs are one of the basic ingredients for the calculation of any observable involving hadrons. The evolution of PDFs is a sensitive test of our understanding of QCD dynamics, which is expressed in the form of PDF evolution equations. Precise knowledge of these PDFs is an essential prerequisite for the identification of any possible signature from physics beyond the SM. On the other hand an accurate evaluation of the errors associated with the PDFs is crucial to generate reliable phe-

nomenological predictions at hadronic colliders, such as the LHC. In Recent times, a substantial amount of theoretical and experimental endeavour has been devoted in the accurate determination of the parton distributions of the nucleon. Particular interests are given in the calculation of the uncertainties associated with various experimental and theoretical inputs, for the sake of precise measurement of collider processes as well as determination of QCD parameters. At present, the preeminent inclusive PDF sets are acquired from a global analysis of hard-scattering data from various processes like DIS, DrellYan, weak vector boson production as well as collider jet production. In global analysis the PDFs are determined unfolding the experimentally measurable structure functions in terms of their parton content, by using the QCD factorization and DGLAP evolution equations. Modern PDFs are constantly developed to incorporate looming theoretical improvement and the most recent data from hadronic experiments. There are various groups extracting PDFs from global data analyses. The LHAPDF [90] library provides a merged and simple computing to all the major PDF sets. The following is a brief description of the major PDF sets available.

GRV/GJR

The GRV global parametrization is a dynamically generated PDFs set advocated by M. Gluck, E. Reya and A. Vogt. defined upto NLO in the $\overline{MS}$ scheme. The GRV group systematically analyze hard scattering data within the framework of perturbative QCD and is very successful in predicting the rapid rise of proton structure function F_2 at small-x, observed at HERA. The GRV1992 PDFs include u, d, s, c and b quarks whereas the GRV1994 include only u, d and s quarks. These PDFs are used in the calculations involving heavier quarks, with non-zero quark masses, in the partonic hard scattering cross section. The GRV1998 global parametrization [31] used H1 and ZEUS high precision data and presents an updated, more accurate, version of valence-like dynamical input distributions. The GRV1998 PDFs compute the light-parton distributions, charm and bottom contributions to F_2 and the scale dependence of α_s in NLO and LO. The parton densities and the F_2 structure functions are determined from interpolation networks covering the regions $0.8 < Q^2 < 10^6$ GeV^2 and $10^{-9} < x < 1$. Moreover, perturbatively fixed parameter-free dynam-

ical prognostications for parton distributions are unfolded to the very small-x region, $10^{-8} \leq x \leq 10^{-5}$ [31], enabling fairly decent evaluations of ultra high energy neutrino-nucleon cross section concerning neutrino astronomy. The LO results corresponds to $\Lambda_{LO}^{(N_f=4)}$=175 MeV which leads to the value of $\alpha_s^{LO}(M_Z^2)$=0.125. The resulting LO input distributions at $Q^2 = \mu_{LO}^2 = 0.26$ GeV^2 for gluon is given by $xg(x, Q^2) = 17.47x^{1.6}(1-x)^{3.8}$. On the other hand the NLO results correspond to $\Lambda_{NLO}^{(N_f=4)}$=246 MeV giving rise to the value of $\alpha_s^{NLO}(M_Z^2)$=0.114. The input distributions have been established employing the 1994 and 1995 HERA F_2^p results [27-30] as well as the fixed target F_2^p data of SLAC, BCDMS, NMC and E665.

The GJR parametrization [32], recommended by M. Gluck, P. Jimenez-Delgado and E. Reya, is the upgraded version of GRV1998 parton distributions. The GJR dynamical distributions generated the small-x ($x \leq 10^{-2}$) structure of dynamical parton distributions from valence-like initial distributions considered at input scale $Q_0 < 1$ GeV. It provides assurance in the trustworthy prediction of the cross sections for heavy quark, $W^{\pm}$, Z_0, and high p_t jet production at the the hadron colliders such as Tevatron and LHC. On the other hand, in the JR09 parametrization [91] the previous LO and NLO global fit analyses for the dynamical parton distributions of the nucleon are extended to NNLO of perturbative QCD utilizing the DIS structure function measurements as well as the hadronic Drell-Yan dilepton production data.

MRST/MSTW

The MRST is a global analysis of parton distributions of the proton recommended by A. D. Martin, R. G. Roberts, W. J. Stirling and Robert Thorne in the $\overline{MS}$ renormalization scheme. MRST2001 PDFs [33] execute a global parton analysis up to NNLO incorporating all the convenient explicit data from DIS and similar hard scattering processes viz. H1, ZEUS, BCDMS, NMC, E665, SLAC and CCFR. This PDFs set is ordinarily suitable to DIS data with $Q^2 > 2$ GeV^2 and $W^2 > 10$ GeV^2, however it concedes the HERA data for Q^2 down to 1.5 GeV^2 to cover the very small-x calculations of F_2. The initial parametrization of the gluon for LO is $xg = 3.08x^{0.10}(1-x)^{6.49}(1-2.96x^{0.5}+9.26x)$, for $\alpha_s(M_Z^2)$=0.130 and $\Lambda_{\overline{MS}}(N_f=4)$=220 MeV [33]. The best global NLO fit is achieved with the initial distribution of the gluon at Q_0^2= 1 GeV^2 and it complements to $\alpha_s(M_Z^2)$=0.119, i.e. $\Lambda_{\overline{MS}}(N_f=4) = 323$ MeV.

These data sets permits the developement of negative input gluon parametrization at small-x. The optimum global NNLO fit is acquired considering the input distribution of the gluon at Q_0^2=1 GeV^2 conforming to $\alpha_s(M_Z^2) = 0.1155$, i.e. $\Lambda_{\overline{MS}}(N_f = 4) = 235$ MeV. The MRST2004 parton sets [34] provide an additional physical parametrization of the gluon distribution for global parton analysis at both NLO and NNLO thereby producing an improved illustration of the W and Z production cross sections at the Tevatron and the LHC in contrast to the earlier set. The complete kinematic domain covered by this PDF sets, where fixed-order DGLAP analysis is convenient, including the corresponding sets of traditional partons, is found to be $W^2 > 15$ GeV^2, $Q^2 > 10$ GeV^2 and $x > 0.005$ at NLO, whereas at NNLO it is given by $W^2 > 15$ GeV^2, $Q^2 > 7$ GeV^2 and $x > 0.005$.

The MSTW2008 [35] is an updated LO, NLO and NNLO PDFs calculated from global analysis of hard scattering data in the $\overline{MS}$ scheme. The MSTW2008 global analysis supersedes all the previous MRST sets and is very convenient in forecasting the accuracy of cross sections and related theoretical calculations of W and Z bosons, Higgs boson and inclusive jet production at the Tevatron and uncertainties at the LHC. This PDFs fit include CCFR/NuTeV di-muon cross sections and Tevatron Run II data on inclusive jet production. Together with α_s there are 30 free PDF parameters in the fit. The MSTW analysis, fits ~ 2700 data points as a whole and the comprehensive nature of the NLO and NNLO fits is identical and perfectly admissible, with $\chi^2/N_{pts} \sim 1$ for nearly all data sets [35]. This fit furthermore determines the uncertainty on the strong coupling α_s, owing to the experimental errors on the data, which is found to be $\alpha_s(M_Z^2) = 0.1202^{+0.0012}_{-0.0015}$ at NLO and $\alpha_s(M_Z^2) = 0.1171^{+0.0014}_{-0.0014}$ at NNLO.

NNPDF

The NNPDF approach is based on the application of neural networks as primary interpolating mechanisms. The neural networks can yield an impartial interpolation which produces the measure for all points, in some ways within a finite range of x and Q^2 where the data sampling is excellent. The NNPDF approach bypasses all the problems present in the usual approach to the determination of the PDFs. These PDF fits determine the probability density in the arena of structure functions for the

proton, deuteron and nonsinglet structure functions calculated from experimental data of the NMC, BCDMS, E665, ZEUS and H1 collaborations. Their results adopt the form of a set of 1000 neural nets, each providing a calculation of F_2 for given x and Q^2. The central value and the statistical moments of the structure functions determined in the NNPDF fit can be computed out of the 1000 nets in accordance with the standard Monte Carlo techniques. NNPDF1.0 [36] is a set of parton distributions of the nucleon, at NLO, from a global set of DIS data employed to estimate the standard W and Z cross sections at the LHC. Including the recent neutrino dimuon production data in combination with a global deep inelastic parton fit, the NNPDF1.2 parton set is constructed and it provides a determination of the strange and antistrange distributions of the nucleon. Apart from being a transitional step towards a fully global fit including hadronic data, this set ia an interesting test of the NNPDF methodology and for the determination of electroweak parameters.

NNPDF2.0 [37] global set of PDFs include DIS with the combined HERA-I dataset, fixed target Drell-Yan production, collider weak boson production and inclusive jet production. It also determines the impact of recent high luminosity D0 Run II lepton asymmetry data and the D0 inclusive muon and electron data. These PDFs sets are very advantageous to the experimentalists in all kinds of circumstances, for example, examining the accuracy of preliminary datasets and their uncertainties, evaluating the validity of viable evidences of new physics, or in improving the design of new experiments using pseudo data. This fit is upgraded to NNPDF2.1 set to including the heavy quark mass effects. These data sets take care of the small-x gluon and are sensitive to the value of the charm mass m_c as well.

HERAPDF

The HERAPDF project determines the quark and gluon distribution functions of the proton from experimental data and has established a statistical combination procedure enhancing the estimation of the average of H1 and ZEUS measurements in a model independent way. The HERAPDF analysis also elucidates the correlated systematic ambiguities enabling cross calibration to lessen the total systematic uncertainty on the combined data. Thereupon the averaged data are utilized in a QCD fit to determine the proton PDFs with an exhaustive interpretation of the experimental

and theoretical uncertainties. HERAPDF0.1 [38] set is a NLO QCD analysis of parton distributions and covers the combined data set of the inclusive deep inelastic cross sections measured by the H1 and ZEUS Collaborations in NC and CC unpolarised $e^{\pm}p$ scattering at HERA. In this analysis the PDFs are parametrized at the starting scale of $Q_0^2 = 4$ GeV^2 and are evolved using the DGLAP evolution equations.The HERAPDF1.0 [39, 92] analysis employs a uniform data set with small associated systematic uncertainties and applies the conventional χ^2 tolerance, $\Delta\chi^2 = 1$ to determine the experimental uncertainties on the PDFs. On account of the precision of the combined data set, the total uncertainties of the HERAPDF1.0 parametrization is of the order of a few percent at small-x, which is much improved compared to the earlier extractions of the PDFs using the individual H1 or ZEUS data. The gluon distribution functions are parametrized by the universal form $xg(x) = A_g x^{B_g}(1-x)^{C_g}$ at the input scale $Q_0^2 = 1.9$ GeV^2, so that $Q_0^2 < m_c^2$ [38]. A_g is the normalization parameter, B_g represents the small-x behaviour whereas C_g represents the high-x behaviour.

The HERAPDF1.0 set has been amended to HERAPDF1.5 by incorporating initial all-inclusive cross section data from HERA-II running. On the other hand the HERAPDF1.6 analysis involves the H1 and ZEUS jet data whereas HERAPDF1.7 fit comprises of all the data sets from HERA-I and II, charm data, low energy data and jet data. Moreover the NLO fits have been continued to NNLO for both HERAPDF1.0 and HERAPDF1.5 [39, 92]. The HERAPDF1.0 NNLO parton set was introduced in 2010 but this has been upgraded to HERAPDF1.5NNLO fit which has an essentially vigorous high-x gluon and provides thorough description of the experimental, model and parametrization uncertainties. The prescribed value for $\alpha_s(M_Z)$ at NNLO is $\alpha_s(M_Z) = 0.1176$ [39]. These HERAPDFs have been affluently encountered both the Tevatron and LHC data on W, Z and jet production.

CTEQ

The CTEQ global QCD analyses of PDFs have been developed over decades. The CTEQ series include CTEQ1, CTEQ2, CTEQ3, CTEQ4, CTEQ5 presented during the period from 1993 to 2000, followed by sets of CTEQ6 published in the period from 2002 to 2006 as well as the ensuing PDF sets CT09 [40, 93-95]. Recently in 2010

CTEQ group presented NLO PDFs named as CT10 and CT10W [40]. These two new PDF sets are built on the contemporary knowledge of the PDFs obtained from global hadronic experiments, mainly the DIS combined data set of HERA-1 cross sections, which supersedes 11 separate HERA-1 data sets, considered in CTEQ6.6 and preceding fits. These PDFs sets have been used in a broad way in phenomenological predictions for the Tevatron, LHC, and other experiments. The CT10 global QCD fits involve a combination of DIS cross sections by the H1 and ZEUS collaborations in HERA-1, measurements of the charge asymmetry of leptons from W boson, Z rapidity distributions, single-inclusive jet cross sections by CDF as well as DØ collaborations at the Tevatron. The CT10 PDFs are derived at NLO in α_s, incorporating the general-mass analysis of charm and bottom quark contributions to hadronic observables. The CT10 NLO QCD analysis is in general compatible with the HERA experiments in the region $Q > 2$ GeV. The net consistency of the CT10 fit with the combined H1 data is somewhat poor than with the separate H1 data sets, due to some increase in $\chi^2/d.o.f.$ for the NC DIS data at $x < 0.001$ and $x > 0.1$ [40]. Both CT10 and CT10W PDF sets contain 26 independent parameters and thus there are 26 eigenvector directions and a total of 52 error sets. These PDF error sets, together with the following α_s error sets, admit a thorough computation of the combined PDF+α_s uncertainties for any observable. Both CT10 and CT10W predict a minor PDF inspired uncertainty in the total cross section for the top-quark pair production at the Tevatron Run-II in contrast to the CTEQ6.6 prediction. The difference between the CT10 and CT10W PDF sets for LHC predictions is very negligible, other than in those observables that are responsive to the ratio of down-quark to up-quark PDFs.

The CT10NNLO [41] global PDF fit is the NNLO analysis of the PDFs recently published by the CTEQ group. It includes basically the same global data sets used in the CT10 and CT10W NLO PDF fits excluding the Tevatron Run-1 inclusive jet data and a subset of the Tevatron Run-2 lepton charged asymmetry data from W boson decays. This fit produces numerous predictions at NNLO precision for both current and upcoming precision measurements from the LHC at CERN. It further analyzes the extent of variations in the gluon distributions initiated by corresponding systematic effects in inclusive jet production.

1.7 Outline of the thesis

This thesis is concerned with the linear DGLAP and nonlinear GLR-MQ evolution equations in the small-x kinematical region and the saturation of gluon density at very small-x due to nonlinear or shadowing corrections to the QCD evolution at very small-x. We present a review of different QCD evolution equations both linear and nonlinear in Chapter 2. Part I of this thesis details the study of the linear DGLAP equation. In chapter 3 we report the semi-numerical solution of the DGLAP equation in the small-x limit for singlet structure functions at LO, NLO and NNLO. The Q^2 and x-dependence of the singlet structure functions have been examined from these solutions and the results are compared with different experimental data and parametrizations. Following this in chapter 4 we extend the study for gluon distribution function by solving the linear DGLAP equation for gluon distribution analytically. The Q^2 and x-dependence of the gluon distribution functions have been obtained upto NNLO.

In part II we turn our attention to the gluon recombination processes which lead to nonlinear corrections to the linear DGLAP evolution equations due to multiple gluon interactions at very small-x. We estimate the importance of the corrections of these higher order QCD effects, which suppress or shadow and eventually saturate the growth of the parton densities in the framework of nonlinear GLR-MQ evolution equation. We solve this equation for both singlet structure and gluon distribution functions in the vicinity of saturation employing the well-known Regge-like ansatz. In chapter 5 we make a deliberate attempt to explore the effect of shadowing corrections to the behaviour of gluon distribution function in the kinematic region of small-x and Q^2 using the nonlinear GLRMQ evolution equation with the shadowing term incorporated. Our predictions are compared with those obtained by the global QCD fits to the parton distribution functions. Moreover we estimate the effect of nonlinearity in our predictions by comparing the results obtained from nonlinear GLR-MQ equation with those obtained from linear DGLAP equation. Chapter 6 is devoted to the study of the singlet structure function with nonlinear or shadowing corrections in the small-x region based on GLR-MQ equation. The obtained results are compared with different experimental data and parametrizations. A comparative study of our results of nonlinear gluon density with those of other nonlinear equations

is accomplished in chapter 7.

Finally, in chapter 8 we give a brief summary and an outlook for future work.

Bibliography

[1] Ball P., *The Elements: A Very short introduction*, Oxford University Press, Oxford, 2004.

[2] Gell-Mann, M. A schematic model of baryons and mesons, *Phys. Lett.* **8**(3), 214 −− 215, 1964.

[3] Zweig, G. An SU(3) Model for strong interaction symmetry and its breaking: II, *CERN Report* **8419/TH.412**, 1964.

[4] Feynman, R. P. *Photon-hadron interactions*, Addison-Wesley Pub. Co.,Boston, 1972.

[5] Aaij, R., et al. Observation of the resonant character of the $Z(4430)^-$ State, *Phys. Rev. Lett.* **112**(22), 222002, 2014.

[6] Oerter, R. *The theory of almost everything: The standard model, the unsung triumph of modern physics*, Kindle ed., Penguin Group., USA, 2006.

[7] Glashow, S.L. Partial-symmetries of weak interactions, *Nucl. Phys.* **22**(4), 579−−588, 1961.

[8] Weinberg, S. A model of Leptons, *Phys. Rev. Lett.*, **19**(21), 1264−−1266, 1967.

[9] Salam, A. Weak and electromagnetic interactions -in elementary particle theory: relativistic groups and analyticity, Proceedings of the eighth Nobel symposium, N. Svartholm, ed. Almqvist & Wiksell, 367-377 (1968).

[10] Arnison, G. et al., Experimental observation of isolated large transverse energy electrons with associated missing energy at $s = 540$ GeV *Phys. Lett. B* **122**(1), 103−−116, 1983.

[11] Abe, F. et al., Observation of top quark production in $p\bar{p}$ collisions with the Collider Detector at Fermilab *Phys. Rev. Lett.* **74**(14), 2626−−2631, 1995.

[12] Kodama, K. et al., Observation of tau neutrino interactions, *Phys. Lett. B* **504**(3,) 218−−224, 2001.

[13] Cho, A. Higgs boson makes its debut after decades-long search, *Science* **337**(6091), 141−−143, 2012.

[14] Accardi, A. et al., Electron Ion Collider: The next QCD frontier - Understanding the glue that binds us all, *arXiv:1212.1701v3* [nucl-ex].

[15] Gross, D. J. and Wilczek, F. Asymptotically free gauge theories. 1, *Phys. Rev. D* **8**(10), 3633, 1973.

[16] Gross D. J. and Wilczek, F. Asymptotically free gauge theories. 2, *Phys. Rev. D* **9**(4), 980, 1974.

[17] Politzer, H. D. Asymptotic Freedom: An approach to strong interactions, *Phys. Rept.* **14**(4), 129, 1974.

[18] Halzen, F. and Martin, A. D. *Quarks and Leptons: An Introductory course in modern particle Physics*, John Wiley and Sons, Canada, 1984.

[19] Fritzsch, H., Gell-Mann, M. and Leutwyler, H. Advantages of the color octet gluon picture, *Phys. Lett. B* **47**(4), 365−−368, 1973.

[20] Prosperi, G. M., Raciti, M. and Simolo, C. On the running coupling constant in QCD, Prog. Part., *Nucl. Phys.* **58**(2), 387−−438, 2007.

[21] Feynman, R. P. Very high-energy collisions of hadrons, *Phys. Rev. Lett.* **23**(24), 1415−−1417, 1969.

[22] Bjorken, J. D. and Paschos, E. A. Inelastic electron-proton and γ-proton scattering and the structure of the nucleon, *Phys. Rev.* **185**(5), 1975−−1982, 1969.

[23] Abelleira Fernandez, J. L. et al., A Large Hadron Electron Collider at CERN: Report on the physics and design concepts for machine and detector, *J.Phys. G: Nucl. Part. Phys.* **39**(7), 075001, 2012.

[24] Bjorken, J.D. Asymptotic sum rules at infinite momentum, *Phys. Rev.* **179**(5), 1547−−553, 1969.

[25] Abbott, L. F., Atwood, W. B. and Michael Barnett, R. Quantum-chromodynamic analysis of eN deep-inelastic scattering data, *Phys. Rev. D* **22**(3), 582−−594, 1980.

[26] Adler, S. L. and Tung, W. Breakdown of Asymptotic sum rules in perturbation theory, *Phys. Rev. Lett.* **22**(18), 978−−981, 1969.

[27] Adloff, C. et al., On the rise of the proton structure function F_2 towards low x, *Phys. Lett. B* **520** (3-4), 183−−190, 2001.

[28] Adloff, C. et al., Measurement and QCD analysis of neutral and charged current cross sections at HERA, *Eur. Phys. J. C* **30**(1), 1−−32, 2003.

[29] Breitweg, J. et al., Measurement of the proton structure function F_2 and $\sigma_{tot}^{\gamma p}$ at low Q^2 and very low x at HERA, *Phys. Lett. B* **407**(3-4), 432−−448, 1997.

[30] Chekanov, S. et al., High-Q^2 neutral current cross sections in e^+p deep inelastic scattering at $\sqrt{s} = 318$ GeV, *Phys. Rev. D* **70**(5), 052001, 2004.

[31] Gluck, M., Reya, E. and Vogt, A. Dynamical parton distributions revisited, *Eur. Phys. J. C* **5**(461), 470, 1998.

[32] Gluck, M. Jimenez-Delgado, P. and Reya, E. Dynamical parton distributions of the nucleon and very small-x physics, *Eur. Phys. J. C* **53**(3), 355−−366, 2008.

[33] Martin, A.D. et al., NNLO global parton analysis, *Phys. Lett. B* **531**(3-4), 216−−224, 2002.

[34] Martin, A.D. et al., Physical gluons and high-E_T jets, *Phys. Lett. B* **604**(1-2), 61−−68, 2004.

[35] Martin, A.D. et al., Parton distributions for the LHC, *Eur.Phys.J. C* **63**(2), 189−−285, 2009.

[36] Ball, R. D. et al., A determination of parton distributions with faithful uncertainty estimation, *Nucl. Phys. B* **809**(1-2), 1−−63, 2009.

[37] Ball, Richard D. A first unbiased global NLO determination of parton distributions and their uncertainties, *Nucl. Phys. B* **838**(12), 136−−206, 2010.

[38] Kretzschmar, J. Proton structure measurements and the HERAPDF fit, *arXiv:0906.1108* [hep-ex].

[39] Cooper-Sarkar, A. PDF Fits at HERA, *arXiv:1112.2107* [hep-ph].

[40] Lai, H-L. et al., New parton distributions for collider physics, *Phys. Rev. D* **82**(7), 074024, 2010.

[41] Gao, J. et al., CT10 next-to-next-to-leading order global analysis of QCD, *Phys. Rev. D* **89**(3), 033009, 2014.

[42] Gribov, L. N., Levin, E. M. and Ryskin, M. G. Semihard processes in QCD, *Phys. Rep.* **100**(1-2), 1−−150, 1983.

[43] Mueller, A.H. and Qiu, J. Gluon recombination and shadowing at small values of x, *Nucl. Phys. B* **268**(2), 427−−452, 1986.

[44] Kwiecinski, J. Theoretical issues of small x physics, *J. Phys. G: Nucl. Part. Phys.* **22**(6), 685−−702, 1996.

[45] Froissart, M. Asymptotic behavior and subtractions in the Mandelstam representation, *Phys. Rev.* **123**(3), 1053−−1057, 1961.

[46] Martin, A. Unitarity and high-energy behavior of scattering amplitudes, *Phys. Rev.* **129**(3), 1432−−1436, 1963.

[47] Laenen, E. and Levin, E. A new evolution equation, *Nucl. Phys. B* **451**(1-2), 207−−230, 1995.

[48] Iancu, E. and McLerran, L. Saturation and universality in QCD at small x, *Phys.Lett. B* **510**(1-4), 145−−154, 2001.

[49] Collins, J. and Kwiecinski, J. Shadowing in gluon distributions in the small-x region, *Nucl. Phys. B.* **335**(1), 1−−260, 1990.

[50] Levin, E., CGC, QCD, Saturation and RHIC data (Kharzeev-Levin-McLerran-Nardi point of view), *Journal of Physics: Conference Series* **5**(1), 127−−147, 2005.

[51] Stasto, A. M., Golec-Biernat, K. and Kwieciski, J. Geometric scaling for the Total $\gamma^* p$ Cross Section in the Low x Region, *Phys. Rev. Lett.* **86**(4), 596, 2001.

[52] McLerran, L. and Praszalowicz, M. Saturation and scaling of multiplicity, mean p_T and p_T distributions from 200 GeV $\leq \sqrt{s} \leq$ 7 TeV, *Acta Phys. Pol. B* **41**(8), 1917−−1926, 2010.

[53] Mueller, A.H. Small-x behavior and parton saturation: A QCD model, *Nucl. Phys. B* **335**(1), 115−−137, 1990.

[54] Bartels, J. Parton evolution and saturation in deep inelastic scattering, *Eur. Phys. J. C* **43**(1-4), 3−−7, 2005.

[55] Laenen, E. and Levin, E. Parton densities at high energy, *Annu. Rev. Nucl. Part. Sci.* **44**, 199−−246, 1994.

[56] Gribov, V.N. and Lipatov, L.N. Deep inelastic $e-p$ scattering in perturbation theory, *Sov. J. Nucl. Phys.* **15**(4), 438−−450, 1972.

[57] Dokshitzer, Y.L. Calculation of structure functions of deep-inelastic scattering and e^+e^- annihilation by perturbation theory in quantum chromodynamics, *Sov. Phys. JETP* **46**(4), 641−−652, 1977.

[58] Altarelli, G. and Parisi, G. Asymptotic freedom in parton language, *Nucl. Phys. B* **126**(2), 298−−318, 1977.

[59] Lipatov, L.N. Reggeization of the vector meson and the vacuum singularity in Nonabelian Gauge Theories, *Sov. J. Nucl. Phys.* **23**, 338−−345, 1976.

[60] Kuraev, E. A., Lipatov, L. N. and Fadin, V. S. The pomeranchuk singularity in nonabelian gauge theories, *Sov. Phys. JETP* **45** (2), 199−−204, 1977.

[61] Balitsky, I.I. and Lipatov, L.N. The pomeranchuk singularity in quantum chromodynamics, *Sov. J. Nucl. Phys.* **28**, 822−−829, 1978.

[62] Zhu, W. A new approach to parton recombination in the QCD evolution equations, *Nucl. Phys. B* **551**(1-2), 245−−274, 1999.

[63] Balitsky, I. Operator expansion for high-energy scattering, *Nucl. Phys. B* **463**(1), 99−−157, 1996.

[64] Kovchegov, Y. V. Small-x F_2 structure function of a nucleus including multiple Pomeron exchanges, *Phys. Rev. D* **60**(3), 034008, 1999.

[65] Zhu, W., Shen, Z. and Ruan, J. A new perspective on gluon distribution at small x, *arXiv:hep-ph/0703309v4*, 2008

[66] Jalilian-Marian, J. et al., The intrinsic glue distribution at very small x, *Phys. Rev. D* **55**(9), 5414−−5428, 1997.

[67] Jalilian-Marian J. et al., The Wilson renormalization group for low x physics: towards the high density regime, *Phys. Rev. D* **59**(1), 014014, 1999.

[68] Levin, E. M. and Ryskin, M. G. High energy hadron collisions in QCD, *Phys. Rep.* **189**(6), 268−−382, 1990.

[69] Iancu, E., Leonidov, A. and McLerran, L. Nonlinear gluon evolution in the color glass condensate: I, *Nucl. Phys. A* **692**(3-4), 583−−645, 2001.

[70] Ferreiro, E. et al., Nonlinear gluon evolution in the color glass condensate: II, *Nucl. Phys. A* **703**(12), 489−−538, 2002.

[71] Gelis, F. et al., The Color Glass Condensate, *Ann. Rev. Nucl. Part. Sci.* **60**, 463−−489, 2010.

[72] Kharzeev, D., Levin, E. and McLerran, L. Parton saturation and N_{part} scaling of semi-hard processes in QCD, *Phys. Lett. B* **561**(12), 93−−101, 2003.

[73] Zhu, W. et al., Contributions of gluon recombination to saturation phenomena, *Phys. Rev. D* **68**(9), 094015:1-11, 2003.

[74] Iancu, E., Itakura, K. and Munier, S. Saturation and BFKL dynamics in the HERA data at small-x, *Phys. Lett. B* **590**(34), 199−−208, 2004.

[75] Levin, E. and Rezaeian, A. H. Gluon saturation and inclusive hadron production at LHC, *Phys. Rev. D* **82**(1), 014022, 2010.

[76] Blaizot, J.P. The status of parton saturation and the CGC, *Nucl. Phys. A* **854**(1), 237−−256, 2011.

[77] Kormilitzin, A., Levin, E. and Miller, J. S. High density QCD and nucleus-nucleus scattering deeply in the saturation region, *Nucl. Phys. A* **859**(1), 87−−113, 2011.

[78] Xiao, B. The search for gluon saturation in pA collisions, *Nucl. Phys. A* **932**, 380−−386, 2014.

[79] Beuf, G. Gluon saturation beyond (naive) leading logs, *Nucl. Phys. A* **932**, 75−−80, 2014.

[80] Whitlow, L. W. et al., Precise measurements of the proton and deuteron structure functions from a global analysis of the SLAC deep inelastic electron scattering cross sections, *Phys. Lett. B* **282**(3-4), 475−−482, 1992.

[81] Chang, C. et al., Observed deviations from scale invariance in high-energy muon scattering, *Phys. Rev. Lett.* **35**(14), 901−−904, 1975.

[82] Gordon, B. A. et al., Measurement of the nucleon structure functions, *Phys. Rev. D* **20**(11), 2645−−2691, 1979.

[83] Benvenuti, A. C. et al., A high statistics measurement of the deuteron structure functions $F_2(x, Q^2)$ and R from deep inelastic muon scattering at high Q^2, *Phys. Lett. B* **237**(3-4), 592−−598, 1990.

[84] Arneodo, M. et al., Measurements of the nucleon structure function in the range $0.002 \leq x \leq 0.17$ and 0.2 Ge$V^2 \leq$ Q2 $\leq$ 8 GeV^2 in deuterium, carbon and calcium, *Nucl. Phys. B* **333**(1), 1−−47, 1990.

[85] Arneodo, M. et al., Measurement of the proton and the deuteron structure functions, F_2^p and F_2^d, *Phys. Lett. B* **364**(2), 107−−115, 1995.

[86] Adams, M. R. et al., Proton and deuteron structure functions in muon scattering at 470-GeV, *Phys. Rev. D* **54**(5), 3006−−3056, 1996.

[87] Aaron, F.D. et al., Combined measurement and QCD analysis of the inclusive $e^{\pm}p$ scattering cross sections at HERA, *JHEP* **2010**(1), 109:1-55, 2010.

[88] Aad, G. Observation of a new particle in the search for the standard model Higgs boson with the ATLAS detector at the LHC, *Phys. Lett. B* **716**(1), 1−−29, 2012.

[89] Chatrchyan S. et al., Observation of a new boson at a mass of 125 GeV with the CMS experiment at the LHC, *Phys. Lett. B* **716**(1), 30−−61, 2012.

[90] http://projects.hepforge.org/lhapdf/.

[91] Jimenez-Delgado, P. and Reya, E. Dynamical NNLO parton distributions, *Phys. Rev. D* **79**(7), 074023, 2009.

[92] Radescu, Voica. Combination and QCD Analysis of the HERA inclusive cross sections, *arXiv:1308.0374*.

[93] Lai, H. L. et al., Global QCD analysis of parton structure of the nucleon:CTEQ5 parton distributions, *Eur. Phy. J. C* **12**(3), 375−−392, 2000.

[94] Pumplin, J. et al., New generation of parton distributions with uncertainties from global QCD analysis, *JHEP* **2002**(JHEP07:012), 1-46, 2002.

[95] Nadolsky, Pavel M. et al., Implications of CTEQ global analysis for collider observables, *Phys. Rev. D* **78**, 013004, 2008.

Chapter 2

Linear and Nonlinear QCD Evolution Equations

2.1 Linear evolution equations

QCD induces higher order corrections to the naive parton model which eventually lead to a breaking of scaling violations. Thus QCD enables the explicit estimation of the dependence of the structure function on Q^2, however, it does not reveal the specific value of F_2 for a given Q^2, but preferably portrays in what manner F_2 varies with Q^2 from a given input. The Q^2 dependence of the PDFs can be computed perturbatively as long as Q^2 is adequately large so that α_s continues to be small. The standard and the basic theoretical frameworks employed to study the scale dependence of the PDFs and eventually the DIS structure functions are the linear Dokshitzer-Gribov-Lipatov-Altarelli-Parisi (DGLAP) [1-4] evolution equations. One can calculate the PDFs for any value of Q^2 making use of the DGLAP equations considering that an initial condition for the PDFs is indeed available at a given initial scale Q_0^2 and then evolving to higher Q^2. The DGLAP approach sums up higher-order α_s contributions enhanced by the logarithm of photon virtuality, i.e. $\alpha_s^n \ln(Q^2)^n$ in the perturbative expansion. Nevertheless, at small-x contributions enhanced by the logarithm of a small momentum fraction, x, carried by gluons, turns out to be essential. Accordingly a different approach is needed to explain the situation of high-energy or in other words small-x scattering. The leading logarithm (LL) contributions of $(\alpha_s \ln(1/x))^n$ are summed up by the Balitsky-Fadin-Kuraev-Lipatov (BFKL) evolution equation

[5-7]. Another evolution equation to study the linear evolution of PDFs in the small-x regime is the so called Catani-Ciafaloni-Fiorani-Marchesini (CCFM) equation [8-10]. The CCFM approach retains the components of both the DGLAP and BFKL realms in the LL approximation. All the aforementioned evolution equations are linear in parton density which have to be modified in a suitable way to add the higher twist approximations at very small-x. A brief account of the linear evolution equations is given below.

2.1.1 DGLAP equation

The evolution of the structure functions or more precisely the quark and gluon distribution functions with Q^2 can be described by the DGLAP evolution equations [1-4]. These equations sum all leading Feynman diagrams that give rise to the logarithmically enhanced $\ln(Q^2)$ contributions to the cross section in order to neglect any kind of higher twist corrections. The associated perturbative resummation is organized in powers $\alpha_s^n \ln(Q^2)^n$. They are the conventional and the fundamental theoretical frameworks for all of the phenomenological perspectives used to interpret hadron interactions at short distances. The DGLAP equations for quark and gluon density can be written as

$$\frac{\partial}{\partial \ln Q^2}\begin{pmatrix} q_i(x,Q^2) \\ g(x,Q^2) \end{pmatrix} = \frac{\alpha_s(Q^2)}{2\pi}\sum_{i=1}^{2N_f}\int_x^1 \frac{dy}{y}\begin{pmatrix} P_{qq}(\frac{x}{y}) & P_{qg}(\frac{x}{y}) \\ P_{gq}(\frac{x}{y}) & P_{gg}(\frac{x}{y}) \end{pmatrix}\begin{pmatrix} q_i(y,Q^2) \\ g(y,Q^2) \end{pmatrix}, \tag{2.1}$$

where the sum runs over all flavors of quarks and anti-quarks. Here $q_i(x,Q^2)$ stands for quark density whereas $g(x,Q^2)$ represents gluon density. P_{qq}, P_{qg}, P_{gq} and P_{gg} are the splitting functions whose interpretations are graphically displayed in Fig.2.1. The splitting functions are elucidated as the probability for finding a parton (quark or gluon) of type i having momentum fraction x arising from a parton (quark or gluon) j with larger momentum fraction $y > x$. They are independent of the quark flavors and are identical for quarks and antiquarks. The leading order splitting functions are given by [11]

$$P_{qq}^{(0)}(z) = C_F\Big(\frac{1+z^2}{(1-z)_+} + \frac{3}{2}\delta(1-z)\Big),$$

$$P_{qg}^{(0)}(z) = \frac{1}{2}\big(z^2+(1-z)^2\big), \;\; P_{gq}^{(0)}(z) = C_F\Big(\frac{1+(1-z)^2}{z}\Big) \text{ and}$$

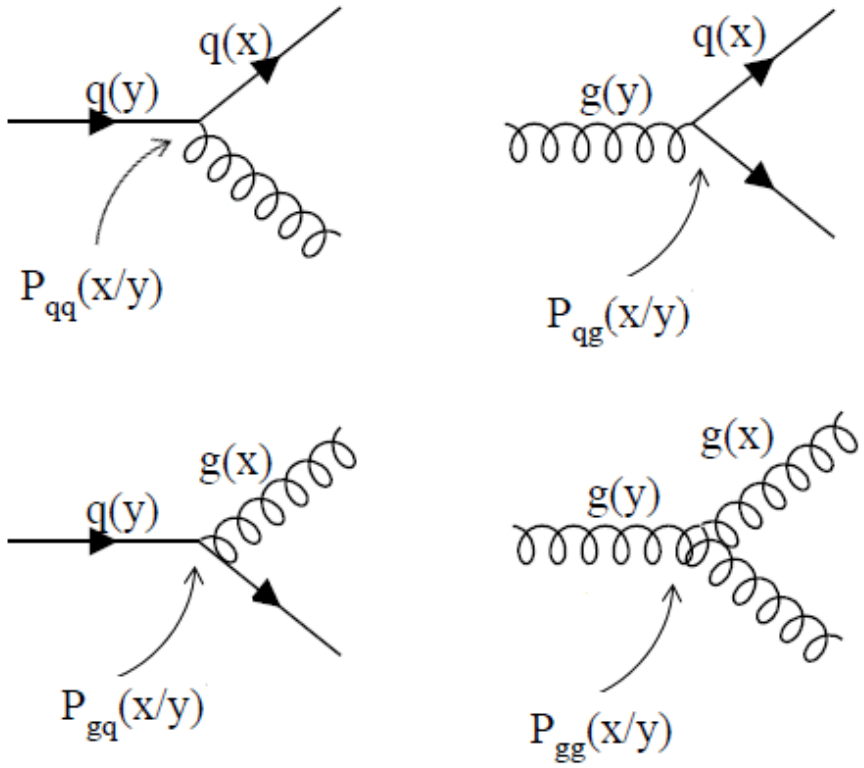

Figure 2.1: Splitting functions

$$P_{gg}^{(0)}(z) = 2N_c\Big(\frac{z}{(1-z)_+} + \frac{1-z}{z} + z(1-z)\Big) + \Big(\frac{11}{2} - \frac{N_f}{3}\Big)\delta(1-z), \tag{2.2}$$

with $C_F = \frac{(N_c^2-1)}{2N_c}$. The "+" distribution is defined by the property [11]

$$\int_0^1 dz \frac{f(z)}{(1-z)_+} = \int_0^1 dz \frac{f(z)-f(1)}{(1-z)}, \tag{2.3}$$

where $(1-z)_+ = 1-z$ for $z < 1$ but is infinite for $z = 1$. The discrepancy at $z = 1$ complements the radiation of soft gluons and is balanced out by the virtual gluon loop contributions.

In perturbation theory, the splitting functions can be expressed as a power series of $\alpha_s(Q^2)$ [11, 12]

$$P_{ab}\big(z, Q^2\big) = P_{ab}^{(0)}(z) + \Big(\frac{\alpha_s(Q^2)}{2\pi}\Big)P_{ab}^{(1)}(z) + \Big(\frac{\alpha_s(Q^2)}{2\pi}\Big)^2 P_{ab}^{(2)}(z) + \cdots, \tag{2.4}$$

with $z = \frac{x}{y}$. These functions are at present working up to next-to-next-to-leading order (NNLO) accuracy. The leading order (LO) expressions $P^{(0)}$ are the well-known Altarelli-Parisi splitting functions [4, 11]. On the other hand, the next-to-leading order (NLO) functions $P^{(1)}$ have been estimated during the time 1977-1980 [13-16], whereas the NNLO terms $P^{(2)}$ are calculated in the period 2004 [17, 18]. The

LO DGLAP evolution sums up the leading log contributions $(\alpha_s \ln(Q^2))^n$, the NLO evolution incorporates the sum of the $\alpha_s(\alpha_s \ln(Q^2))^{n-1}$ terms and so on.

The derivation of the DGLAP equation is founded on the QCD collinear factorization in gluon emission to legitimize the resummation of logarithms in the transverse scale. In consonance with the traditional collinear factorization approach the hadronic observables can be expressed as the convolution of the PDFs with partonic hard-scattering coefficients. The partonic coefficients are computed with the assumption that the hard scattering is originated by a parton collinear to its parent hadron. Customarily the large logarithms are obtained from the region in phase space where

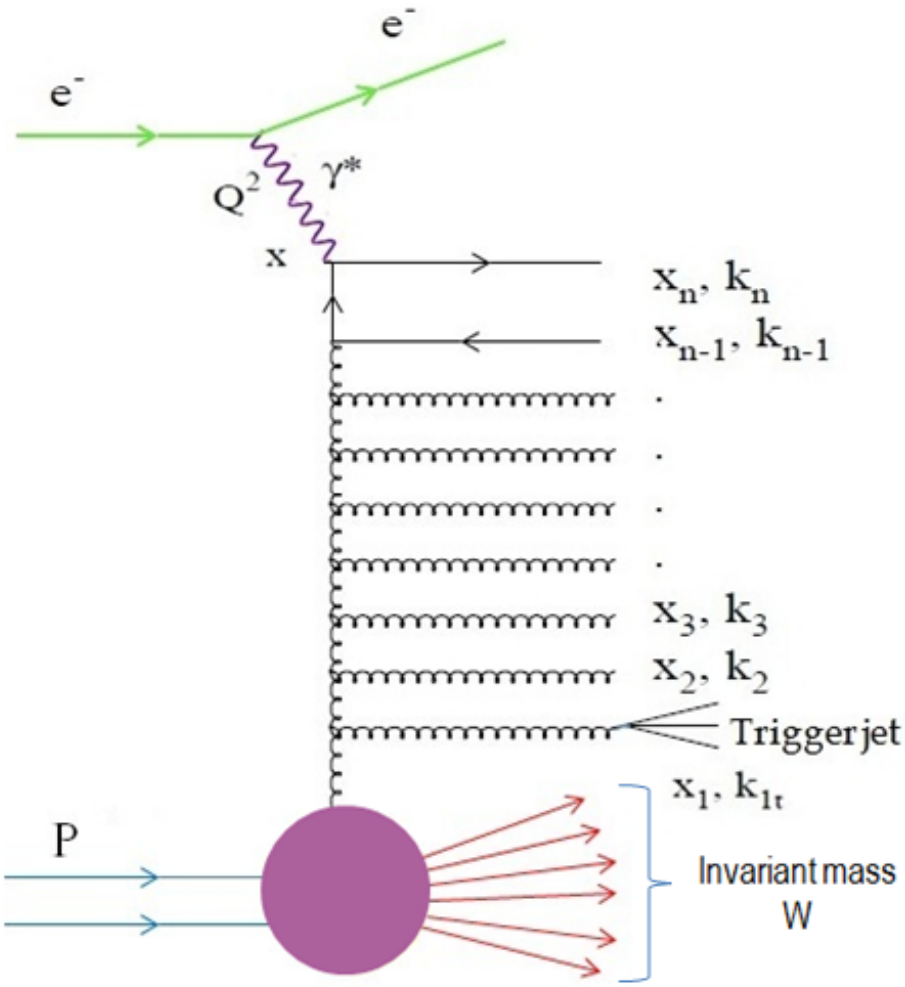

Figure 2.2: Ladder-diagram in LLQ^2 application of DIS

the multiple emissions are strongly set in order in transverse momenta with succeeding emissions having larger momenta, i.e. $Q^2 >> k_n^2 >> \cdots >> k_2^2 >> k_1^2$. Fig.2.2 exhibits a schematic ladder diagram of the quark and gluon emissions in LL(Q^2) application of DIS.

The non-singlet and singlet combinations of the quark flavor group can be defined as [11]

$$q_{NS} \equiv q_i - q_j, \tag{2.5}$$

$$q_S \equiv \sum_i q_i. \tag{2.6}$$

The DGLAP equations for non-singlet and singlet quark distributions are

$$\frac{\partial q_{NS}(x,Q^2)}{\partial \ln Q^2} = \frac{\alpha_s(Q^2)}{2\pi} \int_x^1 \frac{dy}{y} P_{qq}(x/y) q_{NS}(y,Q^2), \tag{2.7}$$

$$\frac{\partial q_S(x,Q^2)}{\partial \ln Q^2} = \frac{\alpha_s(Q^2)}{2\pi} \int_x^1 \frac{dy}{y} \Big(\sum_{i=1}^{2N_f} P_{qq}(x/y) q_i(y,Q^2) + P_{qg}(x/y) g(y,Q^2) \Big). \tag{2.8}$$

As an illustration, the first term of Eq.(2.8) mathematically articulates the fact that a quark with momentum fraction x characterized by $q(x,Q^2)$ (on the left hand side) could have originated form a parent quark with a momentum fraction $y > x$ depicted by $q(y,Q^2)$ (on the right-hand side) which has radiated a gluon. The probability of occurrence of this process is proportional to $\alpha_s P_{qq}(x/y)$. The second term deals with the prospect that a quark with momentum fraction x is the consequence of $q\bar{q}$ pair creation by a parent gluon with momentum fraction $y > x$ and the probability that it happens is proportional to $\alpha_s P_{qg}(x/y)$. The integration appears because of the consideration that the secondary quark with momentum x can come from a parent quark with any momentum fraction $y > x$ [11].

On the other hand, since the gluon distribution does not carry any flavor quantum numbers, it is a flavor singlet and the DGLAP equation for gluon distribution is given by

$$\frac{\partial g(x,Q^2)}{\partial \ln Q^2} = \frac{\alpha_s(Q^2)}{2\pi} \int_x^1 \frac{dy}{y} \Big(\sum_{i=1}^{2N_f} P_{gq}(x/y) q_i(y,Q^2) + P_{gg}(x/y) g(y,Q^2) \Big). \tag{2.9}$$

As soon as the x dependence of quark or gluon distributions are known at some initial scale Q_0^2 then they can be determined for any higher value of Q^2 by using the DGLAP equations. The initial distributions are at present have to be computed from experiment presuming an input form in x which complies with the QCD sum rules. This strategy is adopted in the global analyses of PDFs [19, 20]. As an alternative, one may produce the parton distributions dynamically originating from an input

distribution for the valence quarks and a valence-like input for the sea quarks and gluons [21].

The DGLAP equations neglect higher order contributions of the form $\alpha_s \ln(1/x)$. However, at finite order, the large logarithms in $1/x$ become important in the perturbative expansion at small vales of x, where the evolution is dominated by the gluon cascade and accordingly these leading $\ln(1/x)$ terms have to be resummed. For large-Q^2 this is achieved by the double leading logarithmic approximation (DLLA), which resums the terms that include the leading $\ln(1/x)$ and the leading $\ln(Q^2)$ simultaneously. As a result at small-x one may consider the DLLA of the DGLAP evolution to choose the major contribution to the gluon density growth, analogous to the contribution of the $(\alpha_s \ln(Q^2) \ln(1/x))^n$ terms. The DLLA is valid when $\alpha_s \ln(1/x) \ln(Q^2) \sim 1$ but $\alpha_s \ln(1/x)$ and $\alpha_s \ln(Q^2)$ individually are small. But if Q^2 is not extremely large, then as we move towards smaller values of x the DGLAP equation no longer has its legitimacy. In that case alternative evolution equations, described below, which are appropriate in different regions may be taken into account

2.1.2 BFKL equation

The BFKL equation [5-7] was initially suggested by Balitsky, Fadin, Kuraev, and Lipatov to delineate the high-energy behaviour of processes involving hadrons. Recalling that $x \sim Q^2/s$, where Q^2 is the hard scale of the process and s is c.m.s. energy squared, at small-x, it is essential to sum the terms of the perturbation series enhanced by powers of $\ln(1/x)$. This equation sums up all the leading logarithm contributions of the type $(\alpha_s \ln(1/x))^n$ on the basis of gluon Reggeization. The BFKL approach is usually associated with the evolution equation for the unintegrated gluon distribution, $f(x, k_t)$, which depends on two independent variables, the proton momentum fraction x carried by a gluon and its transverse momentum k_t. An important characteristic of this evolution is distribution of the gluon density in $ln(k_t)$ space. The general form of BFKL evolution equation in LO is

$$\begin{aligned} f(x,k_t^2) &= f^0(x,k_t^2) + \frac{3\alpha_s(k_t^2)}{\pi} k_t^2 \int_x^1 \frac{dz}{z} \int_0^\infty \frac{dk_t'^2}{k_t'^2} \Big[\frac{f(x/z,k_t'^2) - f(x/z,k_t^2)}{\mid k_t'^2 - k_t^2 \mid} \\ &\quad + \frac{f(x/z,k_t^2)}{\sqrt{4k_t'^4 + k_t^4}} \Big], \end{aligned} \tag{2.10}$$

where the function $f^0(x, k_t^2)$ is a suitably defined inhomogeneous term and $k_t'^2$, k_t^2 are the transverse momenta squared of the gluon in the initial and final states respectively. In comparison to the DGLAP equation, this is a more intricate problem on the grounds that the BFKL equation literally involves contributions from operators of higher twists. The BFKL equation, in its ordinary form, not only represents the high-energy behaviour of cross-sections but also describes the amplitudes at non-zero momentum transfer.

2.1.3 CCFM equation

The CCFM equation [8-10] is a theoretical framework proposed by Catani, Ciafaloni, Fiorani and Marchesini (CCFM) which effectively interpolates between the the BFKL evolution and the more familiar DGLAP evolution equations. The primary objective of the CCFM approach is to provide accurate description of both the large-x region, where the summation of $\ln(Q^2)$ dominates, as well as the small-x region, where the large logarithms $\ln(1/x)$ are important. It depends on the comprehensible emission of gluons, that gives rise to an angular arrangement of the gluons along a series of multiple emissions. Similar to the BFKL equation, the CCFM equation is also defined in respect of a unintegrated gluon density f, which determines the possibility of finding a gluon with longitudinal momentum fraction x and transverse momentum k_t. Nonetheless, this distribution has a further dependance on some external scale Q. The CCFM equation is

$$f(x, k_t^2, Q^2) = f^0(x, k_t^2, Q^2)$$
$$+ \int_x^1 dz \int \frac{d^2q}{\pi q^2} \Theta(Q - zq) \Delta_S(Q, z, q) \tilde{P}(z, k_t, q) f(x/z, k_t'^2, q^2). \tag{2.11}$$

The inhomogeneous contribution $f^0(x, k_t^2, Q^2)$ is of non-perturbative origin and is assumed to contribute only for $k_t^2 < q_0^2$. The remaining terms contribute in the region $k_t^2 > q_0^2$. The function $\tilde{P}$ is the gluon-gluon splitting function

$$\tilde{P} = \frac{3\alpha_s}{\pi} \Big(\frac{1}{1-z} + \Delta_R \frac{1}{z} - 2 + z(1-z) \Big), \tag{2.12}$$

where the factors Δ_S and Δ_R are the Sudakov and Regge form factors respectively. The multiplicative factors Δ_S and Δ_R counteract the singularities which are apparent as $z \to 1$ and $z \to 0$ respectively. Unlike Δ_S, the Regee form factor Δ_R not only

depends on the branching variables, but also on the history of the cascade. At large-x one can get the usual DGLAP equation for gluon evolution by fixing $\Delta\Delta = 1$ and evolving Δ_S. On the other hand, at small-x keeping only the $1/z$ piece of P_{gg} and by setting $\Delta_S = 1$ and evolving $\Delta\Delta$ one can obtain the BFKL equation.

2.2 Nonlinear evolution equations

It is very fascinating to observe that the linear QCD evolution equations for parton densities , both the DGLAP and BFKL equations, prognosticate a steep rise of quark and gluon densities in the small-x region which is perceived in the DIS experiments at HERA as well. This sharp growth generates cross sections which in the high-energy limit fail to comply with the unitarity bound or in particular the Froissart bound [22, 23] on and so it will have to eventually slow down in order to restore unitarity. It is a known fact that the hadronic cross sections should obey the Froissart bound which derives from the general assumptions of the analyticity and unitarity of the scattering amplitude. Accordingly, the increasing number of gluon densities, so as to approach small-x, demands a formulation of the QCD at high density, where unitarity corrections are suitably taken into account.

Following DGLAP, the growing number of small-x gluons graphically conforms to higher density of individuals in the same approved region and thus differs from a diluted system at moderate values of x. As a result, at very small values of x the likelihood of interaction between two gluons can no longer be overlooked and it sooner or later engenders a situation in which individual partons inevitably overlap or shadow each other. We recall that, at very high energies, one can get into the region of smaller and smaller values of x and, under these situations, the gluon recombination being more effectual balances gluons splitting at some point. As a result, the abrupt growth of gluon distribution is eventually subdued due to the correlative interactions between gluons. This process is normally referred to as saturation of gluon density and it occurs when the possibility of gluon recombination, i.e. the process $gg \to g$, is as significant as that for a gluon to split into two gluons i.e. $g \to gg$. In deriving the linear DGLAP equations, the correlations among the initial gluons in the physical process of interaction and recombination of gluons are not taken into account. It is indispensable to point out that the linear DGLAP dynamics consider only the

splitting processes in the partonic evolution, i.e. the processes $q \to qg$, $g \to q\bar{q}$ and $g \to gg$. However at small-x, the modifications due to the correlations among initial gluons to the evolutionary amplitude should be treated accordingly. The multiple gluon interactions induce nonlinear or shadowing corrections in the linear evolution equation and so the standard linear DGLAP evolution equation will have to be modified in order to include the contributions of recombination mechanism in the small-x regime.

The DGLAP evolution equations can delineate the available experimental data in a decent manner covering a large domain of x and Q^2 with appropriate parameterizations. But despite the remarkable achievement of the DGLAP approach, some issues come into sight when trying to generate the best possible global fits to the H1 data [24] concurrently in the region of large-Q^2 ($Q^2 > 4$ GeV^2) as well as in the region of small-Q^2 ($1.5 < Q^2 < 4$ GeV^2) [25]. In the NLO analysis of MRST2001 [26] an overall good fit is obtained including both the regions but resulting a negative gluon distribution at $Q_0 = 1$ GeV , thus creating an ambiguity in the interpretation of the PDFs as probability or number density distributions. On the other hand, in the CTEQ collaboration [27], where a slightly higher input scale of $Q_0 = 1.3$ GeV is considered, a very good compatibility with the data are observed in the large-Q^2 region whereas, the consistency with data in the small-Q^2 region becomes poor. The matter of negative gluon distributions also arises in the NLO set of CTEQ6M when evolving backwards to 1 GeV. Nevertheless, the negative gluon distributions are not empowered in LO. These emerging enigmas are really very appealing as they can provide a signal of gluon recombination towards smaller values of x and Q^2. In Ref.[25] the effects of including nonlinear GLRMQ corrections to the LO DGLAP evolution equations are studied by using the HERA data for the structure function $F_2(x, Q^2)$ of the free proton and the PDF sets CTEQ5L and CTEQ6L as a baseline. With the inclusion of the nonlinear corrections, the agreement with the $F_2(x, Q^2)$ data is exhibited to be improved in the region of $x \leq 3 \times 10^{-5}$ and $Q^2 \leq 1.5$ GeV^2, but managing the good fit to the data obtained in the global analyses at large-x and Q^2. Moreover, in Ref.[28] an analysis of HERA $F_2(x, Q^2)$ data is presented adding the effect of absorptive corrections due to parton recombination on the parton distributions. The small-x gluon distribution is found to be enhanced at small scales

due to the absorptive effects, which may possibly avoid the need of a negative gluon distribution at 1 GeV. The gluon recombination effects lead to the nonlinear corrections to the linear DGLAP evolution equations due to multiple gluon interactions and as a result, in the very small-x region the conventional linear evolution equations are likely to breakdown. The nonlinear terms tame the abrupt growth of the gluon distribution in the kinematic region where α_s continues to be small but the density of gluons becomes very high so that a perturbative treatment is possible. Accordingly, the corrections of the higher order QCD effects, which suppress or shadow the growth of the parton densities, turns out to be the center of rigorous studies in the last few years.

The first perturbative QCD calculations reporting the recombination of two gluon ladders into one were carried out by Gribov, Levin and Ryskin (GLR), and Mueller and Qiu (MQ). They suggested that the nonlinear or shadowing corrections due to gluon recombination could be depicted in a new evolution equation with an additional nonlinear term quadratic in the gluon density. This equation, widely known as the GLR-MQ equation [29, 30], can be regarded as the updated version of the usual DGLAP equations with the corrections for gluon recombination. There are several other nonlinear evolution equations reporting the corrections of gluon recombination to the DGLAP and BFKL evolutions. They are the Modified-DGLAP (MD-DGLAP) [31, 32], Balitsky-Kovchegov (BK) [33, 34], Modified-BFKL (MD-BFKL) [35], Jalilian-Marian-Iancu-McLerran-Weigert-Leonidov-Kovner (JIMWLK) [36-38] equations. The BK equation is the most widely studied among these. The nonlinear equations viz. Modified-BFKL (MD-BFKL), BK and JIMWLK are based on BFKL evolution, whereas the MD-DGLAP equation is based on DGLAP evolution. A concise description of all the above mentioned nonlinear evolution equations is given below.

2.2.1 GLR-MQ equation

The shadowing corrections of gluon recombination to the parton distributions were first investigated by Gribov, Levin and Ryskin and then by Mueller and Qiu at the twist-4 level in their pioneering papers [29, 30]. They provided the idea that the nonlinear corrections due to gluon recombination could be portrayed in a new evolution

equation with an additional nonlinear term quadratic in gluon density. This equation, widely known as the GLR-MQ equation, can be considered as the improved version of the usual DGLAP equations with the corrections for gluon recombination. The pictorial representation of the corrections arising from gluon recombination processes is shown in Fig.2.3. Gribov et al. first suggested qualitative modification of the DGLAP

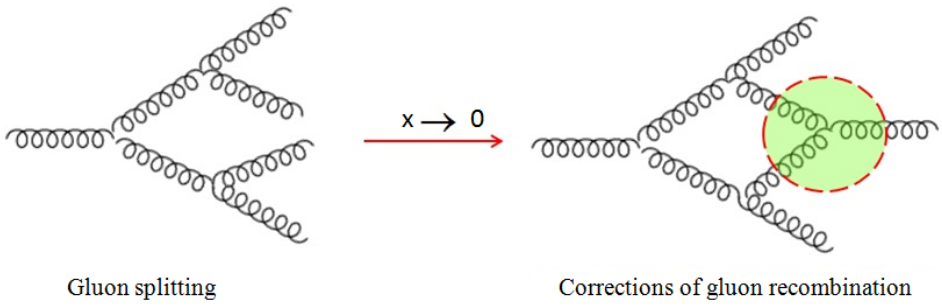

Figure 2.3: Corrections of gluon recombination

gluon evolution equation in order to include the gluon recombination effects based on the Abramovsky-Gribov-Kancheli (AGK) cutting rules [39]. Afterwards Mueller and Qiu completed the equation numerically using a perturbative calculation of the recombination probabilities in the DLLA, which is a significant achievement as it enables the GLR-MQ equation to be applied phenomenologically. This equation was generalized to incorporate the contributions from more higher order corrections in the Glauber-Mueller formula [40].

The GLR-MQ equation is based on two processes in the parton cascade:

(i) The splitting of gluons generated by the QCD vertex : $g \rightarrow g + g$;

(ii)The recombination of gluons promoted by the same vertex : $g + g \rightarrow g$.

For splitting process $1 \rightarrow 2$, the probability is proportional to $\alpha_s \rho$, whereas the probability for recombination process $2 \rightarrow 1$ is in proportion to $\alpha_s r^2 \rho^2$. Here, $\rho = \frac{xg(x,Q^2)}{\pi R^2}$ is the gluon density in the transverse plane, πR^2 is the target area, and R is the correlation radius between two interacting gluons [40]. It is worthwhile to mention that R is non-perturbative in nature and therefore all phenomena that occur at distance scales larger than R is non-perturbative [41]. Here, r is the size of the gluon induced in the recombination process and for DIS $r \sim \frac{1}{Q}$. For, $x \sim 1$ only the emission of gluons is influential since $\rho \ll 1$. At $x \rightarrow 0$, on the other hand, the density of gluons

ρ happens to be so high that the recombination of gluons should also be taken into account. Considering a cell of volume $\Delta \ln Q^2 \Delta \ln(1/x)$ in the phase space, number of gluons increases through splitting and decreases through recombination and this picture allows one to write the modification of the gluonic density as [41, 42]

$$\frac{\partial^2 xg(x,Q^2)}{\partial \ln(1/x) \partial \ln Q^2} = \frac{\alpha_s N_c}{\pi} xg(x,Q^2) - \frac{\alpha_s^2 \gamma}{\pi Q^2 R^2} [xg(x,Q^2)]^2, \tag{2.13}$$

which is known as the GLR-MQ equation. The factor γ is found to be $\gamma = 81/16$ for $N_c = 3$, as evaluated by Mueller and Qiu [30]. Here the gluon distribution is represented by $G(x,Q^2) = xg(x,Q^2)$, where $g(x,Q^2)$ is the gluon density. The quark-gluon emission diagrams are ignored because of their negligible influence in the gluon-dominated small-x domain. The first term in the right hand side of Eq.(2.15) represents the usual DGLAP term in the DLLA and hence linear in gluon field. The second term, having a negative sign controls the growth of the gluon distribution generated by the linear term at small-x and consequently delineates shadowing corrections emerging from recombination of two gluons into one. Likewise, the GLR-MQ equation for sea quark distribution can be written as

$$\frac{\partial xq(x,Q^2)}{\partial \ln(1/x) \partial \ln Q^2} = \frac{\partial G(x,Q^2)}{\partial \ln Q^2}\Big|_{DGLAP} - \frac{27}{160} \frac{\alpha_s^2(Q^2)}{R^2 Q^2} \Big[G\Big(\frac{x}{\omega}, Q^2\Big) \Big]^2 + HT, \tag{2.14}$$

where HT denotes a higher-dimensional gluon distribution term suggested by Mueller and Qiu [30].

In the linear QCD evolution of DIS structure functions like the DGLAP or BFKL only the splitting of quarks and gluons is considered. This leads to a constant increase of the parton densities at small-x eventually violating the unitarity bound and are therefore expected to be tamed by the inverse recombination processes. Therefore, in order to account for gluon recombination processes, apart from the production diagrams, the GLR-MQ equations also include the dominant non-ladder contributions denoted as the fan diagrams. The fan diagrams take into consideration some of the gluon recombination processes that turn significant at small-x and therefore plays the key role in the restoration of unitarity. These diagrams are depicted in Fig.2.4.

The gluon recombination term in the GLR-MQ equation contains a factor $1/Q^2$, whose dimension is balanced by the parameter R representing the size of the region containing the recombining gluons. The size of the nonlinear term varies as $1/R^2$. The value of R depends on how the gluons are distributed within the proton or how

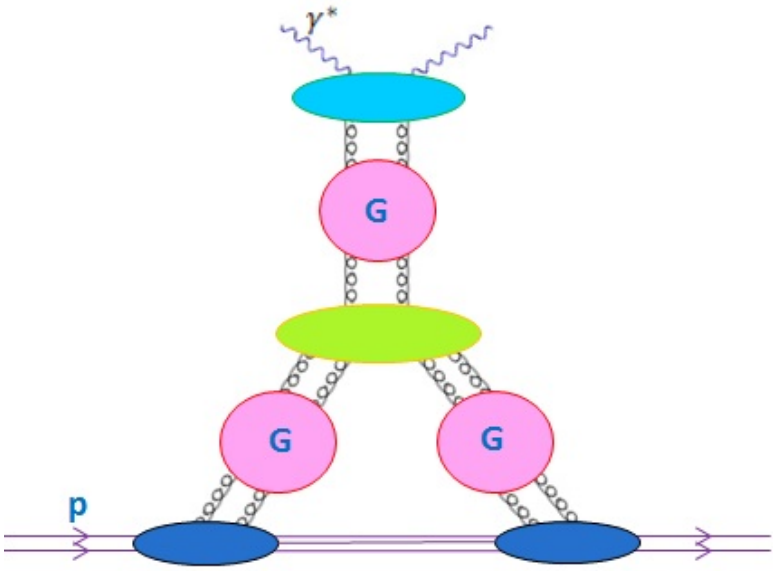

Figure 2.4: Fan-diagrams contributing to the GLR-MQ equation

the gluon ladders couple to each other. The gluon ladders may emerge from different constituents of the proton or from the same constituent. The gluons are supposed to be distributed uniformly across the whole of the proton if the gluon ladders emerge off distinct valence quarks. In that case R is of the order of proton radius R_h, that is to say $R \sim 5$ GeV^{-1} and recombination or shadowing correction is negligibly small [29]. On the other hand, if the gluon ladders couple to the same parton then it leads to a higher gluon density in the parton's vicinity. Such smaller regions within the proton where the gluon density is higher than the average are known as the so-called 'hot spots' [43, 44]. The hot spots could specify the fast onset of gluon-gluon interactions in the environs of the emitting parton and so boost the recombination effect. The value of R for such hot spot, is considered to be of the order of the transverse size of a valence quark i.e $R \sim 2$ GeV^{-1}.

A remarkable feature of the GLR-MQ equation is that it predicts the saturation momentum in the asymptotic region $x \to 0$. Moreover, it predicts a critical line separating the perturbative regime from saturation regime and it is valid only in the vicinity of this critical line [42]. The general benchmark of this equation is that the nonlinear corrections should be small as compared to the linear term, otherwise further corrections must be taken into account and non-perturbative effects could be of significance. As the GLR-MQ equation only includes the first nonlinear term, so

this equation is not legitimate in very high density region where the contributions from the higher order terms become crucial.

2.2.2 MD-DGLAP equation

The MD-DGLAP equation [31, 32] sums up all possible twist-4 cut diagrams in the LL(Q^2) approximation and describes the corrections of parton recombination to the QCD evolution equation. These equations are advocated by Zhu and Ruan. This equation is obtained by aggregating the Feynman diagrams in the framework of the time-ordered perturbation theory (TOPT) [45] instead of the AGK cutting rule [39]. The MD-DGLAP equation for gluon distribution is [31, 32]

$$\begin{aligned}\frac{dxg(x,Q^2)}{dln(Q^2)} &= P_{gg}\otimes G(x,Q^2)+P_{gq}\otimes S(x,Q^2)\\ &+\frac{\alpha_s^2 k}{Q^2}\int_{x/2}^{x} dx_1 x x_1 G^2(x_1,Q^2)\sum_i P_i^{gg\to g}(x_1,x)\\ &-\frac{\alpha_s^2 k}{Q^2}\int_{x}^{1/2} dx_1 x x_1 G^2(x_1,Q^2)\sum_i P_i^{gg\to g}(x_1,x) \qquad (2.15)\end{aligned}$$

and for sea quark distribution is [31, 32]

$$\begin{aligned}\frac{dxq(x,Q^2)}{dln(Q^2)} &= P_{qg}\otimes G(x,Q^2)+P_{qq}\otimes S(x,Q^2)\\ &+\frac{\alpha_s^2 k}{Q^2}\int_{x/2}^{x} dx_1 x x_1 G^2(x_1,Q^2)\sum_i P_i^{gg\to q}(x_1,x)\\ &-\frac{\alpha_s^2 k}{Q^2}\int_{x}^{1/2} dx_1 x x_1 G^2(x_1,Q^2)\sum_i P_i^{gg\to q}(x_1,x), \qquad (2.16)\end{aligned}$$

where P are the evolution kernels of the linear DGLAP equation. The recombination functions are

$$\sum_i P_i^{gg\to g}(x_1,x)=\frac{27}{64}\frac{(2x_1-x)(-136xx_1^3-64x_1x^3+132x_1^2x^2+99x_1^4+16x^4)}{xx_1^5}, \qquad (2.17)$$

$$\sum_i P_i^{gg\to q}(x_1,x)=\frac{1}{48}\frac{(2x_1-x)(36x_1^3+49x_1x^2-14x^3-60x^2x)}{x_1^5}. \qquad (2.18)$$

The nonlinear coefficient k depends on the definition of the double parton distribution and the geometric distributions of partons inside the target. The positive third terms on the right-hand side of both Eq.(2.17) and Eq.(2.18) represent the anti-shadowing effect, whereas the negative fourth term is the result of the shadowing correction. The concurrence of shadowing and anti-shadowing in the QCD

evolution of the parton densities is a usual demand for the local momentum conservation. The shadowing and anti-shadowing terms are defined on distinct kinematic regions $[x, 1/2]$ and $[x/2, x]$ respectively. Hence, the overall recombination effects in Eq.(2.17) are not only associated to the value of gluon density, but also depend on the slope of the gluon distribution in the space $[x/2, x]$. This implies that a steeper gluon distribution has an intense antishadowing effect as compared to a lower gluon distribution.

2.2.3 BK equation

The BK evolution equation [33, 34] is based on the BFKL equation and was derived by Balitsky and Kovchegov in the large-N_c limit, with N_c being the number of colors. The BK equation is an upgraded form of the GLR-MQ equation and it determines the saturation of parton densities at very small-x. This equation is written for the scattering amplitude N. It provides an explanation of the more specific triple-pomeron vertex [46, 47] and can be utilized for the non-forward amplitude. The BK equation is obtained in the leading $\ln(1/x)$ approximation of perturbative QCD, i.e. it sums all contributions of the order $(\alpha_s \ln(1/x))^n$. The contributions of the orders $\alpha_s(\alpha_s \ln(1/x))^n$ and $\alpha_s \ln Q^2(\alpha_s \ln(1/x))^n$ are not included in this equation. The phenomenological analysis of this equation is performed in the dipole model [48, 49] approximation, where the nonlinear terms are supposed to be formed by the dipole splitting and the screening or shadowing effects are emerged from the double scattering of the probe on the final states. The BK equation reads

$$\begin{aligned}\frac{\partial N(r,Y;b)}{\partial Y} &= \frac{\bar{\alpha_s}}{2\pi}\int \frac{d^2r' r^2}{(r-r')^2 r'^2} \\ &\times\Big[2N\big(r',Y;b+\frac{1}{2}(r-r')\big) - N(r,Y;b) \\ &-N\big(r',Y;b-\frac{1}{2}(r-r')\big)N\big(r-r',Y;b-\frac{1}{2}r'\big)\Big], \end{aligned} \tag{2.19}$$

where $\bar{\alpha_s} = (\alpha_s N_c)/\pi$, $N(r,Y;b)$ is the scattering amplitude of interaction for the dipole with the size r and rapidity $Y = \ln(1/x)$, at impact parameter b. In the large N_c limit $C_F = N_c/2$, where N_c is the number of colors.

Eq.(2.21) is an integro-differential equation and it presents the scattering amplitude $N(r,Y;b)$ at all rapidities $Y > 0$ provided the initial condition at $Y = 0$ is known. The physical significance of Eq.(2.21) is that the dipole of size r decays in

two dipoles of sizes r' and $r - r'$ which interact with the target. The linear part of Eq.(2.21) is the usual LO BFKL equation [5-7], which accounts for the evolution of the multiplicity of the color dipoles of fixed size in respect of the rapidity Y. The nonlinear term considers a coexisting interaction of two produced dipoles with the target and it sums the high twist contributions. An outstanding feature of the BK equation is that its solution predicts a limiting form of the scattering amplitude resulting in parton saturation.

2.2.4 MD-BFKL equation

The nonlinear MD-BFKL [35] equation was suggested by Zhu, Shen and Ruan to describes the corrections of the gluon recombination to the BFKL equation, but it differs from the BK equation. The MD-BFKL equation forecasts an intense shadowing effect, which subdues the gluon density. Surprisingly, it generates the extinction of gluons below the saturation region. This unforeseen effect of gluon extinction below the saturation region is induced by an apparent chaotic solution of the equation as suggested in [35]. The MD-BFKL is defined as

$$\begin{aligned} -x\frac{\partial f(x,k_{b0})}{\partial x} &= \frac{\alpha_s N_c}{2\pi^2}\int d^2k_{bc}\frac{k_{b0}^2}{k_{bc}^2 k_{c0}^2}2f(x,k_{bc}) - \frac{\alpha_s N_c}{2\pi^2}f(x,k_{b0})\int d^2k_{bc}\frac{k_{b0}^2}{k_{bc}^2 k_{c0}^2} \\ &\quad -\frac{18\alpha_s^2}{\pi^2 R^2}\frac{N_c^2}{N_c^2-1}\int d^2k_{bc}\frac{1}{k_{bc}^2}\frac{k_{b0}^2}{k_{bc}^2 k_{c0}^2}f^2(x,k_{bc}) \\ &\quad +\frac{9\alpha_s^2}{\pi^2 R^2}\frac{N_c^2}{N_c^2-1}f^2(x,k_{b0})\int d^2k_{bc}\frac{1}{k_{b0}^2}\frac{k_{b0}^2}{k_{bc}^2 k_{c0}^2}. \end{aligned} \tag{2.20}$$

The nonlinear part of the MD-BFKL equation has an infra red (IR) divergence very much alike the BFKL kernel and as a matter of course, it requires the regularization scheme alike the BFKL equation. The evolution kernels in the linear and nonlinear parts of the MD-BFKL equation are fixed by using the same procedure of summations of the real and virtual processes. This equation is derived on the basis of the TOPT cutting rules just as the MD-DGLAP equation to include the contributions from the virtual processes in the linear and nonlinear parts of the MD-BFKL equation. The MD-BFKL and BK equations differ from each other in their assumptions of regularization schemes. In MD-BFKL equation the singularities in the nonlinear real part are aborted by the contributions from the complementary virtual processes, whereas such singularities are assimilated into the double amplitude NN in BK equation.

2.2.5 JIMWLK equation

The JIMWLK evolution equation [36-38], advocated by Jalilian-Marian, Iancu, McLerran, Weigert, Leonidov and Kovner, is the renormalization group equation (RGE) for the Color Glass Condenstate and describes the small-x hadronic physics in the regime of very high gluon density. This is a functional Fokker-Planck equation regarding a classical random color source, which defines the color charge density of the partons with large-x [38]. This equation controls the evolution with rapidity of the statistical weight function for the color glass field.

The JIMWLK equation in the compact form is [50]

$$\partial\tau\hat{Z}_\tau[U] = -\frac{1}{2}i\nabla_x^a\chi_{xy}^{ab}i\nabla_y^b Z_\tau[U], \tag{2.21}$$

where $\hat{Z}_\tau[U]$ is the weight functional and it governs the correlators $O[U]$ of U fields conforming to $\langle O[U]\rangle_\tau = \int \hat{D}[U]O[U]Z_\tau[U]$, with $\hat{D}[U]$ being a functional Haar measure [50]. ∇_x^a are functional form of the left-invariant vector fields affecting U_y in accordance with

$$i\nabla_x^a U_y = U_x t^a \delta_{xy}^{(2)}, \tag{2.22}$$

where U_x are the Wilson line variables representing the kinematically enhanced degrees of freedom. Again

$$\chi_{xy}^{ab} = \frac{\alpha_s}{\pi^2}\int d^2z K_{xyz}[(1-\tilde{U}_x^\dagger\tilde{U}_z)(1-\tilde{U}_z^\dagger\tilde{U}_x)]^{ab},$$

and

$$K_{xyz} = \frac{(x-z).(z-y)}{(x-z)^2(z-y^2)}. \tag{2.23}$$

The deduction of the JIMWLK equation demands an analytic estimation to all orders in the environment of a classical gluon field for a random light cone source. The solution of the JIMWLK equation is normally anticipated to enable the saturation momentum to raise constantly as $y \to \infty$. Moreover its solution is supposed to be universal. In the restrain of weak field the JIMWLK equation scales down to the BFKL equation, whereas in the large N_c limit, it grows to be equivalent to the BK equation.

2.3 Solutions of evolution equations

The QCD evolution equations are the underlying theoretical tools to compute the quark and gluon distributions and eventually the DIS structure functions. On that account the solutions of the evolution equations are drawing attention substantially. The solutions of the DGLAP equation for the QCD evolution of PDFs have been discussed considerably over the past years. There exist two main classes of approaches: those that solve the equation directly in x-space, and those that solve it for Mellin transforms of the parton densities and subsequently invert the transforms back to x-space. Some available programs that deal with DGLAP evolution are CANDIA [51] based on the logarithmic expansions in x-space, QCD PEGASUS [52], which is based on the use of Mellin moments, HOPPET [53] and QCDNUM [54]. HOPPET is a Fortran package for carrying out QCD DGLAP evolution and other common manipulations of PDFs. The Fortran package QCD PEGASUS provides fast, flexible and accurate solutions of the evolution equations for unpolarized and polarized parton distributions of hadrons in perturbative QCD. Similarly QCDNUM is a Fortran program that numerically evolves parton densities or fragmentation functions up to NNLO in perturbative QCD. Most of the methods used for the solution of DGLAP equation are numerical. Laguerre polynomials [55, 56], Brute-Force method [57], Matrix method [58], Mellin transformation [59, 60] etc. are different methods used to solve DGLAP evolution equations. The shortcomings common to all are the computer time required and decreasing accuracy for $x \to 0$. More precise approach to the solution of the DGLAP evolution equations is the matrix approach, but it is also a numerical solution. A numerical solution does not provide the full control on the employed phenomenological parameters, and the transparency and simplicity of physical interpretation are lost if one relies only on the numerical solutions.

As an alternative to the numerical solution, one can study the behavior of quarks and gluons via analytic solutions of the evolution equations. Even though exact analytic solutions of the DGLAP equations cannot be obtained in the whole range of x and Q^2, such solutions are possible under definite conditions and are fairly successful as far as the HERA small-x data are concerned. In recent years, such a scheme in the analytic study of the DGLAP equations has been reported with considerable phenomenological success [61-67]. The Taylor series expansion method, the method

of characteristic and the Regge theory methods are some of the very simple and frugal analytical methods that have been utilized widely to obtain the solutions of DGLAP equations. Part I of this thesis also reports the analytical solutions of the DGLAP equations for DIS structure functions upto NNLO with significant phenomenological triumph.

In contrast to the DGLAP equation, it is very difficult to the solve the BFKL and CCFM equations. Although the solution of the LO BFKL evolution is known, but regardless of a number of attempts, it seems that an exact analytical solution of the NLO BFKL equation, or a general all-order BFKL equation in QCD is still unavailable. Nevertheless, in a conformal field theory without the running of the coupling, i.e. in the N = 4 super Yang-Mills theory, the form of the solution of the BFKL equation to all-order has been identified [68, 69]. The numerical solution of CCFM equation can be obtained by monte-carlo approach CASCADE to study the small-x regime. Although in the single loop approximation the CCFM equatiion can be solved analytically [70], but due the non Sudakov form-factor the solution beyond the single-loop approximation is less apparent.

The solutions of the nonlinear evolution equations, on the other hand, are particularly important for understanding the nonlinear effects of gluon-gluon interaction due to the high gluon density at small-x. The solution of nonlinear evolution equations also provide the determination of the saturation momentum, which incorporates physics in addition to that of the linear evolution equations commonly used to fit the DIS data. It is very difficult to solve the nonlinear equations analytically, unlike the linear DGLAP equations. However the studies on the solutions and viable generalizations of the GLR-MQ type equations in different approaches have been revealed in the last few years [25, 28, 29, 71-80]. In Refs. [29, 71-74] the solutions of GLR-MQ type nonlinear equations are reported in semi classical approach using characteristics method which leads to existence of a critical line separating the perturbative regime from the nonperturbative one. Here it is shown that all characteristics in the region of small-x cannot cross this line but can approach it. Again a new equation is proposed in Ref.[75] which generalizes the GLR equation and allows to probing into smaller distance in the dense parton system considering the shadowing effects more exclusively by including multigluon correlations. The general solution to the

new equation is obtained in in an eikonal approach and fixed α_s. A new approach for searching a solution of the nonlinear GLR-MQ evolution equation in the nonperturbative part of the small-x region is discussed in Ref [76]. Here it is justified that the suggested solution satisfies all physics restrictions and there is only one solution that complements the perturbative DGLAP evolution. A color dipole approach to the solution to the nonlinear GLR-MQ like equation for high parton density is suggested in the full kinematic region including $x \to 0$ in Ref.[77]. The solution replicates the saturation of the gluon density. However due to moderate dependence on the impact parameter, the saturation gives rises to the dipole-target total cross section proportional to $\ln(1/x)$ in the region of very small-x. A numerical analysis of the GLR-MQ equation is presented in Ref. [78] where the signatures of gluon recombination are discussed. They also provide a simple and qualitative idea to explore the H1 [79] experimental data for evidence of gluon recombination. Similarly, a numerical solution of GLR-MQ equation is suggested in Ref.[25], where the effects of the first nonlinear corrections to the DGLAP evolution equations are studied by using the recent HERA data for the structure function $F_2(x, Q^2)$. It is argued in this paper that the nonlinear corrections become important at $x \leq 10^{-3}$ and $Q^2 \leq 10$ GeV^2, but become negligible at large-x and large-Q^2. In Ref.[28] The effect of absorptive corrections due to parton recombination on the parton distributions of the proton is discussed at small-x in a more precise version of the GLRMQ equations using a truncated version of the MRST2001 NLO analysis [26]. Moreover the approximate analytical solutions of the nonlinear GLR-MQ evolution equation have also been reported in recent years [80, 81]. In part II of this thesis we present a semi-analytical approach to solve the GLR-MQ equation in the vicinity of saturation and make a deliberate attempt to explore the effect of nonlinear or shadowing corrections in the kinematic region of small-x and moderate Q^2.

Unlike GLR-MQ the other nonlinear equations are comparatively complicated to solve. The numerical solutions to BK or JIMWLK nonlinear equations in the presence of the impact parameter is very challenging. The JIMWLK equation is difficult to solve, even numerically as it consist of an infinite hierarchy of coupled evolution equations. The BK hierarchy is a special case of the JIMWLK equation where the primary projectile is set and captured by a quark-antiquark pair. For practical

calculations one may use the average field approximation and thereby diminish a full infinite hierarchy to a single closed equation. Even if the full analytical solution of the BK equation is not known, a number of its general properties, such as the existence and shape of limiting solutions, have been determined in both analytical [82-84] and numerical [85-89] approaches in recent years. On the other hand, in Ref.[90] numerical solutions to the MD-DGLAP equation are reported in the small-x region using a with GRV like input distributions. Here the the small-x behavior parton distributions in the nucleus and free proton are predicted numerically and it is seen that gluon recombination at the twist-4 level suppresses the rapid increase of parton densities towards small-x. It is further claimed that saturation and partial saturation occur sooner than the saturation scale Q_s^2 is reached.

Bibliography

[1] Gribov, V. N., Lipatov, L. N. Deep inelastic *ep* scattering in perturbation theory, *Sov. J. Nucl. Phys.* **15**(4), 438−−450, 1972.

[2] Gribov,V. N., Lipatov, L. N. e^+e^- pair annihilation and deep-inelastic *ep* scattering in perturbation theory, *Sov. J. Nucl. Phys.* **15**(4), 675−−684, 1972.

[3] Dokshitzer, Y. L. Calculation of structure functions of deep-inelastic scattering and e^+e^- annihilation by perturbation theory in quantum chromodynamics, *Sov. Phys. JETP* **46**(4), 641−−652, 1977.

[4] Altarelli, G., Parisi, G. Asymptotic freedom in parton language, *Nucl. Phys. B* **126**(2), 298−−318, 1977.

[5] Kuraev, E. A., Lipatov, L. N. and Fadin, V. S. Multi-reggeon processes in the Yang-Mills theory, *Sov. Phys. JETP* **44**(3), 443−−450, 1976.

[6] Kuraev, E. A., Lipatov, L. N. and Fadin, V. S. The Pomeranchuk singularity in nonabelian gauge theories, *Sov. Phys. JETP* **45**(2), 199−−204 ,1977.

[7] Balitsky, L. I., Lipatov, L. N. The Pomeranchuk singularity in quantum chromodynamics, *Sov. J. Nucl. Phys.* **28**, 822−−829, 1978.

[8] Ciafaloni, M. Coherence effects in initial jets at small Q^2/s, *Nucl. Phys. B* **296**(1), 49−−74, 1988.

[9] Catani, S., Fiorani, F. and Marchesini, G. QCD coherence in initial state radiation, *Phys. Lett. B* **234**(3), 339−−345, 1990.

[10] Catani, S., Fiorani, F. and Marchesini, G. Small-x behaviour of initial state radiation in perturbative QCD, *Nucl. Phys. B* **336**(1), 18−−85, 1990.

[11] Halzen, F., Martin, A. D. *Quarks and Leptons: An Introductory Course in Modern Particle Physics*, John Wiley and Sons, Canada, 1984.

[12] Martin, Alan D. Proton structure, Partons, QCD, DGLAP and beyond, *Acta Phys. Polon. B* **39**(9), 2025−−2062, 2008.

[13] Curci, G., Furmanski, W. and Petronzio, R. Evolution of parton densities beyond leading order: The non-singlet case, *Nucl. Phys. B* **175**(1), 27−−92, 1981.

[14] Furmanski, W., Petronzio, R. Singlet parton densities beyond leading order, *Phys.Lett. B* **97**(3-4), 437−−442, 1980.

[15] Gonzalez-Arroyo, A., Lopez, C. and Yndurain, F. Second order contributions to the structure functions in deep inelastic scattering. 1. Theoretical calculations, *Nucl. Phys. B* **153**, 161−−186, 1979.

[16] Floratos, E., Kounnas, C. and Lacaze, R. Higher order QCD effects in inclusive annihilation and deep inelastic scattering, *Nucl. Phys. B* **192**(2), 417−−462, 1981.

[17] Van Neerven, W. L., Vogt, A. NNLO evolution of deep-inelastic structure functions: the singlet case, *Nucl. Phys. B* **588**(1-2), 345−−373, 2000.

[18] Moch, S., Vermaseren, J.A.M. and Vogt, A. The three-loop splitting functions in QCD: The non-singlet case, *Nucl. Phys. B* **688**(1-2), 101−−134, 2004.

[19] Martin, A. D. et al., NNLO global parton analysis, *Phys. Lett. B* **531**(3-4), 216−−224, 2002.

[20] Lai, H. L. et al., Improved parton distributions from global analysis of recent deep inelastic scattering and inclusive jet data, *Phys. Rev. D* **55**(3), 1280, 1997.

[21] Gluck, M., Reya, E. and Vogt, A. Dynamical parton distributions revisited, *Eur. Phys. J. C* **5**(3), 461−−470, 1998.

[22] Froissart, M. Asymptotic behavior and subtractions in the Mandelstam representation, *Phys. Rev.* **123**(3), 1053−−1057, 1961.

[23] Martin, A. Unitarity and high-energy behavior of scattering amplitudes, *Phys. Rev.* **129**(3), 1432−−1436, 1963.

[24] Adloff, C. et al., Deep-inelastic inclusive *ep* scattering at low x and a determination of α_s, *Eur. Phys. J. C* **21**(1), 33−−61, 2001.

[25] Eskola, K. J. et al., Nonlinear corrections to the DGLAP equations in view of the HERA data, *Nucl. Phys. B* **660**(1-2), 211−−224, 2003.

[26] Martin, A. D. et al., MRST2001: partons and S from precise deep inelastic scattering and Tevatron jet data, *Eur. Phys. J. C* **23**(1), 73−−87, 2002.

[27] Pumplin, J. et al., New generation of parton distributions with uncertainties from global QCD analysis, *JHEP* **2002**(JHEP07:012), 1-46, 2002.

[28] Watt, G., Martin, A. D. and Ryskin, M.G. Effect of absorptive corrections on inclusive parton distributions, *Phys. Lett. B* **627**(1-4), 97−−104, 2005.

[29] Gribov, L. N., Levin, E. M. and Ryskin, M. G. Semihard processes in QCD, *Phys. Rep.* **100**(1-2), 1−−150, 1983.

[30] Mueller, A. H., Qiu, J. Gluon recombination and shadowing at small values of x, *Nucl. Phys. B* **268**(2), 427−−452, 1986.

[31] Zhu, W. A new approach to parton recombination in the QCD evolution equations, *Nucl. Phys. B* **551**(1-2), 245−−274, 1999.

[32] Zhu, W., Ruan, J. A new modified Altarelli-Parisi evolution equation with parton recombination in proton, *Nucl. Phys. B* **559**(1-2), 378−−392, 1999.

[33] Balitsky, I. Operator expansion for high-energy scattering, *Nucl. Phys. B* **463**(1), 99−−157, 1996.

[34] Kovchegov, Y. V. Small-x F_2 structure function of a nucleus including multiple Pomeron exchanges, *Phys. Rev. D* **60**(3), 034008, 1999.

[35] Zhu, W., Shen, Z. and Ruan, J. A new perspective on gluon distribution at small x, *arXiv:hep-ph/0703309v4*.

[36] Jalilian-Marian, J. et al., The intrinsic glue distribution at very small x, *Phys. Rev. D* **55**(9), 5414−−5428, 1997.

[37] Jalilian-Marian, J. et al., The Wilson renormalization group for low x physics: towards the high density regime, *Phys. Rev. D* **59**(1), 014014, 1999.

[38] Iancu, E., Leonidov, A. and McLerran, L. Nonlinear gluon evolution in the color glass condensate: I, *Nucl. Phys. A* **692**(3-4), 583−−645, 2001.

[39] Abramovsky, V. A., Gribov, V. N., Kancheli, O. V. Character of inclusive spectra and fluctuations produced in inelastic processes by multi-Pomeron exchange, *Sov.J.Nucl.Phys.* **18**, 308−−317, 1974.

[40] Mueller, A. H. Small-x behavior and parton saturation: A QCD model, *Nucl. Phys. B* **335**(1), 115−−137, 1990.

[41] Laenen, E., Levin, E. Parton densities at high energy, *Annu. Rev. Nucl. Part. Sci.* **44**, 199−−246, 1994.

[42] Laenen, E., Levin, E. A new evolution equation, *Nucl. Phys. B* **451**(1-2), 207−−230, 1995.

[43] Levin, E. M., Ryskin, M. G. Low-x structure function and saturation of the parton density, *Nucl. Phys. B (Proc. Suppl.)* **18**(3), 92−−124, 1991.

[44] Bartels, J., De Roeck, A.and Loewe, M. Measurement of hot spots inside the proton at HERA and LEP/LHC, *Z.Phys. C* **54**(4), 635−−641, 1992.

[45] Sterman, G. *An introduction to Quantum Field Theory*, Cambridge Univ. Press, Cambridge, 1993.

[46] Bartels, J. Unitary corrections to the Lipatov pomeron and the small-x region in deep inelastic scattering in QCD, *Phys. Lett. B* **298**(12), 204−−210, 1993.

[47] Bartels, J., Kutak, K. A momentum space analysis of the triple pomeron vertex in pQCD, *Eur. Phys. J. C* **53**(4), 533−−548, 2008.

[48] Golec-Biernat, K., Stasto, A. M. On solutions of the Balitsky-Kovchegov equation with impact parameter, *Nucl. Phys. B* **668**(12), 345−−363, 2003.

[49] Ikeda, T., McLerran, L. Impact parameter dependence in the Balitsky-Kovchegov Equation, *Nucl. Phys. A* **756**(3-4), 385−−398, 2005.

[50] Rummukainen, K., Weigert, H. Universal features of JIMWLK and BK evolution at small-x, *Nucl. Phys. A* **739**(1-2), 183−−226, 2004.

[51] Cafarella, A., Coriano, C. and Guzzi, M. NNLO logarithmic expansions and exact solutions of the DGLAP equations from x-space: New algorithms for precision studies at the LHC, *Nucl. Phys. B* **748**(1-2), 253−−308, 2006.

[52] Vogt, A. Efficient evolution of unpolarized and polarized parton distributions with QCD-Pegasus, *Comput. Phys. Commun.* **170**(1), 65−−92, 2005.

[53] Salam, G. P., Rojo, J. A Higher order perturbative parton evolution toolkit (HOPPET), *Comput. Phys. Commun.* **180**(1), 120−−156, 2009.

[54] Botje, M. A QCD analysis of HERA and fixed target structure function data, *Eur. Phys. J. C* **14**(2), 285−−297, 2000.

[55] Coriano, C., Savkli, C. QCD evolution equations: Numerical algorithms from the Laguerre expansion, *Comput. Phys. Commun.* **118**(2-3), 236−−258, 1999.

[56] Schoeffel, L. An elegant and fast method to solve QCD evolution equations. Application to the determination of the gluon content of the Pomeron, *Nucl. Instrum. Methods A* **423**(2-3), 439−−445, 1999.

[57] Hirai, M., Kumano, S. and Miyama, M. Numerical solution of Q^2 evolution equations for polarized structure functions, *Comput. Phys. Commun.* **108**(1), 38−−55, 1998.

[58] Ratcliffe, P. G., A matrix approach to numerical solution of the DGLAP evolution equations, *Phys. Rev. D*,**63**(11), 116004, 2001.

[59] Kosower, D. A., Evolution of parton distributions, *Nucl. Phys. B* **506**(1-2), 439−−467, 1997.

[60] Weinzierl, S., Fast evolution of parton distributions, *Comput. Phys. Commun.* **148**(3), 314−−326, 2002.

[61] Kotikov, A.V., Parente, G. The gluon distribution as a function of F_2 and $dF_2/dlnQ^2$ at small x. The next-to-leading analysis, *Phys. Lett. B* **379**(1-4), 195−−210, 1996.

[62] Sarma, J. K., Choudhury, D. K. and Medhi, G. K. x-distribution of deuteron structure function at low-x, *Phys. Lett. B* **403**(1-2), 139−−144, 1997.

[63] Choudhury D. K., Sahariah, P. K. The next-to-leading order (NLO) gluon distribution from DGLAP equation and the logarithmic derivatives of the proton structure function $F_2(x, Q^2)$ at low x, *Pramana J. Phys.* **65**(2), 193−−213, 2005.

[64] Boroun, G. R., Rezaie, A. A solution of the DGLAP equation for gluon distribution as a function of F_2 and $dF_2/dlnQ^2$ at low x: the next-to-leading order analysis, *Chin. Phys. Lett.* **23**(2), 324−−327, 2006.

[65] Baishya, R., Sarma, J.K. Method of characteristics and solution of DGLAP evolution equation in leading and next to leading order at small x, *Phys. Rev. D* **74**(10), 107702, 2006.

[66] Baishya, R., Jamil, U. and Sarma, J. K. Evolution of spin-dependent structure functions from DGLAP equations in leading order and next to leading order, *Phys. Rev. D* **79**(3), 034030, 2009.

[67] Baishya, R., Sarma, J. K. Semi numerical solution of non-singlet Dokshitzer-GribovLipatovAltarelliParisi evolution equation up to next-to-next-to-leading order at small x, *Eur. Phys. J. C* **60**(4), 585−−591, 2009.

[68] Kotikov A., Lipatov, L. NLO corrections to the BFKL equation in QCD and in supersymmetric gauge theories, *Nucl.Phys. B* **582**(1-3), 19−−43, 2000.

[69] Balitsky I., Chirilli, G. A. Conformal kernel for NLO BFKL equation in N=4 SYM, *Phys. Rev. D* **79**(3), 031502, 2009.

[70] Kwiecinski, J. Unintegrated gluon distributions from the transverse coordinate representation of the CCFM equation in the single loop approximation, *Acta Phys. Polon. B* **33**(7), 1809−−1822, 2002.

[71] Collins J. C., Kwiecinski, J. Shadowing in gluon distributions in the small-x region, *Nucl. Phys. B* **335**(1), 89−−100, 1990.

[72] Bartels, J., Blumlein J. and Shuler, G. A Numerical study of the small x behavior of deep inelastic structure functions in QCD *Z. Phys. C* **50**(1), 91−−102, 1991.

[73] Ayala, A. L., Gay Ducati, M. B. and Levin, E. M. QCD evolution of the gluon density in a nucleus, *Nucl. Phys. B* **493**(12), 305−−353, 1997.

[74] Ayala, A. L., Gay Ducati, M. B. and Levin, E. M. Parton densities in a nucleon, *Nucl. Phys. B* **511**(12), 355−−395, 1998.

[75] Laenen, E., Levin, E. A new evolution equation, *Nucl. Phys. B* **451**(12), 207−−230, 1995.

[76] Bartels, J., Levin, E. Solutions to the Gribov-Levin-Ryskin equation in the nonperturbative region, *Nucl. Phys. B* **38**(3), 617−−637, 1992.

[77] Levin E., Tuchin, K. Solution to the evolution equation for high parton density QCD, *Nucl. Phys. B* **573**(3), 833−−852, 2000.

[78] Prytz, K. Signals of gluon recombination in deep inelastic scattering, *Eur. Phys. J. C* **22**(2), 317−−321, 2001.

[79] Adloff, C. et al., Inclusive measurement of diffractive deep inelastic ep scattering, *Z. Phys. C* **76**(4), 613−−629, 1997.

[80] Rezaei, B., Boroun, G. R. Analytical approach for the approximate solution of the longitudinal structure function with respect to the GLR-MQ equation at small x, *Phys. Lett. B* **692**(4), 247−−249, 2010.

[81] Boroun, G. R., Zarrin, S. An approximate approach to the nonlinear DGLAP evaluation equation, *Eur. Phys. J. Plus* **128**(10), 119, 2013.

[82] Levin, E., Tuchin, K. Nonlinear evolution and saturation for heavy nuclei in DIS, *Nucl. Phys. A* **693**(34), 787−−798, 2001.

[83] Munier S., Peschanski, R. Traveling wave fronts and the transition to saturation, *Phys. Rev. D* **69**(3), 034008, 2004.

[84] Levin E., Lublinsky, M. Parton densities and saturation scale from nonlinear evolution in DIS on nuclei, *Nucl. Phys. A* **696**(3-4), 833−−850, 2001.

[85] Lublinsky, M. Scaling phenomena from non-linear evolution in high energy DIS, *Eur. Phys. J. C* **21**(3), 513−−519, 2001.

[86] Albacete J. L. et al., Numerical analysis of the Balitsky-Kovchegov equation with running coupling: Dependence of the saturation scale on nuclear size and rapidity, *Phys. Rev. D* **71**(1), 014003-1-12, 2005.

[87] Kozlov, M., Levin, E. Solution to the Balitsky-Kovchegov equation in the saturation domain, *Nucl. Phys. A* **764**, 498−−514, 2006.

[88] Kutak, K., Placzek, W. and Toton, D. Numerical solution of the integral form of the resummed Balitsky-Kovchegov equation, *Acta Physica Polonica B* **44**(7), 1527−−1536, 2013.

[89] Kutak, K., Surowka, P. Nonlinear evolution of unintegrated gluon density at large values of coupling constant, *Phys. Rev. D* **89**, 026007, 2014.

[90] Zhu, W. et al., Contributions of gluon recombination to saturation phenomena, *Phys. Rev. D* **68**, 094015, 2003.

Chapter 3

NNLO Analysis of Singlet and Non-singlet Structure Functions in the DGLAP Approach

3.1 Introduction

Structure functions in lepton-nucleon DIS are the entrenched observables exploring QCD. They are defined as convolution of the universal parton momentum distributions and coefficient functions, which contain information about the boson-parton interaction. Therefore the structure functions provide exclusive information about the deep structure of hadrons and most importantly, they form the backbone of our knowledge of the parton densities, which are indispensable for analyses of hard scattering processes. Thus the measurements of the structure functions allow perturbative QCD to be precisely tested. The standard and the basic tool for theoretical investigation of DIS structure functions are the DGLAP evolution equations [1-4]. Therefore the solutions of DGLAP evolution equations give quark and gluon distribution functions which ultimately produce proton, neutron and deuteron structure functions.

The solutions of the unpolarized DGLAP equation for the QCD evolution of structure functions have been discussed considerably over the past years. The standard and the most extensively used procedure of studying the hadron structure functions is via the numerical solution of these equations [5-10], with excellent agreement with the DIS data over a wide kinematic region in x and Q^2. However, apart from the

numerical solution, there is the alternative approach of studying analytically these equations at small-x. Although exact analytic solutions of the DGLAP equations cannot be obtained in the entire range of x and Q^2, such solutions are possible under certain conditions [11, 12] and many approximated analytical solutions of DGLAP evolution equations suitable at small-x, have been reported in recent years [13-22] with considerable phenomenological success.

The singlet and non-singlet structure functions in DIS i.e. the flavor independent and flavor dependent contributions to the structure functions play the key role for accurate determination of the quark and gluon densities and therefore they can be considered as the basis for the analysis of other structure functions. In this chapter, by using a Taylor series expansion valid at small-x, we first transform the DGLAP equation, which is an integro-differential equation, into a partial differential equation in the two variables (x, Q^2) and the resulting equation is then solved at LO, NLO and NNLO respectively by the Lagrange's auxiliary method. Inclusion of the NNLO contributions considerably reduces the theoretical uncertainty of determinations of the quark and gluon densities from DIS structure functions. Here, we investigate the impact of the NNLO contributions on the evolution of the singlet and non-singlet structure function respectively considering the corresponding DGLAP evolution equations. The singlet distribution is comparatively complicated to compute as it is coupled to the the gluon densities. We also calculate the Q^2-evolution of deuteron and proton structure functions upto NNLO from the solutions of singlet and non-singlet structure functions. Moreover the x-evolution of deuteron structure function is calculated upto NNLO. We compare our predictions with NMC [23], E665 [24], and H1 [25] experimental data as well as with the NNPDF [26] parametrization based on the NMC and BCDMS data.

3.2 Formalism

3.2.1 General framework

The singlet and non-singlet quark density of a hadron is given by [27]

$$q_S(x, Q^2) = \sum_{i=1}^{N_f} [q_i(x, Q^2) + \overline{q_i}(x, Q^2)], \tag{3.1}$$

$$q_{NS}(x,Q^2) = \sum_{i=1}^{N_f}[q_i(x,Q^2) - \overline{q_i}(x,Q^2)], \tag{3.2}$$

where $q_i(x,Q^2)$ and $\overline{q_i}(x,Q^2)$ represent the number distribution of quarks and anti-quarks, respectively, in the fractional hadron momentum x. The corresponding gluon distribution is denoted by $g(x,Q^2)$. The subscript i indicates the flavour of the quarks or anti-quarks and N_f is the number of effectively massless flavours.

The DGLAP evolution equation in the singlet sector in the standard form is given by [28]

$$\frac{\partial}{\partial \ln Q^2}\begin{pmatrix} q_S \\ g \end{pmatrix} = \begin{pmatrix} P_{qq} & P_{qg} \\ P_{gq} & P_{gg} \end{pmatrix} \otimes \begin{pmatrix} q_S \\ g \end{pmatrix}, \tag{3.3}$$

where P_{qq}, P_{qg}, P_{gq}, P_{gg} are splitting functions. The singlet structure function involves the quark-quark splitting function P_{qq} and gluon-quark splitting function P_{qg}, whereas non-singlet structure function involves only the quark-quark splitting function P_{qq}. The quark-quark splitting function P_{qq} can be expressed as a power series of $\alpha_s(Q^2)$ [10]

$$\begin{aligned} P_{qq}(x,Q^2) &= \frac{\alpha_s(Q^2)}{2\pi}P_{qq}^{(0)}(x) + \Big(\frac{\alpha_s(Q^2)}{2\pi}\Big)^2 P_{qq}^{(1)}(x) + \Big(\frac{\alpha_s(Q^2)}{2\pi}\Big)^3 P_{qq}^{(2)}(x) \\ &\quad + \mathcal{O}P_{qq}^{(3)}(x), \end{aligned} \tag{3.4}$$

where $P_{qq}^{(0)}(x)$, $P_{qq}^{(1)}(x)$ and $P_{qq}^{(2)}(x)$ are LO, NLO and NNLO quark-quark splitting functions respectively. Other splitting functions can be expressed in a similar way. The symbol $\otimes$ stands for the standard Mellin Convolution in the momentum variable defined as

$$a(x) \otimes b(x) \equiv \int_x^1 \frac{d\omega}{\omega} a(\omega) b\Big(\frac{x}{\omega}\Big). \tag{3.5}$$

Thus, using Eq. (3.5), Eq. (3.3) can be written as

$$\frac{\partial}{\partial \ln Q^2}\begin{pmatrix} q_S(x,Q^2) \\ g(x,Q^2) \end{pmatrix} = \int_x^1 \frac{d\omega}{\omega}\begin{pmatrix} P_{qq}(\omega) & P_{qg}(\omega) \\ P_{gq}(\omega) & P_{gg}(\omega) \end{pmatrix}\begin{pmatrix} q_S(x/\omega,Q^2) \\ g(x/\omega,Q^2), \end{pmatrix} \tag{3.6}$$

which implies

$$\frac{\partial q_S(x,Q^2)}{\partial \ln Q^2} = \int_x^1 \frac{d\omega}{\omega}\Big(P_{qq}(\omega)q_S(x/\omega,Q^2) + P_{qg}(\omega)g(x/\omega,Q^2)\Big), \tag{3.7}$$

$$\frac{\partial g(x,Q^2)}{\partial \ln Q^2} = \int_x^1 \frac{d\omega}{\omega}\Big(P_{gq}(\omega)q_S(x/\omega,Q^2) + P_{gg}(\omega)g(x/\omega,Q^2)\Big). \tag{3.8}$$

On the other hand, the DGLAP evolution equation in the non-singlet sector in the standard form is given by [29]

$$\frac{\partial q_{NS}(x,Q^2)}{\partial \ln Q^2} = P_{NS}(x,Q^2) \otimes q_{NS}(x,Q^2), \tag{3.9}$$

where $P_{NS}(x,Q^2)$ is the non-singlet kernel known perturbatively up to the first few orders in $\alpha_s(Q^2)$ [30]. Using equation (3.5), equations (3.9) can be expressed as

$$\frac{\partial q_{NS}(x,Q^2)}{\partial \ln Q^2} = \int_x^1 \frac{d\omega}{\omega} P_{NS}(\omega) q_{NS}(x/\omega, Q^2). \tag{3.10}$$

The quark-quark splitting function P_{qq} in equation (3.6) can be expressed as $P_{qq} = P_{NS} + N_f(P_{qq}^S + P_{\bar{q}q}^S) = P_{NS} + P_{PS}$. P_{qq}^S and $P_{\bar{q}q}^S$ are the flavor-independent contributions to the quark-quark and quark-antiquark splitting functions respectively. The non-singlet contribution P_{NS} dominates P_{qq} at large-x whereas at very small-x the pure singlet term P_{PS} dominates over P_{NS} [31]. The quark-gluon (P_{qg}) and gluon-quark (P_{gq}) entries in equation (3.6) are given by $P_{qg} = N_f P_{q_i g}$ and $P_{gq} = P_{gq_i}$, where $P_{q_i g}$ and P_{gq_i} are the flavor-independent splitting functions.

The running coupling constant $\alpha_S(Q^2)$ has the form [14, 32]

$$\frac{\alpha_s(Q^2)}{2\pi} = \frac{2}{\beta_0 \ln(Q^2/\Lambda^2)}, \tag{3.11}$$

$$\frac{\alpha_s(Q^2)}{2\pi} = \frac{2}{\beta_0 \ln(Q^2/\Lambda^2)} \Big[1 - \frac{\beta_1}{\beta_0^2} \frac{\ln\big(\ln(Q^2/\Lambda^2)\big)}{\ln(Q^2/\Lambda^2)}\Big], \tag{3.12}$$

$$\begin{aligned} \frac{\alpha_s(Q^2)}{2\pi} &= \frac{2}{\beta_0 \ln(Q^2/\Lambda^2)} \Big[1 - \frac{\beta_1}{\beta_0^2} \frac{\ln\big(\ln(Q^2/\Lambda^2)\big)}{\ln(Q^2/\Lambda^2)} + \frac{1}{\beta_0^3 \ln(Q^2/\Lambda^2)} \\ &\quad \times \Big\{ \frac{\beta_1^2}{\beta_0} (\ln^2\big(\ln(Q^2/\Lambda^2)\big) - \ln\big(\ln(Q^2/\Lambda^2)\big) - 1) + \beta_2 \Big\} \Big] \end{aligned} \tag{3.13}$$

at LO, NLO and NNLO respectively. Here

$$\begin{aligned} \beta_0 &= \frac{11}{3} N_c - \frac{4}{3} T_f = 11 - \frac{2}{3} N_f, \\ \beta_1 &= \frac{34}{3} N_c^2 - \frac{10}{3} N_c N_f - 2 C_F N_f = 102 - \frac{38}{3} N_f, \\ \beta_2 &= \frac{2857}{54} N_c^3 + 2 C_F^2 T_f - \frac{205}{9} C_F N_c T_f - \frac{1415}{27} N_c^2 T_f + \frac{44}{9} C_F T_f^2 + \frac{158}{27} N_c T_f^2 \\ &= \frac{2857}{2} - \frac{6673}{18} N_f + \frac{325}{54} N_f^2 \end{aligned}$$

are the one-loop, two-loop and three-loop corrections to the QCD β-function and N_f being the number of quark flavours. Here we use $N_f = 4$, $N_c = 3$. The Casimir operators of the color $SU(3)$ are defined as $C_F = \dfrac{N_c^2 - 1}{2N_c} = \dfrac{4}{3}$ and $T_f = \dfrac{1}{2} N_f$.

3.2.2 LO analysis of singlet and non-singlet structure functions

Substituting the explicit form of the LO splitting functions [4, 11] in Eqs. (3.7) and (3.10) and simplifying, the DGLAP evolution equations for singlet and non-singlet structure functions at LO can be written as

$$\frac{\partial F_2^S(x,t)}{\partial t} = \frac{\alpha_S(t)}{2\pi}\Big[\frac{2}{3}\{3+4\ln(1-x)\}F_2^S(x,t) + I_1^S(x,t)\Big], \tag{3.14}$$

$$\frac{\partial F_2^{NS}(x,t)}{\partial t} = \frac{\alpha_S(t)}{2\pi}\Big[\frac{2}{3}\{3+4\ln(1-x)\}F_2^{NS}(x,t) + I_1^{NS}(x,t)\Big], \tag{3.15}$$

where $F_2^S(x,t) = \sum_{i=1}^{N_f} e_i^2 x[q_i + \overline{q_i}]$, and $F_2^{NS}(x,t) = \sum_{i=1}^{N_f} e_i^2 x[q_i - \overline{q_i}]]$. The integral functions are given by

$$\begin{aligned} I_1^S(x,t) &= \frac{4}{3}\int_x^1 \frac{d\omega}{1-\omega}\Big[(1+\omega^2)F_2^S\Big(\frac{x}{\omega},t\Big) - 2F_2^S(x,t)\Big] \\ &\quad + N_f\int_x^1 \{\omega^2 + (1-\omega)^2\}G\Big(\frac{x}{\omega},t\Big)d\omega, \end{aligned} \tag{3.16}$$

$$I_1^{NS}(x,t) = \frac{4}{3}\int_x^1 \frac{d\omega}{1-\omega}\Big[(1+\omega^2)F_2^{NS}\Big(\frac{x}{\omega},t\Big) - 2F_2^{NS}(x,t)\Big]. \tag{3.17}$$

Here we use a more convenient variable t defined by $t = \ln\Big(\frac{Q^2}{\Lambda^2}\Big)$ with Λ being the QCD cut off parameter, the scale at which partons turn themselves into hadrons.

To simplify and reduce the integro-differential equation to a partial differential equation we introduce a variable $u = 1-\omega$ so that the argument x/ω can be expressed as

$$\frac{x}{\omega} = \frac{x}{1-u} = x + \frac{xu}{1-u}. \tag{3.18}$$

Since $x < \omega < 1$, so we have $0 < u < 1-x$. This implies that the above series is convergent for $|u| < 1$. Now using Eq. (3.18), we can expand $F_2^S(x/\omega,t)$ by Taylor expansion series as

$$\begin{aligned} F_2^S\Big(\frac{x}{\omega},t\Big) &= F_2^S\Big(x + \frac{xu}{1-u},t\Big) \\ &= F_2^S(x,t) + \Big(\frac{xu}{1-u}\Big)\frac{\partial F_2^S(x,t)}{\partial x} + \frac{1}{2}\Big(\frac{xu}{1-u}\Big)^2\frac{\partial^2 F_2^S(x,t)}{\partial^2 x} + \cdots. \end{aligned} \tag{3.19}$$

As x is small in our region of discussion, the terms containing x^2 and higher powers of x can be neglected and therefore Eq. (3.19) takes the form

$$F_2^S\Big(\frac{x}{\omega},t\Big) = F_2^S(x,t) + \frac{xu}{1-u}\frac{\partial F_2^S(x,t)}{\partial x}. \tag{3.20}$$

Similarly,

$$G\Big(\frac{x}{\omega},t\Big) = G(x,t) + \frac{xu}{1-u}\frac{\partial G(x,t)}{\partial x}, \tag{3.21}$$

$$F_2^{NS}\Big(\frac{x}{\omega},t\Big) = F_2^{NS}(x,t) + \frac{xu}{1-u}\frac{\partial F_2^{NS}(x,t)}{\partial x}. \tag{3.22}$$

Putting Eqs. (3.20) and (3.21) in Eq. (3.16) and carrying out the integrations in u we get from Eq. (3.14)

$$\begin{aligned}\frac{\partial F_2^S(x,t)}{\partial t} &= \frac{\alpha_S(t)}{2\pi}\Big[A_1(x)F_2^S(x,t) + A_2(x)\frac{\partial F_2^S(x,t)}{\partial x} + A_3(x)G(x,t) \\ &\quad + A_4(x)\frac{\partial G(x,t)}{\partial x}\Big],\end{aligned} \tag{3.23}$$

where $A_i(x)$ (i=1,2,3,4) are functions of x (see Appendix A). Eq.(3.23) is a first order partial differential equation for the singlet structure function $F_2^S(x,t)$ with respect to the variables x and t. Beyond its traditional use in t or Q^2-evolution ($t = \ln(Q^2/\Lambda^2)$), it also provides x-evolution at small-x. There are various methods for solving the partial differential equations in two variables. We here adopt the Lagrange's auxiliary method as mentioned in the introduction.

The Q^2-evolution of the proton structure function $F_2(x,Q^2)$ is related to the gluon parton densities in the proton $G(x,Q^2)$ and to the strong interaction coupling constant α_S. The gluon parton densities cannot be measured directly through experiments. It is, therefore, important to measure the $G(x,Q^2)$ indirectly using $F_2(x,Q^2)$. Hence the direct relations between $F_2(x,Q^2)$ and the $G(x,Q^2)$ are extremely important because using those relations the experimental values of $G(x,Q^2)$ can be extracted using the data on $F_2(x,Q^2)$. Therefore, in the analytical solutions of DGLAP evolution equations for singlet structure functions or gluon parton densities, a relation between singlet structure function and gluon parton densities has to be assumed. The commonly used relation is $G(x,t) = K(x)F_2^S(x,t)$ [15, 16, 19], where $K(x)$ is a parameter to be determined from phenomenological analysis. We can consider this form as the evolution equations of gluon parton densities and singlet structure functions are in the same forms of derivative with respect to t. Moreover the input singlet and gluon parameterizations, taken from global analysis of PDFs, in particular from the MSTW08 parton set, to incorporate different high precision data, are also functions of x at fixed Q^2 [33]. So the relation between singlet structure function and gluon parton densities will come out in terms of x at fixed-Q^2. However,

the actual functional form of $K(x)$ can be determined by simultaneous solutions of coupled equations of singlet structure functions and gluon parton densities. Further discussions on $K(x)$ are presented in Appendix G.

Hence Eq.(3.23) takes the form

$$-t\frac{\partial F_2^S(x,t)}{\partial t} + L_1^S(x)\frac{\partial F_2^S(x,t)}{\partial x} + M_1^S(x)F_2^S(x,t) = 0, \tag{3.24}$$

where

$$L_1^S(x) = A_f\Big[A_2(x) + K(x)A_4(x)\Big], \tag{3.25}$$

$$M_1^S(x) = A_f\Big[A_1(x) + K(x)A_3(x) + \frac{\partial K(x)}{\partial x}A_4(x)\Big], \tag{3.26}$$

with $A_f{=}\frac{2}{\beta_0}$. Now the general solution of the Eq.(3.24) is

$$F(U,V) = 0, \tag{3.27}$$

where $F(U,V)$ is an arbitrary function of U and V. Here, $U(x,t,F_2^S) = k_1$ and $V(x,t,F_2^S) = k_2$ are two independent solutions of the Lagrange's equation

$$\frac{\partial x}{L_1^S(x)} = \frac{\partial t}{-t} = \frac{\partial F_2^S(x,t)}{-M_1^S(x)F_2^S(x,t)}. \tag{3.28}$$

Then by solving Eq. (3.28) we obtain

$$U(x,t,F_2^S) = t\cdot\exp\Big[\int\frac{1}{L_1^S(x)}dx\Big], \tag{3.29}$$

$$V(x,t,F_2^S) = F_2^S(x,t)\cdot\exp\Big[\int\frac{M_1^S(x)}{L_1^S(x)}dx\Big]. \tag{3.30}$$

Thus we see that it has no unique solution. In this approach we attempt to extract a particular solution that obeys some physical constraints on the structure function. The simplest possibility to get a solution is that a linear combination of U and V should obey the Eq. (3.27) so that

$$\alpha\cdot U + \beta\cdot V = 0, \tag{3.31}$$

where α and β are arbitrary constants to be determined from the boundary conditions on F_2^S. Putting the values of U and V from Eq.(3.29) and Eq.(3.30) in this equation we get

$$\alpha t\cdot\exp\Big[\int\frac{1}{L_1^S(x)}dx\Big] + \beta F_2^S(x,t)\cdot\exp\Big[\int\frac{M_1^S(x)}{L_1^S(x)}dx\Big] = 0, \tag{3.32}$$

which implies

$$F_2^S(x,t) = -\gamma t \cdot \exp\Big[\int \big(\frac{1}{L_1^S(x)} - \frac{M_1^S(x)}{L_1^S(x)}\big)dx\Big], \tag{3.33}$$

where $\gamma = \frac{\alpha}{\beta}$ is a constant. Now at $t = t_0$, where $t_0 = \ln\Big(\frac{Q_0^2}{\Lambda^2}\Big)$ for any lower value $Q^2 = Q_0^2$, we define

$$F_2^S(x,t_0) = -\gamma t_0 \cdot \exp\Big[\int \big(\frac{1}{L_1^S(x)} - \frac{M_1^S(x)}{L_1^S(x)}\big)dx\Big]. \tag{3.34}$$

Then Eqs. (3.33) and (3.34) lead us to

$$F_2^S(x,t) = F_2^S(x,t_0)\Big(\frac{t}{t_0}\Big). \tag{3.35}$$

This gives the t-evolution for singlet structure function at LO at small-x. Again defining at a higher value of $x = x_0$,

$$F_2^S(x_0,t) = -\gamma t \cdot \exp\Big[\int \big(\frac{1}{L_1^S(x)} - \frac{M_1^S(x)}{L_1^S(x)}\big)dx\Big]_{x=x_0}, \tag{3.36}$$

we obtain

$$F_2^S(x,t) = F_2^S(x_0,t) \cdot \exp\Big[\int_{x_0}^{x} \big(\frac{1}{L_1^S(x)} - \frac{M_1^S(x)}{L_1^S(x)}\big)dx\Big]. \tag{3.37}$$

This gives the x-evolutions of singlet structure functions at LO.

Now substituting the approximated form of Taylor expansion of non-singlet structure function from Eq.(3.22) in Eq.(3.17) and performing u-integrations we obtain from Eq.(3.15)

$$\frac{\partial F_2^{NS}(x,t)}{\partial t} = \frac{\alpha_S(t)}{2\pi}\Big[A_1(x)F_2^{NS}(x,t) + A_2(x)\frac{\partial F_2^{NS}(x,t)}{\partial x}\Big], \tag{3.38}$$

which we can rewrite as

$$-t\frac{\partial F_2^{NS}(x,t)}{\partial t} + L_1^{NS}(x)\frac{\partial F_2^{NS}(x,t)}{\partial x} + M_1^{NS}(x)F_2^{NS}(x,t) = 0. \tag{3.39}$$

Here

$$L_1^{NS}(x) = A_f A_2(x), \tag{3.40}$$

$$M_1^{NS}(x) = A_f A_1(x). \tag{3.41}$$

Proceeding in the same way as the singlet case we solve Eq. (3.39) for non-singlet structure function and obtain

$$F_2^{NS}(x,t) = F_2^{NS}(x,t_0)\Big(\frac{t}{t_0}\Big) \tag{3.42}$$

and

$$F_2^{NS}(x,t) = F_2^{NS}(x_0,t) \cdot \exp\Big[\int_{x_0}^{x} \big(\frac{1}{L_1^{NS}(x)} - \frac{M_1^{NS}(x)}{L_1^{NS}(x)}\big)dx\Big], \tag{3.43}$$

which give the t and x-evolutions of non-singlet structure functions respectively at LO respectively.

For phenomenological analysis, we compare our results with various experimental structure functions. The deuteron structure function measured in DIS can be written in terms of the singlet structure function respectively as [11]

$$F_2^d(x,t) = \frac{5}{9}F_2^S(x,t). \tag{3.44}$$

Again the proton structure function measured in DIS can be expressed in terms of the singlet and non-singlet structure function as [11]

$$F_2^p(x,t) = \frac{5}{18}F_2^S(x,t) + \frac{3}{18}F_2^{NS}(x,t). \tag{3.45}$$

Substituting Eqs. (3.35) and (3.37) in Eq. (3.44), the t and x-evolutions of deuteron structure function at LO can be obtained as

$$F_2^d(x,t) = F_2^d(x,t_0)\Big(\frac{t}{t_0}\Big) \tag{3.46}$$

and

$$F_2^d(x,t) = F_2^d(x_0,t) \cdot \exp\Big[\int_{x_0}^{x} \big(\frac{1}{\overline{L_1^S}(x)} - \frac{\overline{M_1^S}(x)}{\overline{L_1^S}(x)}\big)dx\Big]. \tag{3.47}$$

Here the input functions are $F_2^d(x,t_0) = \frac{5}{9}F_2^S(x,t_0)$ and $F_2^d(x_0,t) = \frac{5}{9}F_2^S(x_0,t)$.

On the other hand, substituting Eqs. (3.35) and (3.42) in Eq. (3.45), we get the t-evolutions of proton structure function at LO

$$F_2^p(x,t) = F_2^p(x,t_0)\Big(\frac{t}{t_0}\Big), \tag{3.48}$$

with the input function is $F_2^p(x,t_0) = \frac{5}{18}F_2^S(x,t_0) + \frac{3}{18}F_2^{NS}(x,t_0)$. It is to be noted that the determination of x-evolution of proton structure function like that of deuteron structure function is not suitable by the method adopted here. The reason is that in order to calculate the x-evolution of proton structure function, we have to put Eqs. (3.37) and (3.43) in Eq. (3.45). But the functions inside the integral sign of Eqs. (3.37) and (3.43) are different and so the the input functions $F_2^S(x_0,t)$ and $F_2^{NS}(x_0,t)$ have to be separated from the data points to extract the x-evolution of the proton function, which may contain large errors.

3.2.3 NLO analysis of singlet and non-singlet structure functions

Considering the splitting functions at NLO [12, 34, 35], the DGLAP equations for singlet and non-singlet structure functions at NLO in standard form can be written as

$$\begin{aligned}\frac{\partial F_2^S(x,t)}{\partial t} &= \frac{\alpha_S(t)}{2\pi}\Big[\frac{2}{3}\{3+4\ln(1-x)\}F_2^S(x,t)+I_1^S(x,t)\Big] \\ &\quad+\Big(\frac{\alpha_S(t)}{2\pi}\Big)^2 I_2^S(x,t), \end{aligned} \tag{3.49}$$

$$\begin{aligned}\frac{\partial F_2^{NS}(x,t)}{\partial t} &= \frac{\alpha_S(t)}{2\pi}\Big[\frac{2}{3}\{3+4\ln(1-x)\}F_2^{NS}(x,t)+I_1^{NS}(x,t)\Big] \\ &\quad+\Big(\frac{\alpha_S(t)}{2\pi}\Big)^2 I_2^{NS}(x,t). \end{aligned} \tag{3.50}$$

The integral functions $I_1^S(x,t)$ and $I_1^{NS}(x,t)$ are defined in Eqs. (3.16) and (3.17), whereas

$$\begin{aligned}I_2^S(x,t) &= (x-1)F_2^S(x,t)\int_0^1 f(\omega)d\omega+\int_x^1 f(\omega)F_2^S\Big(\frac{x}{\omega},t\Big)d\omega \\ &\quad+\int_x^1 F_{qq}^S(\omega)F_2^S\Big(\frac{x}{\omega},t\Big)d\omega+\int_x^1 F_{qg}^S(\omega)G\Big(\frac{x}{\omega},t\Big)d\omega, \end{aligned} \tag{3.51}$$

$$I_2^{NS}(x,t)=(x-1)F_2^{NS}(x,t)\int_0^1 f(\omega)d\omega+\int_x^1 f(\omega)F_2^{NS}\Big(\frac{x}{\omega},t\Big)d\omega. \tag{3.52}$$

The explicit forms of the functions $f(\omega)$, $F_{qq}^S(\omega)$ and $F_{qg}^S(\omega)$ are given in Appendix B.

Following the same procedure as in LO, the Eqs. (3.49) and (3.50) can be simplified as

$$-t\frac{\partial F_2^S(x,t)}{\partial t}+L_2^S(x)\frac{\partial F_2^S(x,t)}{\partial x}+M_2^S(x)F_2^S(x,t)=0, \tag{3.53}$$

$$-t\frac{\partial F_2^{NS}(x,t)}{\partial t}+L_2^{NS}(x)\frac{\partial F_2^{NS}(x,t)}{\partial x}+M_2^{NS}(x)F_2^{NS}(x,t)=0. \tag{3.54}$$

Here

$$L_2^S(x)=A_f\Big[\Big(A_2(x)+K(x)A_4(x)\Big)+T_0\Big(B_2(x)+K(x)B_4(x)\Big)\Big], \tag{3.55}$$

$$\begin{aligned}M_2^S(x) &= A_f\Big[\Big(A_1(x)+K(x)A_3(x)+\frac{\partial K(x)}{\partial x}A_4(x)\Big) \\ &\quad+T_0\Big(B_1(x)+K(x)B_3(x)+\frac{\partial K(x)}{\partial x}B_4(x)\Big)\Big], \end{aligned} \tag{3.56}$$

$$L_2^{NS}(x) = A_f\Big[A_2(x) + T_0 B_2(x)\Big], \tag{3.57}$$

$$M_2^{NS}(x) = A_f\Big[A_1(x) + T_0 B_1(x)\Big], \tag{3.58}$$

with $B_i(x)$ (i=1,2,3,4) being the functions of x (see Appendix A). Here we consider the numerical parameter T_0 such that $T^2(t) = T_0 T(t)$ where $T(t)=\frac{\alpha_S(t)}{2\pi}$ and the value of T_0 is determined by phenomenological analysis. This numerical parameter is obtained from a particular range of Q^2 under study and by a suitable choice of T_0 we can reduce the difference between $T^2(t)$ and $T_0 T(t)$ to a minimum. Thus the consideration of the parameter T_0 does not give any abrupt change in our result.

Solving Eq. (3.53) we obtain the t and x-evolutions of singlet structure function at NLO as

$$F_2^S(x,t) = F_2^S(x,t_0)\Big(\frac{t^{1+b/t}}{t_0^{1+b/t_0}}\Big)\cdot\exp\Big(\frac{b}{t}-\frac{b}{t_0}\Big) \tag{3.59}$$

and

$$F_2^S(x,t) = F_2^S(x_0,t)\cdot\exp\Big[\int_{x_0}^{x}\big(\frac{1}{L_2^S(x)}-\frac{M_2^S(x)}{L_2^S(x)}\big)dx\Big], \tag{3.60}$$

where $b=\frac{\beta_1}{\beta_0^2}$. The input functions are defined as

$$F_2^S(x,t_0) = -\gamma t_0^{(1+b/t_0)}\cdot\exp\Big(\frac{b}{t_0}\Big)\cdot\exp\Big[\int\big(\frac{1}{L_2^S(x)}-\frac{M_2^S(x)}{L_2^S(x)}\big)dx\Big], \tag{3.61}$$

$$F_2^S(x_0,t) = -\gamma t^{(1+b/t)}\cdot\exp\Big(\frac{b}{t}\Big)\cdot\exp\Big[\int\big(\frac{1}{L_2^S(x)}-\frac{M_2^S(x)}{L_2^S(x)}\big)dx\Big]_{x=x_0}. \tag{3.62}$$

Now substituting Eqs. (3.59) and (3.60) in Eq. (3.44) we get

$$F_2^d(x,t) = F_2^d(x,t_0)\Big(\frac{t^{1+b/t}}{t_0^{1+b/t_0}}\Big)\cdot\exp\Big(\frac{b}{t}-\frac{b}{t_0}\Big) \tag{3.63}$$

and

$$F_2^d(x,t) = F_2^d(x_0,t)\cdot\exp\Big[\int_{x_0}^{x}\big(\frac{1}{L_2^S(x)}-\frac{M_2^S(x)}{L_2^S(x)}\big)dx\Big], \tag{3.64}$$

which lead us to the t and x-evolutions of deuteron structure function at NLO.

Similarly the t and x-evolutions of the non-singlet structure function at NLO are calculated from Eq. (3.54) and given by

$$F_2^{NS}(x,t) = F_2^{NS}(x,t_0)\Big(\frac{t^{1+b/t}}{t_0^{1+b/t_0}}\Big)\cdot\exp\Big(\frac{b}{t}-\frac{b}{t_0}\Big) \tag{3.65}$$

and

$$F_2^{NS}(x,t) = F_2^{NS}(x_0,t)\cdot\exp\Big[\int_{x_0}^{x}\big(\frac{1}{L_2^{NS}(x)} - \frac{M_2^{NS}(x)}{L_2^{NS}(x)}\big)dx\Big]. \tag{3.66}$$

Thus putting Eqs. (3.59) and (3.65) in Eq. (3.45) we get

$$F_2^{p}(x,t) = F_2^{p}(x,t_0)\Big(\frac{t^{1+b/t}}{t_0^{1+b/t_0}}\Big)\cdot\exp\Big(\frac{b}{t}-\frac{b}{t_0}\Big), \tag{3.67}$$

which lead us to the t-evolution of proton structure function at NLO. It is not possible to evaluate the x-evolution of proton structure function with the present method for the same reason mentioned earlier.

3.2.4 NNLO analysis of singlet and non-singlet structure functions

Using the splitting functions upto NNLO and simplifying [28-31], we get the DGLAP equations for singlet and non-singlet structure functions at NNLO as

$$\begin{aligned}\frac{\partial F_2^S(x,t)}{\partial t} &= \frac{\alpha_S(t)}{2\pi}\Big[\frac{2}{3}\{3+4\ln(1-x)\}F_2^S(x,t)+I_1^S(x,t)\Big]\\ &\quad+\Big(\frac{\alpha_S(t)}{2\pi}\Big)^2 I_2^S(x,t)+\Big(\frac{\alpha_S(t)}{2\pi}\Big)^3 I_3^S(x,t),\end{aligned} \tag{3.68}$$

$$\begin{aligned}\frac{\partial F_2^{NS}(x,t)}{\partial t} &= \frac{\alpha_S(t)}{2\pi}\Big[\frac{2}{3}\{3+4\ln(1-x)\}F_2^{NS}(x,t)+I_1^{NS}(x,t)\Big]\\ &\quad+\Big(\frac{\alpha_S(t)}{2\pi}\Big)^2 I_2^{NS}(x,t)+\Big(\frac{\alpha_S(t)}{2\pi}\Big)^3 I_3^{NS}(x,t).\end{aligned} \tag{3.69}$$

The integral functions I_3^S and I_3^{NS} are given by

$$I_3^S(x,t) = \int_x^1\frac{d\omega}{\omega}\Big[P_{qq}(x)F_2^S\Big(\frac{x}{\omega},t\Big)+P_{qg}(x)G\Big(\frac{x}{\omega},t\Big)\Big], \tag{3.70}$$

$$I_3^{NS}(x,t) = \int_x^1\frac{d\omega}{\omega}P_{NS}^2(x)F_2^{NS}\Big(\frac{x}{\omega},t\Big). \tag{3.71}$$

The explicit forms of the functions $P_{qq}(x)$, $P_{qg}(x)$ and $P_{NS}^2(x)$ are given in Appendix C.

Here we consider the numerical parameter T_1 such that $T^3(t) = T_1T(t)$ where $T(t)$=$\frac{\alpha_S(t)}{2\pi}$. The value of T_1 is determined by phenomenological analysis, like T_0, from a particular range of Q^2 under study and by an appropriate choice of T_1 we can reduce the error to a minimum. Thus Eqs. (3.68) and (3.69) can be simplified as

$$-t\frac{\partial F_2^S(x,t)}{\partial t}+L_3^S(x)\frac{\partial F_2^S(x,t)}{\partial x}+M_3^S(x)F_2^S(x,t)=0, \tag{3.72}$$

$$-t\frac{\partial F_2^{NS}(x,t)}{\partial t} + L_3^{NS}(x)\frac{\partial F_2^{NS}(x,t)}{\partial x} + M_3^{NS}(x)F_2^{NS}(x,t) = 0. \tag{3.73}$$

Here

$$\begin{aligned} L_3^S(x) &= A_f\Big[\Big(A_2(x) + K(x)A_4(x)\Big) + T_0\Big(B_2(x) + K(x)B_4(x)\Big) \\ &\quad + T_1\Big(C_2(x) + K(x)C_4(x)\Big)\Big], \end{aligned} \tag{3.74}$$

$$\begin{aligned} M_3^S(x) &= A_f\Big[\Big(A_1(x) + K(x)A_3(x) + \frac{\partial K(x)}{\partial x}A_4(x)\Big) + T_0\Big(B_1(x) \\ &\quad + K(x)B_3(x) + \frac{\partial K(x)}{\partial x}B_4(x)\Big) + T_1\Big(C_1(x) + K(x)C_3(x) \\ &\quad + \frac{\partial K(x)}{\partial x}C_4(x)\Big)\Big], \end{aligned} \tag{3.75}$$

$$L_3^{NS}(x) = A_f\Big[A_2(x) + T_0B_2(x) + T_1C_2(x)\Big], \tag{3.76}$$

$$M_2^{NS}(x) = A_f\Big[A_1(x) + T_0B_1(x) + T_1C_1(x)\Big] \tag{3.77}$$

with $C_i(x)$ (i=1,2,3,4) being the functions of x (see Appendix A).

We solve Eq. (3.72) following the same procedure as earlier and obtain the t and x-evolutions of singlet structure function at NNLO given by

$$F_2^S(x,t) = F_2^S(x,t_0)\Big(\frac{t^{1+(b-b^2)/t}}{t_0^{1+(b-b^2)/t_0}}\Big)\cdot\exp\Big(\frac{b-c-b^2\ln^2 t}{t} - \frac{b-c-b^2\ln^2 t_0}{t_0}\Big) \tag{3.78}$$

and

$$F_2^S(x,t) = F_2^S(x_0,t)\cdot\exp\Big[\int_{x_0}^{x}\big(\frac{1}{L_3^S(x)} - \frac{M_3^S(x)}{L_3^S(x)}\big)dx\Big] \tag{3.79}$$

respectively. The input functions are defined as

$$\begin{aligned} F_2^S(x,t_0) &= -\gamma t_0^{(1+(b-b^2)/t_0)}\cdot\exp\Big(\frac{b-c-b^2\ln^2 t_0}{t_0}\Big)\cdot\exp\Big[\int\big(\frac{1}{L_3^S(x)} \\ &\quad - \frac{M_3^S(x)}{L_3^S(x)}\big)dx\Big], \end{aligned} \tag{3.80}$$

$$\begin{aligned} F_2^S(x_0,t) &= -\gamma t^{(1+(b-b^2)/t)}\cdot\exp\Big(\frac{b-c-b^2\ln^2 t}{t}\Big)\cdot\exp\Big[\int\big(\frac{1}{L_3^S(x)} \\ &\quad - \frac{M_3^S(x)}{L_3^S(x)}\big)dx\Big]_{x=x_0} \end{aligned} \tag{3.81}$$

with $b = \frac{\beta_1}{\beta_0^2}, c = \frac{\beta_2}{\beta_0^3}$. Accordingly substituting Eqs. (3.78) and (3.79) in Eq. (3.44) we get

$$F_2^d(x,t) = F_2^d(x,t_0)\Big(\frac{t^{1+(b-b^2)/t}}{t_0^{1+(b-b^2)/t_0}}\Big)\cdot\exp\Big(\frac{b-c-b^2\ln^2 t}{t}-\frac{b-c-b^2\ln^2 t_0}{t_0}\Big) \tag{3.82}$$

and

$$F_2^d(x,t) = F_2^d(x_0,t)\cdot\exp\Big[\int_{x_0}^{x}\big(\frac{1}{L_3^S(x)}-\frac{M_3^S(x)}{L_3^S(x)}\big)dx\Big], \tag{3.83}$$

which provide us the t and x-evolutions of deuteron structure functions at NNLO. Thus using Eq.(3.82) we can calculate the evolution of deuteron structure function with t or Q^2 at fixed x at NNLO by choosing an appropriate input distribution $F_2^d(x,t_0)$ at $Q^2 = Q_0^2$. Similarly Eq.(3.83) helps us to estimate the x-evolution of deuteron structure function at fixed t or Q^2 with a suitable input distribution $F_2^d(x_0,t)$ at a given value $x = x_0$.

Similarly, the solution of (3.73) provide us the t and x-evolutions of the non-singlet structure function given by

$$F_2^{NS}(x,t) = F_2^{NS}(x,t_0)\Big(\frac{t^{1+(b-b^2)/t}}{t_0^{1+(b-b^2)/t_0}}\Big)\cdot\exp\Big(\frac{b-c-b^2\ln^2 t}{t}-\frac{b-c-b^2\ln^2 t_0}{t_0}\Big) \tag{3.84}$$

and

$$F_2^{NS}(x,t) = F_2^{NS}(x_0,t)\cdot\exp\Big[\int_{x_0}^{x}\big(\frac{1}{L_3^{NS}(x)}-\frac{M_3^{NS}(x)}{L_3^{NS}(x)}\big)dx\Big] \tag{3.85}$$

respectively. The input functions are defined as

$$\begin{aligned} F_2^{NS}(x,t_0) &= -\gamma t_0^{(1+(b-b^2)/t_0)}\cdot\exp\Big(\frac{b-c-b^2\ln^2 t_0}{t_0}\Big)\cdot\exp\Big[\int\big(\frac{1}{L_3^{NS}(x)} \\ &\quad -\frac{M_3^{NS}(x)}{L_3^{NS}(x)}\big)dx\Big], \end{aligned} \tag{3.86}$$

$$\begin{aligned} F_2^{NS}(x_0,t) &= -\gamma t^{(1+(b-b^2)/t)}\cdot\exp\Big(\frac{b-c-b^2\ln^2 t}{t}\Big)\cdot\exp\Big[\int\big(\frac{1}{L_3^{NS}(x)} \\ &\quad -\frac{M_3^{NS}(x)}{L_3^{NS}(x)}\big)dx\Big]_{x=x_0}. \end{aligned} \tag{3.87}$$

Thus putting Eq.(3.78) and Eq. (3.84) in Eq.(3.45) we obtain

$$F_2^p(x,t) = F_2^p(x,t_0)\Big(\frac{t^{1+(b-b^2)/t}}{t_0^{1+(b-b^2)/t_0}}\Big)\cdot\exp\Big(\frac{b-c-b^2\ln^2 t}{t}-\frac{b-c-b^2\ln^2 t_0}{t_0}\Big), \tag{3.88}$$

which gives the t-evolution of proton structure function. By considering a suitable input distribution $F_2^p(x,t_0)$ at a given value $Q^2 = Q_0^2$, we can determine the evolution of proton structure function with t or Q^2 at some fixed x from Eq.(3.88). The x evolution of proton structure function is not possible at NNLO for the same reason discussed earlier.

For phenomenological analysis of t-evolution, we take the input distributions $F_2^d(x,t_0)$ and $F_2^p(x,t_0)$ from experimental data corresponding to the lowest value of the Q^2 range considered in our study. Similarly the input functions $F_2^d(x_0,t)$ for phenomenological analysis of x-evolution are taken from the experimental data corresponding to the highest value of the x range under consideration.

3.3 Result and discussion

In this chapter, we calculate the Q^2 or t ($t = \ln(Q^2/\Lambda^2)$) and x-evolutions of singlet and non-singlet structure functions. The deuteron and proton structure functions are related to the singlet and non-singlet structure functions as given by the Eqs. (3.48) and (3.49). We calculate the t and x-evolutions of deuteron stucture function at LO, NLO and NNLO respectively. The t-evolution of proton structure function is also obtained up to NNLO. We test the validity of the solutions, by comparing them directly with the available data on deuteron and proton structure function. For our analysis we use the data from the fixed target experiments viz. the NMC [23] in muon-deuteron DIS from the merged data sets at incident momenta 90, 120, 200 and 280 GeV^2, the Fermilab E665 [24] collaboration in muon-deuteron DIS at an average beam energy of 470 GeV^2 and the H1 collaboration of HERA experiment data [25] taken with a 26.7 GeV electron beam in collision with a 820 GeV proton beam. We consider the H1 1995 data because these data sets are available in the range of our consideration. Moreover, we compare our results with those obtained by the fit to F_2^d produced by the NNPDF parametrization [26]. The NNPDF parametrization presents a determination of the probability density in the space of F_2 structure functions for the proton, deuteron and non-singlet structure function, as determined from experimental data of NMC [23], E665 [24], BCDMS [36] and H1 [37] collaborations. Their results take the form of a set of 1000 neural nets, for each of the three structure functions, which give a determination of F_2 for given x and Q^2. The central value and

the errors of the structure functions determined in the NNPDF fit can be computed out of the ensemble of 1000 nets according to standard Monte Carlo techniques. We consider the range $0.0045 \leq x \leq 0.19$ and $0.75 \leq Q^2 \leq 27$ GeV^2 for NMC data, $0.0052 \leq x \leq 0.18$ and $1.094 \leq Q^2 \leq 26$ GeV^2 for E665 data and $0.004 \leq x \leq 0.03$ and $5.5 \leq Q^2 \leq 38$ GeV^2 for H1 data for our phenomenological analysis. Similarly we use the range $0.0045 \leq x \leq 0.095$ and $1.25 \leq Q^2 \leq 26$ GeV^2 to compare our results with the NNPDF parametrization. For the fit we consider $\Lambda_{\overline{MS}} = 323$ MeV for $\alpha_s(M_z^2) = 0.119 \pm 0.002$. The vertical error bars represent the total combined statistical and systematic uncertainties of the experimental data. To compute the dependence of structure functions on Q^2 or in other words for t-evolution, we take the input distributions from the data point corresponding to the lowest value of Q^2 for a particular range of Q^2 under study. Similarly the data point corresponding to the highest value of x of a particular range of x under consideration are taken as input distribution to determine the x dependence of the structure functions.

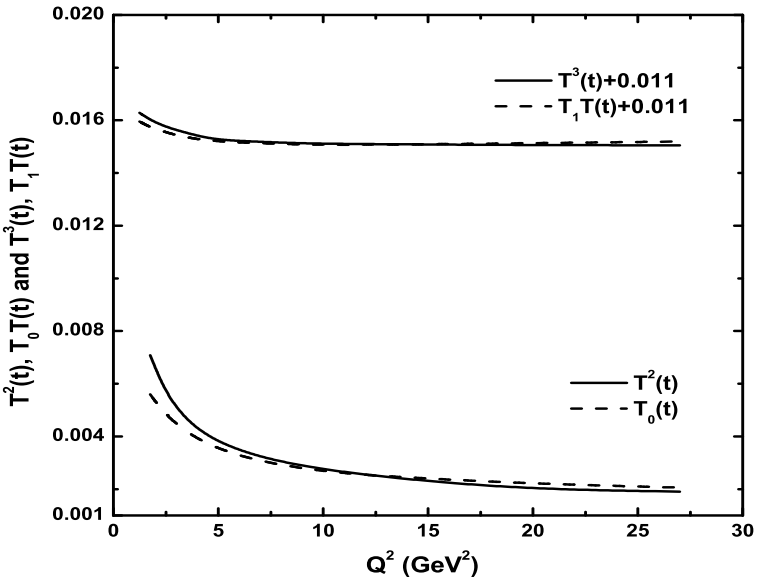

Figure 3.1: Comparison of T^2 and $T_0.T(t)$ as well as T^3 and $T_1.T(t)$ versus Q^2.

As mentioned earlier for the analytical solution of DGLAP evolution equation for singlet structure function we consider a function $K(x)$ which relates the singlet structure function and gluon densities. For simplicity we consider the function $K(x) = K$, where K is an arbitrary constant parameter. We examine the dependence of our predictions on the values of the arbitrary constant K and find that the best fit results

are obtained in the range $0.45 < K < 1.6$ for our entire region of discussion.

As discussed in section 3.2 the numerical parameters T_0 and T_1, considered for the solutions of the DGLAP equations at NLO and NNLO respectively, are obtained for a particular domain of Q^2 under study. To this end in Figure 3.1 we plot $T^2(t)$ and $T_0T(t)$ as well as $T^3(t)$ and $T_1T(t)$ as a function of Q^2. We find that for $T_0 = 0.048$ the difference between $T^2(t)$ and $T_0T(t)$ is reduced to a minimum and for $T_1 = 0.008$ the difference between $T^3(t)$ and $T_1T(t)$ becomes negligible in the range $0.75 < Q^2 < 50$ GeV^2. Therefore the consideration of the parameters T_0 and T_1 does not induce any unexpected change in our results.

In Figure 3.2 we plot the predictions of the deuteron structure function obtained from Eqs.(3.46), (3.63) and (3.82) for LO, NLO and NNLO respectively as functions of Q^2 at four representative values $x = 0.0045, 0.0125, 0.0175$ and 0.025 respectively. Here we compare our results with the NMC experimental data in the range $0.75 \leq Q^2 \leq 27$ GeV^2.

In Figure 3.3 we plot our our set of solutions Eqs. (3.47), (3.64) and (3.83) for deuteron structure function at LO, NLO and NNLO respectively as functions of x for four fixed $Q^2 = 7, 11.5, 20$ and 27 GeV^2 respectively. Our predictions are compared with the NMC experimental data in the range $0.0045 \leq x \leq 0.19$.

Figure 3.4 represent the comparison of our results of t or Q^2 evolution of deuteron structure function calculated from Eqs.(3.46), (3.63) and (3.82) for LO, NLO and NNLO respectively with the E665 experimental data. Here we plot our predictions of deuteron structure function as functions of Q^2 considering the range $1.094 \leq Q^2 \leq 26$ GeV^2 at fixed values of x, viz. $x = 0.0052, 0.00893, 0.0125$ and 0.0173 respectively.

In Figure 3.5 we plot our computed results of deuteron structure function obtained from Eqs.(3.47), (3.64) and (3.83) for LO, NLO and NNLO respectively as functions of x and compare with the E665 experimental data considering the range $0.0052 \leq x \leq 0.18$. The comparison is shown for four fixed $Q^2 = 5.236, 9.795, 18.323$ and 25.061 GeV^2 respectively.

Figure 3.6 shows the Q^2 evolution of deuteron structure function obtained from Eqs.(3.46), (3.63) and (3.82) at LO, NLO and NNLO respectively compared with the NNPDF parametrization in the range $1.25 \leq Q^2 \leq 26$ GeV^2. We perform the comparison for four different values of x, x=0.0045, 0.008, 0.0125 and 0.0175

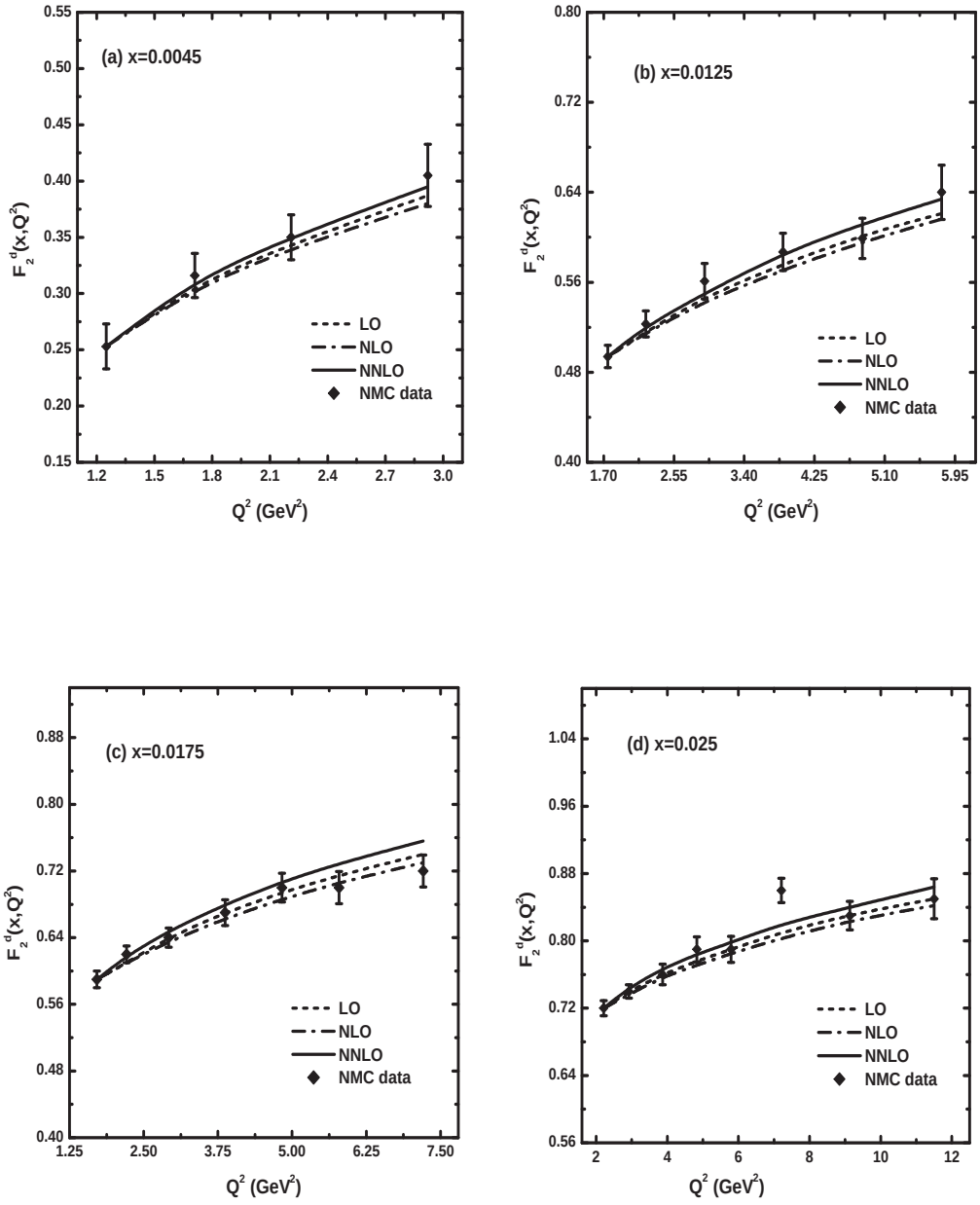

Figure 3.2: Comparison of Q^2 evolution of deuteron structure functions at LO, NLO and NNLO with the NMC data for four fixed values x. The dot lines represent the LO results (Eq.3.46), dash-dot lines represent the NLO results (Eq.3.63) and solid lines represent the NNLO results Eq.(3.82).

respectively.

In Figure 3.7 show the comparison of our results of x-evolutions of deuteron structure function obtained from Eqs.(3.47), (3.64) and (3.83) at LO, NLO and NNLO with those obtained by the NNPDF parametrization in the range $0.0045 \leq x \leq 0.095$. The comparison is done for four fixed values of Q^2 viz. $Q^2 = 5, 9, 15$ and 25 GeV^2

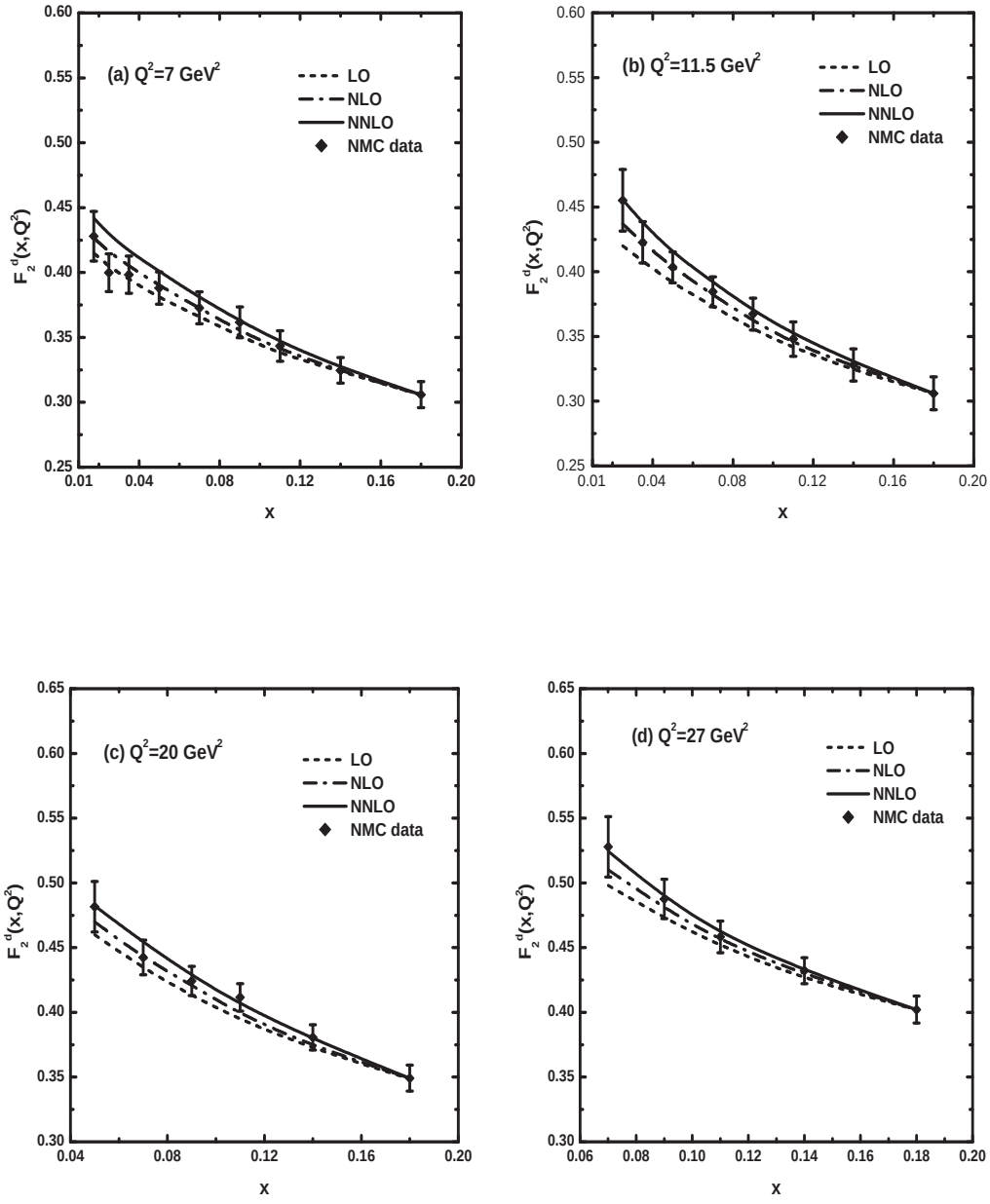

Figure 3.3: Plots of x evolution of deuteron structure function at LO, NLO and NNLO compared with the NMC data for four fixed Q^2. The dot lines represent the LO results (Eq.3.47), dash-dot lines represent the NLO results (Eq.3.64) and solid lines represent the NNLO results Eq.(3.83).

respectively.

We also calculate the t or Q^2-evolution of proton structure function at LO, NLO and NNLO from Eq. (3.48), (3.67) and (3.88). Figure 3.8 show the comparison of our results of proton structure function with those measured at NMC as functions of Q^2 in the range $0.75 \leq Q^2 \leq 27$ GeV^2. We show the comparison for four fixed $x = 0.008, 0.0125, 0.025$ and 0.035 respectively.

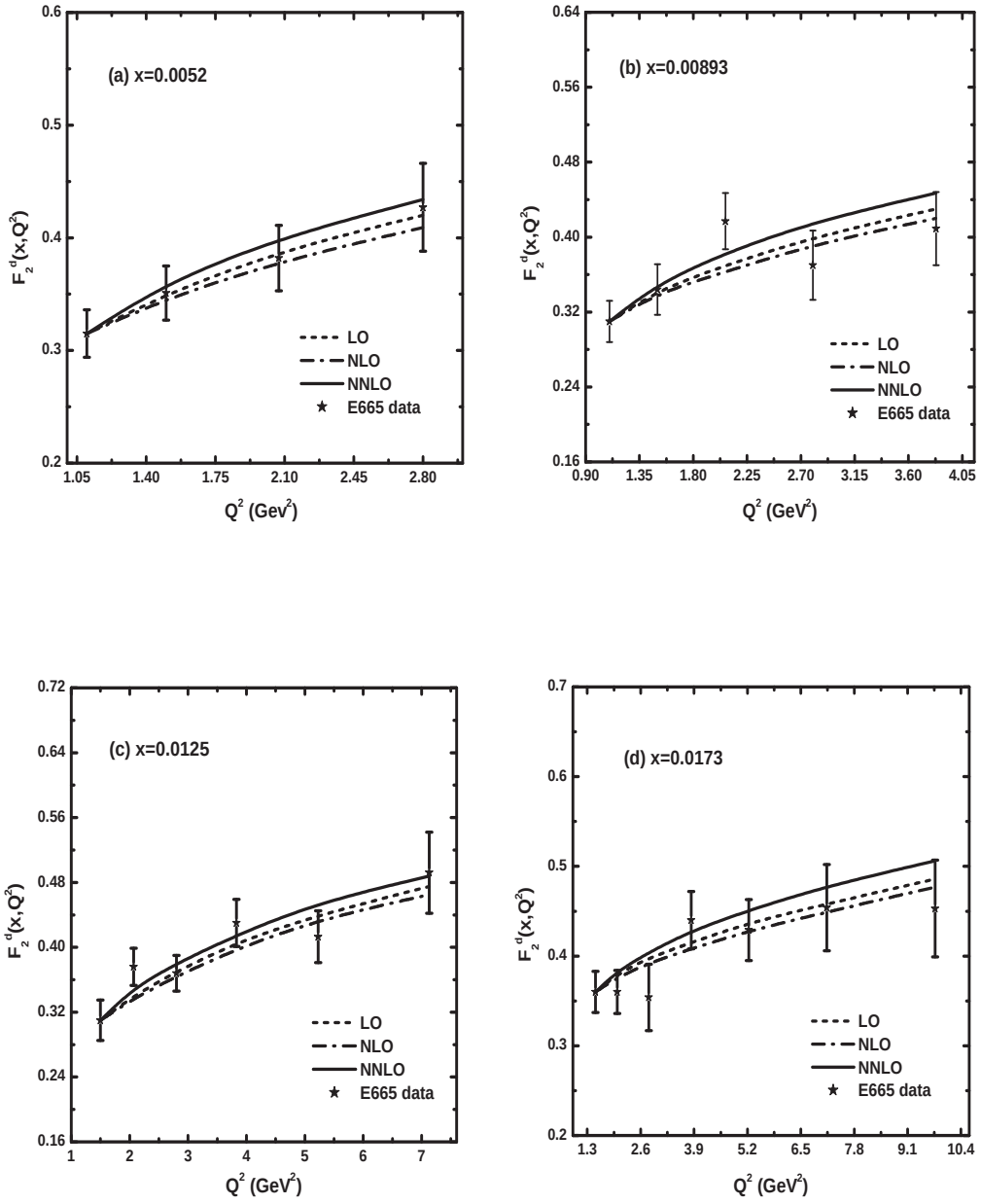

Figure 3.4: Plots of Q^2 evolution of deuteron structure functions at LO, NLO and NNLO compared with the E665 data for four representative x. The dot lines are the LO results (Eq.3.46), dash-dot lines are the NLO results (Eq.3.63) and solid lines are the NNLO results (Eq.3.82).

Figure 3.9 show the comparison of our solution of proton structure function given by Eqs.(3.48), (3.67) and (3.88) for LO, NLO and NNLO respectively with the E665 experimental data in the range $1.094 \leq Q^2 \leq 26$ GeV^2. Here we plot the computed values of proton structure function as functions of Q^2 at four representative values of x, namely $x = 0.00693, 0.01225, 0.0173$ and 0.02449 respectively.

In Figure 3.10 we plot our computed results of proton structure function ob-

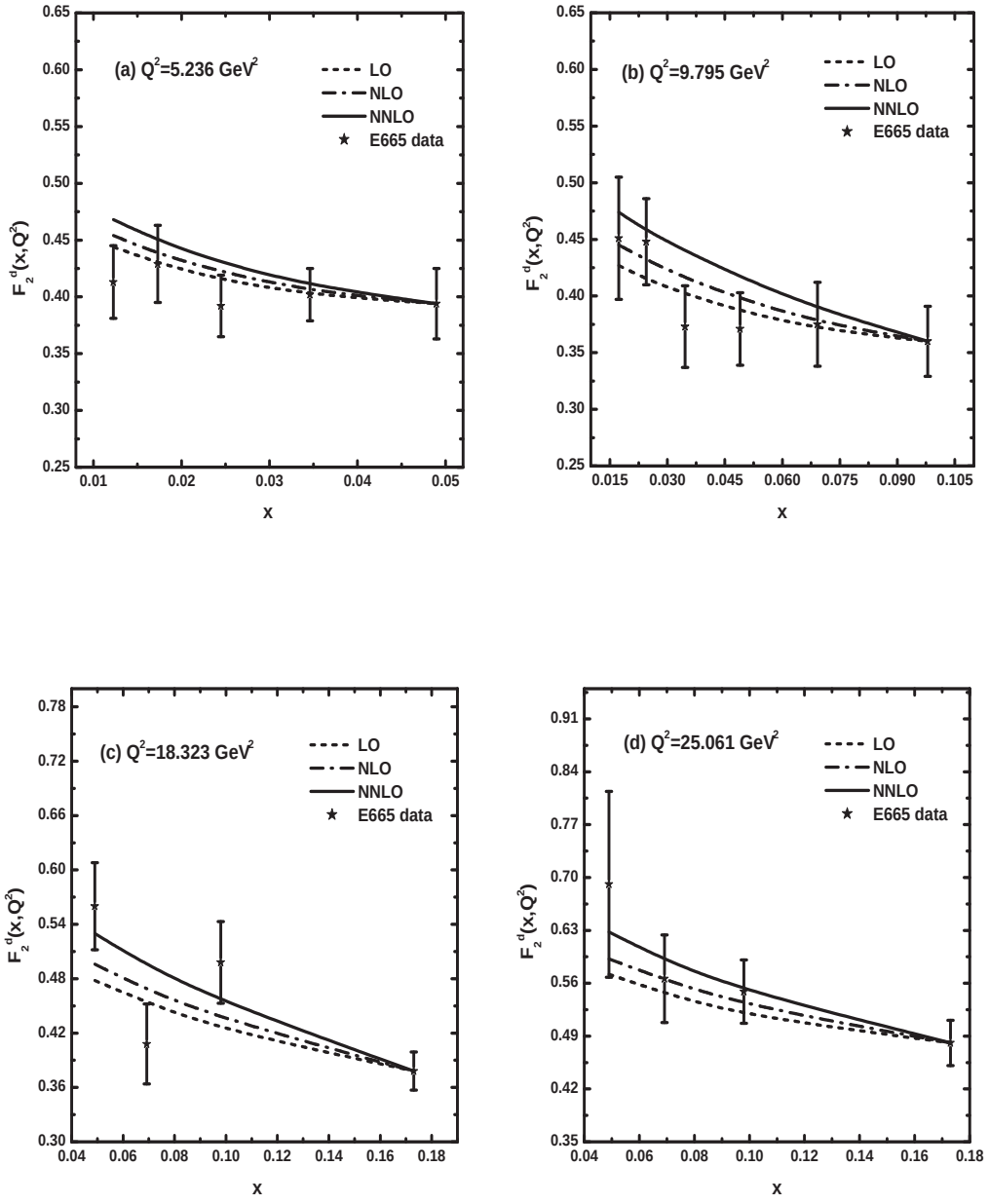

Figure 3.5: Comparison of x evolution of deuteron structure function at LO, NLO and NNLO with the E665 data for four representative values of Q^2 . The dot lines represent the LO results (Eq.3.47), dash-dot lines represent the NLO results (Eq.3.64) and solid lines represent the NNLO results Eq.(3.83).

tained from Eqs.(3.48), (3.67) and (3.88) for LO, NLO and NNLO respectively as functions of Q^2 and compare with the H1 1995 data in the range $5.5 \leq Q^2 \leq 38$ GeV^2. The comparison is done for for four fixed $x = 0.00421, 0.0075, 0.0133$ and 0.0237 respectively.

From the figures we observe that our results of Q^2 and x-evolutions of deuteron

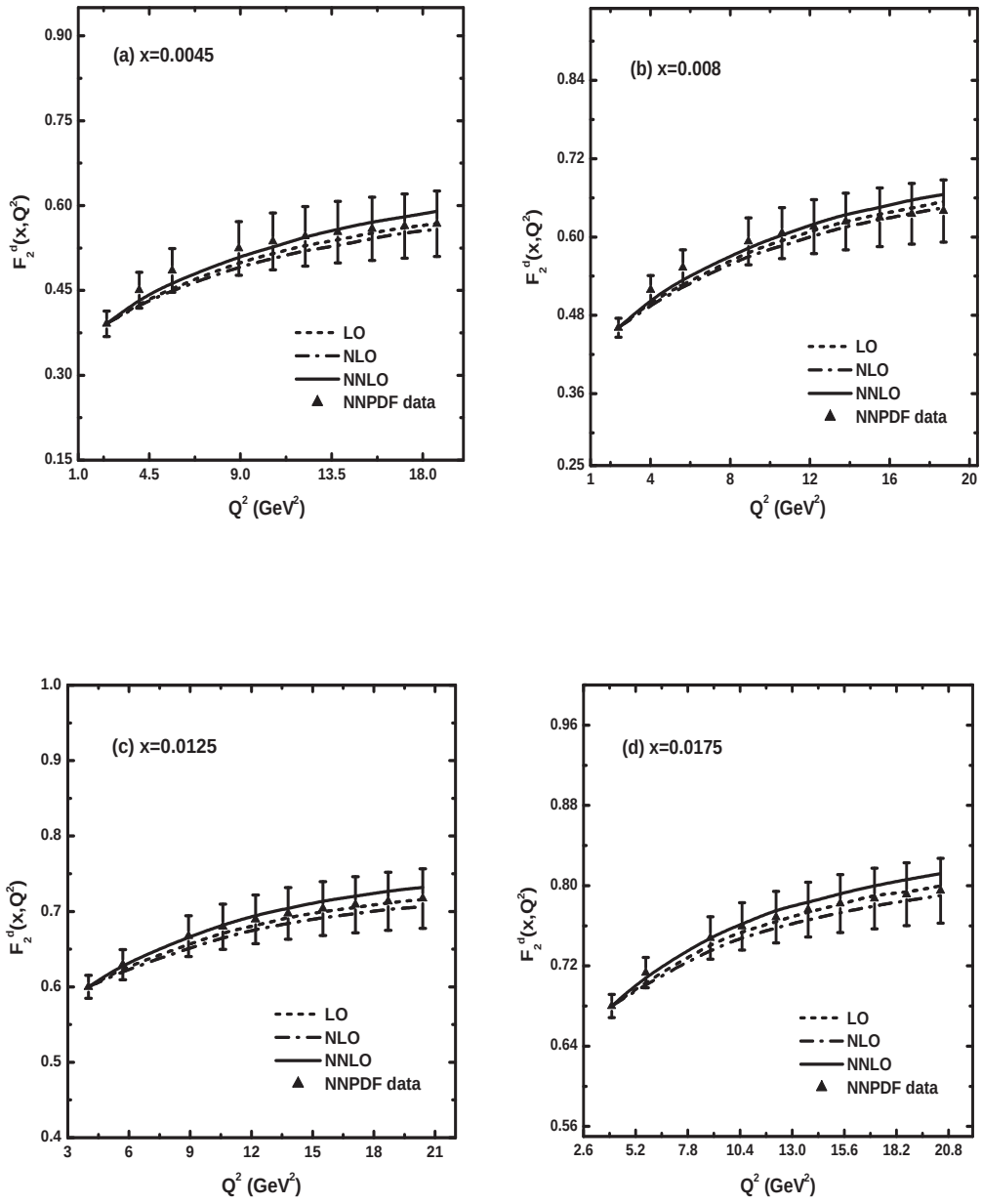

Figure 3.6: Comparison of Q^2 evolution of deuteron structure functions at LO, NLO and NNLO with the NNPDF data for four fixed values x. The dot lines represent the LO results (Eq.3.46), dash-dot lines represent the NLO results (Eq.3.63) and solid lines represent the NNLO results Eq.(3.82).

and proton structure functions are in good consistency with the experimental data and parametrizations. Our predictions at NNLO provide better agreement than LO and NLO results, nevertheless, the difference between the LO, NLO and NNLO results is small. From our analysis in can be anticipated that the region of validity of our method is approximately in the range $10^{-3} \leq x \leq 10^{-1}$ and $0.5 \leq Q^2 \leq 40$

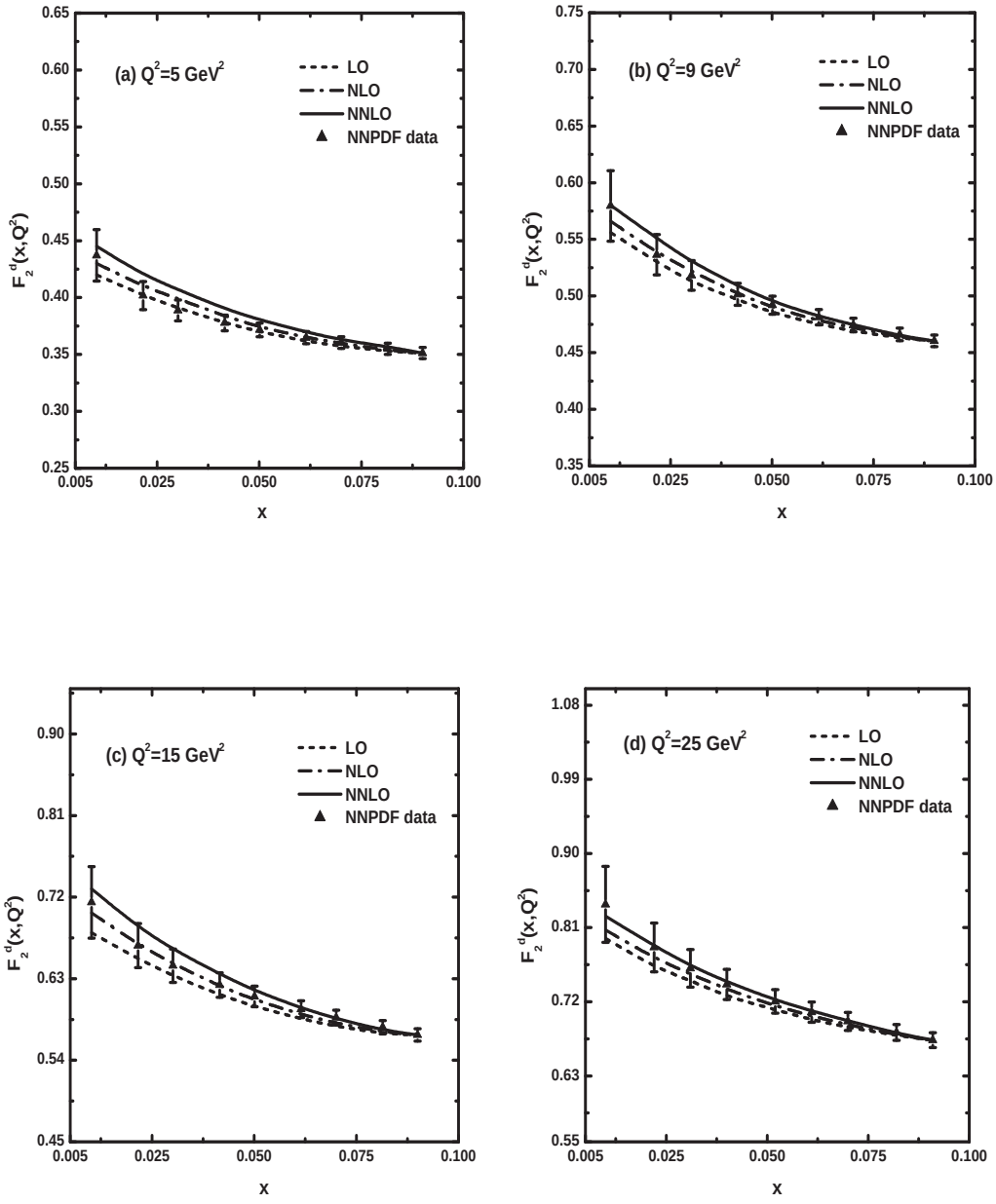

Figure 3.7: Plots showing the comparison of x evolution of deuteron structure function at LO, NLO and NNLO with the NNPDF data for four fixed values of Q^2. The dot lines represent the LO results (Eq.3.47), dash-dot lines represent the NLO results (Eq.3.64) and solid lines represent the NNLO results Eq.(3.83).

GeV^2. But this method may also applicable for other ranges of x and Q^2. Though various methods like Laguerre polynomials [38, 39], Brute-Force method [40], Matrix method [41], Mellin transformation [42, 43] etc. are available in order to obtain a numerical solution of DGLAP evolution equations, our method to solve these equations analytically is also a workable alternative. Here we consider a parameter $K(x)$

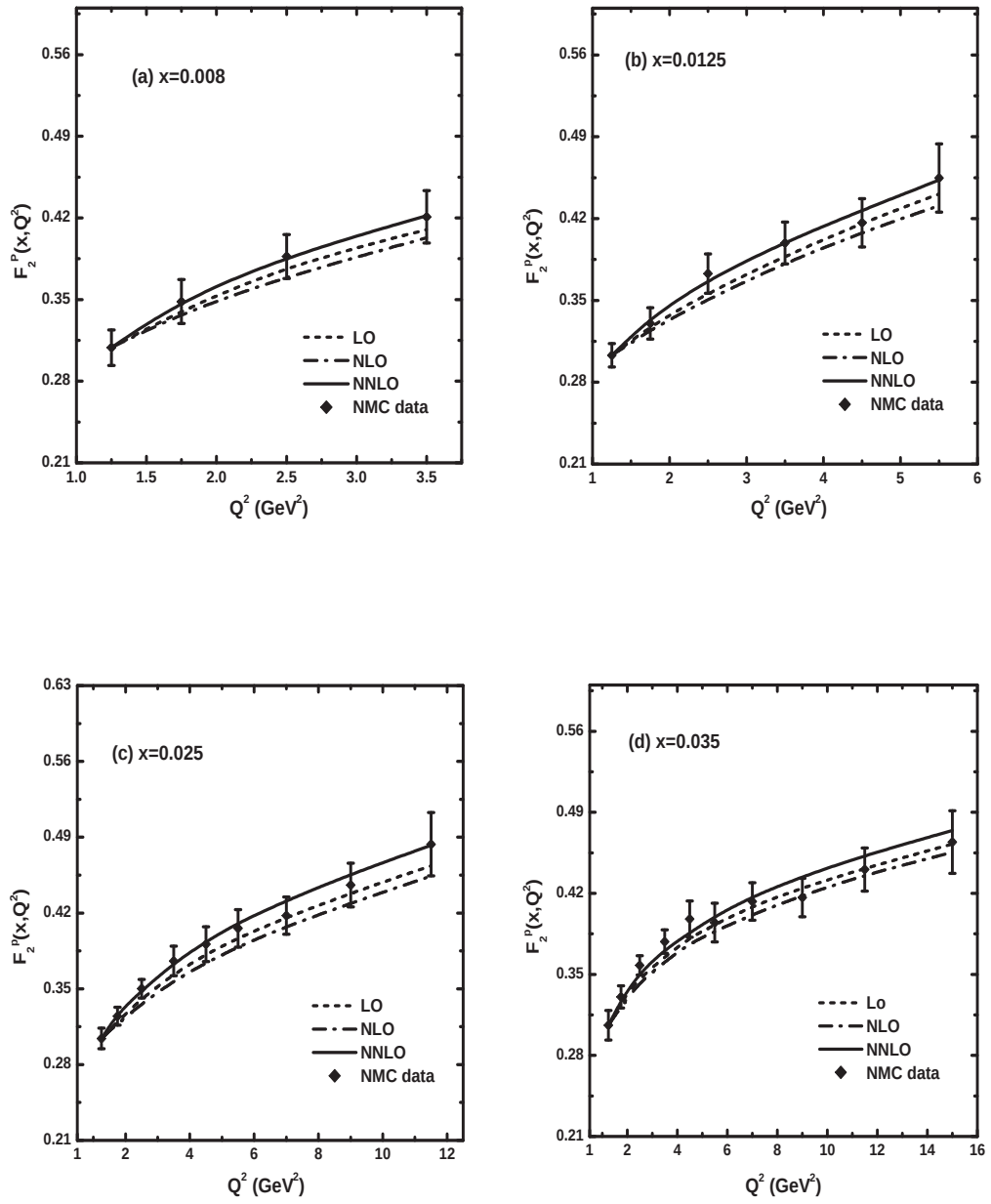

Figure 3.8: Plots of proton structure function at LO, NLO and NNLO vs. Q^2 compared with the NMC data for four particular values of x. The dot lines represent the LO results (Eq.3.48), dash-dot lines represent the NLO results (Eq.3.67) and solid lines represent the NNLO results Eq.(3.88).

in assuming a relation between singlet structure function and gluon parton densities. We have also used two other parameters like T_0 and T_1. However the number of parameters used here are less in comparison to the numerical methods where several parameters have been used mainly in input functions [55, 56]. Moreover, with this method we can calculate the x-evolutions of deuteron structure function in addition

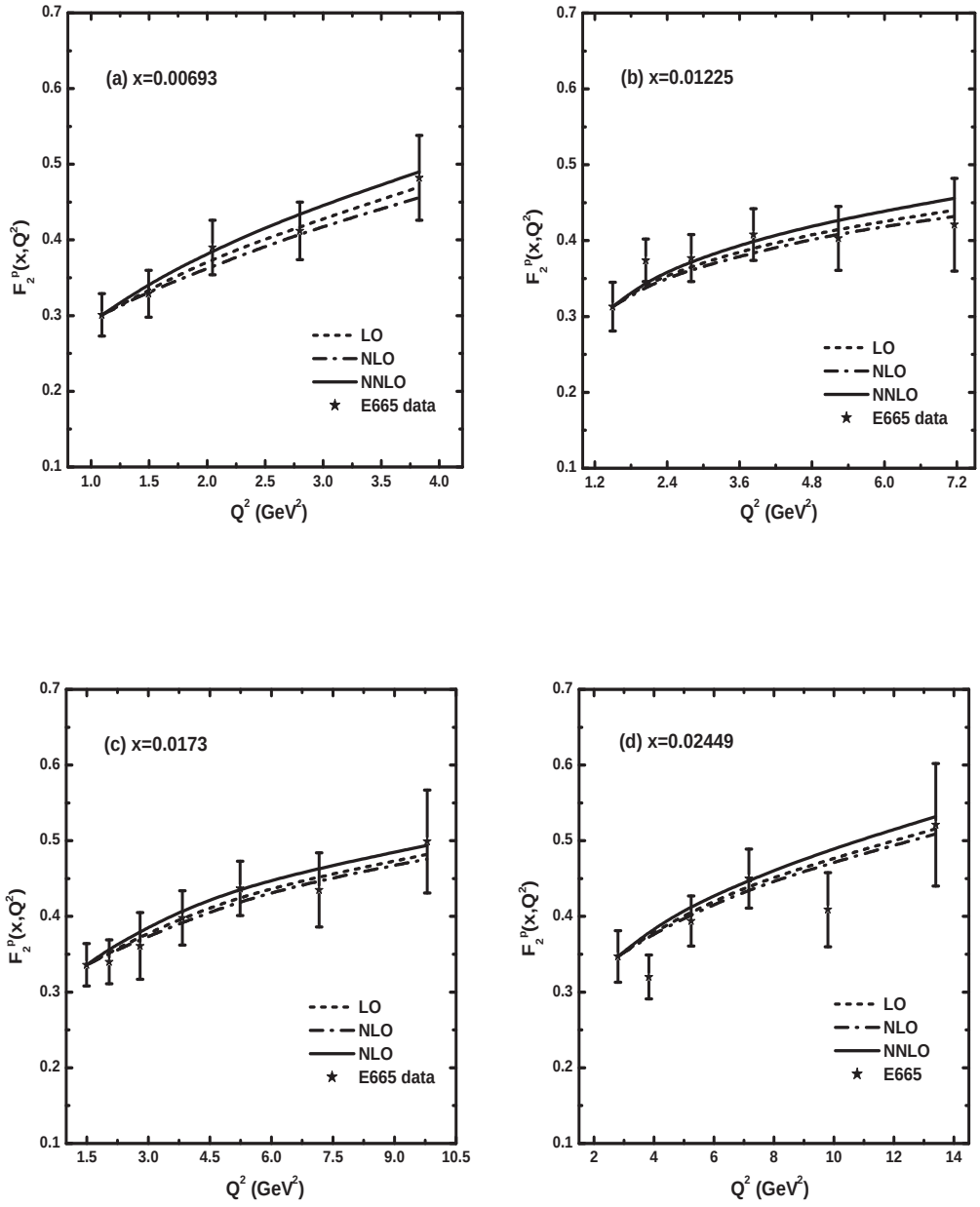

Figure 3.9: Plots showing the comparison of Q^2 evolution of proton structure function at LO, NLO and NNLO with the E665 data for four fixed x. The dot lines represent the LO results (Eq.3.48), dash-dot lines represent the NLO results (Eq.3.67) and solid lines represent the NNLO results Eq.(3.88).

to the t-evolutions.

For a quantitative estimate of the goodness of fit of our results with the experimental data and parametrizations, we perform a χ^2 test. In table 1 we present the χ^2 values for the solutions of deuteron structure function at LO, NLO and NNLO respectively. We observe that our analtical solutions of the deuteron structure function at

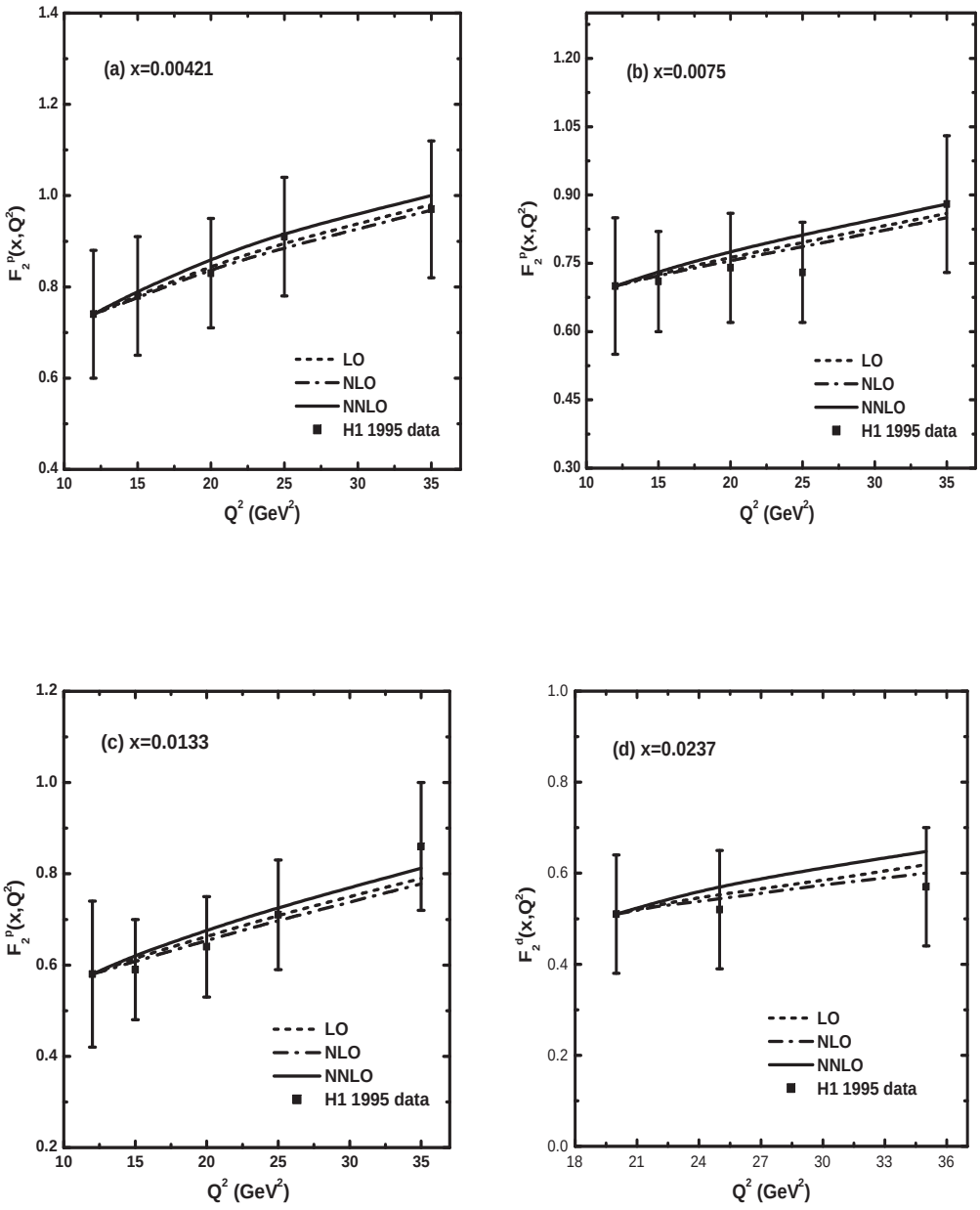

Figure 3.10: Comparison of Q^2 evolution of proton structure function at LO, NLO and NNLO with the H1 1995 data for four fixed x. The dot lines represent the LO results (Eq.3.48), dash-dot lines represent the NLO results (Eq.3.67) and solid lines represent the NNLO results Eq.(3.88).

Table 3.1: χ^2 values for $F_2^d(x, Q^2)$

Order	**NMC**	**E665**	**NNPDF**
LO	3.943	2.215	1.396
NLO	1.733	1.873	0.783
NNLO	1.142	2.07	0.656

LO, NLO and NNLO respectively are in good agreement with the experimental data and parametrizations. However the NNLO results are found to be more compatible.

Table 3.2: χ^2 values for $F_2^p(x, Q^2)$

Order	**NMC**	**E665**	**H1**
LO	2.235	2.477	0.226
NLO	1.097	2.62	0.141
NNLO	0.824	1.92	0.361

Similarly table 2 shows the χ^2 values for the solutions of the proton structure function at LO, NLO and NNLO. Here also we find that our results of proton structure function at LO, NLO and NNLO are almost comparable with the experimental data and parametrizations, nevertheless the NNLO results are more consistent.

3.4 Summary

The Taylor approximated DGLAP equations for the singlet and non-singlet structure functions are solved analytically at LO, NLO and NNLO by the Lagrange's auxilliary method. We also calculate the Q^2 and x-evolutions of deuteron structure function as well as the Q^2-evolution of proton structure function from the solutions of singlet and non-singlet structure functions. The Taylor series expansion changes the integro-differential DGLAP equations into first order partial differential equations which are much easier to solve. This method is comparatively simple and less time consuming for the numerical calculations. We adopt two numerical parameters T_0 and T_1 to evaluate the Q^2 and x-evolutions of singlet and non-singlet structure functions. We also consider the function $K(x) = K$, where K is a constant parameter to relate the singlet and gluon distribution functions and find that K lies in the range $0.45 < K < 1.6$, for our results to be comparable with experimental data and parametrizations. Nevertheless the number of parameters are very few compared to the numerical methods where several parameters are included mainly in the input function. Moreover, with this approch we can calculate the x-evolution of deuteron structure function in addition to the t-evolution. Thus, although various numerical methods are available in order to obtain a numerical solution of DGLAP evolution equations, our approach to solve these equations analytically is also a viable alterna-

tive.

We compare our predictions with the NMC data, E665 data, H1 data as well as with the results of NNPDF parametrization. From our phenomenological analysis we observe that our predicted solutions can explain the general trend of data in a decent manner. Moreover, the inclusion of NNLO contributions provides excellent consistency with the experimental data and parametrizations. Our results show that at fixed x the structure functions increase with increasing Q^2, whereas at fixed Q^2 the structure functions increase with decreasing x which is in agreement with perturbative QCD fits at small-x. By analysing our results we can anticipate that our solutions are valid vis-a-vis the data and parametrizations in the small-x region, roughly in the region $10^{-3} < x < 10^{-1}$. However, our method may loose its validity at very small-x where recombination of gluons have to be taken into account, since these higher order corrections are not included in the derivation of linear DGLAP equations.

Bibliography

[1] Gribov, V. N., Lipatov, L. N. Deep inelastic *ep* scattering in perturbation theory, *Sov. J. Nucl. Phys.* **15**(4), 438−−450, 1972.

[2] Gribov, V. N., Lipatov, L. N. e^+e^- pair annihilation and deep-inelastic *ep* scattering in perturbation theory, *Sov. J. Nucl. Phys.* **15**(4), 675−−684, 1972.

[3] Dokshitzer, Y. L. Calculation of structure functions of deep-inelastic scattering and e^+e^- annihilation by perturbation theory in quantum chromodynamics, *Sov. Phys. JETP* **46**(4), 641−−652, 1977.

[4] Altarelli, G., Parisi, G. Asymptotic freedom in parton language, *Nucl. Phys. B* **126**(2), 298−−318, 1977.

[5] Pascaud, C., Zomer, F. A Fast and precise method to solve the Altarelli-Parisi equations in x space, *arXiv:hep-ph/0104013v1.*

[6] Hirai, M., Kumano, S. and Miyama, M. Numerical solution of Q^2 evolution equations for polarized structure functions, *Comput. Phys. Commun.* **108**(1), 38−−55, 1998.

[7] Coriano, C., Savkli, C. QCD evolution equations: Numerical algorithms from the Laguerre expansion, *Comput. Phys. Commun.* **118**,(2-3), 236−−258, 1999.

[8] Botje, M. A QCD analysis of HERA and fixed target structure function data, *Eur. Phys. J. C* **14**(2), 285−−297, 2000.

[9] Ratcliffe, P. G. Matrix Approach to a numerical solution of the Dokshitzer-Gribov-Lipatov-Altarelli-Parisi evolution equations, *Phys.Rev. D* **63**(11), 116004, 2001.

[10] Cafarella, A., Coriano, C. and Guzzi, M. NNLO logarithmic expansions and exact solutions of the DGLAP equations from x-space: New algorithms for precision studies at the LHC, *Nucl. Phys. B* **748**(1-2), 253−−308, 2006.

[11] Abbott, L. F., Atwood, W. B. and Barnett, R. M. Quantum-chromodynamic analysis of eN deep-inelastic scattering data, *Phys. Rev. D* **22**(3), 582−−593, 1980.

[12] Furmanski, W., Petronzio, R. Lepton-hadron processes beyond leading order in quantum chromodynamics, *Z. Phys. C* **11**(4), 293−−314, 1982.

[13] Ball, R. D., Forte, S. A direct test of perturbative QCD at small x, *Phys. Lett., B* **336**(1), 77−−79, 1994.

[14] Kotikov, A. V., Parente, G. Small x behavior of parton distributions with soft initial conditions, *Nucl. Phys. B* **549**(1-2), 242−−262, 1999.

[15] Sarma, J. K., Choudhury, D. K. and Medhi, G. K. x-distribution of deuteron structure function at low-x, *Phys.Lett. B* **403**(1-2), 139−−144, 1997.

[16] Sarma,J. K., Das, B. t evolutions of structure functions at low-x, *Phys. Lett. B* **304**(3-4), 323−−328, 1993

[17] Choudhury, D. K., Deka, Ranjita and Saikia, A. Gluon distribution and $\frac{dF_2}{d\ln Q^2}$ at small x in the next-to-leading order, *Eur. Phys. J. C* **2**(2), 301−−305, 1998.

[18] Choudhury, D. K., Sahariah, P. K. A solution of the DGLAP equation for gluon at low x, *Pramana J. Phys.* **58**(4), 599−−610, 2002.

[19] Baishya, R., Sarma, J. K. Method of characteristics and solution of DGLAP evolution equation in leading and next to leading order at small x, *Phys. Rev. D* **74**(10), 107702, 2006.

[20] Baishya, R., Sarma, J. K. Semi numerical solution of non-singlet Dokshitzer-Gribov-Lipatov-Altarelli-Parisi evolution equation up to next-to-next-to-leading order at small x, *Eur. Phys. J. C* **60**(4), 585−−591, 2009.

[21] Baishya, R., Jamil, U. and Sarma, J. K. Evolution of spin-dependent structure functions from DGLAP equations in leading order and next to leading order, *Phys. Rev. D* **79**, 034030, 2009.

[22] Choudhury, D. K., Islam, S. An analysis of non-singlet structure function in next-to-next-to-leading order at small-x, *Indian J. Phys.* **85**(2), 319−−328, 2011.

[23] Arneodo, M. et al., Measurement of the proton and deuteron structure functions, F_2^p and F_2^d, and of the ratio σ_L/σ_T, *Nucl. Phys. B* **483**,(1-2), 3−−43, 1997.

[24] Adams, M. R. et al., Proton and deuteron structure functions in muon scattering at 470 GeV, *Phys. Rev. D* **54**(5), 3006−3056, 1996.

[25] Ahmed, T. et al., A measurement of the proton structure function $F_2(x,Q^2)$, *Nucl. Phys. B* **439**(3), 471−−502, 1995.

[26] Forte, S. et al., Neural network parametrization of deep inelastic structure functions, *JHEP* **2002**(JHEP05), 062, 2002.

[27] Halzen, F., Martin, A. D. *Quarks and Leptons: An Introductory Course in Modern Particle Physics*, John Wiley and Sons, Canada, 1984.

[28] Van Neerven, W. L., Vogt, A. NNLO evolution of deep-inelastic structure functions: the singlet case, *Nucl. Phys. B* **588**(1-2), 345−−373, 2000.

[29] Van Neerven, W. L., Vogt, A. NNLO evolution of deep-inelastic structure functions: the non-singlet case, *Nucl. Phys. B* **568**(1-2), 263−−286, 2000.

[30] Moch, S., Vermaseren, J. A. M. and Vogt, A. The three-loop splitting functions in QCD: the non-singlet case, *Nucl. Phys. B* **688**(1-2), 101−−134, 2004.

[31] Vogt, A., Moch, S. and Vermaseren, J. A. M. The three-loop splitting functions in QCD: the singlet case, *Nucl. Phys. B* **691**(1-2), 129−−181, 2004.

[32] Shaikhatdenov, B. G. et al., QCD coupling constant at next-to-next-to-leading order from DIS data, *Phys. Rev. D* **81**(3), 034008, 2010.

[33] Martin, A. D. et al., Parton distributions for the LHC, *Eur. Phys. J. C* **63**(2), 189−−285, 2009.

[34] Furmanski, W., Petronzio, R. Singlet parton densities beyond leading order, *Phys. Lett. B* **97**(3-4), 437−−442, 1980.

[35] Curci, G., Furmanski, W. and Petronzio, R. Evolution of parton densities beyond leading order: The non-singlet case, *Nucl. Phys. B* **175**(1), 27−−92, 1981.

[36] Benvenuti, A. C. et al., A high statistics measurement of the deuteron structure functions $F_2(x, Q^2)$ and R from deep inelastic muon scattering at high Q^2, *Phys. Lett. B* **237**(3-4), 592−−598, 1990.

[37] Adloff, C. et al., Measurement and QCD analysis of neutral and charged current cross sections at HERA, *Eur. Phys. J. C* **30**(1), 1−−32, 2003.

[38] Coriano, C., Savkli, C. QCD evolution equations: Numerical algorithms from the Laguerre expansion, *Comput. Phys. Commun.* **118**(2-3), 236−−258, 1999.

[39] Schoeffel, L. An elegant and fast method to solve QCD evolution equations. Application to the determination of the gluon content of the Pomeron, *Nucl. Instrum. Methods A* **423**(2-3), 439−−445, 1999.

[40] Hirai, M., Kumano, S. and Miyama, M. Numerical solution of Q^2 evolution equations for polarized structure functions, *Comput. Phys. Commun.* **108**(1), 38−−55, 1998.

[41] Ratcliffe, P. G., A matrix approach to numerical solution of the DGLAP evolution equations, *Phys. Rev. D*,**63**(11), 116004, 2001.

[42] Kosower, D. A., Evolution of parton distributions, *Nucl. Phys. B* **506**(1-2), 439−−467, 1997.

[43] Weinzierl, S., Fast evolution of parton distributions, *Comput. Phys. Commun.* **148**(3), 314−−326, 2002.

Chapter 4

NNLO Analysis of Gluon Distribution Function in the DGLAP Approach

4.1 Introduction

The gluon distribution function is one of the extremely indispensable physical observables that controls the physics at high energy or small-x in DIS, where x is the Bjorken variable. Especially, precise knowledge of gluon distribution functions at small-x is of utmost importance in estimating backgrounds and exploring new physics at the Large Hadron Collider. The gluon distribution $G(x, Q^2)$ does not come into sight in the experimentally available proton structure function $F_2(x, Q^2)$. It is determined only via the quark distributions together with the evolution equations. More direct approach to determine the gluon distribution is based on the reconstruction of the kinematics of the interacting partons from the measurement of the hadronic final state in gluon induced processes. They are controlled by different systematic effects and provide a substantive test of perturbative QCD. The proton structure function is measured by the H1 and ZEUS collaboration at HERA [1-3] over a wide kinematic region which makes it possible to know about the gluon distribution in the previously unexplored region of x and Q^2. The fast growth of the proton structure function at small-x observed at HERA brings about much attention because perturbative QCD in conjunction with the DGLAP equation [4-7] attributes this sharp growth to a similar rise of gluon density towards small-x. In the DGLAP formalism the gluon

distribution turns out to be very large at small-x and so it contributes crucially to the evolution of the parton distribution. Subsequently, the gluon distribution governs the structure function $F_2(x, Q^2)$ through the evolution $g \to q\bar{q}$ in the small-x region. In this situation it is very important to explore the possibility of obtaining analytical solutions of DGLAP equations at least in the restricted domain of small-x and many approximated analytical solutions of the gluon distribution function in the framework of DGLAP equation have been reported in recent years with significant phenomenological success [8-14].

In this chapter, we derive an explicit expression for the gluon distribution function upto NNLO by solving the DGLAP evolution equation for gluon distribution function analytically. In such an approach, we use a Taylor series expansion valid at small-x and reframes the DGLAP equations as partial differential equations in the variables x and Q^2 as discussed in chapter 3. The resulting equations at LO, NLO and NNLO are then solved by the Lagrange's auxiliary method to obtain the Q^2 and x-evolutions of the gluon distribution function. The obtained results can be described within the framework of perturbative QCD. To illustrate the method and check the compatibility of our predicted gluon distributions, we use the published values of the gluon distributions from the GRV1998NLO [15], MRST2004NNLO [16], MSTW2008NNLO [17] and JR09NNLO [18] global analyses. We find that the analytic gluon distributions from our solution are consistent with these parametrizations. We also compare our results with the Block-Durand-McKay (BDM) model [14] and observe that our results depict almost the same behaviour as that of BDM model.

4.2 Formalism

4.2.1 General framework

The DGLAP evolution equation for gluon distribution function in the standard form is given by [19]

$$\frac{\partial g(x,Q^2)}{\partial \ln Q^2} = \int_x^1 \frac{d\omega}{\omega}\Big(P_{gq}(\omega)q_S(x/\omega,Q^2) + P_{gg}(\omega)g(x/\omega,Q^2)\Big), \tag{4.1}$$

where the splitting function P_{gq} is defined as

$$\begin{aligned} P_{gq}(x,Q^2) &= \frac{\alpha_s(Q^2)}{2\pi}P_{gq}^{(0)}(x) + \Big(\frac{\alpha_s(Q^2)}{2\pi}\Big)^2 P_{gq}^{(1)}(x) + \Big(\frac{\alpha_s(Q^2)}{2\pi}\Big)^3 P_{gq}^{(2)}(x) \\ &\quad + \mathcal{O}P_{gq}^{(3)}(x). \end{aligned} \tag{4.2}$$

where $P_{gq}^{(0)}(x)$, $P_{gq}^{(1)}(x)$ and $P_{gq}^{(2)}(x)$ are LO, NLO and NNLO quark-gluon splitting functions respectively. The gluon-gluon splitting function P_{gg} can be defined in a Similar fashion. Here q_S is the singlet quark density and g is the gluon density. The representation $G(x,Q^2) = xg(x,Q^2)$ is used here.

4.2.2 LO analysis of gluon distribution function

Substituting the explicit form of the LO splitting functions [7, 21] in Eq.(4.1) and simplifying, the LO DGLAP evolution equation for the gluon distribution function can be written as

$$\frac{\partial G(x,t)}{\partial t} = \frac{\alpha_s(t)}{2\pi}\Big[6\Big(\frac{11}{12} - \frac{N_f}{18} + \ln(1-x)\Big)G(x,t) + 6I_1^g(x,t)\Big], \tag{4.3}$$

where $G(x,Q^2) = xg(x,Q^2)$ is the gluon distribution function. The integral function $I_1^g(x,t)$ is defined as

$$\begin{aligned} I_1^g(x,t) &= \int_x^1 d\omega\Bigg[\frac{\omega G\big(\frac{x}{\omega},t\big) - G(x,t)}{1-\omega} + \Big(\omega(1-\omega) + \frac{1-\omega}{\omega}\Big)G\Big(\frac{x}{\omega},t\Big) \\ &\quad + \frac{2}{9}\Bigg(\frac{1+(1-\omega)^2}{\omega}\Bigg)F_2^S(\frac{x}{\omega}t).\Bigg] \end{aligned} \tag{4.4}$$

Here the variable t is used where $t = \ln(Q^2/\Lambda^2)$. Now, using Taylor expansion method and neglecting higher order terms of x, since we consider the small-x ($x < 0.1$) domain in our analysis, as discussed in the Chapter-3, we can write $G(x/\omega,t)$ as

$$G\Big(\frac{x}{\omega},t\Big) = G(x,t) + \frac{xu}{1-u}\frac{\partial G(x,t)}{\partial x}. \tag{4.5}$$

Similarly, $F_2^S(\frac{x}{\omega},t)$ can be approximated as

$$F_2^S\Big(\frac{x}{\omega},t\Big) = F_2^S(x,t) + \frac{xu}{1-u}\frac{\partial F_2^S(x,t)}{\partial x}. \tag{4.6}$$

Substituting these values of $G(\frac{x}{\omega},t)$ and $F_2^S(\frac{x}{\omega},t)$ in Eq.(4.4) and carrying out the integrations in u we get from Eq.(4.3)

$$\begin{aligned} \frac{\partial G(x,t)}{\partial t} &= \frac{6A_f}{t}\Big[A_1^g(x)G(x,t) + A_2^g(x)\frac{\partial G(x,t)}{\partial x} + A_3^g(x)F_2^S(x,t) \\ &\quad + A_4^g(x)\frac{\partial F_2^S(x,t)}{\partial x}\Big], \end{aligned} \tag{4.7}$$

where $A_i^g(x)$ (i=1,2,3,4) are functions of x (see Appendix D). $\frac{A_f}{t} = \frac{\alpha_s(t)}{2\pi}$ where $A_f = \frac{2}{\beta_0}$ and β_0 is the one-loop correction to the QCD beta function. Eq.(4.7) is a partial differential equation for gluon distribution function with respect to the

variables x and t. Thus using a Taylor expansion valid at small-x we reframe the DGLAP equation for gluon distribution, which is an integro-differential equation, as partial differential equation in two variables x and t or Q^2.

The gluon distribution is coupled to the singlet structure function and therefore to obtain an analytical solution of the DGLAP evolution equation for gluon distribution function a relation between gluon distribution function and singlet structure function has to be assumed. As discussed in chapter 3, here also we assume the relation $G(x,t) = K(x)F_2^S(x,t)$ [22-24] to solve Eq.(4.7) where $K(x)$ is a parameter to be determined from phenomenological analysis. From this relation we get $F_2^S(x,t) = K_1(x)G(x,t)$, where $K_1(x) = 1/K(x)$. Using this relation Eq.(4.7) takes the form

$$-t\frac{\partial G(x,t)}{\partial t} + L_1^g(x)\frac{\partial G(x,t)}{\partial x} + M_1^g(x)G(x,t) = 0, \tag{4.8}$$

with

$$L_1^g(x) = 6A_f\Big[A_2^g(x) + K_1(x)A_4^g(x)\Big], \tag{4.9}$$

$$M_1^g(x) = \frac{12}{\beta_0}\Big[A_1^g(x) + K_1(x)A_3^g(x) + \frac{\partial K_1(x)}{\partial x}A_4^g(x)\Big], \tag{4.10}$$

Now the general solution of the equation (4.8) is

$$F(U,V) = 0, \tag{4.11}$$

where $F(U,V)$ is an arbitrary function of U and V. Here, $U(x,t,G(x,t)) = k_1$ and $V(x,t,G(x,t)) = k_2$ are two independent solutions of the Lagrange's equation

$$\frac{\partial x}{L_1^g(x)} = \frac{\partial t}{-t} = \frac{\partial G(x,t)}{-M_1^g(x)G(x,t)}. \tag{4.12}$$

Solving Eq. (4.12) we obtain

$$U(x,t,G(x,t)) = t\cdot\exp\Big[\int\frac{1}{L_1^g(x)}dx\Big] \tag{4.13}$$

and

$$V(x,t,G(x,t)) = G(x,t)\cdot\exp\Big[\int\frac{M_1^g(x)}{L_1^g(x)}dx\Big]. \tag{4.14}$$

Thus we see that it has no unique solution. In this approach we attempt to extract a particular solution that obeys some physical constraints on the structure

function. The simplest possibility to get a solution is that a linear combination of U and V should obey the Eq.(4.11) so that

$$\alpha \cdot U + \beta \cdot V = 0, \tag{4.15}$$

where α and β are arbitrary constants to be determined from the boundary conditions on singlet structure function. Putting the values of U and V from Eq.(4.13) and Eq.(4.14) respectively in Eq.(4.15) we get

$$\alpha t \cdot \exp\Big[\int \frac{1}{L_1^g(x)}dx\Big] + \beta G(x,t) \cdot \exp\Big[\int \frac{M_1^g(x)}{L_1^g(x)}dx\Big] = 0, \tag{4.16}$$

which implies,

$$G(x,t) = -\gamma t \cdot \exp\Big[\int \Big(\frac{1}{L_1^g(x)} - \frac{M_1^g(x)}{L_1^g(x)}\Big)dx\Big] \tag{4.17}$$

where $\gamma = \frac{\alpha}{\beta}$ is another constant. Now at $t = t_0$, where $t_0 = \ln\frac{Q_0^2}{\Lambda^2}$ for any lower value $Q^2 = Q_0^2$, we define

$$G(x,t_0) = -\gamma t_0 \cdot \exp\Big[\int (\frac{1}{L_1^g(x)} - \frac{M_1^g(x)}{L_1^g(x)})dx\Big]. \tag{4.18}$$

Then Eqs.(4.17) and (4.18) lead us to

$$G(x,t) = G(x,t_0)\Big(\frac{t}{t_0}\Big). \tag{4.19}$$

This gives the t or Q^2-evolution ($t = \ln(Q^2/\Lambda^2)$) for gluon distribution function at LO at a particular value small-x. Again we define

$$G(x_0,t) = -\gamma t \cdot \exp\Big[\int (\frac{1}{L_1^g(x)} - \frac{M_1^g(x)}{L_1^g(x)})dx\Big]_{x=x_0}, \tag{4.20}$$

at a higher value of $x = x_0$. Then from Eq.(4.17) and Eq.(4.20) we get

$$G(x,t) = G(x_0,t) \cdot \exp\Big[\int_{x_0}^{x} (\frac{1}{L_1^g(x)} - \frac{M_1^g(x)}{L_1^g(x)})dx\Big]. \tag{4.21}$$

which gives the x-evolutions of gluon distribution function at LO for a given value of Q^2.

4.2.3 NLO analysis of gluon distribution function

Substituting the NLO splitting functions [25-27] in Eq.(4.1) and simplifying, we get the DGLAP equation for gluon distribution function at NLO in standard form as

$$\begin{aligned}\frac{\partial G(x,t)}{\partial t} &= \frac{\alpha_s(t)}{2\pi}\Big[6\Big(\frac{11}{12} - \frac{N_f}{18} + \ln(1-x)\Big)G(x,t) + 6I_1^g(x,t)\Big] \\ &\quad + \Big(\frac{\alpha_S(t)}{2\pi}\Big)^2 I_2^g(x,t),\end{aligned} \tag{4.22}$$

where the integral function $I_2^g(x,t)$ is defined as

$$I_2^g(x,t) = \int_x^1 d\omega \Big[P_{gg}^1(\omega) G\big(\frac{x}{\omega}, t\big) + A(\omega) F_2^S\Big(\frac{x}{\omega}, t\Big)\Big] \tag{4.23}$$

The explicit forms of $P_{gg}^1(\omega)$ and $A(\omega)$ are given in Appendix E.

Following the same procedure as in LO, the Eq.(4.22) can be simplified as

$$-\Big(\frac{t^2}{t - b\ln t}\Big)\frac{\partial G(x,t)}{\partial t} + L_2^g(x)\frac{\partial G(x,t)}{\partial x} + M_2^g(x) G(x,t) = 0. \tag{4.24}$$

Here

$$L_2^g(x) = \frac{2}{\beta_0}\Big[6\Big(A_2^g(x) + K_1(x)A_4^g(x)\Big) + T_0\Big(B_2^g(x) + K_1(x)B_4^g(x)\Big)\Big], \tag{4.25}$$

$$\begin{aligned} M_2^g(x) &= \frac{2}{\beta_0}\Big[6\Big(A_1^g(x) + K_1(x)A_3^g(x) + \frac{\partial K_1(x)}{\partial x}A_4^g(x)\Big) \\ &\quad + T_0\Big(B_1^g(x) + K_1(x)B_3^g(x) + \frac{\partial K_1(x)}{\partial x}B_4^g(x)\Big)\Big], \end{aligned} \tag{4.26}$$

where $B_i^g(x)$, (i=1,2,3,4) are functions of x (see Appendix D). Here we consider the numerical parameter T_0 such that $T^2(t) = T_0 T(t)$ where $T(t)$=$\frac{\alpha_S(t)}{2\pi}$. As discussed in chapter 3, this parameter is chosen in such a way that the difference between $T^2(t)$ and $T_0T(t)$ is negligible in the specified range under study.

Thus proceeding in the same way we solve Eq.(4.24) we obtain the t or Q^2 and x-evolutions of gluon distribution function at NLO as

$$G(x,t) = G(x,t_0)\Big(\frac{t^{1+b/t}}{t_0^{1+b/t_0}}\Big)\cdot\exp\Big(\frac{b}{t} - \frac{b}{t_0}\Big) \tag{4.27}$$

and

$$G(x,t) = G(x_0,t)\cdot\exp\Big[\int_{x_0}^{x}\big(\frac{1}{L_2^g(x)} - \frac{M_2^g(x)}{L_2^g(x)}\big)dx\Big] \tag{4.28}$$

with $b = \frac{\beta_1}{\beta_0^2}$. The input functions $G(x,t_0)$ and $G(x_0,t)$ can be determined by applying the initial conditions at $t = t_0$ as well as at $x = x_0$ as in the previous case.

4.2.4 NNLO analysis of gluon distribution function

Using the splitting functions upto NNLO [28-30] and simplifying, we get the DGLAP equations for gluon distribution function at NNLO as

$$\begin{aligned} \frac{\partial G(x,t)}{\partial t} &= \frac{\alpha_s(t)}{2\pi}\Big[6\Big(\frac{11}{12} - \frac{N_f}{18} + \ln(1-x)\Big)G(x,t) + 6I_1^g(x,t)\Big] \\ &\quad + \Big(\frac{\alpha_S(t)}{2\pi}\Big)^2 I_2^g(x,t) + \Big(\frac{\alpha_S(t)}{2\pi}\Big)^3 I_3^g(x,t), \end{aligned} \tag{4.29}$$

where, the integral functions I_3^g is given by

$$I_3^g(x,t) = \int_x^1 d\omega \Big[P_{gg}^2(\omega) G\Big(\frac{x}{\omega}, t\Big)\Big]. \tag{4.30}$$

The explicit forms of the function P_{gg}^2 is given in Appendix F. In this case we overlook the quark contribution to the gluon distribution function. The reason behind this approximation is that at very small values of x, the gluons, being the most abundant parton, dominate over the quarks. Moreover, it simplifies the calculations involving the NNLO splitting functions which otherwise are very complicated to solve analytically.

To obtain an analytical solution of Eq.(4.29) we consider the numerical parameter T_1 such that $T^3(t) = T_1 T(t)$, where $T(t)$=$\frac{\alpha_S(t)}{2\pi}$. The value of T_1 is determined by phenomenological analysis, like T_0, from a particular range of Q^2 under study and by an appropriate choice of T_1 the error can be reduced to a minimum. Thus Eq. (4.29) can be simplified as

$$-\Big(\frac{t^2}{t - b\ln t + b^2(\ln^2 t - \ln t - 1) + c}\Big) + L_3^g(x)\frac{\partial G(x,t)}{\partial x} + M_3^g(x) G(x,t) = 0. \tag{4.31}$$

Here

$$\begin{aligned} L_3^g(x) &= \frac{2}{\beta_0}\Big[6\Big(A_2^g(x) + K_1(x)A_4^g(x)\Big) + T_0\Big(B_2^g(x) + K_1(x)B_4^g(x)\Big) \\ &\quad + T_1 C_2^g(x)\Big], \end{aligned} \tag{4.32}$$

$$\begin{aligned} M_3^g(x,t) &= \frac{2}{\beta_0}\Big[6\Big(A_1^g(x) + K_1(x)A_3^g(x) + \frac{\partial K_1(x)}{\partial x}A_4^g(x)\Big) + T_0\Big(B_1^g(x) \\ &\quad + K_1(x)B_3^g(x) + \frac{\partial K_1(x)}{\partial x}B_4^g(x)\Big) + T_1 C_1^g(x)\Big], \end{aligned} \tag{4.33}$$

where $C_i^g(x)$, (i=1,2) are functions of x (see Appendix D).

Following the same procedure as earlier, we solve Eq.(4.31) and obtain the t or Q^2 and x-evolutions of gluon distribution function at NNLO as

$$G(x,t) = G(x,t_0)\Big(\frac{t^{1+(b-b^2)/t}}{t_0^{1+(b-b^2)/t_0}}\Big) \cdot \exp\Big(\frac{b - c - b^2\ln^2 t}{t} - \frac{b - c - b^2\ln^2 t_0}{t_0}\Big) \tag{4.34}$$

and

$$G(x,t) = G(x_0,t) \cdot \exp\Big[\int_{x_0}^{x} \Big(\frac{1}{L_3^g(x)} - \frac{M_3^g(x)}{L_3^g(x)}\Big)dx\Big], \tag{4.35}$$

where $b = \frac{\beta_1}{\beta_0^2}$ and $c = \frac{\beta_2}{\beta_0^3}$. The input functions $G(x,t_0)$ and $G(x_0,t)$ can be determined by applying the initial conditions at $t = t_0$ as well as at $x = x_0$ as earlier.

4.3 Result and discussion

In this chapter, obtain the Q^2 or t ($t = \ln(Q^2/\Lambda^2)$) and x-evolutions of the gluon distribution function solving the DGLAP evolution equation for gluon density up to NNLO approximation. The analysis is performed in the range $5 \leq Q^2 \leq 110$ GeV^2 and $10^{-4} \leq x \leq 0.1$. The computed results of gluon distribution function at LO, NLO and NNLO are compared with the available GRV1998NLO [15], MRST2004NNLO [16], MSTW2008NNLO [17] and JR09NNLO [18] global QCD analysis. We also compare our results with the results of the BDM model [14]. The BDM model obtains an analytic solution for the LO gluon distribution function directly from the proton structure function using the accurate Froissart-bound [31] type parametrization of proton structure function. In this model, it is shown that using an analytic expression that successfully reproduces the known experimental data for proton structure function in a domain $x_{min}(Q^2) \leq x \leq x_{max}(Q^2)$ and $Q^2_{min} \leq Q^2 \leq Q^2_{max}$ in DIS, the gluon distribution $G(x, Q^2)$ can be uniquely determined in the same domain of x and Q^2. In all the graphs, the lowest-Q^2 and highest-x points are taken as input for

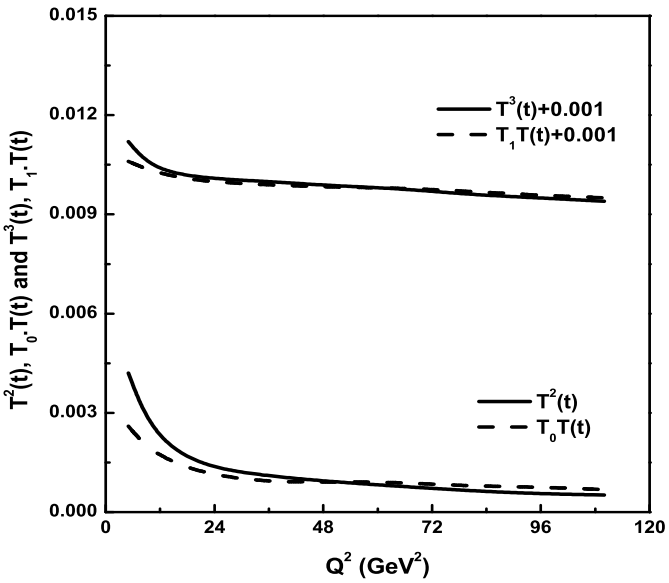

Figure 4.1: Comparison of T^2 and $T_0.T(t)$ as well as T^3 and $T_1.T(t)$ versus Q^2.

$G(x, t_0)$ and $G(x_0, t)$ respectively. As mentioned earlier for the analytical solution of DGLAP equation for gluon distribution function we consider a function $K_1(x)$ which relates the gluon distribution and the singlet structure function. For simplicity we consider the function $K_1(x) = K_1$, where K_1 is a constant parameter. The acceptable

range of the arbitrary constant K_1 is found to be $0.14 \leq K_1 \leq 0.85$. In each figure the dot lines represent our LO results, the dash-dot lines represent our NLO results whereas the solid lines represent the NNLO results. As expected the improvement is found to be better at NNLO than at NLO and LO.

In the calculation of gluon distribution function at NLO and NNLO, we consider two numerical parameters T_0 and T_1 to linearise the equations in α_s as discussed in section 4.2. These numerical parameters are obtained for a particular range of Q^2 under study. Figure 4.1 shows the plot of $T^2(t)$ and $T_0T(t)$ as well as $T^3(t)$ and $T_1T(t)$ versus Q^2 in the range $2 < Q^2 < 110$ GeV^2. It is observed that for $T_0 = 0.035$ and $T_1 = 0.0042$ the differences between $T^2(t)$ and $T_0T(t)$ as well as $T^3(t)$ and $T_1T(t)$ becomes negligible in the Q^2 range under study. Therefore, the consideration of the parameters T_0 and T_1 does not induce any unexpected change in our results.

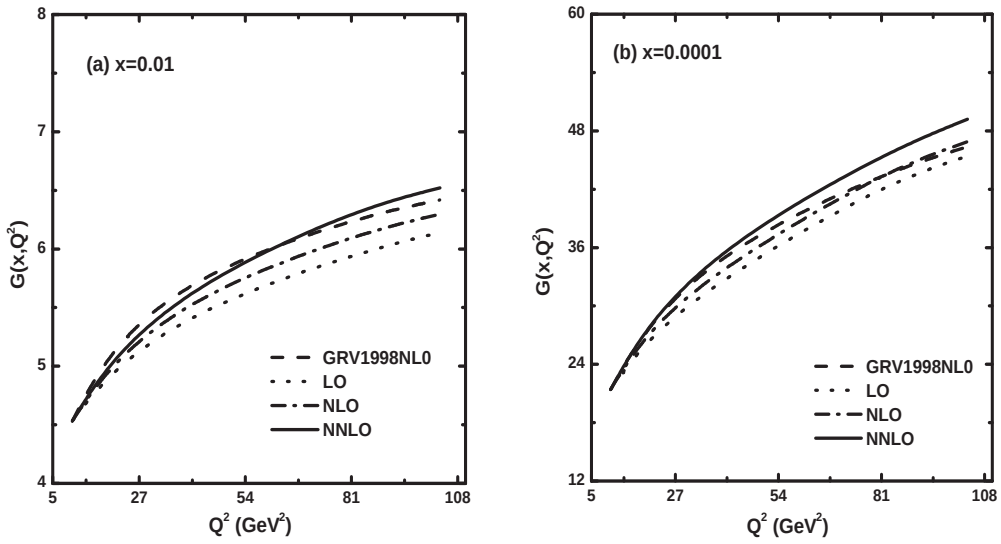

Figure 4.2: Q^2 evolution of gluon distribution functions at LO, NLO and NNLO compared with GRV1998NLO for two fixed values x. The dot lines represent the LO results (Eq.4.19), dash-dot lines represent the NLO results (Eq.4.27) and solid lines represent the NNLO results Eq.(4.34).

Figure 4.2 and Figure 4.3 show the comparison of the analytical gluon distributions obtained by solving the DGLAP equation for gluon distribution at LO, NLO and NNLO with the published results of GRV1998NLO. In Figure 4.2 we plot the computed values of $G(x, Q^2)$ from Eqs.(4.19), (4.27) and (4.34) for LO, NLO and NNLO respectively vs. Q^2 at $x = 0.01$ and $x = 0.0001$ respectively in the range $10 \leq Q^2 \leq 105$ Gev^2. It is seen from the figures that the predictions at NNLO

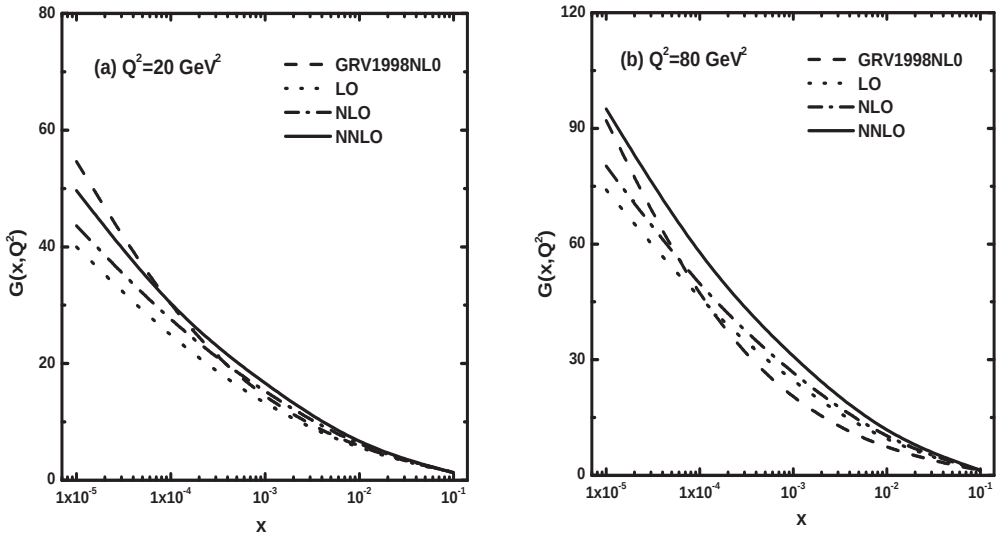

Figure 4.3: x evolution of gluon distribution functions at LO, NLO and NNLO compared with GRV1998NLO data for two fixed Q^2. The dot lines represent the LO results (Eq.4.21), dash-dot lines represent the NLO results (Eq.4.28) and solid lines represent the NNLO results Eq.(4.35).

approximation show better agreement with the GRV results at $x = 0.01$. On the other hand in Figure 4.3 the computed values of $G(x, Q^2)$ obtained from Eqs.(4.21), (4.28) and (4.35) for LO, NLO and NNLO respectively are plotted against x for two representative Q^2, viz. $Q^2 = 20\ GeV^2$ and $Q^2 = 80\ GeV^2$ respectively in the range $10^{-4} \leq x \leq 0.1$.

Figure 4.4 represent the comparison of our results of Q^2 or t ($t = \ln(Q^2/\Lambda^2)$) evolution of gluon distribution function $G(x, Q^2)$ calculated from Eqs.(4.19), (4.27) and (4.34) for LO, NLO and NNLO respectively with the MRST2004NNLO global analysis. Here we plot our predictions of $G(x, Q^2)$ as functions of Q^2 for some fixed values of x, viz. at $x = 0.01, 0.001, 0.0005$ and 0.0001 considering the Q^2 domain $5 \leq Q^2 \leq 100$ GeV^2. The NNLO predictions show the better compatibility with MRST2004 result particularly at $x = 0.001$.

In Figure 4.5 we plot our computed results of gluon distribution $G(x, Q^2)$ obtained from Eqs.(4.21), (4.28) and (4.35) for LO, NLO and NNLO respectively as functions of x for $Q^2 = 20, 40, 60$ and 80 GeV^2 respectively. Here we compare our results with the MRST2004NNLO predictions in the x range $10^{-4} \leq x \leq 0.1$. The NNLO approximation improves the agreement of the predicted values of $G(x, Q^2)$ with MRST2004NNLO global analysis.

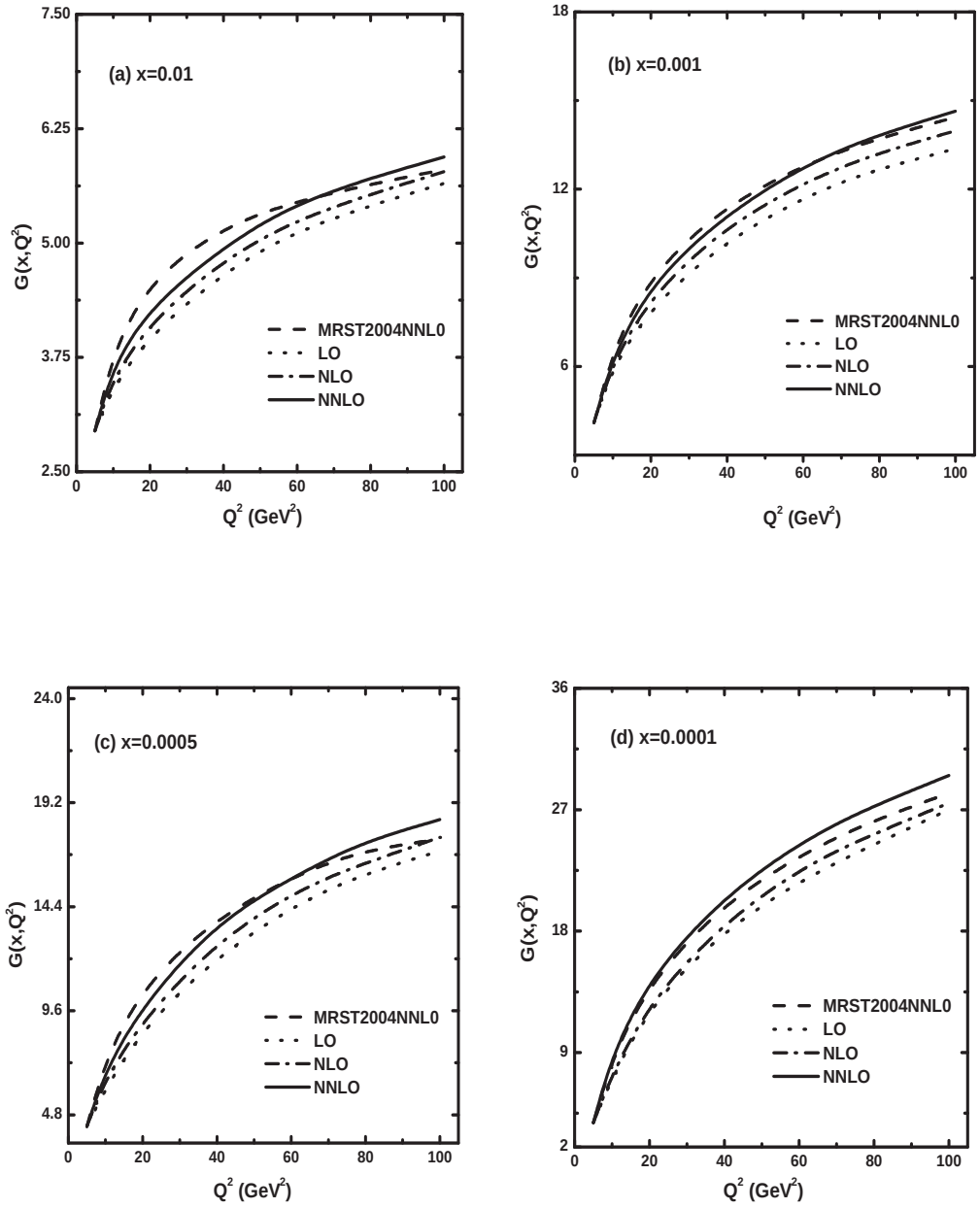

Figure 4.4: Comparison of Q^2 evolution of gluon distribution functions at LO, NLO and NNLO with MRST2004NNLO parametrization for four fixed values x. The dot lines represent the LO results (Eq.4.19), dash-dot lines represent the NLO results (Eq.4.27) and solid lines represent the NNLO results Eq.(4.34).

Figure 4.6 depict the Q^2-evolution of $G(x, Q^2)$ at LO, NLO and NNLO obtained from Eqs. (4.19), (4.27) and (4.34) respectively in the range $5 \leq Q^2 \leq 105$ GeV^2. Here our predictions are compared with the MSTW2008NNLO parametrization and the comparison is performed for four fixed x values, namely x=0.01, 0.005, 0.001 and 0.0001. For each x, the NNLO result show good consistency with the MSTW2008NNLO predictions.

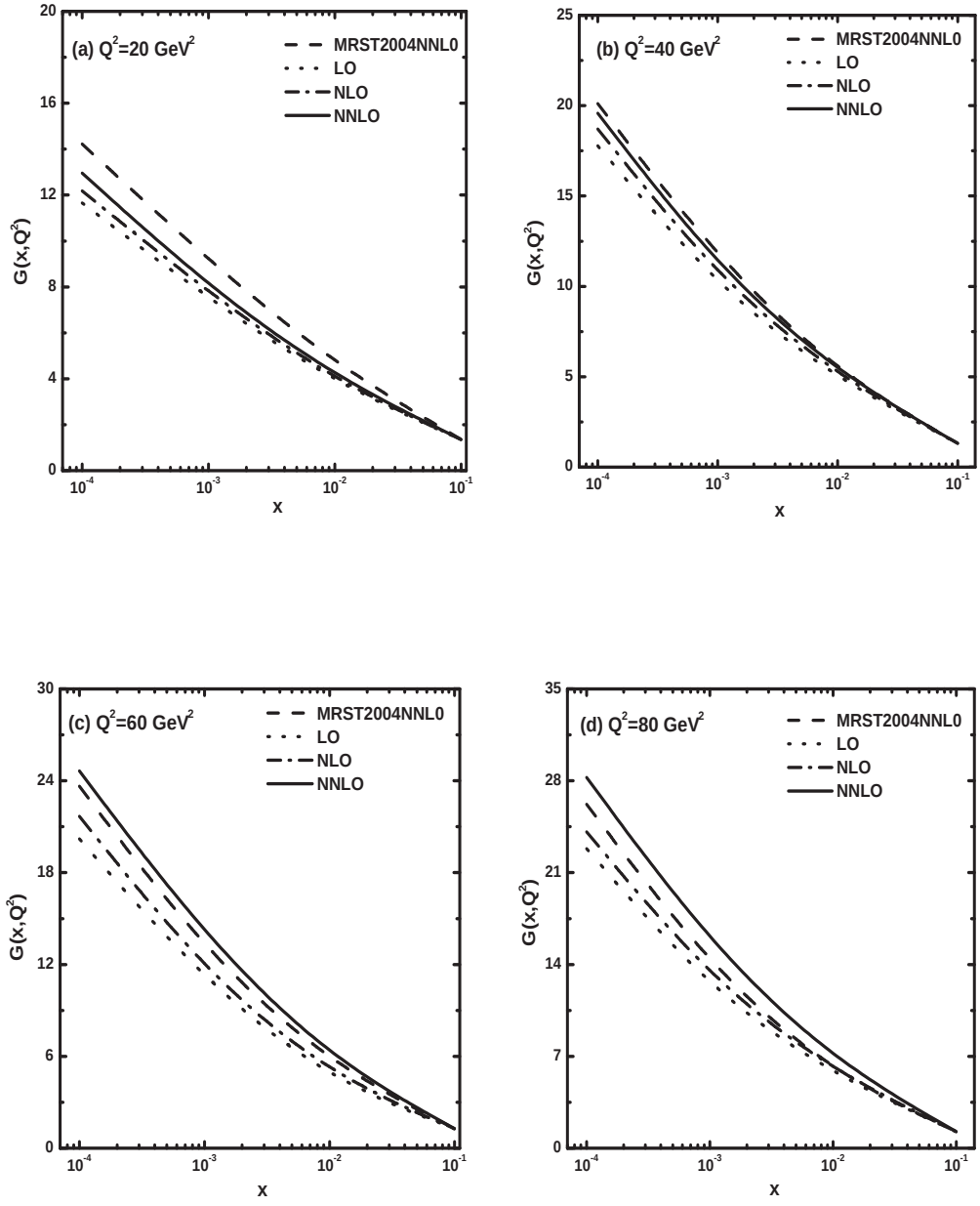

Figure 4.5: Comparison of the values of gluon distribution function at LO, NLO and NNLO plotted against x with the MRST2004NNLO parametrization for four representative Q^2. The dot lines represent the LO results (Eq.4.21), dash-dot lines represent the NLO results (Eq.4.28) and solid lines represent the NNLO results Eq.(4.35).

Figure 4.7 shows the comparison of our results of x-evolutions of $G(x, Q^2)$ at LO, NLO and NNLO obtained from Eqs.(4.21), (4.28) and (4.35) with those obtained by the MSTW2008NNLO parametrization in the range $10^{-4} \leq x \leq 0.1$. The comparison is done for four representative $Q^2 = 30, 50, 80$ and 100 GeV^2. It can be seen that the NNLO result for each Q^2 agrees well with the MSTW2008NNLO parametrization.

We also compare the predicted results of x dependence of gluon distribution

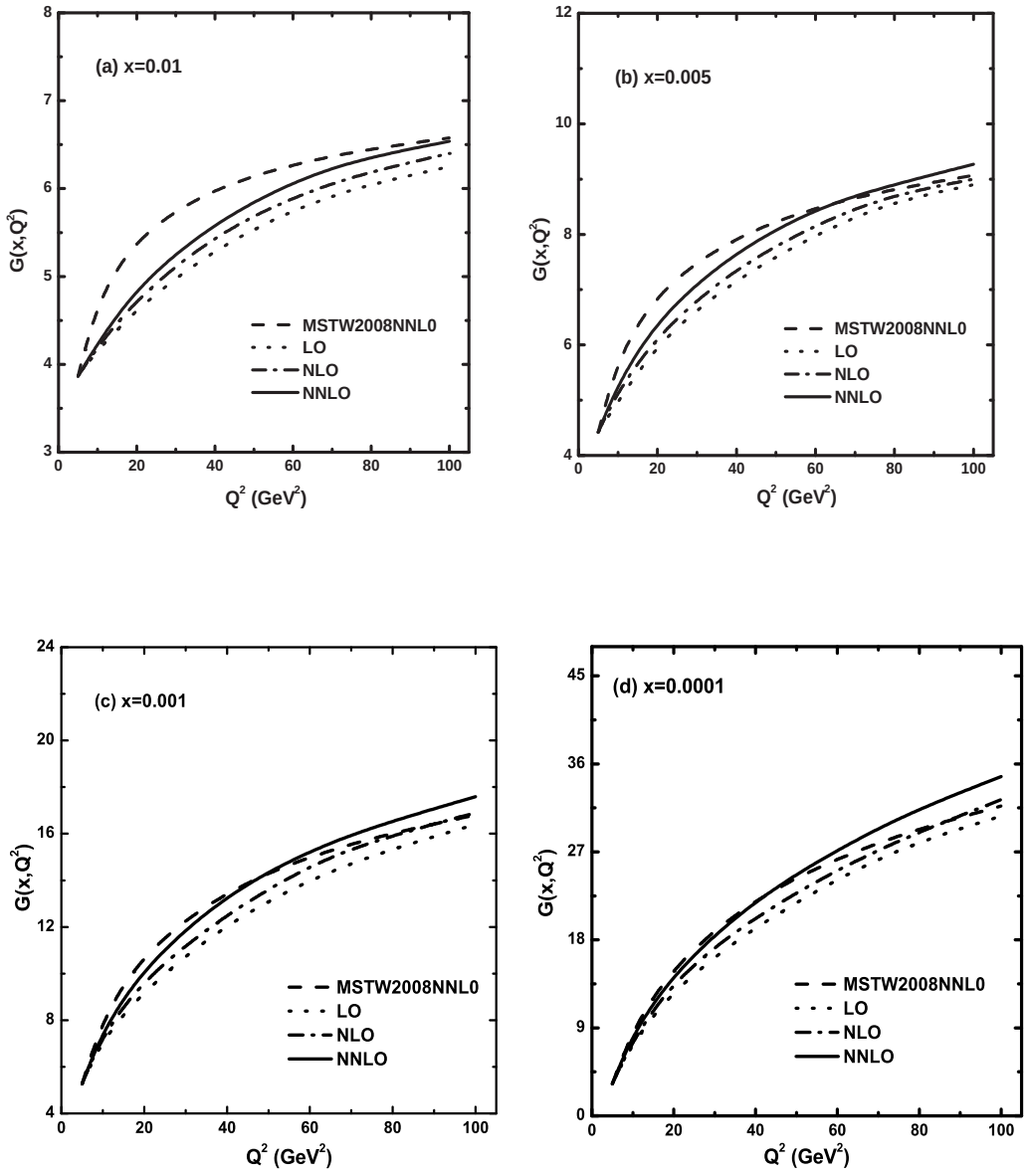

Figure 4.6: Q^2 evolution of gluon distribution function at LO, NLO and NNLO compared with MSTW2008NNLO parametrization for four fixed x values. The dot lines represent the LO results (Eq.4.19), dash-dot lines represent the NLO results (Eq.4.27) and solid lines represent the NNLO results Eq.(4.34).

function $G(x, Q^2)$ with the JR09NNLO global parton analysis [18] as well as with the results of BDM model [14]. This comparison is portrayed in Figure 4.8 where we plot the computed values of $G(x, Q^2)$ at LO, NLO and NNLO using Eqs. (4.26), (4.33) and (4.40) versus x in the range $10^{-4} \leq x \leq 0.1$ for $Q^2 = 5$ GeV^2 and $Q^2 = 20$ GeV^2. Our predictions of $G(x, Q^2)$ at NNLO show very good agreement with the JR09NNLO. Our results also show similar behaviour with those of BDM model, however the BDM

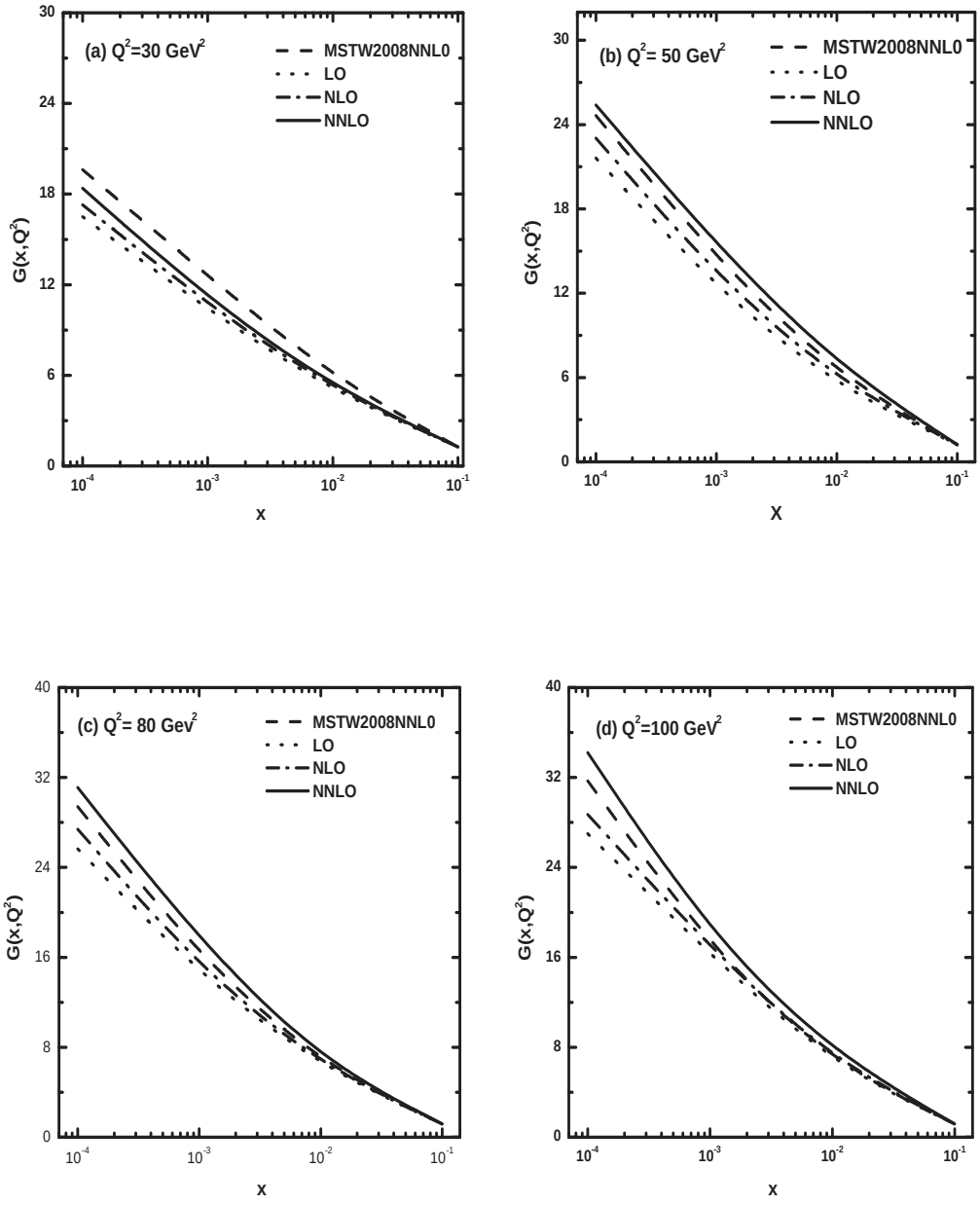

Figure 4.7: Comparison of the values of gluon distribution function at LO, NLO and NNLO plotted against x with the MSTW2008NNLO parametrization for four representative Q^2. The dot lines represent the LO results (Eq.4.21), dash-dot lines represent the NLO results (Eq.4.28) and solid lines represent the NNLO results Eq.(4.35).

model gives much larger gluon distribution towards small x. Figures indicate that the compatibility of our predictions with the JR09NNLO parametrization much better that that of BDM model.

To check the compatibility of our results of gluon distribution function at LO, NLO and NNLO respectively with different parametrizations, we perform a χ^2 test shown in Table 4.1. From this we observe that our results are almost comparable

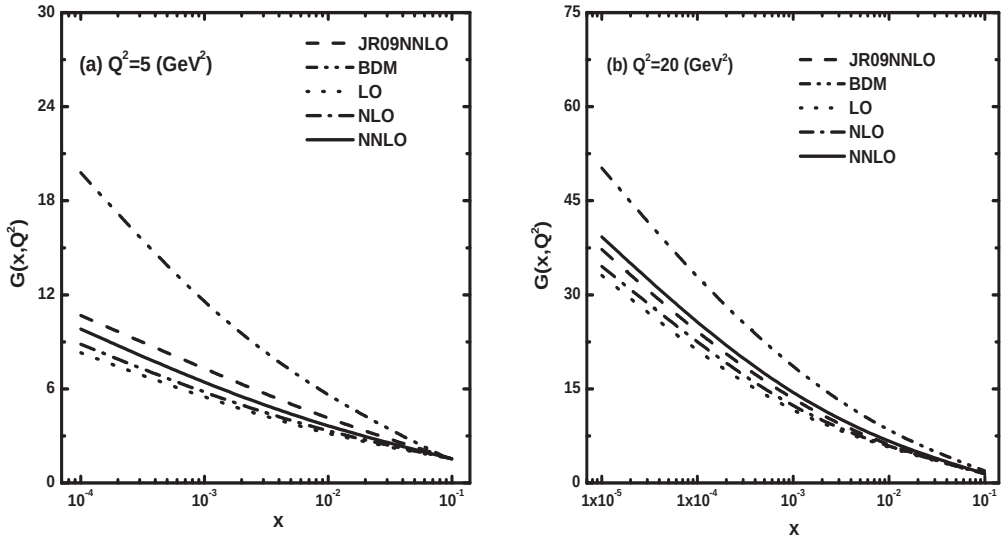

Figure 4.8: Comparison of our predictions of gluon distribution function at LO, NLO and NNLO with JR09NNLO global fit as well as with the BDM model for two representative Q^2. The dot lines are the LO results of obtained from Eq.(4.21), dash-dot lines are NLO results from Eq.(4.28) and solid lines are the NNLO results from Eq.(4.35). The dash curves are from the JR09NNLO parametrization and dash-dot-dot curves are the results of BDM model.

Table 4.1: χ^2 text for $G(x, Q^2)$

Order	**GRV1998**	**MRST2004**	**MSTW2008**	**JR09**
LO	4.03	2.34	3.18	2.38
NLO	3.16	1.63	2.16	1.24
NNLO	2.96	0.85	1.72	0.61

with different parametrizations and the inclusion of NNLO contributions improve the consistency.

4.4 Summary

To summarise the evolution of gluon distribution function with respect to x and Q^2 at LO, NLO and NNLO are presented by solving the DGLAP evolution equation for gluon distribution analytically. Here the DGLAP equation is first transformed into a partial differential equation in the two variables x and Q^2 by using the Taylor series expansion valid at small-x. Following this the resulting equation is solved at LO, NLO and NNLO respectively by the Lagrange's auxiliary method to obtain the Q^2 and x evolutions of the gluon distribution function. We compare our predictions with the GRV1998NLO, MRST2004NNLO, MSTW2008NNLO and JR09NNLO global QCD

analysis as well as with the BDM model. The obtained results of gluon distribution can be described within the framework of perturbative QCD. Our results show that at fixed x the gluon distribution function increases with increasing Q^2, whereas at fixed Q^2 it increases as x decreases which is in agreement with perturbative QCD fits at small-x. We perform our analysis in the Q^2 and x range, viz. $5 \leq Q^2 \leq 110$ GeV^2 and $10^{-4} \leq x \leq 0.1$ and note that in this domain our predicted solutions are comparable with different global analysis of parton distributions. We consider the function $K_1(x) = K_1$, where K_1 is a constant parameter, in defining the relation between gluon and singlet structure functions and obtain our best fitted results in the range $0.14 \leq K_1 \leq 0.85$. Moreover we consider the numerical parameters T_0 and T_1 to linearise the equations at NLO and NNLO in α_s. These parameters are chosen from phenomenological analysis for a particular range of Q^2 under study and therefore, the use of the parameters T_0 and T_1 does not produce any abrupt change in our results. From our phenomenological analysis we observe that our computed results of gluon distribution function at NNLO show significantly better agreement with different parameterizations than those of LO and NLO. Thus we can say that the NNLO approximation has appreciable contribution to the gluon distribution function in the particular range of x and Q^2 under study. However, in the very small-x region, where the number density of gluons become very high, the gluon recombination processes may take place inducing nonlinear corrections to the QCD evolution and in that case the solution suggested in this chapter may not be sufficient to explain the available data at very small-x. The nonlinear GLR-MQ evolution equation may provide a good description of the high density QCD at very small-x, which we will discuss in the next chapter.

Bibliography

[1] Adloff, C. et al., On the rise of the proton structure function F_2 towards low x, *Phys. Lett. B* **520** (3-4), 183−−190, 2001.

[2] Adloff, C. et al., Deep-inelastic inclusive *ep* scattering at low x and a determination of α_s, *Eur. Phys. J. C* **21**(1), 33−−61 2001.

[3] Chekanov, S. et al., Measurement of the neutral current cross section and F_2 structure function for deep inelastic e^+p scattering at HERA, *Eur. Phys. J. C* **21**(3),443−−471, 2001.

[4] Gribov, V. N., Lipatov, L. N. Deep inelastic *ep* scattering in perturbation theory, *Sov. J. Nucl. Phys.* **15**(4), 438−−450, 1972.

[5] Gribov, V. N., Lipatov, L. N. e^+e^- pair annihilation and deep-inelastic *ep* scattering in perturbation theory, *Sov. J. Nucl. Phys.* **15**(4), 675−−684, 1972.

[6] Dokshitzer, V. Calculation of structure functions of deep-inelastic scattering and e^+e^- annihilation by perturbation theory in quantum chromodynamics, *Sov. Phys. JETP* **46**(4), 641−−652, 1977.

[7] Altarelli, G., Parisi, G. Asymptotic freedom in parton language, *Nucl. Phys. B* **126**(2), 298−−318, 1977.

[8] Prytz, K. Approximate determination of the gluon density at low-x from the F_2 scaling violations, *Physics Letters B* **311**(1-4), 286−−290, 1993.

[9] Prytz, K. An approximate next-to-leading order relation between the low-x F_2 scaling violations and the gluon density, *Phys. Lett. B* **332**(3-4), 393−−397, 1994.

[10] Sarma, J. K., Medhi, G. K. Regge behaviour of structure function and gluon distribution at low-x in leading order, *Eur. Phys. J. C* **16**(3), 481487, 2000.

[11] Choudhury, D. K., Deka, Ranjita and Saikia, A. Gluon distribution and $\frac{dF_2}{d\ln Q^2}$ at small x in the next-to-leading order, *Eur. Phys. J. C* **2**(2), 301−−305, 1998.

[12] Choudhury, D. K., Sahariah, P. K. A solution of the DGLAP equation for gluon at low x, *Pramana J. Phys.* **58**(4), 599−−610, 2002.

[13] Choudhury, D. K., Sahariah, P. K. The next-to-leading order (NLO) gluon distribution from DGLAP equation and the logarithmic derivatives of the proton structure function $F_2(x, Q^2)$ at low x, *Pramana J. Phys.* **65**(2), 193−−213, 2005.

[14] Block, Martin M., Durand, Loyal and McKay, Douglas W. Analytic derivation of the leading-order gluon distribution function $G(x, Q^2)$ from the proton structure function $F_2^p(x, Q^2)$, *Phys. Rev. D* **77**(9), 094003, 2008.

[15] Gluck, M., Reya, E. and Vogt, A. Dynamical parton distributions revisited, *Eur. Phys. J. C* **5**(3), 461−−470, 1998.

[16] Martin, A. D. et al., Physical gluons and high-ET jets, *Physics Letters B* **604**(1-2), 61−−68, 2004.

[17] Martin, A. D. et al., Parton distributions for the LHC, *Eur. Phys. J. C* **63**(2), 189−−285, 2009.

[18] Jimenez-Delgado, P., Reya, E. Dynamical NNLO parton distributions, *Phys. Rev. D* **79**(7), 074023, 2009.

[19] Van Neerven, W. L., Vogt, A. NNLO evolution of deep-inelastic structure functions: the singlet case, *Nucl. Phys. B* **588**(1-2), 345−−373, 2000.

[20] Shaikhatdenov, B. G. et al., QCD coupling constant at next-to-next-to-leading order from DIS data, *Phys. Rev. D* **81**(3), 034008, 2010.

[21] Abbott, L. F., Atwood, W. B. and Michael Barnett, R. Quantum-chromodynamic analysis of eN deep-inelastic scattering data, *Phys. Rev.* **22**(3), 582−−594, 1980.

[22] Sarma, J. K., Das, B. t evolutions of structure functions at low-x, *Phys. Lett. B* **304**(3-4), 323−−328, 1993.

[23] Sarma, J. K., Choudhury, D. K. and Medhi, G. K. x-distribution of deuteron structure function at low-x, *Phys.Lett. B* **403**(1-2), 139−−144, 1997.

[24] Baishya, R., Sarma, J. K. Method of characteristics and solution of DGLAP evolution equation in leading and next to leading order at small x, *Phys. Rev. D* **74**(10), 107702, 2006.

[25] Furmanski, W., Petronzio, R. Lepton-hadron processes beyond leading order in quantum chromodynamics, *Z. Phys. C* **11**(4), 293−−314, 1982.

[26] Furmanski, W., Petronzio, R. Singlet parton densities beyond leading order, *Phys.Lett. B* **97**(3-4), 437−−442, 1980.

[27] Curci, G., Furmanski, W. and Petronzio, R. Evolution of parton densities beyond leading order: The non-singlet case, *Nucl. Phys. B* **175**(1), 27−−92, 1981.

[28] Van Neerven, W. L., Vogt, A. NNLO evolution of deep-inelastic structure functions: the singlet case, *Nucl. Phys. B* **588**(1-2), 345−−373, 2000.

[29] Vogt, A., Moch, S. and Vermaseren, J. A. M. The three-loop splitting functions in QCD: the singlet case, *Nucl. Phys. B* **691**(1-2), 129−−181, 2004.

[30] Ellis, R. K., Kunszt, Z. and Levina, E. M. The evolution of parton distributions at small x, *Nuclear Physics B* **420**(3), 517−−549, 1994.

[31] Froissart, M. Asymptotic Behavior and Subtractions in the Mandelstam Representation, *Phys. Rev.* **123**(3), 1053−−1057, 1961.

Chapter 5

Shadowing Corrections to the Small-x Behaviour of Gluon Distribution Function

5.1 Introduction

The dynamics of the the high density QCD, the regime of large gluon densities, is one of the present-day extremely demanding undecided issues in the area of high energy or small-x physics, where x is the small fraction of proton's momentum conveyed by the struck parton. Enormous theoretical and experimental endeavours towards the perception of hadron structure in the high density regime at small-x occurs from DIS at HERA to the proton-(anti)proton collisions at LHC. The gluon saturation is one of the most fascinating problems of the small-x physics, which is presumed on theoretical basis and there is emerging indications of its existence [1-3]. The linear QCD evolution equations at the twist-2 level like DGLAP [4-6] predicts an abrupt rise of the gluon densities towards small-x which is also perceived in the DIS experiments at HERA. This sharp growth of gluon density generates cross sections which in the high-energy limit violate the Froissart bound [7, 8] on physical cross sections. Accordingly a new formulation of the QCD at high partonic density is essential, in the very small-x region, to incorporate the unitarity corrections in a suitable way. In general it is anticipated that, the gluon recombination processes provide the mechanism responsible for the unitarization of the cross section at high energies. As we move towards small-x at fixed Q^2 the number of gluons of fixed size

$\sim 1/Q$ increases and at some critical value of x, the entire transverse area inhabited by gluons turns out to be analogous to or larger than the transverse area of a proton. Thus, the likelihood of interaction between two gluons can no longer be overlooked and it sooner or later engenders a situation in which individual partons inevitably overlap or shadow each other. In the derivation of the linear DGLAP equation the correlations among the initial gluons in the physical process of interaction and recombination of gluons are not usually taken into account. But at small-x the corrections of the correlations among the initial gluons to the evolutionary amplitude should be considered which eventually leads to a control of the maximum gluon density per unit of phase-space. The conventional linear DGLAP evolution equation will have to be modified accordingly in order to take these into effect. The multiple gluon interactions take part in the evolution nonlinearly, taming the growth of the gluon density in the kinematic domain where α_s remains small but the density of gluons evolves into very high. The pioneering perturbative QCD studies reporting the recombination of two gluon ladders into one were performed by Gribov, Levin and Ryskin [9], and by Mueller and Qiu [10, 11]. They insinuated that the shadowing or nonlinear corrections due to gluon recombination could be expressed in a new evolution equation with an additional nonlinear term quadratic in gluon density. This equation, widely known as the GLR-MQ equation, can be regarded as the upgraded version of the linear DGLAP equation.

The GLR-MQ equation incorporates all fan diagrams, that is, all workable $2 \to 1$ ladder recombinations, in the double leading logarithmic approximation (DLLA) in order to deal with the gluon recombination processes. The fan diagrams portrays the decisive role in the restoration of unitarity by taking into consideration some of the gluon recombination processes that become vital at small-x. Gribov, Levin and Ryskin at the outset introduced the concept of shadowing, arising from gluon recombination, based on the Abramovsky-Gribov-Kancheli (AGK) cutting rule [12] in the DLLA. Later Mueller and Qiu successfully carried out a perturbative calculation of the recombination probabilities in the DLLA which empowers the equation to be applied phenomenologically [10]. The GLR-MQ equation prognosticate a critical line separating the perturbative regime from the saturation regime and it is legitimate only in the vicinity of this critical line. Moreover it predicts a saturation of the gluon

density at very small-x. Therefore the study of the GLR-MQ equation is extremely important for understanding the nonlinear effects of gluon recombination at small enough x as well as for the determination of the saturation momentum (Q_S) that incorporates physics in addition to that of the linear evolution equations commonly used to fit DIS data.

Until now the majority of our knowledge on the modifications of the higher order QCD effects is established on the semi-classical approach [9, 13-15] and on numerical studies [16-21]. The approximate analytical solutions of the nonlinear GLR-MQ evolution equation have also been reported in recent years [22, 23]. In this thesis we attempt to use, to a feasible extent, semi-analytic methods to solve this equation. We report, in this chapter, the approximate semi-analytical solution of the nonlinear GLR-MQ equation as well as the validity of the well known Regge-like ansatz in the region of small-x and moderate virtuality of photon. The aim of this work is to check the evidence for gluon recombination at very small-x. We investigate the effect of shadowing corrections on the small-x behavior of gluon distribution at fixed virtuality of photon from the solution of GLR-MQ equation in LO with considerable phenomenological success. Moreover, we obtain the Q^2-dependence of gluon distribution with shadowing corrections at fixed small-x. Our resulting gluon distributions are compared with different experimental data and parametrizations. Our predictions for nonlinear gluon density are further compared with different models based on GLR-MQ equation. Moreover, we examine the extent of nonlinearity in our predictions by comparing the gluon distributions obtained from nonlinear GLR-MQ equation with those obtained from linear DGLAP equation.

5.2 Formalism

5.2.1 General framework

The GLR-MQ equation depends on two processes in the parton cascade, namely the gluon emission generated by the QCD vertex $g \to g + g$ as well as the gluon recombination by the same vertex $g + g \to g$. The probability that a gluon splits into two gluons is proportional to $\alpha_s \rho$ whereas the probability of gluon recombination is proportional to $\alpha_s^2 r^2 \rho^2$. Here, ρ is the density of gluons in the transverse plane and r is the size of the gluon produced in the recombination process and for DIS, $r \propto \frac{1}{Q}$.

It is very clear that, at $x \sim 1$ only the production of new partons (quarks or gluons) is essential because $\rho \ll 1$, however at $x \to 0$ the value of ρ becomes so large that the recombination of gluons turns into crucial. The number of partons in a phase space cell $(\Delta \ln(1/x) \Delta \ln Q^2)$, thus, increases through gluon splitting and decreases through gluon recombination and correspondingly the balance equation for emission and recombination of partons can be written as [9-11]

$$\frac{\partial^2 \rho(x,Q^2)}{\partial \ln(1/x) \partial \ln Q^2} = \frac{\alpha_s(Q^2) N_c}{\pi} \rho(x,Q^2) - \frac{\alpha_s^2(Q^2)\gamma}{Q^2} [\rho(x,Q^2)]^2, \tag{5.1}$$

which is referred to as the GLR-MQ equation. Here $\rho = \frac{xg(x,Q^2)}{\pi R^2}$, where πR^2 is the target area and R is the correlation radius between two interacting gluons i.e. the size of the relevant region for the gluon recombination processes. The factor γ is found to be $\gamma = \frac{81}{16}$ for $N_c = 3$, as evaluated by Mueller and Qiu [10]. In terms of gluon distribution function the above equation can be expressed as

$$\frac{\partial^2 xg(x,Q^2)}{\partial \ln(1/x) \partial \ln Q^2} = \frac{\alpha_s(Q^2) N_c}{\pi} xg(x,Q^2) - \frac{\alpha_s^2(Q^2)\gamma}{\pi Q^2 R^2} [xg(x,Q^2)]^2, \tag{5.2}$$

The first term in the r.h.s. is the usual DGLAP term in the DLLA and and is therefore linear in the gluon field. The second term carries a negative sign and it reduces the growth of the gluon distribution once the fan diagrams become admissible. It expresses the nonlinearity in respect of the square of the gluon distribution. Here, the representation for the gluon distribution $G(x,Q^2) = xg(x,Q^2)$ is used, where $g(x,Q^2)$ is the gluon density. The quark-gluon emission diagrams are not given attention here due to their little importance in the gluon-rich small-x region. A general criterion for the validity of Eq.(5.2) is that the nonlinear correction term should not be larger than the first term since in that case further corrections must be considered and non-perturbative effects could be of importance [24].

The parameter R does not become operative as long as one uses the DGLAP evolution equation, which is linear in gluon density. Nonetheless, this size parameter becomes relevant in the GLR-MQ equation where one takes into account the first nonlinear term in the evolution and therefore it is essential to define it precisely. Since the size parameter R in the denominator and the gluon distribution G in the numerator appear in the second term of Eq.(5.2) as squared, so they are extremely decisive for the magnitude of the recombination effect. R is of the order of proton

radius R_h, that is $R \sim 5$ GeV^{-1} if the gluons are distributed uniformly across the whole of the proton and in that case recombination or shadowing corrections can be negligibly small [10, 25]. On the other hand, R is of the order of the transverse size of a valence quark i.e. $R \sim 2$ GeV^{-1} if the gluons are condensed in the hot spots [10, 25, 26] inside the proton. The hot spots can enumerate rapid commencement of gluon-gluon interactions in the environs of the parton and and so uplift the recombination effect. Accordingly in such hot-spots the shadowing corrections are expected to be large.

5.2.2 Solution of GLR-MQ equation for gluon distribution function and effect of gluon shadowing

In order to study the effect of nonlinear or shadowing corrections on the behaviour of gluon density we rewrite the GLR-MQ equation given by Eq.(5.2) in a convenient form

$$\frac{\partial G(x,Q^2)}{\partial \ln Q^2} = \frac{\partial G(x,Q^2)}{\partial \ln Q^2}\Big|_{DGLAP} - \frac{81}{16}\frac{\alpha_s^2(Q^2)}{R^2Q^2}\int_x^1 \frac{d\omega}{\omega}\Big[G\Big(\frac{x}{\omega},Q^2\Big)\Big]^2, \tag{5.3}$$

We perform the analysis in the leading twist approximation and therefore have taken the strong coupling constant $\alpha_s(Q^2) = \frac{4\pi}{\beta_0 \ln(Q^2/\Lambda^2)}$, where $\beta_0 = 11 - \frac{2}{3}N_f$. At small-$x$ gluons essentially turn out to be the most abundant partons and therefore, the quark contributions to the gluon distribution function can be overlooked in the small-x region. Accordingly the first term in the r.h.s. of Eq. (5.3) can be expressed as [27]

$$\begin{aligned}\frac{\partial G(x,Q^2)}{\partial \ln Q^2}\Big|_{DGLAP} &= \frac{3\alpha_s(Q^2)}{\pi}\Bigg[\Big(\frac{11}{12} - \frac{N_f}{18} + \ln(1-x)\Big)G(x,Q^2) \\ &\quad + \int_x^1 d\omega\Big\{\frac{\omega G\Big(\frac{x}{\omega},Q^2\Big) - G(x,Q^2)}{1-\omega} \\ &\quad + \Big(\omega(1-\omega) + \frac{1-\omega}{\omega}\Big)G\Big(\frac{x}{\omega},Q^2\Big)\Big\}\Bigg].\end{aligned} \tag{5.4}$$

To obtain an analytical solution of the GLR-MQ equation in the small-x region we incorporate a Regge-like behavior of gluon distribution function. The behaviour of structure functions at small-x can be described effectively in terms of Regge-like ansatz [28]. The Regge theory is a highly ingenuous parameterization of all total cross sections and supposed to be applicable at large-Q^2 values if x is small enough $x < 0.01$ [29]. Moreover, as advocated in Refs.[30, 31], the Regee behavior is anticipated to

be valid at small-x and some intermediate Q^2, where Q^2 must be small but not so small that $\alpha_s(Q^2)$ is too large. Since the total center of mass energy squared is defined as $s^2 = Q^2\left(\frac{1}{x} - 1\right)$, therefore the small-$x$ behaviour of structure functions for fixed Q^2 emulates the high energy behaviour of total cross section with increasing s^2 [32]. For this reason the Regge pole exchange picture [28] sounds convenient for the theoretical description of this behaviour. Again, as the structure functions are proportional to the total virtual photon-nucleon cross section, therefore they are expected to have Regge behaviour corresponding to pomeron or reggeon exchange [30]. According to the Donnachie-Landshoff (DL) model, the high energy attitude of hadronic cross sections as well as structure functions will be governed by two contributions, especially by a pomeron proliferating the rise of structure function at small-x and by reggeons related with meson trajectories. The high energy i.e. small-x behaviour of both gluons and sea quarks are conducted by the same singularity factor in the complex angular momentum plane [31] in accordance with Regge theory. The Regge behavior of the sea-quark distribution for small-x is given by $q_{sea}(x) \sim x^{-\alpha_P}$ corresponding to a pomeron exchange with an intercept of $\alpha_P = 1$. But the valence-quark distribution for small x given by $q_{val}(x) \sim x^{-\alpha_R}$ corresponds to a reggeon exchange with an intercept of $\alpha_R = 0.5$. The x dependence of the parton densities is often estimated at moderate Q^2 and thus the leading order calculations in $\ln(1/x)$ with fixed α_s predict a steep power-law behavior of $xg(x, Q^2) \sim x^{-\lambda_G}$, where $\lambda_G = (4\alpha_s N_c/\pi)\ln 2 \simeq 0.5$ for $\alpha_s \simeq 0.2$, as relevant for $Q^2 \sim 4\ GeV^2$.

Furthermore, the Regge theory is presumed to be applicable if W^2, the mass invariant squared in a DIS process, is much greater than all the other variables [33] and so, models based upon this idea have been fruitful in explaining the DIS cross-section when x is small enough ($x < 0.7$), whatsoever be the value of Q^2 [33-35]. The small-x limit of DIS corresponds to the case when $2M\nu >> Q^2$, where $x = Q^2/2M\nu$, but Q^2 is still maintained large i.e. $Q^2 > \Lambda^2$, with Λ being the QCD cut off parameter. The limit $2M\nu >> Q^2$ is equivalent to $s >> Q^2$ and is therefore the Regge limit of DIS. Moreover, as Q remains greater than the QCD cut off parameter Λ so it enables us to use perturbative QCD calculations and therefore Regge theory is applicable in the region of large s, i.e. in the region of small-x [28, 29]. Hence it is feasible to use Regge theory for the study of the GLR-MQ equation which is an improved version

of DGLAP equation in the very small-x region. The Regge pole model gives the parametrization of the DIS structure function $F_2(x, Q^2)$ at small-x as $F_2 \propto x^{-\lambda}$ with $\lambda > 0$ being a constant or depending on Q^2 or x [29, 33].

On that account, we employ the Regee like ansatz of gluon distribution function to solve the nonlinear GLR-MQ equation at small-x. We assume a simple form of Regge ansatz for gluon distribution function given as

$$G(x, Q^2) = H(Q^2)x^{-\lambda_G}, \tag{5.5}$$

where $H(Q^2)$ is a function of Q^2 and λ_G is the Regge intercept for gluon distribution function. This form of Regge behaviour is extensively used by many authors with considerable success [33, 36, 37]. With this ansatz the term $G(\frac{x}{\omega}, Q^2)$ can be written as

$$G\Big(\frac{x}{\omega}, Q^2\Big) = \omega^{\lambda_G} G(x, Q^2). \tag{5.6}$$

One of the applications of the Regge behaviour is the DL two pomeron model where the rise of structure function is described by powers of $1/x$. In the DL model it is assumed that the exchange of two pomerons contribute to the amplitude, however, at small-x the gluon distribution function is dominated exclusively by the hard pomeron exchange [33]. In the DL two pomerons exchange model, the hard pomeron has an intercept $\epsilon_h = 0.418$. Moreover, as the values of Regge intercepts for all the spin-independent singlet, non-singlet and gluon structure functions should be close to 0.5 in quite a broad range of small-x [37], so we also consider the value of λ_G to be 0.5 in our analysis and expect to obtain our best fit results with this value of λ_G.

To simplify our calculations we consider a variable t, such that $t = \ln(\frac{Q^2}{\Lambda^2})$. Then using the Eqs.(5.5) and (5.6) together with the Eq.(5.4), Eq.(5.3) can be simplified as

$$\begin{aligned}\frac{\partial G(x,t)}{\partial t} &= \frac{3\alpha_s(t)}{\pi} G(x,t)\Big[\Big(\frac{11}{12} - \frac{N_f}{18} + \ln(1-x)\Big) + \int_x^1 d\omega\Big\{\frac{\omega^{\lambda_G+1}-1}{1-\omega} \\ &\quad + \Big(\omega(1-\omega) + \frac{1-\omega}{\omega}\Big)\omega^{\lambda_G}\Big\}\Big] - \frac{81}{16}\frac{\alpha_s^2(t)}{R^2\Lambda^2 e^t} G^2(x,t)\int_x^1 \omega^{2\lambda_G-1} d\omega.\end{aligned} \tag{5.7}$$

Now rearranging the terms Eq. (5.7) can be expressed as

$$\frac{\partial G(x,t)}{\partial t} = \gamma_1(x)\frac{G(x,t)}{t} - \gamma_2(x)\frac{G^2(x,t)}{t^2 e^t}, \tag{5.8}$$

where the x dependent functions $\gamma_1(x)$ and $\gamma_2(x)$ are defined as

$$\gamma_1(x) = 3A_f\Big[\frac{11}{12} - \frac{N_f}{18} + \ln(1-x) + \int_x^1 d\omega\Big\{\frac{\omega^{\lambda_G+1}-1}{1-\omega} + \Big(\omega(1-\omega) + \frac{1-\omega}{\omega}\Big)\omega^{\lambda_G}\Big\}\Big], \tag{5.9}$$

$$\gamma_2(x) = \frac{81}{16}\frac{A_f^2\pi^2}{R^2}\int_x^1 \omega^{2\lambda_G-1}d\omega. \tag{5.10}$$

where $A_f = \frac{4}{\beta_0}$.

Eq.(5.8) is a partial differential equation for the gluon distribution function with respect to the variables x and Q^2 ($t = \ln(Q^2/\Lambda^2)$). Thus apart from its conventional use in Q^2-evolution, Eq.(5.8) can also be used to examine the x-dependence of gluon distribution. Solution of Eq.(5.8) then leads us to a solution for the nonlinear gluon density as given below

$$G(x,t) = \frac{t^{\gamma_1(x)}}{C + \gamma_2(x)\int t^{\gamma_1(x)-2}e^{-t}dt}, \tag{5.11}$$

where C is a constant to be determined from initial boundary conditions. Thus we solve Eq.(5.3) by employing the Regge ansatz for gluon distribution given by Eq.(5.5) and obtain a solution of the nonlinear gluon density. As the Regge behaviour is supposed to be legitimate at small-x and some intermediate Q^2, therefore the solution of the GLR-MQ equation in the form of Eq.(5.11) is expected to be worthwhile. We believe that our solution is correct in the vicinity of the saturation where all our assumptions look natural. Now to determine the Q^2 ($t = \ln(Q^2/\Lambda^2)$) and x-dependence of the gluon distribution we apply the following two physically plausible boundary conditions

$$G(x,t) = G(x,t_0) \tag{5.12}$$

at some lower value $Q^2 = Q_0^2$, where $t_0 = \ln(Q_0^2/\Lambda^2)$ and

$$G(x,t) = G(x_0,t), \tag{5.13}$$

at some high $x = x_0$.

The boundary condition (5.12) gives us

$$G(x,t_0) = \frac{t_0^{\gamma_1(x)}}{C + \gamma_2(x)\int {t_0}^{\gamma_1(x)-2}e^{-t_0}dt_0}, \tag{5.14}$$

From this equation the constant C can be evaluated by considering an appropriate input distribution $G(x,t_0)$ at a given value of Q_0^2. Now Eq.(5.11) and Eq.(5.14) lead us to the Q^2-evolution of gluon distribution function for fixed x given as

$$G(x,t)=\frac{t^{\gamma_1(x)}G(x,t_0)}{t_0^{\gamma_1(x)}+\gamma_2(x)\Big[\int t^{\gamma_1(x)-2}e^{-t}dt-\int {t_0}^{\gamma_1(x)-2}e^{-t_0}dt_0\Big]G(x,t_0)}. \tag{5.15}$$

Thus we have obtained an expression for the Q^2-evolution of nonlinear gluon density at LO by solving the nonlinear GLR-MQ evolution equation semi-analytically. From this expression we can easily compute the dependence of gluon distribution function on Q^2 for a particular value of x by choosing an appropriate input distribution at a given value of Q_0^2. Eq.(5.15) also assist us to investigate the nonlinear or shadowing corrections to the gluon distribution functions at moderate values of Q^2.

Similarly, the boundary condition (5.13) yields

$$G(x_0,t)=\frac{t^{\gamma_1(x_0)}}{C+\gamma_2(x_0)\int t^{\gamma_1(x_0)-2}e^{-t}dt}, \tag{5.16}$$

so that using Eqs. (5.11) and (5.16) we obtain

$$G(x,t)=\frac{t^{\gamma_1(x)}G(x_0,t)}{t^{\gamma_1(x_0)}+\Big[\gamma_2(x)\int t^{\gamma_1(x)-2}e^{-t}dt-\gamma_2(x_0)\int t^{\gamma_1(x_0)-2}e^{-t}dt\Big]G(x_0,t)}. \tag{5.17}$$

Thus Eq. (5.17) provides the solution of the GLR-MQ equation for gluon distribution at small-x for fixed Q^2. Accordingly from Eq. (5.17) we can easily predict the small-x dependence of nonlinear gluon distribution function for a particular value of Q^2 by picking out a suitable input distribution at an initial value of $x=x_0$. The effect of nonlinear or shadowing corrections to the gluon distribution functions at small-x can be studied as well by employing Eq. (5.17).

We analyze the region of validity of our solution given by Eq.(5.11) and we expect that the solution is only valid in the region of small-x and intermediate values of Q^2. It is clear from Eq.(5.11) that at large Q^2 ($t=\ln(Q^2/\Lambda^2)$), we can neglect the nonlinear corrections and our solution takes the form

$$G(x,t)=\frac{t^{\gamma_1(x)}}{C+\gamma_2(x)\int t^{\gamma_1(x)-2}e^{-t}dt}\xrightarrow{t\gg 1} t^{\gamma_1(x)}/C, \tag{5.18}$$

However, in the region where Q^2 is not very large, the corrections for the nonlinear term in Eq.(5.11) can not be neglected and in that case Eq.(5.11) does not reduce to Eq.(5.18). In our analysis we consider intermediate values of Q^2 ($1\leq Q^2\leq 30$

GeV^2) to calculate the gluon distribution function. In this region the corrections for the nonlinear term $\gamma_2(x) \int t^{\gamma_1(x)-2} e^{-t} dt$ cannot be neglected in comparison to C, where C is defined by Eq.(5.14), and so our solution given by Eq.(5.11) does not reduce to Eq.(5.18).

On the other hand we observe that in the region $10^{-5} \leq x \leq 10^{-2}$ Eq.(5.11) predicts an increase of gluon distribution with decreasing-x, which is in accordance with the Regge ansatz of Eq.(5.5). Nevertheless Eq.(5.11) yields a slower growth of gluon density towards small-x in comparison to the solution of linear DGLAP equation, since the nonlinear effects due to gluon-gluon interactions play a significant role in the small-x ($x \leq 10^{-2}$) region. However in the region of very small-x ($x < 10^{-5}$) but fixed Q^2, we can neglect the dependence of the functions $\gamma_1(x)$ and $\gamma_2(x)$ on x. Accordingly the solution suggested in Eq.(5.11) does not depend on x taking the form

$$G_{x\to 0}(x,t) = \frac{t^{\gamma_{10}}}{C + \gamma_{20} \int t^{\gamma_{10}} e^{-t} dt}, \tag{5.19}$$

where the r.h.s is a constant. In that case the solution to the nonlinear equation given by Eq.(5.11) contradicts the ansatz of Eq.(5.5). So we can conclude that Eq.(5.11) is not a valid solution at very small-x ($x < 10^{-5}$). It is to note that in the region of $x > 10^{-2}$ the process of gluon-recombination does not play an important role on the QCD evolution and therefore nonlinear corrections to the DGLAP equation is not essential. In other words in the region of $x > 10^{-2}$ DGLAP equation is sufficient to explain the available experimental data. So we can interpret that the solution given by Eq.(5.11) may not be applicable in the region of $x < 10^{-5}$ as well as $x > 10^{-2}$. But in the kinematic region $10^{-5} \leq x \leq 10^{-2}$ the x-dependence of the functions $\gamma_1(x)$ and $\gamma_2(x)$ can not be neglected and under this situation Eq.(5.11) does not reduce to Eq.(5.19) and thus it does not contradict the ansatz given by Eq.(5.5). Hence we can conclude that the solution suggested in Eq.(5.11) is expected to be a valid solution of the nonlinear GLR-MQ equation in the kinematic region $1 \leq Q^2 \leq 30$ GeV^2 and $10^{-5} \leq x \leq 10^{-2}$ and it can delineate the small-x dependence of nonlinear gluon density in a satisfactory manner.

5.2.3 Comparative analysis of DGLAP and GLRMQ equations

To estimate the effect of shadowing corrections for the gluon distribution function in our predictions we make a comparative study of the nonlinear GLR-MQ equation with the linear DGLAP approach. For this purpose we solve the linear DGLAP equation at small-x at LO defined by Eq.(5.4) by employing the Regge ansatz of gluon distribution function and compare it with the solution of the GLR-MQ equation discussed above. Using the Regge ansatz of Eq.(5.5), Eq.(5.4) can be simplified as

$$\frac{\partial G(x,t)}{\partial t}\Big|_{DGLAP} = \gamma_1(x)\frac{G(x,t)}{t}, \tag{5.20}$$

which can be easily solved to have

$$G(x,t) = At^{\gamma_1(x)}. \tag{5.21}$$

Here A is a constant to be fixed by initial boundary conditions. The x dependent function $\gamma_1(x)$ is defined in Eq.(5.9). Now defining

$$g_{10} = G(x,t_0) = At_0^{\gamma_1(x)} \tag{5.22}$$

at some lower value $Q^2 = Q_0^2$, we get from Eq.(5.21)

$$G(x,t) = g_{10}\Big(\frac{t}{t_0}\Big)^{\gamma_1(x)}. \tag{5.23}$$

Eq.(5.23) provides the solution of the linear DGLAP equation at LO for gluon distribution with the ansatz of Eq.(5.5) and it describes the Q^2 dependence of linear gluon density for a fixed value of x, provided a suitable input distribution g_{10} has been chosen from the initial boundary condition.

Again, defining

$$g_{20} = G(x_0,t) = At^{\gamma_1(x_0)} \tag{5.24}$$

at some initial higher value $x = x_0$, Eq.(5.21) can be expressed as

$$G(x,t) = g_{20}t^{\gamma_1(x)-\gamma_1(x_0)}. \tag{5.25}$$

Eq.(5.25) is the solution of the linear DGLAP equation at LO for gluon distribution at small-x with the ansatz of Eq.(5.5) and it describes the small-x behavior of

linear gluon density for a particular value of Q^2 by choosing an appropriate input distribution g_{20} from the initial boundary condition.

The effect of shadowing corrections to the gluon distribution function can be examined considering the solutions of the DGLAP and GLR-MQ equations respectively. To do this we calculate the ratio R_G of the predicted values of gluon distribution function obtained from the solution of nonlinear GLR-MQ equation given by Eq. (5.17) to that obtained using the linear DGLAP equation given by Eq.(5.25)

$$R_G = \frac{G^{GLR-MQ}(x,t)}{G^{DGLAP}(x,t)}, \tag{5.26}$$

as a function of variable x for different values of Q^2. By evaluating this ratio we have observed a taming behavior of gluon distribution in the HERA kinematic region ($3 \leq \ln(1/x) \leq 12$) due to shadowing corrections to the linear evolution. Thus employing the expression (5.26) we can interpret the influence of nonlinear or shadowing corrections as a consequence of gluon recombinations on the behavior of gluon distribution at small-x. It also assists us to understand whether Froissart bound can be restored at small-x. We have explored the phenomenological aspect of Eq.(5.26) in section 3.

5.2.4 Compatibility of Regge like solutions of gluon density with the DLA solution

The DGLAP evolution equation predicts that the gluon distribution function rises steeply as a power of x toward small-x which is observed at HERA too. This is in accordance with the Double Logarithmic Approximation (DLA) at small-x and large photon virtualities Q^2. The DLA accounts for only the leading double logarithmic contributions ($\alpha_s \ln(Q^2/Q_0^2) \ln(1/x)$) to multiparton cross sections. In DLA it is considered that $\frac{\alpha_s}{\pi} \ll 1$, $\frac{\alpha_s}{\pi} \ln Q^2 \ll 1$, $\frac{\alpha_s}{\pi} \ln^2 Q^2 \sim 1$ [38]. DLA analysis manifests the structure of intrajet parton cascades and as a matter of fact, the DLA predictions provide an assumption for the parton picture. The parton cascade is an excellent replica in consideration of DLA ladder diagrams. The DLA is applicable to perturbative QCD evolution in the asymptotic regime characterized by $Q^2 \gg Q_0^2$ and $x \ll x_0$, $x_0 \leq 0.1$, [39]. The proton structure function data explored at HERA have been demonstrated to evolve in consonance with DLA as suggested in Ref. [30]. The DLA asymptotics of the structure function derived by the addition of diagrams

corresponding to $(\alpha_s \ln(Q^2/Q_0^2))^n$ and of those $(\alpha_s \ln(1/x))^n$ occur simultaneously and produce the solution of the DGLAP equation in the form $\sim \exp\left(\sqrt{\ln\frac{t}{t_0}\ln\frac{x_0}{x}}\right)$ [9]. The gluon distribution produced by the DLA DGLAP evolution naturally portrays the data in a satisfactory manner exclusively in a somewhat confined kinematic domain of small-x and large-Q^2.

Any LO solution of DGLAP equation is presumed to be consistent with the DLA result. That being so, it is worthwhile to investigate the prospect of compatibility of our Regge type solution of DGLAP equation with the DLA one. Even though Regge behavior is not in agreement with the DLA in general, but, when x is small enough ($x < 0.7$) the Regge theory is assumed to be applicable, whatsoever the value of Q^2 [34, 35]. Accordingly the Regge type solution of DGLAP equation is expected to be valid. The conventional DLA formula [38] for gluon distribution function is

$$G^{DLA}(x,t) = G(x,t_0)\exp\left(2\sqrt{\frac{N_c}{\pi b}\ln\left(\frac{t}{t_0}\right)\ln\left(\frac{x_0}{x}\right)}\right), \tag{5.27}$$

with the function $b = \frac{11N_c - 2N_f}{12\pi}$. Here $N_c = 3$ is the number of color. Our solution of linear DGLAP equation given by Eq. (5.25) is in agreement with DLA formula of Eq. (5.27) as long as the following condition is satisfied,

$$\frac{\ln\left(\frac{G^{DLA}(x,t_0)}{G^{DGLAP}(x_0,t)}\right)}{\big(\gamma_1(x)-\gamma_1(x_0)\big)t} + \frac{2\sqrt{\frac{12N_c}{11N_c-2N_f}\ln\left(\frac{t}{t_0}\right)\ln\left(\frac{x_0}{x}\right)}}{\big(\gamma_1(x)-\gamma_1(x_0)\big)t} = 1. \tag{5.28}$$

An analysis of the phenomenological aspects of Eq.(5.28) is presented in section 3 where we denote the l.h.s. of Eq.(5.28) as $P(x,Q^2)$.

5.3 Result and discussion

We solve the nonlinear GLR-MQ evolution equation by considering the Regge like behavior of gluon distribution function and examine the effects of adding the nonlinear GLR-MQ corrections due to gluon recombination processes at small-x to the LO DGLAP evolution equations. We investigate the behavior of gluon distribution function at small-x and moderate Q^2 from the predicted solution of the GLR-MQ equation. The solutions suggested in Eqs.(5.15) and (5.17) are directly related to the initial conditions. Our predictions of x and Q^2 dependence of gluon distribution function $G(x,Q^2)$ are compared with with those obtained by the global QCD

fits to the parton distribution functions, viz. GRV1998LO [40], GJR2008LO [41], MRST2001LO [42], MSTW2008LO [43], NNPDF [44], HERAPDF0.1 [45, 46] and CT10 [47, 48] parametrizations respectively. To evolve our solutions, we use the GRV1998LO input and MRST2001LO input for two different representations of our solutions.

Furthermore, we present a comparative analysis of our computed results with the results of the EHKQS [20] and BZ models [23]. In the EHKQS model the effects of the first nonlinear corrections to the DGLAP evolution equations are studied by using the recent HERA data for the structure function $F_2(x, Q^2)$ of the free proton and the parton distributions from CTEQ5L and CTEQ6L as a baseline [49]. The EHKQS model shows that the nonlinear corrections improve the agreement with the $F_2(x, Q^2)$ data in the region of $x \sim 3 \times 10^{-5}$ and $Q^2 \sim 1.5$ GeV^2. On the other hand in BZ model using a Laplace-transform technique, the behavior of the gluon distribution is obtained by solving the GLR-MQ evolution equation with the nonlinear shadowing term incorporated.

Figure 5.1 represent our predictions of the gluon distribution function with the effect of nonlinear or shadowing corrections obtained from Eq.(5.15), plotted against Q^2 for four fixed values of x, viz. $x = 10^{-2}, 10^{-3}, 10^{-4}$ and 10^{-5} respectively. We compare our predictions with GRV1998LO, GJR2008LO, MRST1001LO and MSTW2008LO global parton analysis as well as with the EHKQS model. The input distribution is taken from the GRV1998LO. The red solid curve represents the effect of the shadowing correction of gluon distribution function predicted by using Eq.(5.15) for the hot spots with $R = 2$ GeV^{-1} whereas the results for $R = 5$ GeV^{-1} is shown by the blue solid line.

Similarly, in Figure 5.2 we plot our computed results of the gluon distribution function obtained from Eq.(5.15) vs. Q^2, considering the MRST2001LO input gluon distribution, for $x = 10^{-2}, 10^{-3}, 10^{-4}$ and 10^{-5} respectively as before. Here also the red and blue solid lines represent our predictions of nonlinear gluon density for $R = 2$ GeV^{-1} and $R = 5$ GeV^{-1} respectively. We perform a comparison of our results with different parametrizations namely, HERAPDF0.1, CT10 and NNPDF.

Figure 5.3 represent the small-x behavior of the gluon distribution with the effect shadowing corrections to the gluon distribution function determined from Eq.(5.17)

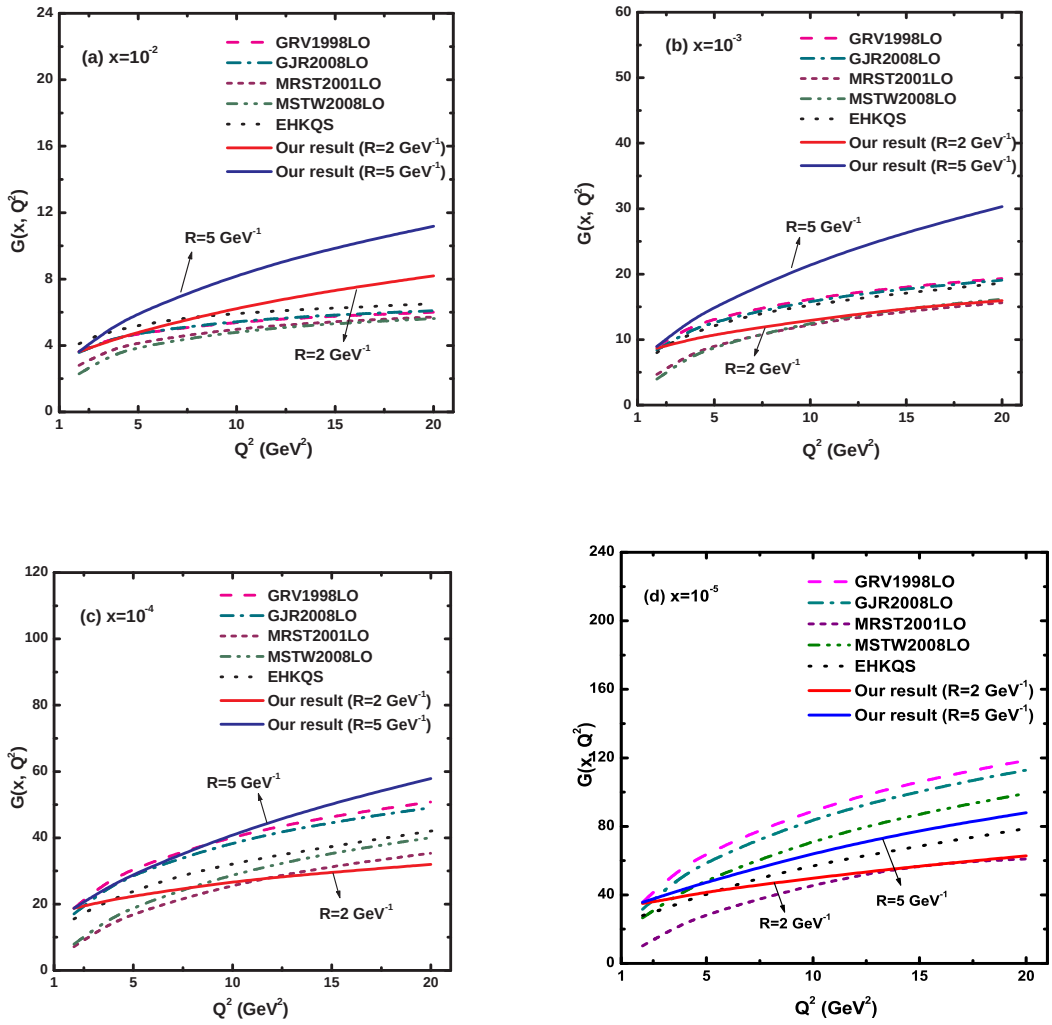

Figure 5.1: Q^2 dependence of gluon distribution with shadowing corrections obtained from Eq.(5.15) for four fixed values of x at $R = 2\ GeV^{-1}$ (red solid curves) and $R = 5\ GeV^{-1}$ (blue solid curves) respectively. Our predictions are compared with GRV1998LO (dash), GJR2008LO (dash-dot), MRST2001LO (short-dash) and MSTW2008LO (dash-dot-dot) parametrizations as well as with the EHKQS model (dot). The input gluon distribution is taken from GRV1998LO.

as a function of x for four fixed values of Q^2, viz. $Q^2 = 5, 10, 15$ and 20 GeV^2. Here the input gluon distribution is taken from GRV1998LO to evolve our solutions and our predictions of the small-x behaviour of nonlinear gluon density are compared with the global QCD analysis namely GRV1998LO, GJR2008LO, MRST2001LO, MSTW2008LO as well as with the H1 data. The red and blue solid lines represent our best fit results of nonlinear gluon density for $R = 2$ GeV^{-1} and $R = 5$ GeV^{-1} respectively.

On the other hand, our predictions of gluon distribution function with the shadowing corrections evaluated from Eq. (5.17) using the MRST2001LO input are plotted in Figure 5.4 as a function of x for four fixed Q^2, viz. $Q^2 = 5, 10, 15$ and and

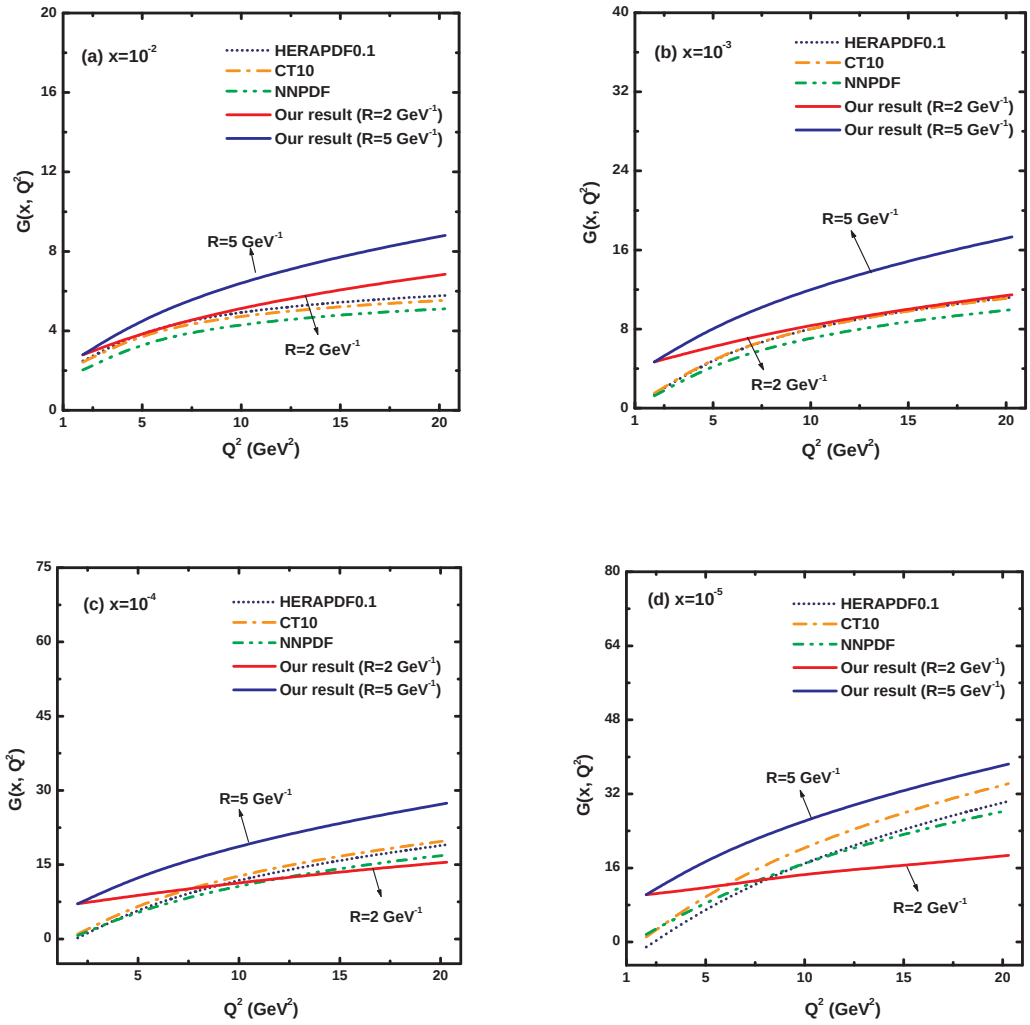

Figure 5.2: Q^2 dependence of gluon distribution function incorporating shadowing corrections computed from Eq.(5.15) for four fixed values of x at $R = 2\ GeV^{-1}$ (red solid curves) and $R = 5\ GeV^{-1}$ (blue solid curves) respectively. Our predictions are compared with HERAPDF0.1 (short-dot), CT10 (dash-dot) and NNPDF (dash-dot-dot) parametrizations. The input gluon distribution is taken from MRST2001LO.

20 GeV^2 as in the previous case. We make a comparison of our computed results of nonlinear gluon density with the HERAPDF0.1, CT10, NNPDF parametrizations as well as with the results of BZ model. Here too the computed results of the small-x behaviour of nonlinear gluon density corresponding to $R = 2$ GeV^{-1} and $R = 5$ GeV^{-1} are represented by the red and blue solid lines respectively.

From Figure 5.1 to Figure 5.4 we have observed that our results are in good agreement with different experimental data, global parametrizations and also with different models. The gluon distribution increases with increasing Q^2 and decreasing x, which complements the perturbative QCD fits at small-x, but this behaviour is tamed with respect to the nonlinear terms in GLR-MQ equation. It is very interesting to observe that our predictions for the x and Q^2 dependence of nonlinear gluon

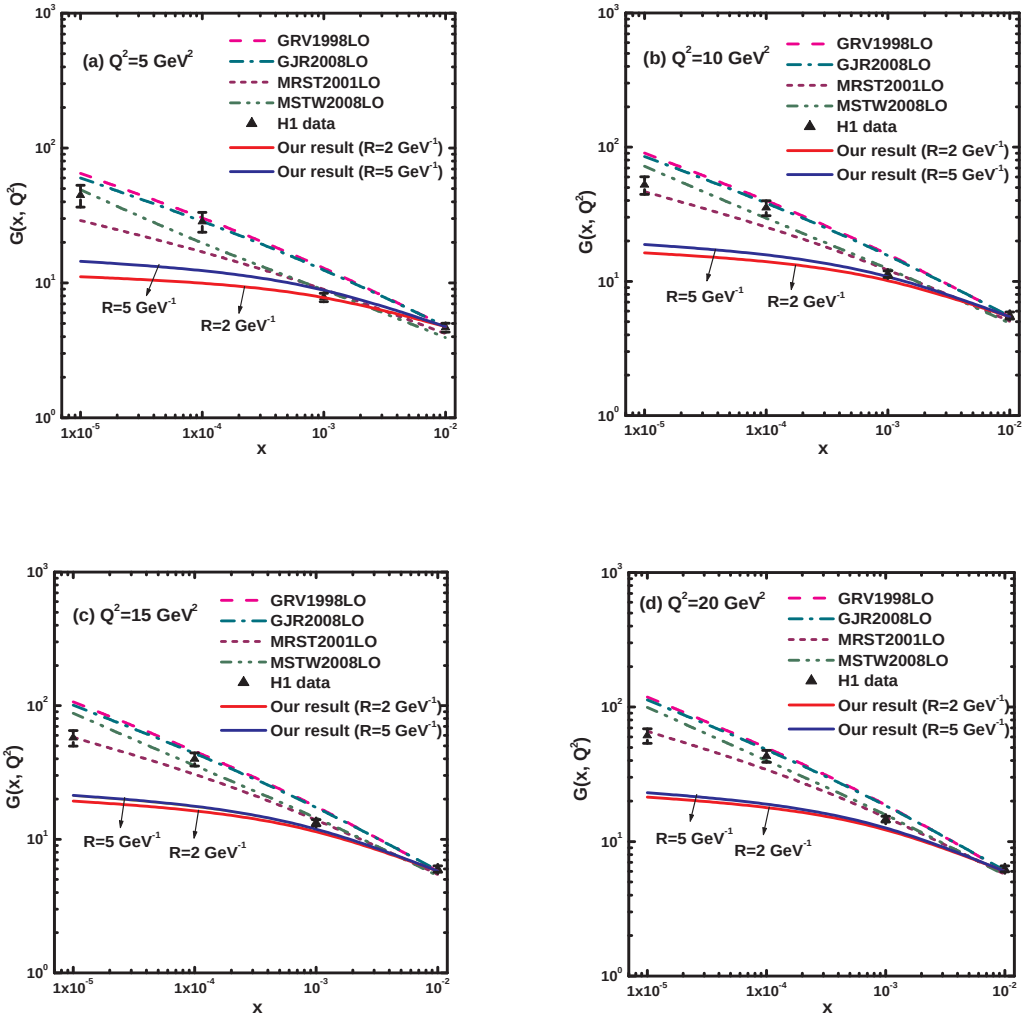

Figure 5.3: Small-x behaviour of gluon distribution with shadowing corrections obtained from Eq.(5.17) for four fixed values of Q^2 at $R = 2\ GeV^{-1}$ (red solid curves) and $R = 5\ GeV^{-1}$ (blue solid curves) respectively. Our results are compared with GRV1998LO (dash), GJR2008LO (dash-dot), MRST2001LO (short-dash), MSTW2008LO (dash-dot-dot) parametrizations as well as with H1 data (up-triangle). The input gluon distribution is taken from GRV1998LO.

density are in excellent agreement with the gluon density function obtained from HERAPDF0.1 and CT10 parametrizations. Moreover, we observe from Figure 5.2 that our results of the effect of shadowing corrections to the moderate-Q^2 behaviour of gluon distribution function are comparable with those obtained in a similar analysis by the EHKQS model. We further note that, our results follow the general trend of H1 data but they get saturated towards very small-x due to shadowing corrections. Similarly, we see that the shapes of the curves in Figure 5.4 representing the small-x behaviour of nonlinear gluon density are almost similar to the results of BZ model. Therefore we can say that the Regge type solution of the GLR-MQ equation for the nonlinear gluon distribution suggested in Eq.(5.11) can describe the available data in

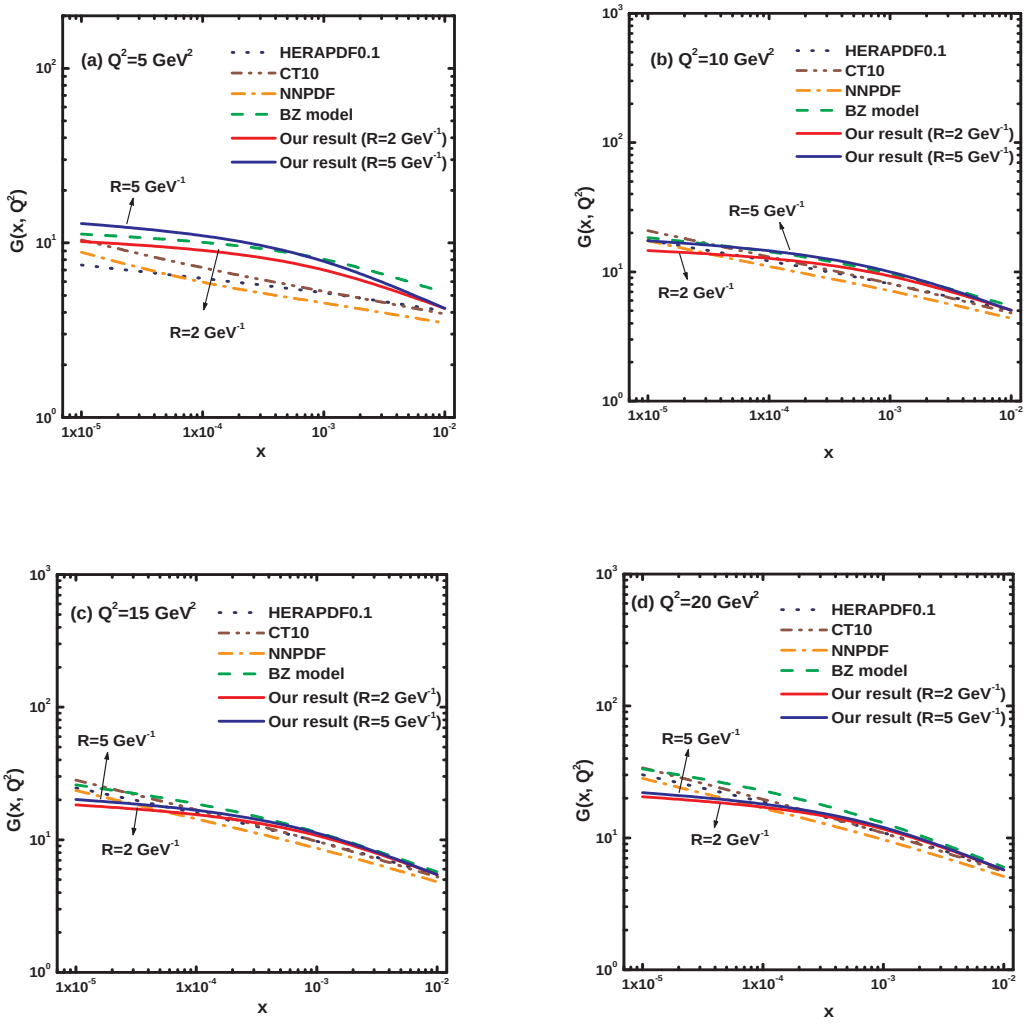

Figure 5.4: Small-x behaviour of gluon distribution considering shadowing corrections calculated from Eq.(5.17) for four fixed values of Q^2 at $R = 2\ GeV^{-1}$ (red solid curves) and $R = 5\ GeV^{-1}$ (blue solid curves) respectively. Our results are compared with HERAPDF0.1 (dot), CT10 (dash-dot-dot) and NNPDF (dash-dot) parametrizations and BZ model (dash). The input gluon distribution is taken from MRST2001LO.

a satisfactory manner. We perform our analysis in the kinematic region $1 \leq Q^2 \leq 30$ GeV^2 and $10^{-5} \leq x \leq 10^{-2}$ and our solution of the nonlinear gluon density is found to be legitimate in this kinematic domain. The effect of shadowing corrections as a consequence of gluon recombination processes in our predictions is observed to be very high at the hot-spots with $R = 2$ GeV^{-1} when the gluons are centered within the proton, compared to at $R = 5$ GeV^{-1} when the gluons are disseminated throughout the entire proton.

Moreover, to examine the effects of nonlinear or shadowing corrections to the gluon distributions in our prediction, we have plotted the ratio R_G of the gluon distribution function obtained from the solution of nonlinear GLR-MQ equation for $R = 2$ GeV^{-1} to that obtained from the solution of linear DGLAP equation using Eq.(5.26)

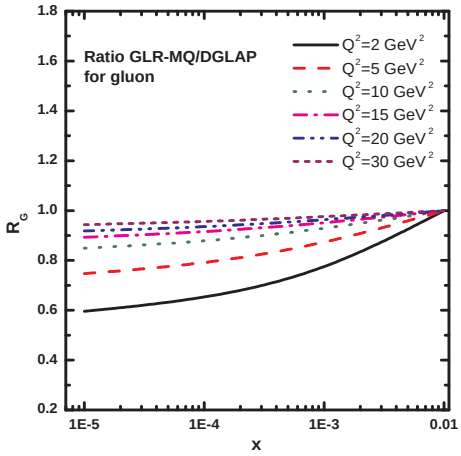

Figure 5.5: A comparison of the gluon distribution function in terms of R_G defined in Eq.(5.26). The comparison is shown for six different bins in $Q^2 = 2, 5, 10, 15, 20$ and 30 GeV^2.

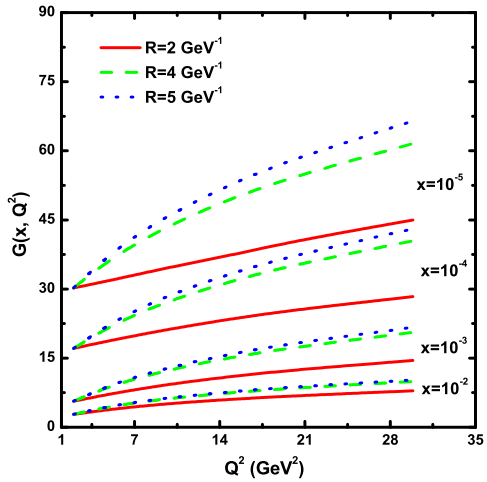

Figure 5.6: Sensitivity of the correlation radius R in our predictions for four values of x.

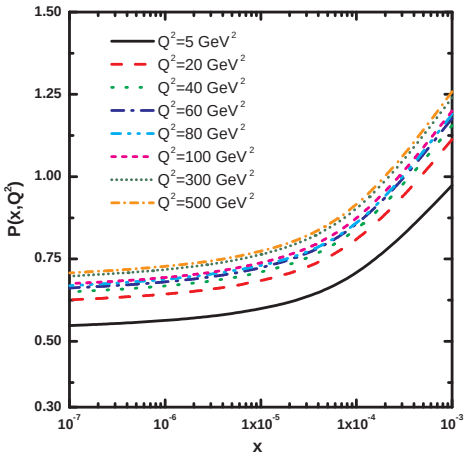

Figure 5.7: Compatibility of our LO solution of DGLAP equation with the DLA one using Eq.(5.28).

in Figure 5.5. This comparison helps us to estimate the shadowing corrections for the gluon distribution function. We plot the ratio R_G for gluon distribution as a function of the variable x for six representative values $Q^2 = 2, 5, 10, 15, 20$ and 30 GeV^2 respectively. We observe that as x grows smaller the GLR-MQ/DGLAP ratios decrease which implies that the effect of nonlinearity increases towards small-x due to gloun recombination. The fall of the ratio at small-x ($x < 10^{-2}$) is a consequence of the gluon recombination or shadowing corrections. Results also clearly indicates that towards smaller values of Q^2 the value of the ratio between nonlinear gluon density and linear gluon density also goes smaller. In other words, gluon recombination plays an important role in the region of small-x and Q^2 whereas, with the evolution to large-Q^2 ($Q^2 > 30\ GeV^2$) and large-x ($x \geq 10^{-2}$), gluon recombinations play less of a role, and as a consequence the nonlinear effects have a very little impact.

We have further investigated the effect of nonlinearity in our results by performing an analysis to check the sensitivity of the correlation radius R between two interacting gluons. For this analysis our computed values of $G(x, Q^2)$ from Eq. (5.15) for $R = 2, 4$ and 5 GeV^{-1} respectively are plotted against Q^2 in Figure 5.6 for four fixed values of x, $x = 10^{-2}, 10^{-3}, 10^{-4}$ and 10^{-5}. For this analysis we take the input distribution from MRST2001LO global parametrization for a given value of Q_0^2. The gluon distribution function is observed to be more tamed at $R = 2$ GeV^1, where gluons are supposed to be condensed in the hot-spots within the proton, compared to at $R = 4$ GeV^{-1} and $R = 5$ GeV^{-1} where gluons are almost scattered over the entire proton. Moreover, we note that that the differences between the data as we approach from $R = 2$ GeV^{-1} to $R = 5$ GeV^{-1} increase with decreasing x as anticipated.

Figure 5.7 represents the plot of $P(x, Q^2)$ vs. x for different values of Q^2, where $P(x, Q^2)$ represents the l.h.s of Eq.(5.28) which represents the condition of compatibility of the Regge like solution of DGLAP equation to the DLA one. This figure illustrates that our Regge type solution of linear DGLAP equation given by Eq.(5.23) is comparable with the DLA result of Eq.(5.27) in a finite domain of x and Q^2 as long as the constraint given by Eq.(5.28) is fulfilled. It is obvious from the figure that for each value of Q^2, there is a corresponding value of x for which the l.h.s and r.h.s. of Eq.(5.28) are identical and the value of x, where this happens, switches to lower limit as Q^2 increases. We observe that for the Q^2 values $5 \leq Q^2 \leq 500$ GeV^2,

considered in our analysis, the condition of compatibility is satisfied in the region of x between 10^{-4} and 10^{-3}. Accordingly the Regge like solution of the linear DGLAP equation in LO is expected to be applicable in the region of $10^{-4} \leq x \leq 10^{-3}$ and high-Q^2 if it is appealed to be consistent with the DLA one.

5.4 Summary

In summary, the behavior of gluon distributions in the region of small-x and moderate-Q^2 are semi-analytically predicted by solving the nonlinear GLR-MQ equation in leading twist approximation incorporating the well known Regge ansatz. We make a deliberate attempt to explore the effect of nonlinear or shadowing corrections arises due to the gluon recombination processes on the behavior of gluon distribution at small-x and moderate-Q^2. We observe that the gluon distribution function increases with increasing Q^2 and decreasing x, but with the inclusion of the nonlinear terms, this behaviour of gluon density is slowed down relative to DGLAP gluon distribution. We investigate how the inclusion of nonlinear effects changes the behavior of gluon density and it is interesting to observe that although the gluon distribution increases with increasing Q^2 and decreasing x as usual, which is in agreement with the perturbative QCD fits at small-x, however the gluon recombination processes tame the rapid growth of gluon densities towards small-x. This suggests that the gluon distributions unitarize leading to the restoration of Froissart bound in the small-x region where density of gluons becomes very high. For the gluon distribution the nonlinear effects are found to play an increasingly important role at $x \leq 10^{-3}$. The nonlinearities, however, vanish rapidly at larger values of x. Furthermore, our results manifest that the nonlinearity increases with decreasing value of correlation radius R as expected which is very fascinating.

Our results indicates that the nonlinear effects or shadowing corrections, emerged as a consequence of recombination of two gluon ladders, play a significant role on QCD evolution for gluon distribution in the kinematic region of small-x and moderate-Q^2. Accordingly the suggested solution of the GLR-MQ equation for gluon distribution function is anticipated to be legitimate only in the vicinity of saturation i.e. in the kinematic region $1 \leq Q^2 \leq 30$ GeV^2 and $10^{-5} \leq x \leq 10^{-2}$. Our phenomenological analysis also supports this as the obtained results of nonlinear gluon density using

the Regge ansatz are in accordance with different parametrization as well as models.

Finally, we derive the condition of compatibility of the LO solution of linear DGLAP equation for gluon, obtained by employing the Regge ansatz, with the DLA solution in a finite range of the variables x and Q^2. From our phenomenological analysis we understand that in the Q^2 region $5 \leq Q^2 \leq 500\ GeV^2$, considered in our study, the condition of compatibilty is satisfied in the region of x between 10^{-4} and 10^{-3}. Accordingly we can expect the Regge type solution of the linear DGLAP equation in LO to be applicable in the region of $10^{-4} \leq x \leq 10^{-3}$ and high-Q^2 if we demand it to be consistent with the DLA one.

Bibliography

[1] Stasto, A. M., Golec-Biernat, K. J. and Kwiecinski, J. Geometric scaling for the total $\gamma^* p$ cross section in the low x region, *Phys. Rev. Lett.* **86**(4), 596−−599, 2001.

[2] Albacete, J. L., Marquet, C. Azimuthal correlations of forward dihadrons in d+Au collisions at RHIC in the color glass condensate, *Phys. Rev. Lett.* **105**(16), 162301, 2010.

[3] Dumitru, A. et al., The ridge in proton-proton collisions at the LHC, *Phys. Lett. B* **697**(1), 21−−25, 2011.

[4] Dokshitzer, Y. L. Calculation of structure functions of deep-inelastic scattering and e^+e^- annihilation by perturbation theory in quantum chromodynamics, *Sov. Phys. JETP* **46**(4), 641−− 652, 1977.

[5] Altarelli, G., Parisi, G. Asymptotic freedom in parton language, *Nucl. Phys. B* **126**(2), 298−−318, 1977.

[6] Gribov, V. N., Lipatov, L. N. Deep inelastic ep scattering in perturbation theory, *Sov. J. Nucl. Phys.* **15**(4), 438−−450, 1972.

[7] Froissart, M. Asymptotic behavior and subtractions in the Mandelstam representation, *Phys. Rev.* **123**(3), 1053−−1057, 1961.

[8] Martin, A. Unitarity and high-energy behavior of scattering amplitudes, *Phys. Rev.* **129**(3), 1432−−1436, 1963.

[9] Gribov, L. N., Levin, E. M. and Ryskin, M. G. Semihard processes in QCD, *Phys. Rep.* **100**(1-2), 1−−150, 1983.

[10] Mueller, A. H., Qiu, J. Gluon Recombination and Shadowing at Small Values of x, *Nucl. Phys. B* **268**(2), 427−−452, 1986.

[11] Mueller, A. H. Small-x behavior and parton saturation: A QCD model, *Nucl. Phys. B* **335**(1), 115−−137, 1990.

[12] Abramovsky, V. A., Gribov, V. N., Kancheli, O. V. Character of inclusive spectra and fluctuations produced in inelastic processes by multi-Pomeron exchange, *Sov.J.Nucl.Phys.* **18**, 308−−317, 1974.

[13] Collins J. C., Kwiecinski, J. Shadowing in gluon distributions in the small-x region, *Nucl. Phys. B* **335**(1), 89−−100, 1990.

[14] Ayala, A. L., Gay Ducati, M. B. and Levin, E. M. QCD evolution of the gluon density in a nucleus, *Nucl. Phys. B* **493**(12), 305−−353, 1997.

[15] Ayala, A. L., Gay Ducati, M. B. and Levin, E. M. Parton densities in a nucleon, *Nucl. Phys. B* **511**(12), 355−−395, 1998.

[16] Bartels, J., Levin, E. Solutions to the Gribov-Levin-Ryskin equation in the nonperturbative region, *Nucl. Phys. B* **38**(3), 617−−637, 1992.

[17] Levin E., Tuchin, K. Solution to the evolution equation for high parton density QCD, *Nucl. Phys. B* **573**(3), 833−−852, 2000.

[18] Prytz, K. Signals of gluon recombination in deep inelastic scattering, *Eur. Phys. J. C* **22**(2), 317−−321, 2001.

[19] Bartels, J., Blumlein J. and Shuler, G. A Numerical study of the small x behavior of deep inelastic structure functions in QCD, *Z. Phys. C* **50**(1), 91−−102, 1991.

[20] Eskola, K. J. et al., Nonlinear corrections to the DGLAP equations in view of the HERA data, *Nucl. Phys. B* **660**(1-2), 211−−224, 2003.

[21] Watt, G., Martin, A. D. and Ryskin, M. G. Effect of absorptive corrections on inclusive parton distributions, *Phys. Lett. B* **627**(1-4), 97−−104, 2005.

[22] Rezaei, B., Boroun, G. R. Analytical approach for the approximate solution of the longitudinal structure function with respect to the GLR-MQ equation at small x, *Phys. Lett. B* **692**(4), 247−−249, 2010.

[23] Boroun, G. R., Zarrin, S. An approximate approach to the nonlinear DGLAP evaluation equation, *Eur. Phys. J. Plus* **128**(10), 119, 2013.

[24] Laenen, E., Levin, E. A new evolution equation, *Nucl. Phys. B* **451**(1-2), 207−−230, 1995.

[25] Laenen, E., Levin, E. Parton densities at high energy, *Annu. Rev. Nucl. Part. Sci.* **44**, 199−−246, 1994.

[26] Levin, E. M., Ryskin, M. G. Low-x structure function and saturation of the parton density, *Nucl. Phys. B (Proc. Suppl.)* **18**(3), 92−−124, 1991.

[27] Abbott, L. F., Atwood, W. B. and Michael Barnett, R. Quantum-chromodynamic analysis of eN deep-inelastic scattering data, *Phys. Rev. D* **22**(3), 582−−594, 1980.

[28] Collins, P. D., *An Introduction to Regge Theory and High-Energy Physics*, Cambridge University Press, Cambridge, 1997.

[29] Donnachie, A., Landshoff, P. V. Total cross sections, *Phys. Lett. B* **296**(1-2), 227−− 232, 1992.

[30] Ball, R. D., Forte, S. Double asymptotic scaling at HERA, *Phys. Lett. B* **335**(1), 77−−86, 1994

[31] Kotikov, A. V. Small x Behaviour of parton distributions in proton, *Mod. Phys. Lett. A* **11**(2), 103, 1996.

[32] Kwiecinski, J. Theoretical issues of small x physics, *J. Phys. G: Nucl. Part. Phys.* **22**(6), 685−−702, 1996.

[33] Donnachie, A., Landshoff, P. V. Small x: two pomerons!, *Phys. Lett. B* **437**(3-4), 408−−416, 1998.

[34] Bartels, J. et al., The dipole picture and saturation in soft processes, *Phys. Lett. B* **556**(3-4), 114−−122, 2003.

[35] Martin, A. D., Ryskin, M. G. and Watt, G. Simultaneous QCD analysis of diffractive and inclusive deep-inelastic scattering data, *Phys. Rev. D* **70**(9), 091502, 2004.

[36] Badelek, B. Spin Dependent Structure Function $g_1(x, Q^2)$ at Low x and Low Q^2, *Acta Phys. Polon. B* **34**(6), 2943−−2962, 2003.

[37] Soffer, J., Teryaev, O. V. Neutron spin-dependent structure function, Bjorken sum rule, and first evidence for singlet contribution at low x, *Phys. Rev. D* **56**(3), 1549, 1997.

[38] Dokshitzer, Y. L., Khoze, V. A., Mueller, A. H. and Troyan, S. I. *Basics of Perturbative QCD*, Editions Frontieres, Fong and Sons Printers Pte. Ltd, Singapore, 1991.

[39] De Rujula, A. et al., Possible non-Regge behavior of electroproduction structure functions, *Phys. Rev. D* **10**(5), 1649, 1974.

[40] Gluck, M., Reya, E. and Vogt, A. Dynamical parton distributions revisited, *Eur. Phys. J. C* **5**(461), 470, 1998.

[41] Gluck, M., Jimenez-Delgado, P. and Reya, E. Dynamical parton distributions of the nucleon and very small-x physics, *Eur. Phys. J. C* **53**(3), 355−−366, 2008.

[42] Martin, A. D. et al., MRST2001: partons and α_s from precise deep inelastic scattering and Tevatron jet data, *Eur. Phys. J. C* **23**(1), 73−−87, 2002.

[43] Martin, A. D. et al., Parton distributions for the LHC, *Eur. Phys. J. C* **63**(2), 189−−285, 2009.

[44] Forte, S. et al., Neural network parametrization of deep inelastic structure functions, *JHEP* **2002**(JHEP05), 062, 2002.

[45] Adloff, C. et al., Measurement and QCD analysis of neutral and charged current cross sections at HERA, *Eur. Phys. J. C* **30**(1), 1−−32, 2003.

[46] S. Chekanov et al., An NLO QCD analysis of inclusive cross-section and jet-production data from the ZEUS experiment, *Eur. Phys. J. C* **42**(1), 1−−16, 2005.

[47] Guzzi, M. et al., CT10 parton distributions and other developments in the global QCD analysis, *arXiv:1101.0561v1.*

[48] Lai, H. L. et al., New parton distributions for collider physics, *Phys. Rev. D* **82**(7), 074024, 2010.

[49] Pumplin, J. et al., New generation of parton distributions with uncertainties from global QCD analysis, *JHEP* **2002**(07), 012, 2002.

Chapter 6

Shadowing Corrections to the Singlet Structure Function and Behaviour of F_2 Slope

6.1 Introduction

Perturbative QCD manifests that the sea quark distributions, in a hadron evolves rapidly with $\ln(1/x)$ at fixed Q^2 in the same manner as the gluon distribution $xg(x, Q^2)$. However in the region of very small-x the sharp growth of the sea quark density is expected to slow down eventually in order to restore the Froissart bound [1, 2] on physical cross sections. In general the gluon recombination processes, which lead to the nonlinear or shadowing corrections to the linear QCD evolution, is considered to be responsible for this taming behaviour. The sea quark distribution, which overshadows the valence quarks at small x, is supposed to be generated through gluons and therefore it is extensively believed that the gluon and sea quark distribution functions almost feel the same effect of shadowing. The nonlinear or shadowing corrections in DIS arise due to two processes, one is the taming of the gluon density as a result of gluon recombination $gg \to g$ and the other is the Glauber-like rescattering of the $q\bar{q}$ fluctuations off gluons [3]. The second process can also be regarded as a parton recombination, particularly as a recombination of gluons into a quark-antiquark pair, $gg \to q\bar{q}$. Gribov, Levin and Ryskin (GLR-MQ) [4], at the onset, investigated the shadowing corrections of gluon recombination to the parton distributions i.e quark and gluon distribution. Following that Mueller and Qiu (MQ) [3, 5] completed the

equation numerically using a perturbative calculation of the recombination probabilities in the DLLA, and also formulated the equation for the conversion of gluons to sea quarks. This is a triumph of great significance as it empowers the GLR-MQ equation to be applied phenomenologically and thus provides the connection to experiments. This equation was made widely applicable in order to include the contributions from more higher order corrections in the Glauber-Mueller formula [3].

In this chapter, we solve the GLR-MQ equation for sea quark distribution incorporating the well known Regge like ansatz and investigate the effect of shadowing corrections on the small-x and moderate-Q^2 behaviour of singlet structure function. Our predictions of x and Q^2 dependence of singlet structure function with shadowing corrections are compared with NMC [6] and E665 [7] experimental data as well with the NNPDF collaboration [8]. Moreover, we perform a comparison of our predictions of singlet structure function obtained from nonlinear GLR-MQ equation with those obtained from linear DGLAP equation to examine the effect of nonlinear or shadowing corrections on the behaviour of singlet structure function. We further predict the logarithmic derivative of the singlet structure function and compare the results with H1 data [9, 10].

6.2 Formalism

6.2.1 General framework

The nonlinear corrections arising from the recombination of two gluon ladders into one gluon or a $q\bar{q}$ pair, modify the evolution equations of sea qurak distribution as [11]

$$\frac{\partial xq(x,Q^2)}{\partial \ln Q^2} = \frac{\partial xq(x,Q^2)}{\partial \ln Q^2}\Big|_{DGLAP} - \frac{27}{160}\frac{\alpha_S^2(Q^2)}{R^2Q^2}[xg(x,Q^2)]^2 + HT. \tag{6.1}$$

This equation is known as the GLR-MQ evolution equation for sea quark distribution. Here $q(x,Q^2)$ is the quark density and $g(x,Q^2)$ is the gluon density. The representation for the gluon distribution $G(x,Q^2) = xg(x,Q^2)$ is used. The first term on the right-hand side is given by standard linear DGLAP equation whereas the term quadratic in G is the result of gluon recombination into quarks. The negative sign in front of the non-linear term tames the strong growth of sea quark distribution generated by the linear term at very small-x and it describes the shadowing correc-

tions. HT stands for an additional term revealed by Mueller and Qiu but it is not given in all respects. Therefore this term is not taken into account in our analysis presented below. The parameter γ is calculated by Mueller and Qiu in perturbation theory and is found to be $\gamma = \frac{81}{16}$ for $N_c = 3$. The size of the nonlinear term crucially depends on the value of the correlation radius R between two interacting gluons. πR^2 is the target area occupied by the gluons. If the gluons originate from sources which occupy distinct regions in longitudinal coordinate space then R is of the order of proton radius, i.e. $R = 5$ GeV^{-1}. In that case recombination probability is very negligible [12, 13]. On the other hand, a considerable effect of recombination or shadowing corrections is expected if the gluons are condensed in hot spots [14] inside the proton, where R is considered to be of the order of the transverse size of a valence quark, i.e. $R = 2$ GeV^{-1}.

In the QCD improved parton model approximation, the structure functions are usually identified by summing quark distributions weighted by squared charges as usual

$$F_2(x, Q^2) = \sum_i e_i^2 x q_i(x, Q^2) \tag{6.2}$$

where the sum implies summation over all flavours of quarks and anti-quarks and e_i is the electric charge of a quark of type i. The F_2 structure functions measured in DIS can be written in terms of singlet and non-singlet quark distribution functions as [15]

$$F_2 = \frac{5}{18} F_2^S + \frac{3}{18} F_2^{NS} \tag{6.3}$$

As the structure function in the small-x region is mainly dominated by the gluon and sea quark distributions, therefore at small-x the non-singlet contribution can be neglected. It is reasonable to consider this from the experimental point of view as well. The H1 Collaboration presents a global fit of their data of the singlet quark distribution, $q_S = u + \bar{u} + d + \bar{d} + s + \bar{s}$, which determines practically the $F_2(x, Q^2)$ behaviour at small-x in the form $xq_S(x) = Ax^B(1-x)^C(1+Dx)$ where A, B, C and D are numerical constants at $Q^2 = 4$ GeV^2 and $x > 2 \times 10^{-4}$. At $x \leq 10^{-2}$, one can rewrite this expression as $xq_S(x) = Ax^B$ and one may neglect the non-singlet contribution within a few percent accuracy. Similarly ZEUS Collaboration presented their data for singlet quark distribution in a similar form $xq_S(x) = Ax^B(1-x)^C(1+$

$D\sqrt{x} + Ex$) with the numerical constants A, B, C, D and E at $Q^2 = 7$ GeV^2 and $x > 0.67 \times 10^{-4}$. Also in this case one can rewrite the expression in the form $xq_S(x) = Ax^B$.

Thus the contribution of the non-singlet part of the structure function can be ignored in the small-x region and in that situation Eq.(6.1) can be approximated as

$$\frac{\partial F_2^S(x,Q^2)}{\partial \ln Q^2} = \frac{5}{18}\frac{\partial F_2^S(x,Q^2)}{\partial \ln Q^2}\Big|_{DGLAP} - \frac{5}{18}\frac{27}{160}\frac{\alpha_S^2(Q^2)}{R^2Q^2}G^2(x,Q^2), \tag{6.4}$$

Again the first term of Eq.(6.4), which is the linear DGLAP equation for singlet structure function, in the leading twist approximation is given by [28]

$$\begin{aligned}\frac{\partial F_2^S(x,Q^2)}{\partial \ln Q^2}\Big|_{DGLAP} &= \frac{\alpha_s(Q^2)}{2\pi}\Bigg[\frac{2}{3}\Big(3 + 4\ln(1-x)\Big)F_2^S(x,Q^2) \\ &+ \frac{4}{3}\int_x^1 \frac{d\omega}{1-\omega}\Big\{(1+\omega^2)F_2^S\Big(\frac{x}{\omega},Q^2\Big) - 2F_2^S(x,Q^2)\Big\} \\ &+ N_F\int_x^1 \Big(\omega^2 + (1-\omega)^2\Big)G\Big(\frac{x}{\omega},Q^2\Big)d\omega\Bigg].\end{aligned} \tag{6.5}$$

6.2.2 Solution of GLR-MQ equation for singlet structure function and effects of gluon shadowing

Now to solve the GLR-MQ equation for singlet structure function we employ a Regge like behaviour of singlet structure function As discussed in chapter 5, the Regge ansatz can successfully describe the behaviour of structure functions at small-x [16]. The Regge theory is supposed to be applicable if x is small enough [17, 18] as long as Q^2 is sufficiently large that a perturbative treatment is possible. The Regge pole model gives the parametrization of the DIS structure function $F_2(x,Q^2)$ at small-x as $F_2 \propto x^{-\lambda}$ with $\lambda > 0$ [15]. To this end, we take into account a simple form of Regge like behaviour of singlet structure function as

$$F_2^S(x,Q^2) = J(Q^2)x^{-\lambda_S}, \tag{6.6}$$

where $J(Q^2)$ is a function of Q^2 and λ_S is the Regge intercepts for singlet structure function. According to Regge viewpoint, the high energy or small-x behaviour of both gluons and sea quarks are controlled by the same singularity factor in the complex angular momentum plane [16] since the same power is expected for sea quarks and gluons. Therefore likewise the value of the Regge intercept λ_G for gluon distribution function, the values of λ_S in our analysis is also taken to be 0.5 .

Again to obtain a solution of the GLR-MQ equation for singlet structure function, we have to assume a relation between singlet structure function and gluon distribution function as discussed in chapter 3 and chapter 4. The frequently used relation is [19-21]

$$G(x,Q^2) = K(x)F_2^S(x,Q^2), \tag{6.7}$$

with the ad hoc parameter $K(x)$ to be determined from phenomenological analysis.

Now employing the Regge ansatz of Eq.(6.6) for singlet structure function and using the relation defined by Eq.(6.7) in Eq.(6.4) we arrive at

$$\frac{\partial F_2^S(x,Q^2)}{\partial Q^2} = p_1(x)\frac{F_2^S(x,Q^2)}{\ln(Q^2/\Lambda^2)} - p_2(x)\frac{\left[F_2^S(x,Q^2)\right]^2}{Q^2\ln(Q^2/\Lambda^2)}, \tag{6.8}$$

The explicit forms of the functions $p_1(x)$ and $p_2(x)$ are

$$\begin{aligned} p_1(x) &= \frac{5}{9\beta_0}\Bigg[\frac{2}{3}\Big(3+4\ln(1-x)\Big) + \frac{4}{3}\int_x^1 \frac{d\omega}{1-\omega}\Big(\{(1+\omega^2)\omega^{\lambda_S} - 2\Big) \\ &\quad + N_F\int_x^1 \Big(\omega^2+(1-\omega)^2\Big)\omega^{\lambda_S}K(x)d\omega\Bigg], \end{aligned} \tag{6.9}$$

$$p_2(x) = \frac{27}{36}\frac{\pi^2\big(K(x)\big)^2}{\beta_0^2 R^2}. \tag{6.10}$$

Here we consider the leading twist approximation of the strong coupling constant $\alpha_s(Q^2) = \frac{4\pi}{\beta_0\ln(Q^2/\Lambda^2)}$ with $\beta_0 = 11-\frac{2}{3}N_f$ and N_f being the number of active quark flavours. Eq.(6.8) is a partial differential equation for the singlet structure function $F_2^S(x,Q^2)$ with respect to the variables x and Q^2. This equation can be used to examine the x-evolution of singlet structure function apart from its conventional use in Q^2-evolution. Solving of Eq.(6.8) we get

$$F_2^S(x,t) = \frac{t^{p_1(x)}}{C + p_2(x)\int t^{p_1(x)-2}e^{-t}dt}, \tag{6.11}$$

which leads us to the solution for the singlet structure function with nonlinear or shadowing corrections. Here we have use the variables $t = \ln(\frac{Q^2}{\Lambda^2})$ for convenience and C is a constant to be determined from initial boundary conditions. We note that in the kinematic region $0.6 \leq Q^2 \leq 30$ GeV^2 and $10^{-4} \leq x \leq 10^{-1}$ the solution given by Eq.(6.11) is in good agreement with the Regge ansatz of Eq.(6.6) and and satisfactorily describes the shadowing corrections to the singlet structure function.

So we restrict our analysis in this kinematic region and observe that the solution of singlet structure function with the inclusion of shadowing corrections given by Eq.(6.11) is valid in the region of small-x and moderate values of Q^2. However the solution suggested in Eq.(6.11) loose its validity at large-x and large-Q^2 where the effect of gluon recombination on the QCD evolution is very trivial.

Now we can determine the Q^2 and small-x dependence of singlet structure function from Eq.(6.11) using the appropriate boundary conditions. The physically plausible boundary conditions are

$$F_2^S(x,t) = F_2^S(x,t_0) \tag{6.12}$$

at $t = t_0$ where $t_0 = \ln\left(\frac{Q_0^2}{\Lambda^2}\right)$ for some lower value of $Q^2 = Q_0^2$ and

$$F_2^S(x,t) = F_2^S(x_0,t), \tag{6.13}$$

at some high $x = x_0$.

The boundary condition (6.12) leads us to

$$F_2^S(x,t_0) = \frac{t_0^{p_1(x)}}{C + p_2(x)\int {t_0}^{p_1(x)-2}e^{-t_0}dt_0}, \tag{6.14}$$

where $t_0 = \ln\left(\frac{Q_0^2}{\Lambda^2}\right)$. From this equation the constant C can be determined by choosing a suitable input distribution $F_2^S(x,t_0)$ at a given value of Q_0^2. Now from Eqs.(6.11) and (6.14) we get the Q^2-evolution of shadowing singlet structure function for fixed x given as

$$F_2^S(x,t) = \frac{t^{p_1(x)}F_2^S(x,t_0)}{t_0^{p_1(x)} + p_2(x)\Big[\int t^{p_1(x)-2}e^{-t}dt - \int {t_0}^{p_1(x)-2}e^{-t_0}dt_0\Big]F_2^S(x,t_0)}. \tag{6.15}$$

This expression gives the Q^2-evolution of shadowing singlet structure function at LO. We can easily compute the dependence of singlet structure function on Q^2 for a particular value of x by choosing an appropriate input distribution at a given value of Q_0^2 using Eq.(6.15). The effect of nonlinear or shadowing corrections to the singlet structure functions for a set of Q^2 can also be studied from this equation.

Similarly, the boundary condition (6.13) yields

$$F_2^S(x_0,t) = \frac{t^{p_1(x_0)}}{C + p_2(x_0)\int t^{p_1(x_0)-2}e^{-t}dt}, \tag{6.16}$$

so that using Eqs. (6.11) and (6.16) we obtain

$$F_2^S(x,t) = \frac{t^{p_1(x)} F_2^S(x_0,t)}{t^{p_1(x_0)} + \Big[p_2(x)\int t^{p_1(x)-2}e^{-t}dt - p_2(x_0)\int t^{p_1(x_0)-2}e^{-t}dt\Big] F_2^S(x_0,t)}. \quad (6.17)$$

Thus Eq.(6.17) provides us the solution of the GLR-MQ equation for singlet structure function at small-x for fixed Q^2. Using this equation the small-x dependence of nonlinear singlet structure function can be predicted for a particular value of Q^2 taking a convenient input distribution at an initial value of $x = x_0$. Eq.(6.17) further helps us to examine the effect of shadowing corrections to the singlet structure functions at small-x.

6.2.3 Comparative analysis of DGLAP and GLR-MQ equations for singlet structure function

In this section we find a solution of the linear DGLAP equation (Eq.(6.5)) for singlet structure function at LO employing the Regge ansatz of Eq.(6.6) and compare it with the solution of the GLR-MQ equation for singlet structure function discussed above. This comparison assists us to estimate the effect of shadowing corrections in our predictions of singlet structure function. Now employing the Regge ansatz of Eq.(6.6) the solution of Eq.(6.5) is obtained as

$$F_2^S(x,t) = Dt^{p_1(x)}, \quad (6.18)$$

where D is a constant to be fixed by initial boundary condition. The x dependent function $p_1(x)$ is defined in Eq.(6.9). We define

$$f_{10} = F_2^S(x,t_0) = Dt_0^{p_1(x)} \quad (6.19)$$

at $t = t_0$ at some lowe value $Q^2 = Q_0^2$. Then Eq.(6.18) and Eq.(6.19) leads us to

$$F_2^S(x,t) = f_{10}\Big(\frac{t}{t_0}\Big)^{p_1(x)}. \quad (6.20)$$

which provides the solution of the linear DGLAP equation for singlet structure function with the ansatz of Eq.(6.6) and it describes the Q^2-evolution of linear singlet structure function for a fixed value of x provided a suitable input distribution f_{10} has been chosen from the initial boundary condition.

Again, defining

$$f_{20} = F_2^S(x_0,t) = Dt^{p_1(x_0)} \quad (6.21)$$

at some initial higher value $x = x_0$, Eq.(6.18) can be expressed as

$$F_2^S(x, Q^2) = f_{20} t^{p_1(x)-p_1(x_0)}. \tag{6.22}$$

Eq.(6.22) is the solution of the linear DGLAP equation for singlet structure function at small-x with the ansatz of Eq.(6.6) and it describes the small-x behavior of linear singlet structure function for a particular value of Q^2 by choosing an appropriate input distribution f_{20} from the initial boundary condition.

Now considering the solutions of the linear DGLAP and nonlinear GLR-MQ equations respectively we can examine how the gluon recombination processes effect the linear QCD evolution of singlet structure functions. For this purpose we calculate the ratio of the solution of nonlinear GLR-MQ equation to that of linear DGLAP equation for singlet structure function using the Eqs.(6.17) and (6.22)

$$R_{F_2^S} = \frac{F_2^{S^{GLR-MQ}}(x,t)}{F_2^{S^{DGLAP}}(x,t)}, \tag{6.23}$$

as a function of variable x for different values of Q^2. From this ratio we can investigate the effect of shadowing corrections as a consequence of gluon recombination on the behavior of singlet structure function at small-x. The phenomenological analysis of Eq.(6.23) is presented in section 3.

6.2.4 Derivative of the singlet structure function with respect to $\ln Q^2$

It is very interesting to study the logarithmic derivative of the F_2 structure function with a shadowing corrections interpretation which provides information pertinent to the Regge analyses of F_2 in x and Q^2 kinematic domains. We make an attempt to study the Q^2 dependence of $\partial F_2^s/\partial \ln Q^2$ at given fixed value of x and examine the effect of shadowing corrections. There are several methods suggesting the relation between the scaling violations of $F_2(x, Q^2)$ to the gluon density at small-x [22-26]. These methods are based on the fact that at very small-x the structure function becomes gluon dominated. We use the the following approximate relation between the gluon density and the scaling violation of $F_2(x, Q^2)$ at some point x [26]

$$\frac{\partial F_2^S}{\partial \ln Q^2} = \frac{5\alpha_S(Q^2)}{9\pi} \int_x^1 \Big(\omega^2 + (1-\omega)^2\Big) G\Big(\frac{x}{\omega}, Q^2\Big) d\omega, \tag{6.24}$$

for four flavours. Since the non-singlet contributions of the structure function can be neglected in the small-x region, therefore we have considered the F_2 structure function as equivalent to F_2^S. The nonlinear gluon distribution function has a Regge like behavior

$$G(x,Q^2) = H(Q^2)x^{-\lambda_G}, \tag{6.25}$$

in the small-x region as discussed earlier in chapter 5. Thus the function $G(x/\omega, Q^2)$ can be expressed as

$$G\Big(\frac{x}{\omega}, Q^2\Big) = \omega^{\lambda_G} G(x,Q^2), \tag{6.26}$$

Using Eq.(6.24) along with the Eq.(6.26), we can express Eq.(6.4) in terms of gluon distribution function as

$$\frac{\partial F_2^S(x,Q^2)}{\partial \ln(Q^2)} = \frac{5\alpha_s(Q^2)}{9\pi} M(x) G(x,Q^2) - \frac{3\alpha_s^2(Q^2)}{64R^2Q^2} G^2(x,Q^2), \tag{6.27}$$

with,

$$M(x) = \int_x^1 \Big(\omega^2 + (1-\omega)^2\Big)\omega^{\lambda_G}. \tag{6.28}$$

Thus from Eq.(6.27) we can determine the effect of shadowing corrections on the behaviour of the logarithmic derivative of the singlet structure function. For phenomenological analysis of Eq.(6.27) we take the results of the gluon distribution function $G(x,Q^2)$ obtained in chapter 5 of this thesis. Due to the negative nonlinear term as a result of gluon recombination Eq.(6.27) is expected to predict a slower growth of $\partial F_2^s/\partial \ln Q^2$ towards small-x.

6.3 Result and discussion

We have solved the nonlinear GLR-MQ evolution equation by considering the Regge like behavior of singlet and gluon structure function and examine the effects of shadowing corrections due to gluon recombination processes at small-x to the LO DGLAP evolution equations. The behavior of singlet structure function at small-x and moderate Q^2 is investigated for both at $R = 2$ GeV^{-1} and $R = 5$ GeV^{-1} from the predicted solution of the GLR-MQ equation. Our computed values of singlet structure function with shadowing corrections are compared with the CERN's NMC [6], Fermilab E665

Collaboration [7] as well as with those obtained in the NNPDF [8] collaboration. It is worthwhile to mention here that the NMC and E665 experiments measured the deuteron structure function F_2^d from which F_2^S can be extracted using the relation $F_2^d = \frac{5}{9}F_2^S$. We perform our analysis in the kinematic region $0.6 \leq Q^2 \leq 30$ GeV^2

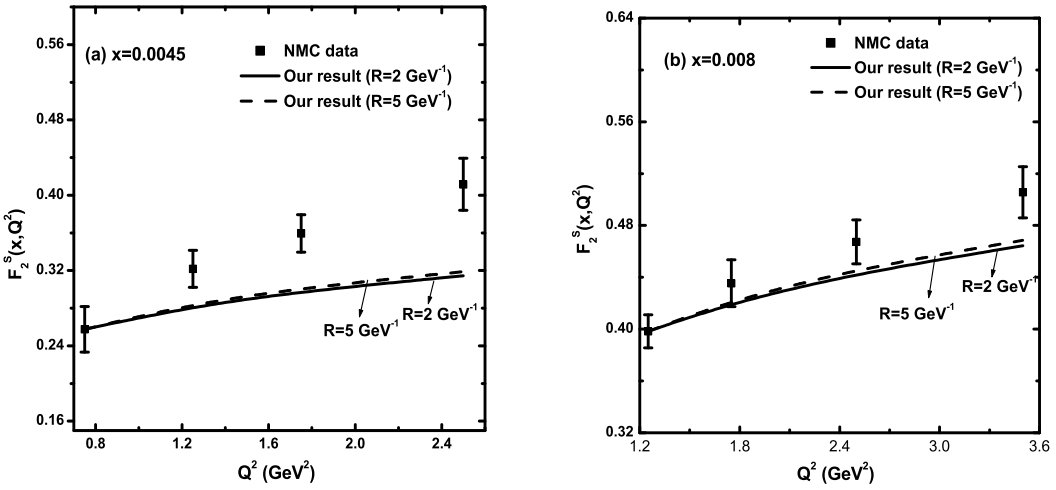

Figure 6.1: Q^2 dependence of singlet structure function with shadowing corrections for $R = 2$ GeV^{-1} (solid lines) and $R = 5$ GeV^{-1} (dash lines) computed from Eq. (6.15) compared with the NMC data [6].

and $10^{-4} \leq x \leq 10^{-1}$ where the suggested solution of the GLR-MQ equation for singlet structure function given by Eq.(6.11) is found to be legitimate. We consider the range $0.6 < Q^2 < 3.6$ GeV^2 and $10^{-4} < x < 0.013$ for NMC data, $1 < Q^2 < 4$ GeV^2 and $10^{-4} < x < 0.01$ for E665 data and $1 < Q^2 < 27$ GeV^2 and $10^{-4} < x < 0.011$ for NNPDF data in our phenomenological analysis. To compute the dependence of structure functions on Q^2 we take the input distributions from the data point corresponding to the lowest value of Q^2 for a particular range of Q^2 under study. On the other hand, the data point corresponding to the highest value of x of a particular range of x under consideration are taken as input distribution to determine the x dependence of the structure functions. In the present analysis we consider the function $K(x) = K$, where K is a constant parameter, to relate the singlet structure function and gluon densities as a simplest assumption and find that the best fit results are obtained in the range $0.28 < K < 1.2$ for our entire region of discussion. The vertical error bars represent the total combined statistical and systematic uncertainties of the experimental data.

In Figure 6.1 we plot the Q^2 dependence of singlet structure function with shad-

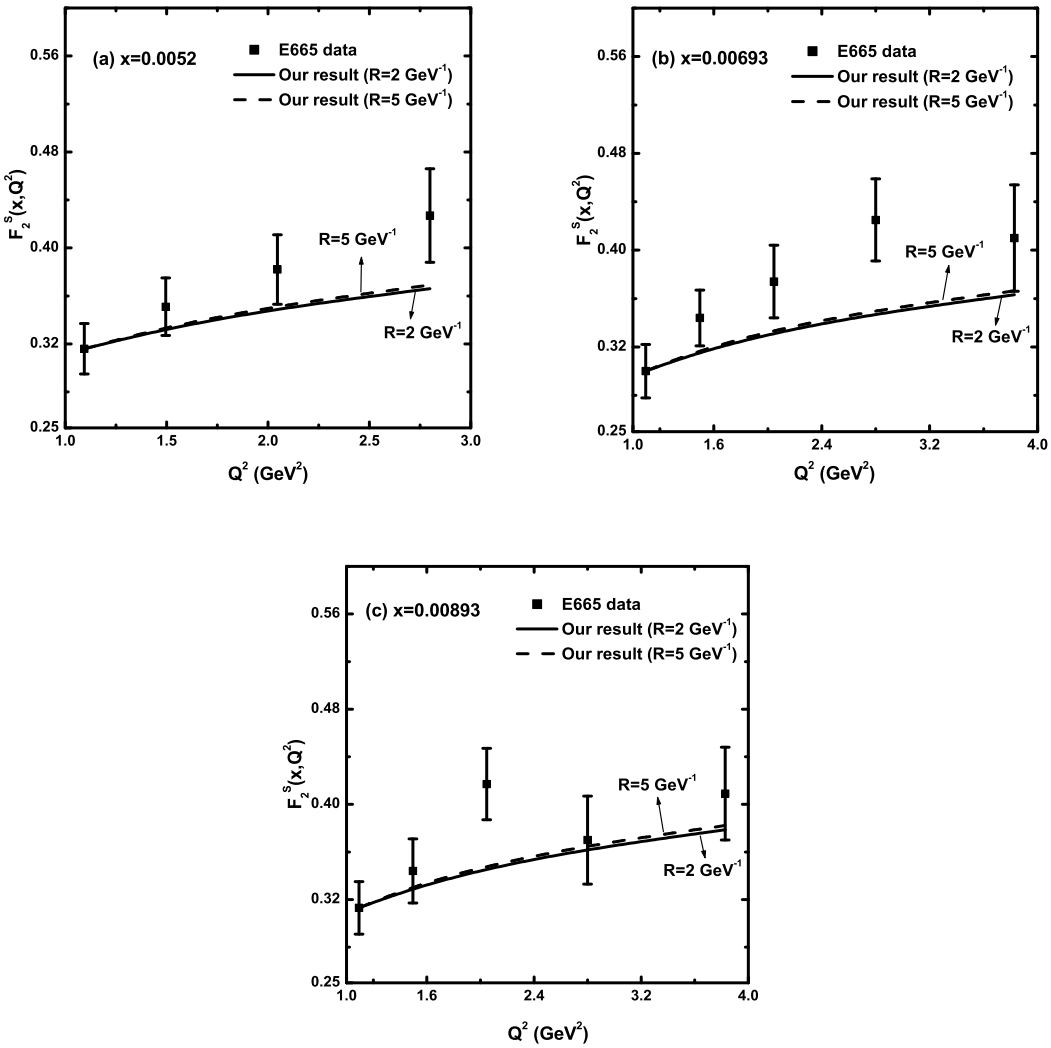

Figure 6.2: A plot showing the Q^2 dependence of singlet structure function with shadowing corrections for $R = 2$ GeV^{-1} (solid lines) and $R = 5$ GeV^{-1} (dash lines) computed from Eq. (6.15) compared with the E665 data [7].

owing corrections computed from Eq.(6.15) for $R = 2$ GeV^{-1} and $R = 5$ GeV^{-1} and check the compatibility of our predictions with the NMC data at two representative $x = 0.0045$ and 0.008 respectively. The solid lines represent the predictions of singlet structure function for the hot spots with $R = 2$ GeV^{-1} whereas the results for $R = 5$ GeV^{-1} is shown by the dash lines.

In Figure 6.2 we show the comparison of our predictions of the singlet structure function for $R = 2$ GeV^{-1} and $R = 5$ GeV^{-1} obtained from Eq.(6.15) with the E665 data. Here the predicted values of singlet structure function with shadowing corrections are plotted against Q^2 at some fixed $x = 0.0052, 0.00693$ and 0.00893 respectively. The solid lines represent the results for $R = 2$ GeV^{-1} whereas the dash

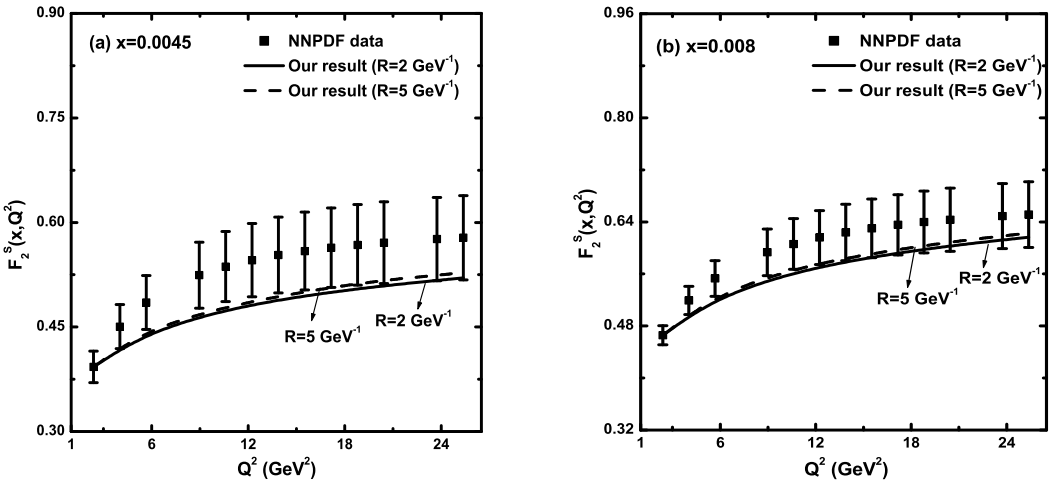

Figure 6.3: Q^2 dependence of singlet structure function with shadowing corrections for $R = 2$ GeV^{-1} (solid lines) and $R = 5$ GeV^{-1} (dash lines) obtained from Eq.(6.15) compared to NNPDF data [8].

lines represent the results for $R = 5$ GeV^{-1}.

Similarly, in Figure 6.3 the Q^2 dependence of the singlet structure function with shadowing corrections obtained from Eq.(6.15) for $R = 2$ GeV^{-1} and $R = 5$ GeV^{-1} are compared with the NNPDF parametrizations. Here the plots are shown for two values of x, viz. $x = 0.0045$ and 0.008. The results for $R = 2$ GeV^{-1} are depicted by the solid lines and the results for $R = 5$ GeV^{-1} are shown by the dash lines.

On the other hand, Figure 6.4 represents the small-x behavior of singlet structure function with shadowing corrections computed from Eq.(6.17) for $R = 2$ GeV^{-1} and $R = 5$ GeV^{-1} respectively. The consistency of our results are examined with the NMC data at fixed values of $Q^2 = 1.25, 1.75$ and 2.5 GeV^2 respectively. The results for $R = 2$ GeV^{-1} are shown by the solid lines whose those for $R = 5$ GeV^{-1} are shown by the dash lines.

In Figure 6.5 we show the comparison of the small-x behavior of singlet structure function with shadowing corrections computed from Eq.(6.17) for $R = 2$ GeV^{-1} and $R = 5$ GeV^{-1} with E665 data. The comparison is shown for four representative Q^2, viz. $Q^2 = 1.094, 1.496, 2.046$ and 2.799 GeV^2 respectively. The solid lines represent the results for $R = 2$ GeV^{-1} whereas the dash lines represent the results for $R = 5$ GeV^{-1}.

Figure 6.6 shows the plots of singlet structure function with shadowing corrections computed from Eq.(6.17) for $R = 2$ GeV^{-1} and $R = 5$ GeV^{-1} vs. x compared with

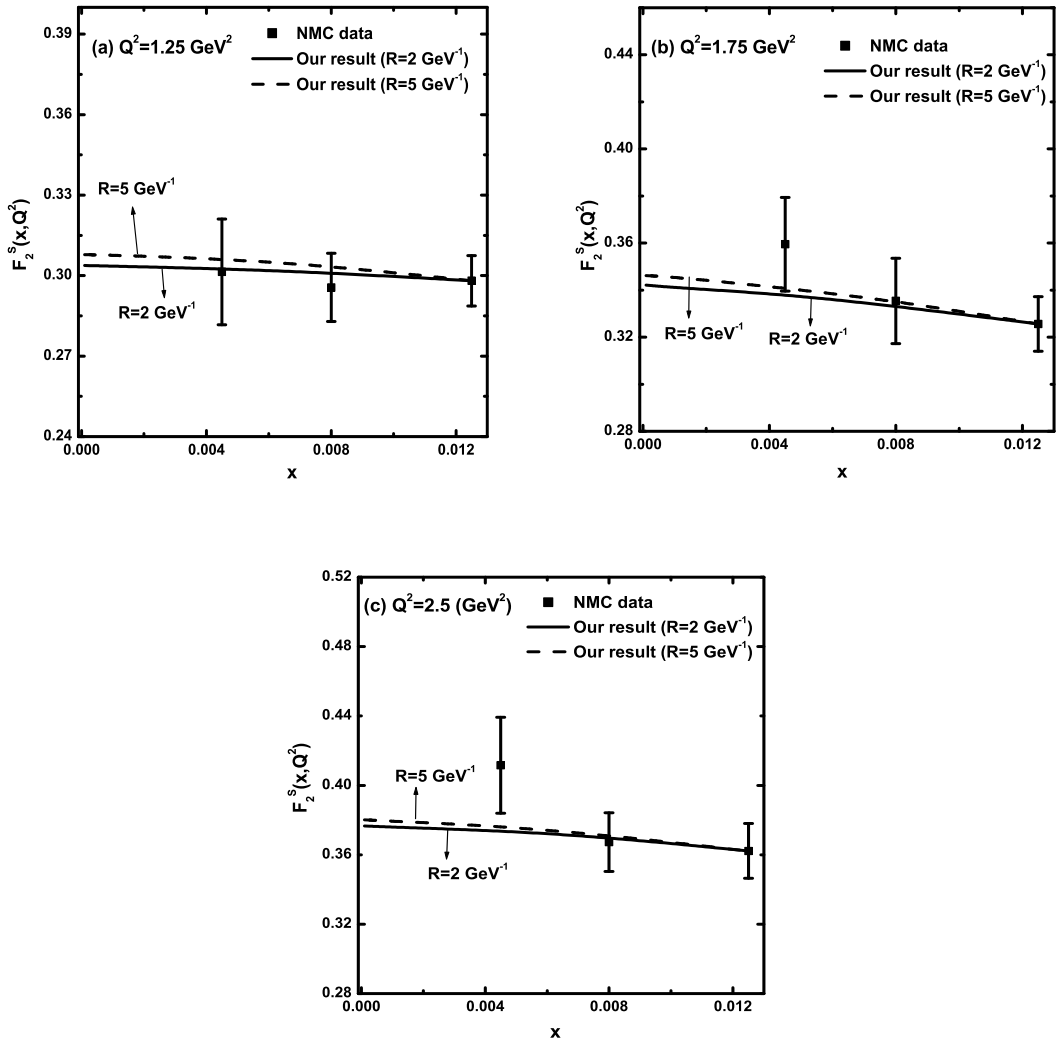

Figure 6.4: Small-x behavior of singlet structure function with shadowing corrections for $R = 2$ GeV^{-1} (solid lines) and $R = 5$ GeV^{-1} (dash lines)from Eq.(6.17) compared to NMC data [6].

the NNPDF data at four representative Q^2, viz. $Q^2 = 4.03, 8.958, 12.242$ and 18.808 GeV^2 respectively. The solid lines represent the results for $R = 2$ GeV^{-1} whereas the dash lines represent the results for $R = 5$ GeV^{-1}.

From Figure 6.1 to Figure 6.6 we observe that the obtained results of singlet structure function with shadowing corrections show the general trend of experimental data and parametrization. The singlet structure function increases with increasing Q^2 and decreasing x, but this attitude is tamed with respect to the nonlinear terms in the GLR-MQ equation. The effect of shadowing corrections as a consequence of gluon recombination processes in our predictions is observed to be very high at the hot-spot with $R = 2$ GeV^{-1} when the gluons are centered within the proton, compared to at $R = 5$ GeV^{-1} when the gluons are disseminated throughout the entire proton.

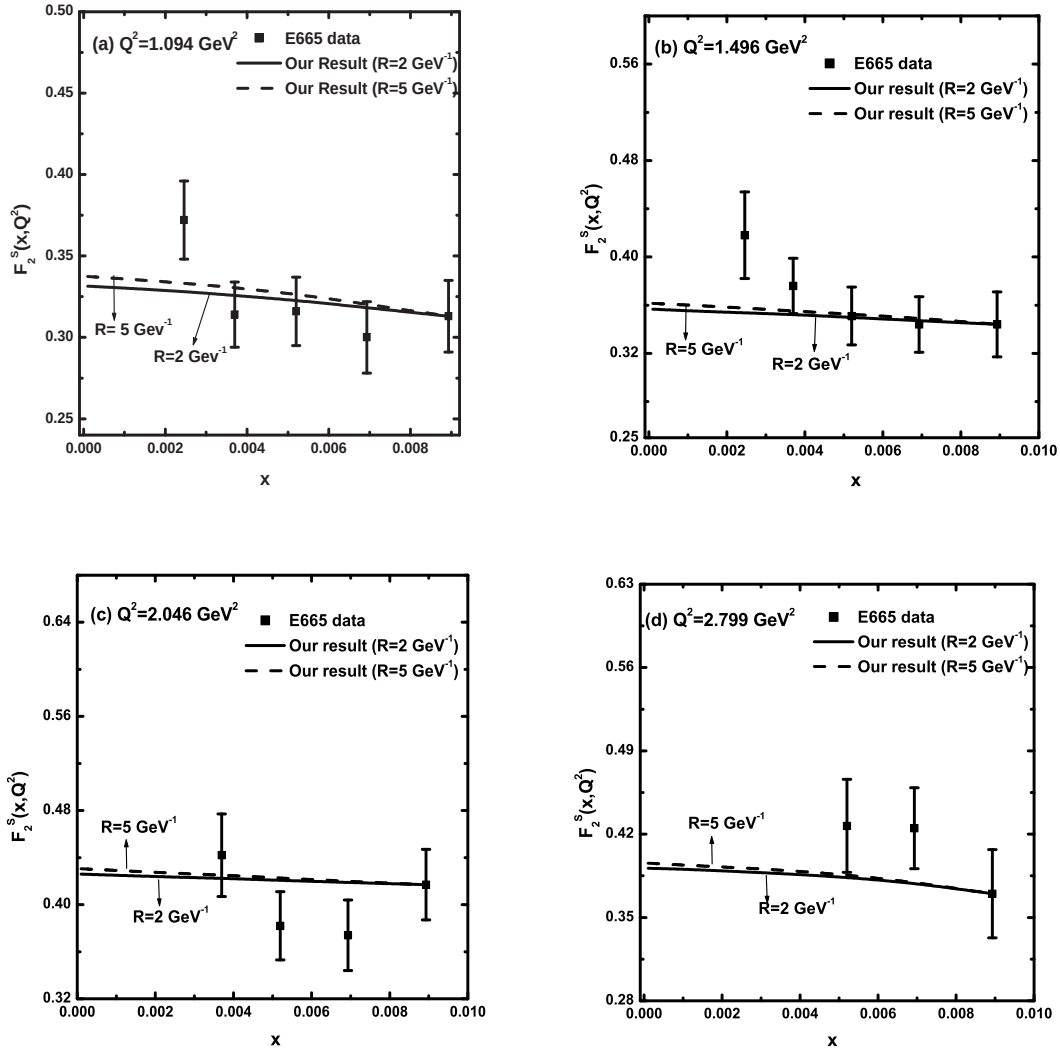

Figure 6.5: Small-x behaviour of singlet structure function with shadowing corrections for $R = 2$ GeV^{-1} (solid lines) and $R = 5$ GeV^{-1} (dash lines) computed from Eq.(6. 17) compared to E665 data [7].

Moreover, to examine the effect of nonlinear or shadowing corrections to the singlet structure function in our prediction, we plot the ratio of the solution of nonlinear GLR-MQ equation to that of the linear DGLAP equation for singlet structure function in Figure 6.7. The ratio $R_{F_2^S}$ defined in Eq.(6.22) is plotted against the variable x in the range $10^{-4} \leq x \leq 10^{-2}$ for five representative values $Q^2 = 4.03, 5.675, 8.958, 12.242$ and 18.808 GeV^2 respectively. We observe that as x grows smaller the GLR-MQ/DGLAP ratio for singlet structure function decreases which implies that the effect of nonlinearity increases towards small-x due to gluon recombination. We also observe that towards smaller values of Q^2 the value of the ratio goes smaller.

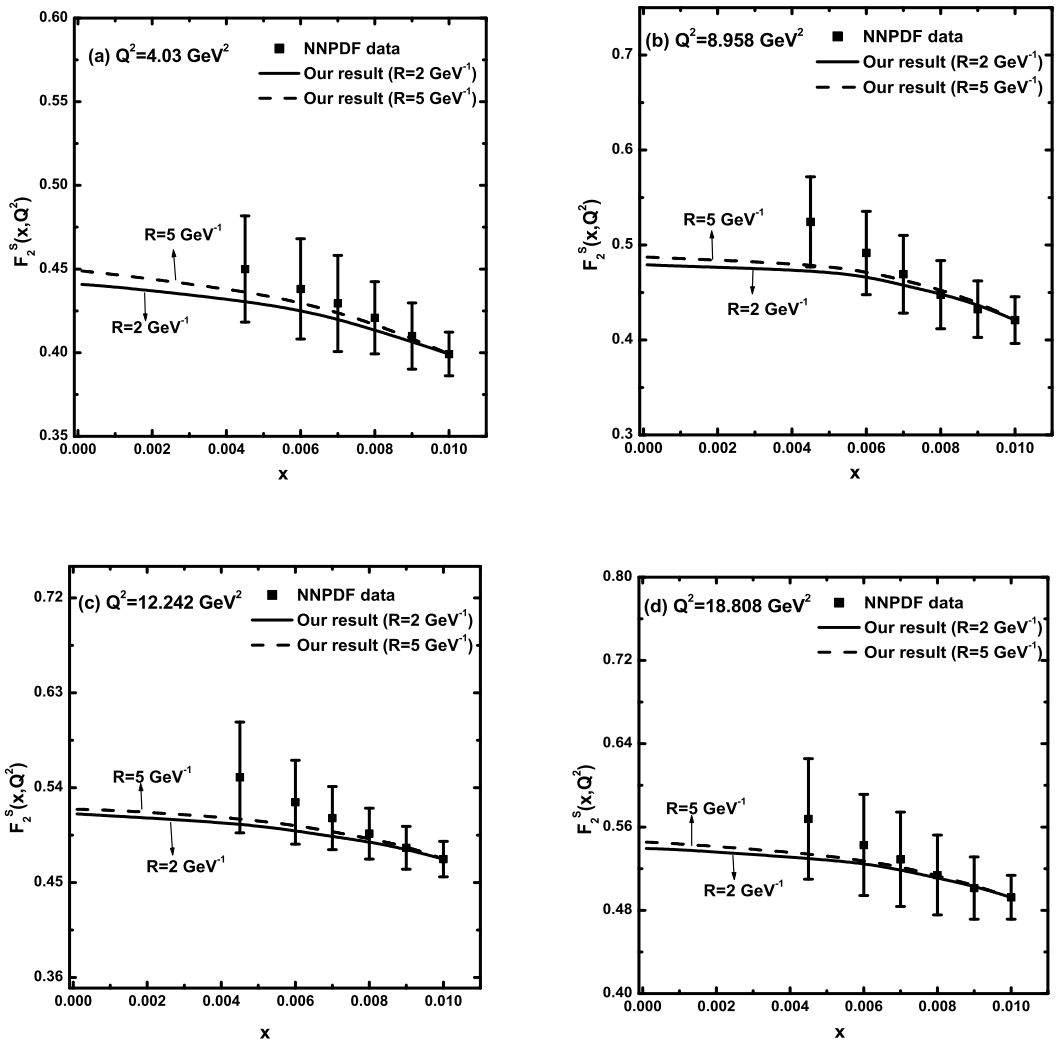

Figure 6.6: Small-x behavior of singlet structure function with shadowing corrections for $R = 2$ GeV^{-1} (solid lines) and $R = 5$ GeV^{-1} (dash lines) computed from Eq.(6.17) compared to NNPDF data [8].

In Figure 6.8 we show a plot of logarithmic derivative of the singlet structure function obtained at the hot-spot point $R = 2$ GeV^{-1} from Eq.(6.27) vs. Q^2 at three fixed values of $x = 0.0005, 0.005$ and 0.008 respectively. We compare our results with the H1 [9, 10] data. The corresponding values of $G(x, Q^2)$ are obtained from Eq.(5.15) of chapter 5 using the MRST2001LO [26] input gluon parametrization. Similarly, we show a plot of logarithmic slop of the singlet structure function for a set of x values in Figure 6.9 at two different bins in Q^2, viz. $Q^2 = 2.2$ and 7.4 GeV^2 respectively. Here also we check the consistency of our results with the H1 [9, 10] data. The corresponding values of $G(x, Q^2)$ are obtained from Eq.(5.17) of chapter 5 using the MRST2001LO [27] input gluon parametrization. We observe that the derivative of the singlet structure function with respect to $\ln Q^2$ has a tamed behavior

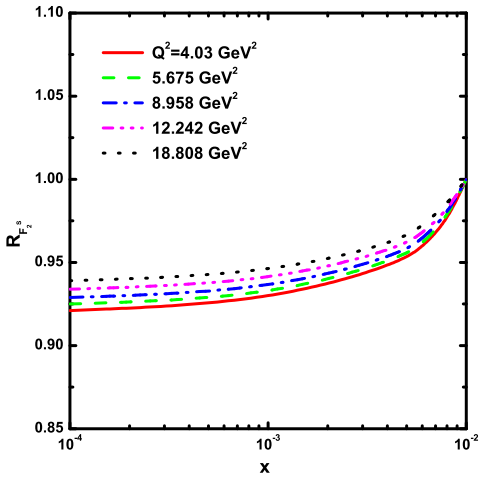

Figure 6.7: A plot of the GLR-MQ/DGLAP ratio for singlet structure function for five different bins in $Q^2 = 4.03, 5.675, 8.958, 12.242$ and 18.808 GeV^2.

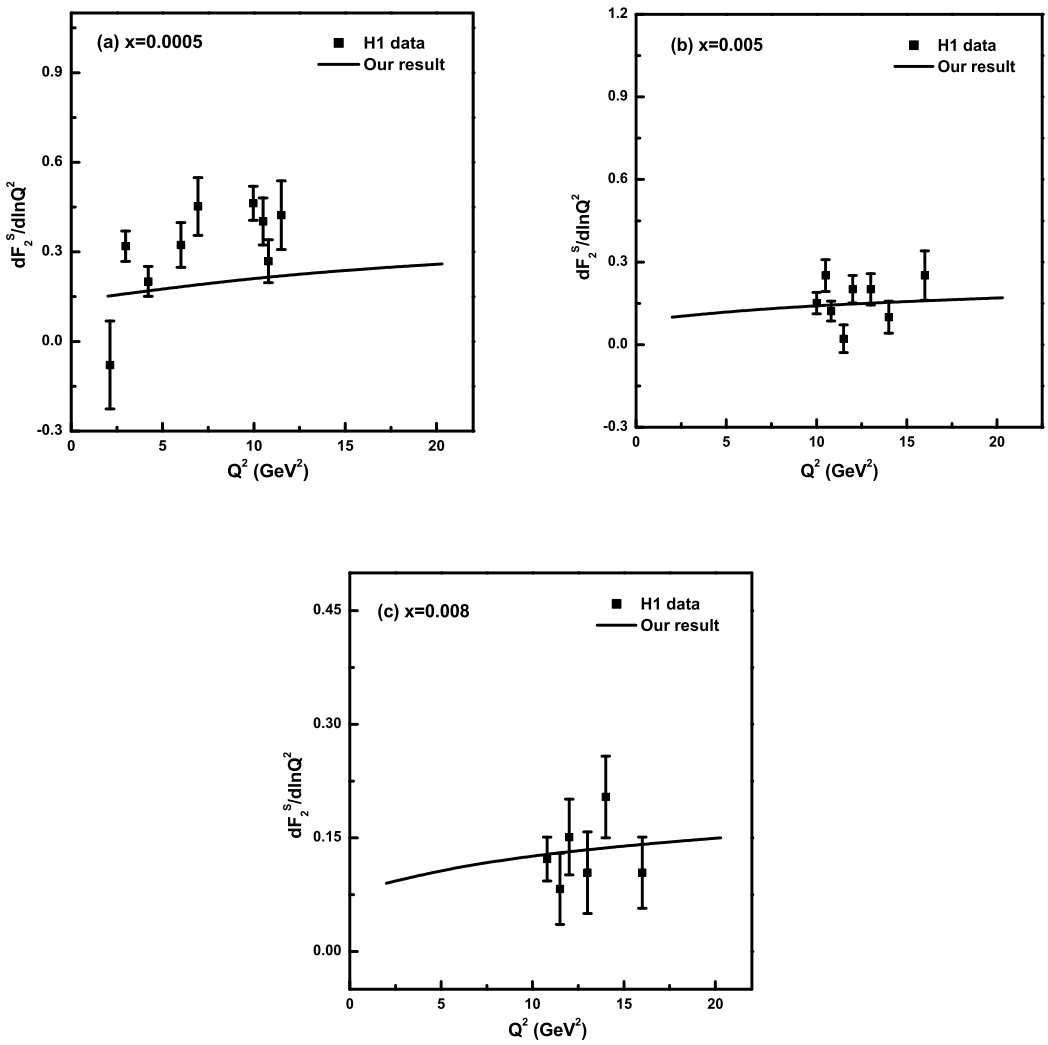

Figure 6.8: A plot of the derivative of the singlet structure function with respect to $\ln(Q^2)$ vs. Q^2 compared with the H1 data [9, 10] at $x = 0.0005, 0.005$ and 0.008 respectively.

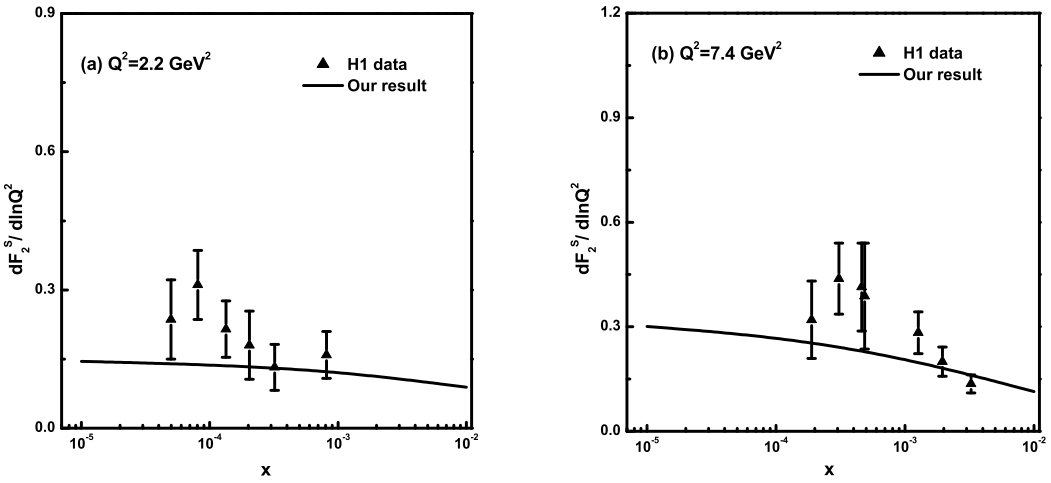

Figure 6.9: A plot of the derivative of the singlet structure function with respect to $\ln(Q^2)$ vs. x compared with the H1 data [9, 10] at $Q^2 = 2.2$ and 7.4 GeV^2.

due to gluon recombination as x grows smaller. It can be easily seen from the figure that the H1 data shows a steep rise of the logarithmic derivative of the structure function towards small-x, however this steep behavior is observed to be tamed for $x \leq 10^{-4}$. This tamed behaviour is correlated with the shadowing corrections as a result of gluon recombination at very small-x. It is very interesting to note that our results obtained in the GLR-MQ framework are comparable with the H1 data in the small-x region.

6.4 Summary

To summaries, we solve the nonlinear GLR-MQ equation for sea quark distribution function in leading twist approximation incorporating the well known Regge ansatz and investigate the effect of nonlinear or shadowing corrections arises due to the gluon recombination processes on the behavior of singlet structure function at small-x and moderate-Q^2. We note that the solution of the GLR-MQ equation for singlet structure function with shadowing corrections suggested in this work is found to be valid only in the kinematic domain $0.6 \leq Q^2 \leq 30$ GeV^2 and $10^{-4} \leq x \leq 10^{-1}$, where the gluon recombination processes play an important role on the QCD evolution. Our predictions of singlet structure function is found to show the general trend of experimental data and parametrization, nevertheless with the inclusion of the nonlinear terms, this behaviour of singlet structure function is slowed down towards small-x

leading to a restoration of the Froissart bound. Moreover the effect of shadowing corrections on the behaviour of singlet structure function with decreasing x become significant at the hot spot with $R = 2$ GeV^{-1} when the gluons and the sea quarks are assumed to condensed in a small region within the proton. The predictions of the GLR-MQ/DGLAP ratio for $F_2^S(x, Q^2)$ also indicate that the gluon recombination processes become significant towards smaller values of x and Q^2 . Moreover our results show that the behavior of the derivative of the singlet structure function with respect to $\ln Q^2$ is consistent with the H1 experimental data. Our results show that in the small-x region the logarithmic derivative of the singlet structure function has a tamed behavior related to shadowing corrections due to gluon recombination.

Bibliography

[1] Froissart, M. Asymptotic behavior and subtractions in the Mandelstam representation, *Phys. Rev.* **123**(3), 1053−−1057, 1961.

[2] Martin, A. Unitarity and high-energy behavior of scattering amplitudes, *Phys. Rev.* **129**(3), 1432−−1436, 1963.

[3] Mueller, A. H., Qiu, J. Gluon recombination and shadowing at small values of x, *Nucl. Phys. B* **268**(2), 427−−452, 1986.

[4] Gribov, L. N., Levin, E. M. and Ryskin, M. G. Semihard processes in QCD, *Phys. Rep.* **100**(1-2), 1−−150, 1983.

[5] Mueller, A. H. Small-x behavior and parton saturation: A QCD model, *Nucl. Phys. B* **335**(1), 115−−137, 1990.

[6] Arneodo, M. et al., Measurement of the proton and deuteron structure functions, F_2^p and F_2^d, and of the ratio $\sigma_L\sigma_T$, *Nucl. Phys. B* **483**(1-2), 3−−43, 1997.

[7] Adams, M. R. et al., Proton and deuteron structure functions in muon scattering at 470 GeV, *Phys. Rev. D* **54**(5), 3006−3056, 1996.

[8] Forte, S. et al., Neural network parametrization of deep inelastic structure functions, *JHEP* **2002**(JHEP05), 062, 2002.

[9] Adloff, C. et al., Measurement of neutral and charged current cross-sections in positron-proton collisions at large momentum transfer, *Eur. Phys. J. C* **13**(4), 609−−639, 2000.

[10] Adloff, C. et al., Deep-inelastic inclusive ep scattering at low x and a determination of α_s, *Eur. Phys. J. C* **21**(1), 33−−61, 2001.

[11] Prytz, K. Signals of gluon recombination in deep inelastic scattering, *Eur. Phys. J. C* **22**(2), 317−−321, 2001.

[12] Laenen, E., Levin, E. A new evolution equation, *Nucl. Phys. B* **451**(1-2), 207−−230, 1995.

[13] Laenen, E., Levin, E. Parton densities at high energy, *Annu. Rev. Nucl. Part. Sci.* **44**, 199−−246, 1994.

[14] Levin, E. M., Ryskin, M. G. Low-x structure function and saturation of the parton density, *Nucl. Phys. B (Proc. Suppl.)* **18**(3), 92−−124, 1991.

[15] Abbott, L. F., Atwood, W. B. and Michael Barnett, R. Quantum-chromodynamic analysis of eN deep-inelastic scattering data, *Phys. Rev. D* **22**(3), 582−−594, 1980.

[16] Collins, P. D., *An Introduction to Regge Theory and High-Energy Physics*, Cambridge University Press, Cambridge, 1997.

[17] Donnachie, A., Landshoff, P. V. Total cross sections, *Phys. Lett. B* **296**(1-2), 227−− 232, 1992.

[18] Donnachie, A., Landshoff, P. V. Small x: two pomerons!, *Phys. Lett. B* **437**(3-4), 408−−416, 1998.

[19] Sarma, J. K., Choudhury, D. K. and Medhi, G. K. x-distribution of deuteron structure function at low-x, *Phys.Lett. B* **403**(1-2), 139−−144, 1997.

[20] Sarma, J. K., Das, B. t evolutions of structure functions at low-x, *Phys. Lett. B* **304**(3-4), 323−−328, 1993.

[21] Baishya, R., Sarma, J. K. Method of characteristics and solution of DGLAP evolution equation in leading and next to leading order at small x, *Phys. Rev. D* **74**(10), 107702, 2006.

[22] Prytz, K. Approximate determination of the gluon density at low-x from the F_2 scaling violations, *Physics Letters B* **311**(1-4), 286−−290, 1993.

[23] Prytz, K. An approximate next-to-leading order relation between the low-x F_2 scaling violations and the gluon density, *Phys. Lett. B* **332**(3-4), 393−−397, 1994.

[24] Bora, K., Choudhury, D. K. Finding the gluon distribution of the proton at low x from F_2, *Phys. Lett. B* **354**(1-2), 151−−154, 1995.

[25] Gay Ducati, M. B., Goncalves, P. B. Analysis of low-x gluon density from the F_2 scaling violations, *Phys. Lett. B* **390**(1-4), 401−−404, 1997.

[26] Boroun, G. R. Analysis of the Logarithmic Slope of F_2 from the Regge Gluon Density Behavior at Small x, *J. of Expt. and Theor. Phys.* **111**(4), 567−−569, 2010.

[27] Martin, A. D. et al., MRST2001: partons and α_s from precise deep inelastic scattering and Tevatron jet data, *Eur. Phys. J. C* **23**(1), 73−−87, 2002.

Chapter 7

Comparative Analysis of Various Nonlinear Evolution Equations

7.1 Introduction

The growth of total hadronic cross sections at very high energies is one of the most challenging problems of QCD and accordingly the study of the high density QCD turns out to be the center of intensive studies in the last few years. The attempts to understand the aspects of the higher twist phenomena led to many different kinds of model in the past times. The corrections of the higher order QCD effects, which suppress or shadow the growth of the parton densities, leading to a possible restoration of the Froissart bound on physical cross-section in the very small-x region are at the onset accounted for by Gribov, Levin and Ryskin, and Mueller and Qiu in the GLR-MQ [1-3] equations. Several other nonlinear evolution equations are proposed in later times reporting the corrections of the gluon recombination to the linear DGLAP [4-6] and BFKL [7-9] evolutions, viz. the Modified-DGLAP (MD-DGLAP) [10, 11], Balitsky-Kovchegov (BK) [12, 13], Modified-BFKL (MD-BFKL) [14] and Jalilian-Marian-Iancu-McLerran-Weigert-Leonidov-Kovner (JIMWLK) [15-17] equations. The nonlinear equations viz. Modified-BFKL (MD-BFKL), BK and JIMWLK are based on BFKL evolution, whereas, the MD-DGLAP equation is based on DGLAP evolution. The BK and the MD-DGLAP equations are the most widely studied among these . The GLR-MQ equation takes the double leading logarithmic approximation (DLLA) for both Q^2 and $1/x$, keeping only the $\ln(Q^2/\Lambda^2)\ln(1/x)$ fac-

tor in the solutions of the evolution equation, whereas, the MD-DGLAP equation is derived under the leading logarithmic LL(Q^2) approximation. Unlike the GLR-MQ equation, the MD-DGLAP equation sums the Feynman diagrams in the framework of the time-ordered perturbation theory (TOPT) [18] instead of using the AGK cutting rule [19]. Moreover, apart from the shadowing corrections, the MD-DGLAP equation also takes into account the antishadowing effects which balance the momentum lost in the shadowing process. The antishadowing corrections may change the predictions of the GLR-MQ equations. On the other hand, the BK equation is an upgraded version of the GLR-MQ equation and it determines the saturation of parton densities at very small-x. The BK equation considers the more precise triple-pomeron vertex [20, 21] and can be used for the non-forward amplitude. The BK equation is obtained in the leading $\ln(1/x)$ approximation of perturbative QCD, i.e. it sums all contributions of the order $(\alpha_s \ln(1/x))^n$.

In this chapter we present a comparative analysis of the GLR-MQ equation with the MD-DGLAP and BK equations. Here the gluon distribution function obtained from the semi analytical solution of the GLR-MQ equation discussed in chapter 5 are compared with the results of MD-DGLAP and BK equations in the region of small-x. To compare our predictions in the GLR-MQ approach with those of MD-DGLAP and BK equations we have used the results of Ref.[22] and Ref.[23] respectively where the numerical analysis of these equations are presented.

7.2 Formalism

The GLR-MQ equation for the gluon distribution function can be expressed as [1-3, 24]

$$\frac{\partial G(x,Q^2)}{\partial \ln Q^2} = \frac{\partial G(x,Q^2)}{\partial \ln Q^2}\Big|_{DGLAP} - \frac{81}{16}\frac{\alpha_s^2(Q^2)}{R^2Q^2}\int_x^1 \frac{d\omega}{\omega}\Big[G\Big(\frac{x}{\omega},Q^2\Big)\Big]^2, \tag{7.1}$$

In chapter 5 we have solved this equation semi analytically and investigated the effect of shadowing corrections on the behaviour of small-x and Q^2-dependence of gluon distribution function using a simple form of Regge like ansatz. Here we have used these results to perform a comparative analysis of the small-x dependence of gluon distribution function obtained in the GLR-MQ approach with the results of MD-DGLAP and BK equations respectively. For convenience, we rewrite here some of

the important results of chapter 5.

By incorporating the Regge like behaviour of the gluon distribution function, i.e., $G(x,Q^2) = H(Q^2)x^{-\lambda_G}$ with the Regge intercept λ_G, the solution of Eq.(7.1) is obtained as

$$G(x,t) = \frac{t^{\gamma_1(x)}}{C + \gamma_2(x)\int t^{\gamma_1(x)-2}e^{-t}dt}. \tag{7.2}$$

Here $t = \ln(Q^2/\Lambda^2)$ and the constant C is determined from initial boundary conditions. So we use the physically plausible boundary condition at some high $x = x_0$ in Eq.(7.2) and obtain the x dependence of the gluon distribution function as

$$G(x,t) = \frac{t^{\gamma_1(x)}G(x_0,t)}{t^{\gamma_1(x_0)} + \Big[\gamma_2(x)\int t^{\gamma_1(x)-2}e^{-t}dt - \gamma_2(x_0)\int t^{\gamma_1(x_0)-2}e^{-t}dt\Big]G(x_0,t)}. \tag{7.3}$$

This equation helps us to predict the effect of shadowing corrections to small-x behaviour of nonlinear gluon distribution function by picking out suitable input distribution at an initial value of $x = x_0$. The Regge type solution of the GLR-MQ equation is found to be valid in the kinematic region $1 \leq Q^2 \leq 30$ GeV^2 as well as $10^{-5} \leq x \leq 10^{-2}$ as discussed in chapter 5.

The MD-DGLAP equation [10, 11] derived by Zhu and Ruan sums up all possible twist-4 cut diagrams in the LL(Q^2) approximation and describes the corrections of parton recombination to the QCD evolution equation. For gluon distribution the MD-DGLAP equation is given by [22]

$$\begin{aligned}\frac{dxG(x,Q^2)}{d\ln(Q^2)} &= P_{gg}\otimes G(x,Q^2) + P_{gq}\otimes S(x,Q^2) \\ &\quad + \frac{\alpha_s^2 k}{Q^2}\int_{x/2}^{x} dx_1 x x_1 G^2(x_1,Q^2)\sum_i P_i^{gg\to g}(x_1,x) \\ &\quad - \frac{\alpha_s^2 k}{Q^2}\int_{x}^{1/2} dx_1 x x_1 G^2(x_1,Q^2)\sum_i P_i^{gg\to g}(x_1,x)\end{aligned} \tag{7.4}$$

where P_{gg} and P_{gq} are the evolution kernels of the linear DGLAP equation. The explicit form of the recombination function is

$$\sum_i P_i^{gg\to g}(x_1,x) = \frac{27}{64}\frac{(2x_1 - x)(-136xx_1^3 - 64x_1x^3 + 132x_1^2x^2 + 99x_1^4 + 16x^4)}{xx_1^5}. \tag{7.5}$$

The nonlinear coefficient k is based on the definition of the double parton distribution and the geometric distributions of partons inside the target. The positive third term

on the right-hand side represents the anti-shadowing effect, whereas the negative fourth term is the result of the shadowing correction.

In Ref.[22] an analysis of MD-DGLAP equation is presented by W. Zhu et al., where the parton distributions in the small-x region in the nucleus and free proton are numerically predicted considering the GRV-like input distributions with and without anti-shadowing corrections. Here the Q^2 and x behaviour of the parton distributions at high gluon density are studied in LL(Q^2) approximation using the MD-DGLAP equation. The initial gluon density in the GRV98LO set is used as the input distribution at $Q_0^2 = 0.34$ GeV^2, i.e.,

$$xg(x, Q_0^2) = 17.47x^{1.6}(1-x)^{3.8}, \tag{7.6}$$

with the representation $G(x, Q^2) = xg(x, Q^2)$. The results obtained in Ref.[22] show that the growth of the predicted gluon distribution in the proton toward small-x is slower than $\ln(1/x)$ for $x < 10^{-6}$ which implies that the gluon recombination at twist 4 level suppresses the rapid growth of gluon densities with decrease in x. We consider the results of Ref.[22] for a comparative analysis of our predictions of gluon distribution obtained from the solution of GLR-MQ equation with the MD-DGLAP results.

The BK equation [12, 13] is derived by Balitsky and Kovchegov in the LL($1/x$) approximation of perturbative QCD, i.e. it sums all contributions of the order $(\alpha_s \ln(1/x))^n$. This equation is written in coordinate space in terms of the dipole scattering amplitude N. This equation provides the basic indication of the fact that the correct degrees of freedom at high energies in QCD are colour dipoles. It provides an explanation of the more specific triple-pomeron vertex [20, 21] and can be utilized for the non-forward amplitude. The BK equation reads

$$\begin{aligned}\frac{\partial N(r,Y;b)}{\partial Y} &= \frac{\bar{\alpha_s}}{2\pi}\int \frac{d^2r' r^2}{(r-r')^2 r'^2} \\ &\times\Big[2N\big(r', Y; b+\frac{1}{2}(r-r')\big) - N(r,Y;b) \\ &-N\big(r', Y; b-\frac{1}{2}(r-r')\big)N\big(r-r', Y; b-\frac{1}{2}r'\big)\Big],\end{aligned} \tag{7.7}$$

where $\bar{\alpha_s} = (\alpha_s N_c)/\pi$, $N(r, Y; b)$ is the scattering amplitude of interaction for the dipole with the size r and rapidity $Y = \ln(1/x)$, at impact parameter b. In the large N_c limit $C_F = N_c/2$, where N_c is the number of colors. Eq.(7.7) implies

that the dipole of size r decays in two dipoles of sizes r' and $r - r'$ which interact with the target. The linear part of Eq.(7.7) represents the conventional LO BFKL equation [7-9]. The non-linear term accounts for the simultaneous interaction of two produced dipoles with the target and the high twist contributions. A fascinating characteristics of the BK equation is that its solution predicts a limiting form of the scattering amplitude resulting in parton saturation. For small dipole densities N the quadratic term in the brackets is negligible and Eq.(7.7) reduces to the conventional BFKL equation, whereas, sauration is reached when $N = 1$.

In Ref.[23] the solution of the LO BK equation is reported where the authors include the impact parameter dependence of the amplitude at initial values of rapidity $Y = \ln(1/x)$ and find the amplitude in each point of impact parameter space. The gluon density is related to the dipole amplitude as

$$G(x, Q^2) = \frac{4}{\pi^3} \int_x^1 \frac{dx'}{x'} \int_{4/Q^2}^{\infty} \frac{dr^2}{r^2} \int d^2b 2N(r, x'; b), \tag{7.8}$$

where the representation $G(x, Q^2) = xg(x, Q^2)$ is used. The calculated results of the gluon density function in Ref.[23] are found to be in good agreement with the GRV parametrization. Here we use the results of Ref.[23] to perform a comparative analysis of our results of gluon distribution obtained from the solution of GLR-MQ equation with those of the BK equation.

7.3 Result and discussion

The x dependence of gluon distribution function with shadowing corrections calculated in the framework of GLR-MQ equation is compared with the results of MD-DGLAP and BK equations taken from the Refs.[22] and [23] respectively. We perform these comparisons in the kinematic region $1 \leq Q^2 \leq 30$ GeV^2 and $10^{-5} \leq x \leq 10^{-2}$ as our predicted solution of GLR-MQ equation is found to be valid only in this domain. In Figure 7.1 the gluon distribution function calculated from Eq.(7.3) at the hot spots $R = 2$ GeV^{-1} are plotted as a function of x for fixed values of Q^2=2.2, 3, 5, 10 and 20 GeV^2 respectively. Our results manifest that the gluon density increases with the decreasing x but this behavior is tamed as x grows smaller due to nonlinear or shadowing corrections. For each Q^2 our predictions obtained in the framework of GLR-MQ equation are in very good agreement with the results of the BK equation.

Moreover, concerning the shape of the curves we observe that the shapes of the curves found in the GLR-MQ approach are very similar to the shape of the BK curves. On the other hand, we note that our predictions do not match with the results of MD-DGLAP equation, as the MD-DGLAP curves have opposite concavities in the region of $x > 10^{-3}$. However in the region $x \leq 10^{-3}$ the shape of our results is almost similar to that of the MD-DGLAP equation with a completely different slope. The MD-DGLAP equation predicts a steeper gluon distribution towards small-x which implies the presence of strong antishadowing effect in the results of MD-DGLAP equation, whereas our predictions show significant effect of shadowing corrections as a consequence of gluon recombination processes towards small-x which results in a flatter gluon distribution.

7.4 Summary

To summarize, the gluon distribution function obtained in the framework of nonlinear GLR-MQ equation in leading twist approximation is compared with the MD-DGLAP and BK equations. We make the comparison in the kinematic domain $1 \leq Q^2 \leq 30$ GeV^2 and $10^{-5} \leq x \leq 10^{-2}$ as the predicted solution of GLR-MQ equation is found to be valid only in this region. It is a very captivating finding that the predictions of nonlinear gluon density obtained from the GLR-MQ equation are very compatible with the results of the BK equation. Our results of nonlinear gluon density are also found to almost comparable with those of the MD-DGLAP equation but with a completely different slope. The MD-DGLAP equation predicts a steeper gluon distribution due to a relatively stronger antishadowing effect, whereas a flatter gluon distribution is observed in our predictions due to significant shadowing corrections at small-x. In this work we have not considered other nonlinear equations such as the JIMWLK equation for comparative analysis with the GLR-MQ equation, owing to the fact that the JIMWLK equation deals with the process dependent unintegrated parton distributions and the cross sections whereas the GLR-MQ equation considers the shadowing in the process independent parton distributions.

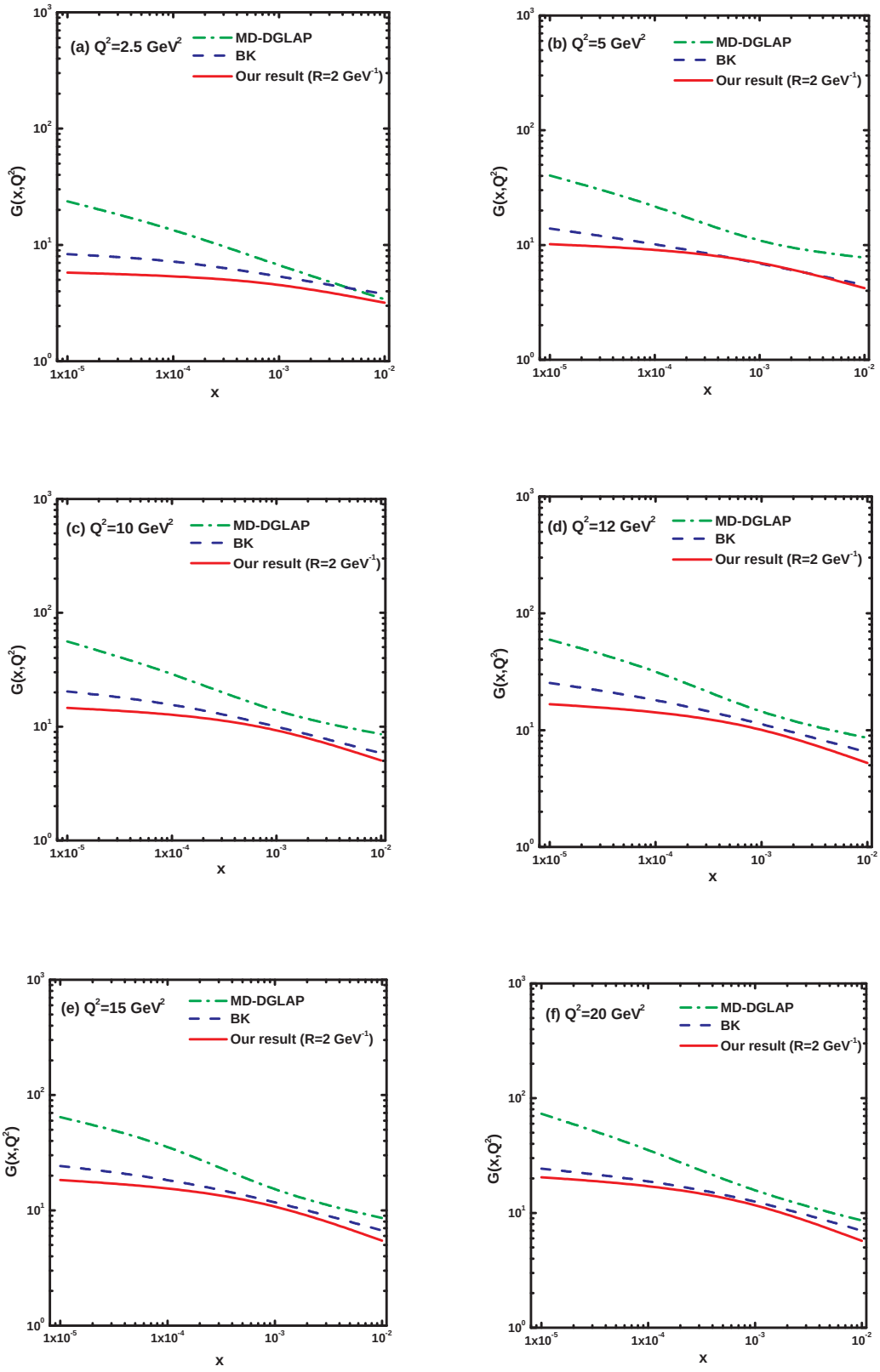

Figure 7.1: Comparison of the gluon distribution function obtained from Eq.(7.3) in the GLR-MQ approach with the MD-DGLAP results [22] as well as the BK results [23].

Bibliography

[1] Gribov, L. N., Levin, E. M. and Ryskin, M. G. Semihard processes in QCD, *Phys. Rep.* **100**(1-2), 1−−150, 1983.

[2] Mueller, A. H., Qiu, J. Gluon recombination and shadowing at small values of x, *Nucl. Phys. B* **268**(2), 427−−452, 1986.

[3] Mueller, A. H. Small-x behavior and parton saturation: A QCD model, *Nucl. Phys. B* **335**(1), 115−−137, 1990.

[4] Gribov, V. N., Lipatov, L. N. Deep inelastic ep scattering in perturbation theory, *Sov. J. Nucl. Phys.* **15**(4), 438−−450, 1972.

[5] Dokshitzer, Y. L. Calculation of structure functions of deep-inelastic scattering and e^+e^- annihilation by perturbation theory in quantum chromodynamics, *Sov. Phys. JETP* **46**(4), 641−−652, 1977.

[6] Altarelli, G., Parisi, G. Asymptotic freedom in parton language, *Nucl. Phys. B* **126**(2), 298−−318, 1977.

[7] Kuraev, E. A., Lipatov, L. N. and Fadin, V. S. Multi-reggeon processes in the Yang-Mills theory, *Sov. Phys. JETP* **44**(3), 443−−450, 1976.

[8] Kuraev, E. A., Lipatov, L. N. and Fadin, V. S. The Pomeranchuk singularity in nonabelian gauge theories, *Sov. Phys. JETP* **45**(2), 199−−204 ,1977.

[9] Balitsky, L. I., Lipatov, L. N. The Pomeranchuk singularity in quantum chromodynamics, *Sov. J. Nucl. Phys.* **28**, 822−−829, 1978.

[10] Zhu, W. A new approach to parton recombination in the QCD evolution equations, *Nucl. Phys. B* **551**(1-2), 245−−274, 1999.

[11] Zhu, W., Ruan, J. A new modified Altarelli-Parisi evolution equation with parton recombination in proton, *Nucl. Phys. B* **559**(1-2), 378−−392, 1999.

[12] Balitsky, I. Operator expansion for high-energy scattering, *Nucl. Phys. B* **463**(1), 99−−157, 1996.

[13] Kovchegov, Y. V. Small-x F_2 structure function of a nucleus including multiple Pomeron exchanges, *Phys. Rev. D* **60**(3), 034008, 1999.

[14] Zhu, W., Shen, Z. and Ruan, J. A new perspective on gluon distribution at small x, *arXiv:hep-ph/0703309v4*.

[15] Jalilian-Marian, J. et al., The intrinsic glue distribution at very small x, *Phys. Rev. D* **55**(9), 5414−−5428, 1997.

[16] Jalilian-Marian, J. et al., The Wilson renormalization group for low x physics: towards the high density regime, *Phys. Rev. D* **59**(1), 014014, 1999.

[17] Iancu, E., Leonidov, A. and McLerran, L. Nonlinear gluon evolution in the color glass condensate: I, *Nucl. Phys. A* **692**(3-4), 583−−645, 2001.

[18] Sterman, G. *An introduction to Quantum Field Theory*, Cambridge Univ. Press, Cambridge, 1993.

[19] Abramovsky, V. A., Gribov, V. N., Kancheli, O. V. Character of inclusive spectra and fluctuations produced in inelastic processes by multi-Pomeron exchange, *Sov.J.Nucl.Phys.* **18**, 308−−317, 1974.

[20] Bartels, J. Unitary corrections to the Lipatov pomeron and the small-x region in deep inelastic scattering in QCD, *Phys. Lett. B* **298**(12), 204−−210, 1993.

[21] Bartels, J., Kutak, K. A momentum space analysis of the triple pomeron vertex in pQCD, *Eur. Phys. J. C* **53**(4), 533−−548, 2008.

[22] Wei Zhu et al., Contributions of gluon recombination to saturation phenomena, *Phys. Rev. D* **68**(9), 094015, 2003.

[23] Bondarenko, S. Gluon density and F_2 functions from BK equation with impact parameter dependence, *Physics Letters B* **665**(2-3), 72−−78, 2008.

[24] Laenen, E., Levin, E. A new evolution equation, *Nucl. Phys. B* **451**(1-2), 207−−230, 1995.

Chapter 8

Conclusion and Outlook

In this thesis we have examined the behaviour of DIS structure functions in the framework of both linear DGLAP and non-linear GLR-MQ evolution equations at small-x. The small-x behavior of quark and gluon densities, where x is the Bjorken scaling variable, is one of the challenging issues of QCD. A key discovery of the past years is the prevalent role of gluons with very small fractional momentum x in nucleons when observed by a high energy probe. On that account, the study of lepton-nucleon DIS or in particular the determination of the gluon density in the region of small-x is of great significance. The increase of energy generates a rapid growth of the gluon density in the limit $x \to 0$ which is eventually expected to saturate in order to preserve unitarity. Accordingly, the corrections of the higher order QCD effects, which suppress or shadow the growth of the parton densities, have been rigorously studied in the last few years.

The linear DGLAP evolution equations are the standard and the basic theoretical tools to explore the scale dependence of the PDFs and ultimately the DIS structure functions are. In part I of this thesis we have solved the DGLAP equations for the singlet and non-singlet structure functions, as well as the gluon distribution function at LO, NLO and NNLO respectively in an analytical approach by using the Taylor series expansion method. The Taylor series expansion transforms the integro-differential DGLAP equations into first order partial differential equations which are much easier to solve. The resulting equations are then solved by the Lagrange's auxiliary method to obtain Q^2 and x evolutions of the singlet and non-singlet structure functions and the gluon distribution functions. We have also calculated the Q^2 and x evolutions of

deuteron structure function as well as the Q^2 evolution of proton structure function from the solutions of the singlet and non-singlet structure functions. We compare our predictions of deuteron and proton structure function with the NMC data, E665 data, H1 data as well as with the results of NNPDF parametrization. Our results show that at fixed x the structure functions increase with increasing Q^2 whereas at fixed Q^2 the structure functions decrease as x decreases which is in agreement with perturbative QCD fits at small-x. We further observe that our computed results can explain the general trend of data in a decent manner in the kinematic region $10^{-3} < x < 10^{-1}$ and $0.5 \leq Q^2 \leq 40$ GeV^2. On the other hand, our results of gluon distribution function obtained by solving DGLAP equation are compared with the GRV1998NLO, MRST2004NNLO, MSTW2008NNLO and JR09NNLO global QCD analysis as well as with the BDM model. The obtained results can be described within the framework of perturbative QCD. We perform our analysis in the x and Q^2 range, viz. $10^{-4} \leq x \leq 0.1$ and $5 \leq Q^2 \leq 110$ GeV^2 and find that in this domain our predictions are comparable with different global analysis of parton distributions. It is observed from our phenomenological analysis that the inclusion of the NNLO contributions provides better agreement of our results with the experimental data and parametrizations. The Taylor series expansion is a very feasible and convenient method for analytical solution of DGLAP equations. We have considered some numerical parameters to obtain the solution of DGLAP equations, however the number of parameters are less compared to the numerical. Moreover, this approach also enables us to calculate the x-evolution of deuteron structure function in addition to the Q^2-evolution. Even though various numerical methods are available in order to obtain the solution of DGLAP evolution equations, but it is always interesting to obtain an analytical solution and in this regard the Taylor series expansion method is a good alternative.

In the very small-x region the growth of the gluon distribution is incredibly enunciated. Accordingly at small-x the likelihood of interaction between two gluons can no longer be overlooked and therefore, gluon recombination will be as important as gluon splitting. So the standard linear DGLAP evolution equation will have to be modified in order to include the the modifications due to the correlations among initial gluons to the evolutionary amplitude. A traditional tool in this research is the

GLR-MQ equation that takes into account the nonlinear corrections arising from the recombination of two gluon ladders into one gluon. In part II of this thesis we have made an deliberate attempt to explore the higher order QCD effects of the gluon recombination processes at very small-x in the framework of nonlinear GLR-MQ equation. We have solved the GLR-MQ equation in the leading twist approximation in a semi-analytical approach by employing the well-known Regge-like ansatz with considerable phenomenological success. We have investigated the behavior of the gluon distributions in the vicinity of saturation region. Our resulting gluon distributions are compared with different global QCD fits to the parton distribution functions, viz. GRV1998LO, GJR2008LO, MRST2001LO, MSTW2008LO, NNPDF, HERAPDF0.1, CT10 as well as with the H1 experimental data, and are found to be quite compatible. Furthermore, we present a comparative analysis of our computed results with the results of the EHKQS and BZ models. We have examined how the inclusion of nonlinear effects changes the behavior of gluon density and it is interesting to observe that although the gluon distribution increases with increasing Q^2 and decreasing x, but the rapid growth of gluon densities is tamed due to shadowing corrections as x grows smaller. This indicates that the gluon distributions unitarize leading to the restoration of Froissart bound in the small-x region. This tamed behaviour of gluon density is observed to be more the the hot-spots when the correlation radius between two interacting gluons is of the order of the transverse size of a valance quark, i.e. $R = 2$ GeV^{-1}. We have further checked the effect of shadowing corrections in our results by comparing the gluon distributions obtained in the nonlinear GLR-MQ approach with those obtained in the linear DGLAP approach. Careful investigation of our results indicates that the nonlinear effects or shadowing corrections, emerged as a result of recombination of two gluon ladders, play a significant role on QCD evolution for gluon distribution in the kinematic region of small-x ($10^{-5} \leq x \leq 10^{-2}$) and moderate Q^2 ($1 \leq Q^2 \leq 30$ GeV^2).

We have also obtained a semi analytical solution of the GLR-MQ equation for sea quark distribution in leading twist approximation using the Regge like ansatz. The solution of the GLR-MQ equation for singlet structure function with shadowing corrections is found to be legitimate in the kinematic domain $10^{-4} \leq x \leq 10^{-1}$ and $0.6 \leq Q^2 \leq 30$ GeV^2. We have examined the effect of shadowing corrections on the

small-x and moderate-Q^2 behaviour of singlet structure function and compared our predictions with the NMC and E665 experimental data as well with the NNPDF collaboration. Our predictions are found to show the general trend of experimental data and parametrization, nevertheless with the inclusion of the nonlinear terms, the behaviour of singlet structure function is slowed down towards small-x leading to a restoration of the Froissart bound. Moreover we note that in the small-x region the logarithmic derivative of the singlet structure function has a tamed behavior related to shadowing corrections due to gluon recombination.

We have further made a comparative analysis of our predictions obtained in the framework of GLR-MQ equation in a semi-analytical approach with the results of the MD-DGLAP and BK equations. It is very fascinating to note that the predictions of nonlinear gluon density obtained from the GLR-MQ equation are in a very good agreement with the results of the BK equation. Our results are also found to almost comparable with those of the MD-DGLAP equation but with a completely different slope. The MD-DGLAP equation predicts a steeper gluon distribution caused by strong antishadowing effect, whereas a flatter gluon distribution is observed in our predictions due to significant shadowing corrections at small-x.

As a future prospect, this work encourages a more detailed study of the properties of the high density parton system. The GLR-MQ equation only includes the first non-linear term reporting the recombination of two gluon ladders into one. Therefore although it predicts saturation in the asymptotic regime, but its validity does not extend to very high density regime where significant contributions from the higher twist effects should be taken into account. Moreover, the suggested Regge type solution of the GLR-MQ equation has a limited range of validity. Nevertheless for more reliable predictions beyond this range, towards much smaller-Q^2 or smaller-x, further analysis is required incorporating the evolution dynamics at higher order. It will be interesting to study the other nonlinear equations relevant at high gluon density.

Appendices

Appendix A

The explicit forms of the functions $A_i(x)$, $B_i(x)$ and $C_i(x)$ (where i=1,2,3,4) are

$$A_1(x) = 2x + x^2 + 4\ln(1-x), \tag{1}$$

$$A_2(x) = x - x^3 - 2x\ln(x), \tag{2}$$

$$A_3(x) = 2N_f\big(\frac{2}{3} - x + x^2 - \frac{2}{3}x^3\big), \tag{3}$$

$$A_4(x) = 2N_f\big(-\frac{5}{3}x + 3x^2 - 2x^3 + \frac{2}{3}x^4 - x\ln(x)\big), \tag{4}$$

$$B_1(x) = x\int_0^1 f(\omega)d\omega - \int_0^x f(\omega)d\omega + \frac{4}{3}N_f\int_x^1 F_{qq}(\omega)d\omega, \tag{5}$$

$$B_2(x) = x\int_x^1 \big[f(\omega) + \frac{4}{3}N_f F_{qg}^s(\omega)\big]\frac{1-\omega}{\omega}d\omega, \tag{6}$$

$$B_3(x) = \int_x^1 F_{qg}^S(\omega)d\omega, \tag{7}$$

$$B_4(x) = x\int_x^1 \frac{1-\omega}{\omega}F_{qg}^S(\omega)d\omega, \tag{8}$$

where the functions $f(\omega)$, $F_{qq}(\omega)$ and $F_{qg}^S(\omega)$ are defined in Appendix B. Again,

$$C_1(x) = N_f\int_0^{1-x}\frac{\omega d\omega}{1-\omega}R_1(\omega), \tag{9}$$

$$C_2(x) = N_f\int_0^{1-x}\frac{\omega x d\omega}{(1-\omega)^2}R_1(\omega), \tag{10}$$

$$C_3(x) = N_f\int_0^{1-x}\frac{\omega x d\omega}{(1-\omega)^2}R_1(\omega), \tag{11}$$

$$C_4(x) = N_f\int_0^{1-x}\frac{\omega x d\omega}{(1-\omega)^2}R_2(\omega), \tag{12}$$

with,

$$
\begin{aligned}
R_1(\omega) &= \{\ln(\omega)\ln(1-\omega)[-173.1+46.18\ln(1-\omega)]+178.04\ln(1-\omega) \\
&+6.892\ln^2(1-\omega)+\frac{40}{27}[\ln^4(1-\omega)-2\ln^3(1-\omega)]\}+\omega\{\ln(\omega) \\
&(-163.9(1-\omega)^{-1}-7.208(1-\omega)\big)+151.49+44.51(1-\omega) \\
&-43.12(1-\omega)^2+4.82(1-\omega)^3\}+\omega^2\{-5.926\ln^3(\omega) \\
&-9.751\ln^2(\omega)-72.11\ln(\omega)+177.4+392.9(1-\omega) \\
&-101.4(1-\omega)^2-57.04\ln(1-\omega)\ln(\omega)-661.6\ln(1-\omega) \\
&+131.4\ln^2(1-\omega)-\frac{400}{9}\ln^3(1-\omega)+\frac{160}{27}\ln^4(1-\omega) \\
&-506.0(1-\omega)^{-1}-\frac{3584}{27}(1-\omega)^{-1}\ln(1-\omega)\}+N_f\omega\{1.778\ln^2(\omega) \\
&+5.944\ln(\omega)+100.1-125.2(1-\omega)+49.26(1-\omega)^2 \\
&-12.59(1-\omega)^3-1.889\ln(1-\omega)\ln(\omega)+61.75\ln(1-\omega) \\
&+17.89\ln^2(1-\omega)+\frac{32}{27}\ln^3(1-\omega)+\frac{256}{81}(1-\omega)^{-1}\} \qquad (13)
\end{aligned}
$$

$$
\begin{aligned}
R_2(\omega) &= \{\frac{100}{27}\ln^4(\omega)-\frac{70}{9}\ln^3(\omega)-120.5\ln^2(\omega)+104.42\ln(\omega)+2522 \\
&-3316(1-\omega)+2126(1-\omega)^2-252.5(1-\omega)\ln^3(1-\omega) \\
&+\ln(\omega)\ln(1-\omega)\big(1823-25.22\ln(1-\omega)\big)+424.9\ln(1-\omega) \\
&+881.5\ln^2(1-\omega)-\frac{44}{3}\ln^3(1-\omega)+\frac{536}{27}\ln^4(1-\omega)-1268.3 \\
&(1-\omega)^{-1}-\frac{896}{3}(1-\omega)^{-1}\ln(1-\omega)\}+N_f\{\frac{20}{27}\ln^3(\omega)+\frac{200}{27}\ln^2(\omega) \\
&-5.496\ln(\omega)-252.0+158.0(1-\omega)+145.4(1-\omega)^2 \\
&-139.28(1-\omega)^3-98.07(1-\omega)\ln^2(1-\omega)+11.70(1-\omega) \\
&\times\ln^3(1-\omega)-\ln(\omega)\ln(1-\omega)(53.09+80.616\ln(1-\omega)) \\
&-254.0\ln(1-\omega)-90.80\ln^2(1-\omega)-\frac{376}{27}\ln^3(1-\omega) \\
&-\frac{16}{9}\ln^4(1-\omega)+\frac{1112}{243}(1-\omega)^{-1}\} \qquad (14)
\end{aligned}
$$

Appendix B

The functions involved in the DGLAP equations for singlet and non-singlet structure functions at NLO are

$$f(\omega) = C_F^2[P_F(\omega) - P_A(\omega)] + \frac{1}{2}C_F C_A[P_G + P_A(\omega)] + C_F T_R N_f P_{N_f}(\omega), \tag{15}$$

$$F_{qq}^S(\omega) = 2C_F T_R N_f F_{qq}(\omega), \tag{16}$$

$$F_{qg}^S(\omega) = C_F T_R N_f F_{qg}^1(\omega) + C_G T_R N_f F_{qg}^2(\omega) \tag{17}$$

where,

$$F_{qq}(\omega) = \frac{20}{9\omega} - 2 + 6\omega - \frac{56}{9}\omega^2 + \Big(1 + 5\omega + \frac{8}{3}\omega^2\Big)\ln(\omega) - (1+\omega)\ln^2(\omega), \tag{18}$$

$$\begin{aligned} F_{qg}^1(\omega) &= 4 - 9\omega - (1-4\omega)\ln(\omega) - (1-2\omega)\ln^2(\omega) + 4\ln(1-\omega) \\ &\quad + \Big[2\ln^2(\frac{1-\omega}{\omega}) - 4\ln(\frac{1-\omega}{\omega}) - \frac{2}{3}\pi^2 + 10\Big]P_{qg}^1(\omega), \end{aligned} \tag{19}$$

$$\begin{aligned} F_{qg}^2(\omega) &= \frac{182}{9} + \frac{14}{9}\omega + \frac{40}{9\omega} + \Big(\frac{136}{3}\omega - \frac{38}{3}\Big)\ln(\omega) - 4\ln(1-\omega) \\ &\quad -(2+8\omega)\ln^2(\omega) + \Big[-\ln^2(\omega) + \frac{44}{3}\ln(\omega) - 2\ln^2(1-\omega) \\ &\quad +4\ln(1-\omega) + \frac{\pi^2}{3} - \frac{218}{3}\Big]P_{qg}(\omega) \\ &\quad +2P_{qg}(-\omega)\int_{\frac{\omega}{1+\omega}}^{\frac{1}{1+\omega}} \frac{dz}{z}\ln\frac{1-z}{z}, \end{aligned} \tag{20}$$

Here, the Casimir operators of the color group SU(3) are defined as $C_G \equiv N_C = 3$, $C_F = \dfrac{N_c^2 - 1}{2N_c} = \dfrac{4}{3}$ and $T_R = \frac{1}{2}$.

$$P_{N_f}(\omega) = \frac{2}{3}\Big[\frac{1+\omega^2}{1-\omega}(-\ln\omega - \frac{5}{3}) - 2(1-\omega)\Big], \tag{21}$$

$$\begin{aligned} P_F(\omega) &= -\frac{2(1+\omega^2)}{(1-\omega)}\ln(\omega)\ln(1-\omega) - \Big(\frac{3}{1-\omega} + 2\omega\Big)\ln\omega - \frac{1}{2}(1+\omega)\ln\omega \\ &\quad + \frac{40}{3}(1-\omega), \end{aligned} \tag{22}$$

$$\begin{aligned} P_G(\omega) &= \frac{(1+\omega^2)}{(1-\omega)}\Big(\ln^2(\omega) + \frac{11}{3}\ln(\omega) + \frac{67}{9} - \frac{\pi^2}{3}\Big) - \frac{1}{2}(1+\omega)\ln\omega \\ &\quad + \frac{40}{3}(1-\omega), \end{aligned} \tag{23}$$

$$P_A(\omega) = \frac{2(1+\omega^2)}{(1+\omega)}\int_{(\frac{\omega}{1+\omega})}^{(\frac{1}{1+\omega})}\frac{dk}{k}\ln\Big(\frac{1-k}{k}\Big) + 2(1+\omega)\ln(\omega)+4(1-\omega). \quad (24)$$

Appendix:C

The functions involved in the DGLAP equations for singlet and non-singlet structure functions at NNLO are given below.

The three-loop quark-quark splitting function is

$$P^2_{qq} = P^2_{NS} + P^2_{PS}, \quad (25)$$

The third-order pure-singlet contribution to the quark-quark splitting function is

$$\begin{aligned} P^{(2)}_{PS}(x) \simeq & \Big[N_f(-5.92L_1^3 - 9.751L_1^2 - 72.11L_1 + 177.4 + 392.9x - 101.4x^2 \\ & -57.04L_0L_1 - 661.61L_0 + 131.4L_0^2 - \frac{400}{9}L_0^3 + \frac{160}{27}L_0^4 - 506.0x^{-1} \\ & -\frac{3584}{27}x^{-1}L_0) + N_f^2(1.778L_1^2 + 5.944L_1 + 100.1 - 125.2x + 49.26x^2 \\ & -12.59x^3 - 1.889L_0L_1 + 61.75L_0 + 17.89L_0^2 + \frac{32}{27}L_0^3 + \frac{256}{81}x^{-1})\Big](1-x), \end{aligned} \quad (26)$$

with $L_0 = \ln(x)$, $L_1 = \ln(1-x)$.

The non-singlet splitting function calculated upto third order is given by

$$\begin{aligned} P^{(2)}_{NS}(x) = & N_f\Big[\{L_1(-163.9x^{-1} - 7.208x) + 151.49 + 44.51x - 43.12x^2 \\ & +4.82x^3\}(1-x) + L_0L_1(-173.1 + 46.18L_0) + 178.04L_0 \\ & +6.892L_0^2 + \frac{40}{27}(L_0^4 - 2L_0^3)\Big]. \end{aligned} \quad (27)$$

The three-loop quark-gluon splitting function is

$$\begin{aligned} P^{(2)}_{qg}(x) \simeq & N_f\big(\frac{100}{27}L_1^4 - \frac{70}{9}L_1^3 - 120.5L_1^2 + 104.42L_1 + 2522 - 3316x + 2126x^2 \\ & +L_0L_1(1823 - 25.22L_0) - 252.5xL_0^3 + 424.9L_0 + 881.5L_0^2 - \frac{44}{3}L_0^3 \\ & +\frac{536}{27}L_0^4 - 1268.3x^{-1} - \frac{896}{3}x^{-1}L_0\big) + N_f^2\big(\frac{20}{27}L_1^3 + \frac{200}{27}L_1^2 - 5.496L_1 \\ & -252.0 + 158.0x + 145.4x^2 - 98.07xL_0^2 + 11.70xL_0^3 - L_0L_1(53.09 \\ & +80.616L_0) - 254.0L_0 - 90.80L_0^2 - \frac{376}{27}L_0^3 - \frac{16}{9}L_0^4 + \frac{1112}{243}x^{-1}\big). \end{aligned} \quad (28)$$

Appendix:D

The explicit forms of the functions $A_i^g(x)$, $B_i^g(x)$ (i=1,2,3,4) and $C_i^g(x)$ (i=1,2) are

$$A_1^g(x) = -\frac{11}{6} + 2x - \frac{1}{2}x^2 + \frac{1}{3}x^3 - \ln(x), \tag{29}$$

$$A_2^g(x) = 1 + \frac{4}{3}x - 3x^2 + x^3 - \frac{1}{4}x^4 + 2x\ln(x). \tag{30}$$

$$A_3^g(x) = \frac{2}{9}(-\frac{3}{2} + 2x - \frac{1}{2}x^2 - 2\ln(x)), \tag{31}$$

$$A_4^g(x) = \frac{2}{9}(2 + \frac{1}{2}x - 3x^2 + \frac{1}{2}x^3 + 4x\ln(x), \tag{32}$$

$$B_1^g(x) = -\frac{52}{3}\ln(x), \tag{33}$$

$$B_2^g(x) = -\frac{52}{3}(1 - x + x\ln(x)), \tag{34}$$

$$B_3^g(x) = \int_x^1 A(\omega)d\omega, \tag{35}$$

$$B_4^g(x) = x\int_x^1 \frac{1-\omega}{\omega}A(\omega)d\omega, \tag{36}$$

$$C_1^g(x) = \int_x^1 P_{gg}^2(\omega)d\omega, \tag{37}$$

$$C_2^g(x) = x\int_x^1 \frac{1-\omega}{\omega}P_{gg}^2(\omega). \tag{38}$$

Here, the functions $A(\omega)$ and $P_{gg}^2(\omega)$ are defined in Appendices E and F respectively.

Appendix:E

The functions involved in the DGLAP equations for gluon distribution functions at NLO are

$$\begin{aligned} P_{gg}^1(\omega) &= C_F T_F(-16 + 8z + \frac{20}{3}z^2 + \frac{4}{3}z - (6+10z)\ln(z) - (2+2z)lnz^2) \\ &+C_A T_F(2 - 2z + \frac{26}{9}(z^2 - 1/z) - \frac{4}{3}(1+z)\ln(z) - \frac{20}{9}P_{gg}(z)) \\ &+C_A^2(\frac{27}{2}(1-z) + \frac{26}{9}(z^2 - 1/z) - (\frac{25}{3} - \frac{11}{3}z + \frac{44}{3}z^2)\ln(z) \\ &+4(1+z)\ln(z^2) + 2P_{gg}(-z)S_2(z) + (\frac{67}{9} - 4\ln(z)\ln(1-z) \\ &+\ln(z^2) - \frac{\pi^2}{3})P_{gg}(z)). \end{aligned} \tag{39}$$

$$A(\omega) = C_F^2 A_1(\omega) + C_F C_G A_2(\omega) + C_F T_R N_F A_3(\omega) \tag{40}$$

where

$$\begin{aligned} A_1(\omega) &= -\frac{5}{2} - \frac{7}{2}\omega + (2 + \frac{7}{2}\omega) + (-1 + \frac{\omega}{2}) \ln^2 \omega - 2\omega . \ln(1-\omega) \\ &\quad + (-3\ln(1-\omega) - \ln^2(1-\omega)) \frac{1 + (1-\omega)^2}{\omega}, \end{aligned} \tag{41}$$

$$\begin{aligned} A_2(\omega) &= \frac{28}{9} + \frac{65}{18}.\omega + \frac{44}{9}\omega^2 + (-12 - 5\omega - \frac{8}{3}\omega^2) \ln\omega + (4+\omega)\ln^2\omega \\ &\quad + 2\omega \ln(1-\omega) + (-2\ln\omega\ln(1-\omega) + \frac{1}{2}\ln^2\omega + \frac{11}{3}\ln(1-\omega) \\ &\quad + \ln^2(1-\omega) - \frac{1}{6}\pi^2 + \frac{1}{2}) \frac{1 + (1-\omega)^2}{\omega} \\ &\quad - \frac{1 + (1+\omega)^2}{\omega} \int_{\omega/1+\omega}^{1/1+\omega} \frac{dz}{z} \ln(\frac{1-z}{z}), \end{aligned} \tag{42}$$

$$A_3(\omega) = -\frac{4}{3}\omega - (\frac{20}{9} + \frac{4}{3}\ln(1-\omega))(\frac{1 + (1-\omega)^2}{\omega}). \tag{43}$$

Appendix:F

The functions involved in the DGLAP equations for gluon distribution functions at NNLO are

$$\begin{aligned} P_{gg}^2(\omega) &= 2643.524 D_0 + 4425.894\delta(1-z) + 3589 L_1 - 20852 + 3968z - 3363z^2 \\ &\quad + 4848z^3 + L_0 L_1 (7305 + 8757 L_0) + 274.4 L_0 - 7471 L_0^2 + 72 L_0^3 - 144 L_0^4 + \\ &\quad \frac{142141}{z} + \frac{2675.81}{z} L_0 + N_f (412.142 D_0 - 528.723\delta(1-z) - 320 l_1 \\ &\quad - 350.2 + 755.7z - 713.8z^2 + 559.3z^3 + L_0 L_1 (26.85 - 808.7 L_0) + 1541 L_0 \\ &\quad + 491.3 L_0^2 + \frac{832}{9} L_0^3 + \frac{512}{27} L_0^4 + \frac{182.961}{z} + \frac{157.271}{z} L_0) \\ &\quad + N_f^2 (-\frac{16}{9} D_0 + 6.4630\delta(1-z) - 13.878 + 153.4z - 187.7z^2 + 52.75z^3 \\ &\quad L_0 L_1 (115.6 - 85.25z + 63.23 L_0) - 3.422 L_0 + 9.680 L_0^2 - \frac{32}{27} L_0^3 \\ &\quad - \frac{680}{2431z}) \end{aligned} \tag{44}$$

where, L_0=ln(z), L_1=ln$(1-z)$ and D_0=$\frac{1}{(1-z)}$.

Appendix G

To obtain the analytical solutions of DGLAP evolution equations for singlet structure function or gluon distribution function, we assume the following ansatz [a-c]

$$G(x,Q^2) = K(x)F_2^S(x,Q^2) \tag{45}$$

which gives the possibility to extract the gluon distribution function directly from the experimental data. Here $K(x)$ is a function of x or may be a suitable parameter which can be determined by phenomenological analysis.

In the DGLAP formalism the gluon distribution turns out to be very large at small-x and so it contributes crucially to the evolution of the parton distribution. Subsequently, the gluon distribution governs the structure function $F_2(x,Q^2)$ through the evolution $g \to q\bar{q}$ in the small-x region. For lower Q^2 ($Q^2 \approx \Lambda^2$), however, there is no such clear cut distinction between the two. Thus for small-x and high Q^2, the gluons are expected to more dominant than the sea quarks and therefore the determination of gluon density in the small-x region is particularly interesting. But the gluon distribution function $G(x,Q^2)$ cannot be measured directly through experiments. It is determined only via the quark distributions together with the evolution equations. The most precise determinations of the gluon momentum distribution in the proton can be obtained from a measurement of the deep inelastic scattering (DIS) proton structure function $F_2(x,Q^2)$ and its scaling violation. The Q^2-evolution of the proton structure function $F_2(x,Q^2)$ is related to the gluon distribution function $G(x,Q^2)$ in the proton and to the strong interaction coupling constant α_S. It is, therefore, important to measure the $G(x,Q^2)$ indirectly using $F_2(x,Q^2)$. Hence the direct relations between $F_2(x,Q^2)$ and $G(x,Q^2)$ are extremely important because using those relations the experimental values of $G(x,Q^2)$ can be extracted using the data on $F_2(x,Q^2)$. A plausible way of realizing this is through the above ansatz. The evolution equations of gluon distribution function and singlet structure function are in the same forms of derivative with respect to Q^2. Moreover the input singlet and gluon parameterizations, taken from global analysis of PDFs, in particular from the GRV1998, MRST2001, MSTW2008 parton sets [d-f], to incorporate different high precision data, are also functions of x at fixed Q^2. So the relation between singlet structure function and gluon parton densities can be expressed in terms of x at fixed-Q^2. Accordingly the above assumption is justifiable.

The function K(x) may be assumed to have some standard functional form such as $K(x) = K$, ax^b, ce^{dx} where K, a, b, c, d are suitable parameters which can be determined by phenomenological analysis, however we can not rule out the other possibilities [a-c, g, h]. The actual functional form of $K(x)$ can be determined by simultaneous solutions of coupled equations of singlet structure functions and gluon parton densities, nevertheless it is beyond the scope of thesis. In this thesis we perform our analysis considering the function $K(x)$ as an arbitrary constant parameter K for a particular range of x and Q^2 in defining the relation between gluon and singlet structure functions as the simplest assumption. But, we need to adjust its value for satisfactory description of different experiments. The best fit graphs are obtained by choosing an appropriate value of K for a proper description of each experiment.

Our phenomenological analysis reveals that the best fit results of singlet structure functions obtained from the solutions of linear DGLAP equations are in very good agreement with NMC data in the range $0.0045 \leq x \leq 0.19$ and $0.75 \leq Q^2 \leq 27$ GeV^2 for $0.92 < K < 1.2$, E665 data in the range $0.0052 \leq x \leq 0.18$ and $1.094 \leq Q^2 \leq 26$ GeV^2 for $0.45 < K < 0.87$ and NNPDF parametrizations in the range $0.0045 \leq x \leq 0.095$ and $1.25 \leq Q^2 \leq 26$ GeV^2 for $1.1 < K < 1.6$ respectively. Thus the parameter K lies in the range $0.45 < K < 1.6$ to obtain the best fit results of singlet structure functions compared with different experiments and parametrizations for the entire domain of x and Q^2 under study. Similarly we perform our analysis for gluon distribution functions obtained from the solutions of DGLAP equations in the x and Q^2 domain, viz. $10^{-4} \leq x \leq 0.1$ and $5 \leq Q^2 \leq 110$ GeV^2 and obtain our best fit results compared with different global analysis of parton distributions in the range $0.14 < K_1 < 0.85$, where $K_1 = 1/K$. We observe that our results show excellent consistency with the global parametrizations namely GRV1998, MRST2004, MSTW2008, JR09 and with the BDM model for $0.72 < K_1 < 0.85$, $0.5 < K_1 < 0.64$, $0.14 < K_1 < 0.48$, $0.56 < K < 0.68$ and $0.62 < K < 0.78$ respectively. On the other hand from the phenomenological analysis of singlet structure functions obtained from the solution of nonlinear GLR-MQ equation we note that the best fit results are obtained in the range $0.28 < K < 1.2$ for the entire domain of x and Q^2 under study. The computed values of singlet structure functions with shadowing corrections are found to be quite compatible with NMC data in the range $0.6 < Q^2 < 3.6$ GeV^2 and

$10^{-4} < x < 0.013$ for $0.52 < K < 0.9$, E665 data in the range $1 < Q^2 < 4$ GeV^2 and $10^{-4} < x < 0.01$ for $0.28 < K < 0.86$ and with the NNPDF parametrization in the range $1 < Q^2 < 27$ GeV^2 and $10^{-4} < x < 0.011$ for $0.72 < K < 1.2$ respectively.

To conclude, we examine the dependence of our predictions on the values of the arbitrary parameters K and K_1 for different experimental data or parametrizations and observe that the values of K or K_1 lie in a very small range. Therefore it is legitimate to take these parameters as constant parameters.

References:

(a) Sarma, J. K., Choudhury, D. K. and Medhi, G. K. x-distribution of deuteron structure function at low-x, *Phys.Lett. B* **403**(1-2), 139−−144, 1997.

(b) Sarma, J. K., Das, B. t evolutions of structure functions at low-x, *Phys. Lett. B* **304**(3-4), 323−−328, 1993.

(c) Baishya, R., Sarma, J. K. Method of characteristics and solution of DGLAP evolution equation in leading and next to leading order at small x, *Phys. Rev. D* **74**(10), 107702, 2006.

(d) Gluck, M., Reya, E. and Vogt, A. Dynamical parton distributions revisited, *Eur. Phys. J. C* **5**(3), 461−−470, 1998.

(e) Martin, A. D. et al., MRST2001: partons and α_s from precise deep inelastic scattering and Tevatron jet data, *Eur. Phys. J. C* **23**(1), 73−−87, 2002.

(f) Martin, A. D. et al., Parton distributions for the LHC, *Eur. Phys. J. C* **63**(2), 189−−285, 2009.

(g) Jamil, U., Sarma, J. K. Regge behaviour of distribution functions and t and x-evolutions of gluon distribution function at low-x, *Pramana J. Phys* **69**(2), 167−−180, 2007.

(h) Rajkhowa, R., Sarma, J. K. Particular and unique solutions of DGLAP evolution equation in leading order and gluon structure function at small-x, *Int. J. Sci. Eng. Res.* **4**(11), 1185−−1192, 2013.

List of Publications

In Referred Journals:

1. **Devee, M.,** Sarma, J. K., Analysis of the small-x behavior of gluon distribution and a search for gluon recombination, ***Nucl. Phys. B 885*** 571--582, 2014.

2. **Devee, M.,** Sarma, J. K., Nonlinear GLR-MQ evolution equation and Q^2-evolution of gluon distribution function, ***Eur. Phys. J. C 74*** (2) 2751, 2014.

3. **Devee, M.,** Baishya, R., Sarma, J. K., Evolution of singlet structure functions from DGLAP equation at next-to-next-to-leading order at small-x, ***Eur. Phys. J. C 72*** (6) 2036, 2012.

4. **Devee, M.,** Baishya, R., Sarma, J. K., Solution of singlet Dokshitzer-Gribov-Lipatov-Altarelli-Parisi evolution equation in next-to-next-to-leading order at small-x, ***Indian J. Phys. 86*** (2) 141--144, 2012.

5. **Devee, M.,** Sarma, J. K., Gluon distribution from the solution of DGLAP equation at small-x: the next-to-next-to-leading order analysis, ***Eur. Phys. J. A,*** (Under Review).

6. **Devee, M.,** Sarma, J. K., Shadowing corrections to the evolution of singlet structure function in the framework of GLR-MQ equation, ***Nucl. Phys. B,*** (Under Review).

In Conference Proceedings:

1. **Devee, M.,** Sarma, J. K., Solution of nonlinear Gribov-Levin-Ryskin-Mueller-Qiu evolution equation for gluon distribution Function, ***Journal of Phys: Conf. Series*** **481** 012026, 2014.

2. **Devee, M.,** Sarma, J. K., Analytical approach for the solution of the nonlinear GLR-MQ equation, ***Proceedings of INSA*** **81** (1) 16--21, 2015.